

Vol. 25, no. 4, 2025

eISSN 2687-1653

PEER-REVIEWED SCIENTIFIC AND PRACTICAL JOURNAL

Advanced Engineering Research (Rostov-on-Don)

Mechanics

Machine Building
and Machine Science

Information Technology,
Computer Science
and Management



www.vestnik-donstu.ru
DOI 10.23947/2687-1653



Advanced Engineering Research (Rostov-on-Don)

Peer-reviewed scientific and practical journal

eISSN 2687–1653

Published since 2000

Periodicity – 4 issues per year

DOI: 10.23947/2687–1653

Founder and Publisher — Don State Technical University (DSTU), Rostov-on-Don, Russian Federation

The journal is aimed at informing the readership about the latest achievements and prospects in the field of mechanics, mechanical engineering, computer science and computer technology. The publication is a forum for cooperation between Russian and foreign scientists, it contributes to the convergence of the Russian and world scientific and information space.

The journal is included in the List of the leading peer-reviewed scientific publications (Higher Attestation Commission under the Ministry of Science and Higher Education of the Russian Federation), where basic scientific results of dissertations for the degrees of Doctor and Candidate of Science in scientific specialties and their respective branches of science should be published.

The journal publishes articles in the following fields of science:

- Theoretical Mechanics, Dynamics of Machines (Engineering Sciences)
- Deformable Solid Mechanics (Engineering, Physical and Mathematical Sciences)
- Mechanics of Liquid, Gas and Plasma (Engineering Sciences)
- Mathematical Simulation, Numerical Methods and Program Systems (Engineering Sciences)
- System Analysis, Information Management and Processing, Statistics (Engineering Sciences)
- Automation and Control of Technological Processes and Productions (Engineering Sciences)
- Software and Mathematical Support of Machines, Complexes and Computer Networks (Engineering Sciences)
- Computer Modeling and Design Automation (Engineering, Physical and Mathematical Sciences)
- Computer Science and Information Processes (Engineering Sciences)
- Machine Science (Engineering Sciences)
- Machine Friction and Wear (Engineering Sciences)
- Technology and Equipment of Mechanical and Physicotechnical Processing (Engineering Sciences)
- Engineering Technology (Engineering Sciences)
- Welding, Allied Processes and Technologies (Engineering Sciences)
- Methods and Devices for Monitoring and Diagnostics of Materials, Products, Substances and the Natural Environment (Engineering Sciences)
- Hydraulic Machines, Vacuum, Compressor Equipment, Hydraulic and Pneumatic Systems (Engineering Sciences)

<i>Registration</i>	Extract from the Register of Registered Mass Media ЭЛ № ФС 77 – 78854 dated August 07, 2020, issued by the Federal Service for Supervision of Communications, Information Technology and Mass Media
<i>Indexing and Archiving</i>	Scopus, RSCI, RISC (core), CyberLeninka, CrossRef, Dimensions, DOAJ, EBSCO, Index Copernicus, Internet Archive, Google Scholar
<i>Website</i>	https://vestnik-donstu.ru
<i>Address of the Editorial Office</i>	1, Gagarin sq., Rostov-on-Don, 344003, Russian Federation
<i>E-mail</i>	vestnik@donstu.ru
<i>Telephone</i>	+7 (863) 2–738–372
<i>Date of Publication No.4,2025</i>	30.12.2025





ДОНСКОЙ ГОСУДАРСТВЕННЫЙ
ТЕХНИЧЕСКИЙ УНИВЕРСИТЕТ

Advanced Engineering Research (Rostov-on-Don)

Рецензируемый научно-практический журнал

eISSN 2687–1653

Издается с 2000 года

Периодичность – 4 выпуска в год

DOI: 10.23947/2687–1653

Учредитель и издатель — Федеральное государственное бюджетное образовательное учреждение высшего образования «Донской государственный технический университет» (ДГТУ), г. Ростов-на-Дону

Создан в целях информирования читательской аудитории о новейших достижениях и перспективах в области механики, машиностроения, информатики и вычислительной техники. Издание является форумом для сотрудничества российских и иностранных ученых, способствует сближению российского и мирового научно-информационного пространства.

Журнал включен в перечень рецензируемых научных изданий (К2), в котором должны быть опубликованы основные научные результаты диссертаций на соискание ученой степени кандидата наук, на соискание ученой степени доктора наук (Перечень ВАК) по следующим научным специальностям:

- 1.1.7 – Теоретическая механика, динамика машин (технические науки)
- 1.1.8 – Механика деформируемого твердого тела (технические, физико-математические науки)
- 1.1.9 – Механика жидкости, газа и плазмы (технические науки)
- 1.2.2 – Математическое моделирование, численные методы и комплексы программ (технические науки)
- 2.3.1 – Системный анализ, управление и обработка информации, статистика (технические науки)
- 2.3.3 – Автоматизация и управление технологическими процессами и производствами (технические науки)
- 2.3.5 – Математическое и программное обеспечение вычислительных систем, комплексов и компьютерных сетей (технические науки)
- 2.3.7 – Компьютерное моделирование и автоматизация проектирования (технические, физико-математические науки)
- 2.3.8 – Информатика и информационные процессы (технические науки)
- 2.5.2 – Машиноведение (технические науки)
- 2.5.3 – Трение и износ в машинах (технические науки)
- 2.5.5 – Технология и оборудование механической и физико-технической обработки (технические науки)
- 2.5.6 – Технология машиностроения (технические науки)
- 2.5.8 – Сварка, родственные процессы и технологии (технические науки)
- 2.5.9 – Методы и приборы контроля и диагностики материалов, изделий, веществ и природной среды (технические науки)
- 2.5.10 – Гидравлические машины, вакуумная, компрессорная техника, гидро- и пневмосистемы (технические науки)

Регистрация	Выписка из реестра зарегистрированных средств массовой информации ЭЛ № ФС 77 – 78854 от 07 августа 2020 г., выдано Федеральной службой по надзору в сфере связи, информационных технологий и массовых коммуникаций
Индексация и архивация	Scopus, RSCI, ПИНЦ (ядро), CyberLeninka, CrossRef, Dimensions, DOAJ, EBSCO, Index Copernicus, Internet Archive, Google Scholar
Сайт	https://vestnik-donstu.ru
Адрес редакции	344003, Российская Федерация, г. Ростов-на-Дону, пл. Гагарина, 1
E-mail	vestnik@donstu.ru
Телефон	+7 (863) 2–738–372
Дата выхода №4, 2025 в свет	30.12.2025



Editorial Board

Editor-in-Chief

Alexey N. Beskopylny, Dr.Sci. (Eng.), Professor, Don State Technical University (Rostov-on-Don, Russian Federation)

Deputy Chief Editor

Alexandr I. Sukhinov, Corresponding Member, Russian Academy of Sciences, Dr.Sci. (Phys.-Math.), Professor, Don State Technical University (Rostov-on-Don, Russian Federation)

Executive Editor

Manana G. Komakhidze, Cand.Sci. (Chemistry), Don State Technical University (Rostov-on-Don, Russian Federation)

Executive Secretary

Nadezhda A. Shevchenko, Don State Technical University (Rostov-on-Don, Russian Federation)

Ahilan Appathurai, National Junior Research Fellow, Anna University Chennai (India)

Ahmet Uyumaz, PhD (Eng.), Professor, Burdur Mehmet Akif Ersoy University (Turkey)

Alexander T. Rybak, Dr.Sci. (Eng.), Professor, Don State Technical University (Rostov-on-Don, Russian Federation)

Ali M. Hasan, PhD (Computer Engineering), Al Nahrain University (Baghdad, Iraq)

Andrey V. Nasedkin, Dr.Sci. (Phys.-Math.), Professor, Southern Federal University (Rostov-on-Don, Russian Federation)

Arestak A. Sarukhanyan, Dr.Sci. (Eng.), Professor, National University of Architecture and Construction of Armenia (Armenia)

Arkady N. Solov'yev, Dr.Sci. (Phys.-Math.), Professor, Crimean Engineering and Pedagogical University the name of Fevzi Yakubov (Simferopol, Republic of Crimea)

Batyr M. Yazyev, Dr.Sci. (Eng.), Professor, Don State Technical University (Rostov-on-Don, Russian Federation)

Bertram Torsten, Dr.Sci. (Eng.), Professor, TU Dortmund University (Germany)

Evgenii A. Demekhin, Dr.Sci. (Phys.-Math.), Professor, Financial University under the RF Government, Krasnodar branch (Krasnodar, Russian Federation)

Geny V. Kuznetsov, Dr.Sci. (Phys.-Math.), Professor, Tomsk Polytechnic University (Tomsk, Russian Federation)

Gultekin Basmaci, PhD (Eng.), Professor, Burdur Mehmet Akif Ersoy University (Turkey)

Hamid A. Jalab, PhD (Computer Science & IT), University of Malaya (Malaysia)

Hubert Anysz, PhD (Eng.), Assistant Professor, Warsaw University of Technology (Republic of Poland)

Huchang Liao, Professor, IAAM Fellow, IEEE Business School Senior Fellow, Sichuan University (China)

Igor M. Verner, PhD (Eng.), Professor, Technion — Israel Institute of Technology (Israel)

Ilya I. Kudish, PhD (Phys.-Math.), Kettering University (USA)

Imad R. Antipas, Cand.Sci. (Eng.), Don State Technical University (Rostov-on-Don, Russian Federation)

Janusz Witalis Kozubal, Dr.Sci. (Eng.), Wrocław Polytechnic University (Republic of Poland)

José Carlos Quadrado, PhD (Electrical Engineering and Computers), DSc Habil, Polytechnic Institute of Porto (Portugal)

Kamil S. Akhverdiev, Dr.Sci. (Eng.), Professor, Rostov State Transport University (Rostov-on-Don, Russian Federation)

Karen O. Egiazaryan, Dr.Sci. (Eng.), Professor, Tampere University of Technology (Finland)

Konstantin V. Podmaster'ev, Dr.Sci. (Eng.), Professor, Orel State University named after I.S. Turgenev (Orel, Russian Federation)

LaRoux K. Gillespie, Dr.Sci. (Eng.), Professor, President-Elect of the Society of Manufacturing Engineers (USA)

Mezhlum A. Sumbatyan, Dr.Sci. (Phys.-Math.), Professor, Southern Federal University (Rostov-on-Don, Russian Federation)

Mikhail A. Tamarkin, Dr.Sci. (Eng.), Professor, Don State Technical University (Rostov-on-Don, Russian Federation)

Murat Tezer, Professor, Near East University (Turkey)

Murman A. Mukutadze, Dr.Sci. (Eng.), Professor, Rostov State Transport University (Rostov-on-Don, Russian Federation)

Muzafer H. Saračević, Full Professor, Novi Pazar International University (Serbia)

Nguyen Dong Ahn, Dr.Sci. (Phys.-Math.), Professor, Academy of Sciences and Technologies of Vietnam (Vietnam)

Nguyen Xuan Chiem, Dr.Sci. (Eng.), Le Quy Don Technical University (Vietnam)

Nikolay E. Galushkin, Dr.Sci. (Eng.), Professor, Institute of Service and Business, DSTU branch (Shakhty, Russian Federation)

Nikolay N. Prokopenko, Dr.Sci. (Eng.), Professor, Don State Technical University (Rostov-on-Don, Russian Federation)

Oleg V. Dvornikov, Dr.Sci. (Eng.), Professor, Belarusian State University (Belarus)

Revaz Z. Kavtaradze, Dr.Sci. (Eng.), Professor, Raphael Dvali Institute of Machine Mechanics (Georgia)

Roman N. Polyakov, Dr.Sci. (Eng.), Associate Professor, Orel State University named after I.S. Turgenev (Orel, Russian Federation)

Sergei A. Voronov, Dr.Sci. (Eng.), Associate Professor, Russian Foundation of Fundamental Research (Moscow, Russian Federation)

Sergey G. Parshin, Dr.Sci. (Eng.), Associate Professor, St. Petersburg Polytechnic University (St. Petersburg, Russian Federation)

Sergey M. Aizikovitch, Dr.Sci. (Phys.-Math.), Professor, Don State Technical University (Rostov-on-Don, Russian Federation)

Tamaz M. Natriashvili, Academician, Raphael Dvali Institute of Machine Mechanics (Georgia)

Umid M. Turdaliev, Dr.Sci. (Eng.), Professor, Andijan Machine-Building Institute (Uzbekistan)

Valentin L. Popov, Dr.Sci. (Phys.-Math.), Professor, Berlin University of Technology (Germany)

Valery N. Varavka, Dr.Sci. (Eng.), Professor, Don State Technical University (Rostov-on-Don, Russian Federation)

Victor A. Ereemev, Dr.Sci. (Phys.-Math.), Professor, Southern Scientific Center of RAS (Rostov-on-Don, Russian Federation)

Victor M. Kureychik, Dr.Sci. (Eng.), Professor, Southern Federal University (Rostov-on-Don, Russian Federation)

Vilor L. Zakovorotny, Dr.Sci. (Eng.), Professor, Don State Technical University (Rostov-on-Don, Russian Federation)

Vladimir I. Lysak, Dr.Sci. (Eng.), Professor, Volgograd State Technical University (Volgograd, Russian Federation)

Vladimir I. Marchuk, Dr.Sci. (Eng.), Professor, Institute of Service and Business, DSTU branch (Shakhty, Russian Federation)

Vladimir M. Mladenovic, Dr.Sci. (Eng.), Professor, University of Kragujevac (Serbia)

Vladimir N. Sidorov, Dr.Sci. (Eng.), Russian University of Transport (Moscow, Russian Federation)

Vyacheslav G. Tsybulin, Dr.Sci. (Phys.-Math.), Associate Professor, Southern Federal University (Rostov-on-Don, Russian Federation)

Yuri O. Chernyshev, Dr.Sci. (Eng.), Professor, Don State Technical University (Rostov-on-Don, Russian Federation)

Редакционная коллегия

Главный редактор

Бескопыйный Алексей Николаевич, доктор технических наук, профессор, Донской государственный технический университет (Ростов-на-Дону, Российская Федерация)

Заместитель главного редактора

Сухинов Александр Иванович, член-корреспондент РАН, доктор физико-математических наук, профессор, Донской государственный технический университет (Ростов-на-Дону, Российская Федерация)

Ответственный редактор

Комахидзе Манана Гивиевна, кандидат химических наук, Донской государственный технический университет (Ростов-на-Дону, Российская Федерация)

Ответственный секретарь

Шевченко Надежда Анатольевна, Донской государственный технический университет (Ростов-на-Дону, Российская Федерация)

Айзикович Сергей Михайлович, доктор физико-математических наук, профессор, Донской государственный технический университет (Ростов-на-Дону, Российская Федерация)

Антибас Имад Ризакалла, кандидат технических наук, Донской государственный технический университет (Ростов-на-Дону, Российская Федерация)

Ахилан Аппатурай, младший научный сотрудник, Инженерно-технологический колледж PSN, Университет Анны Ченнаи (Индия)

Ахвердиев Камил Самед Оглы, доктор технических наук, профессор, Ростовский государственный университет путей сообщения (Ростов-на-Дону, Российская Федерация)

Варавка Валерий Николаевич, доктор технических наук, профессор, Донской государственный технический университет (Ростов-на-Дону, Российская Федерация)

Вернер Игорь Михайлович, доктор технических наук, профессор, Технологический институт в Израиле (Израиль)

Воронов Сергей Александрович, доктор технических наук, доцент, Российский фонд фундаментальных исследований (Москва, Российская Федерация)

Галушкин Николай Ефимович, доктор технических наук, профессор, Институт сферы обслуживания и предпринимательства, филиал ДГТУ (Шахты, Российская Федерация)

Лару Гиллеси, доктор технических наук, профессор, Президент Общества машиностроителей (США)

Аныш Губерт, доктор наук, доцент, Варшавский технологический университет (Польша)

Басмачи Гюльтекин, доктор наук, профессор, Университет Бурдура Мехмета Акифа Эрсоя (Турция)

Дворников Олег Владимирович, доктор технических наук, профессор, Белорусский государственный университет (Беларусь)

Демехин Евгений Афанасьевич, доктор физико-математических наук, профессор, Краснодарский филиал Финансового университета при Правительстве РФ (Краснодар, Российская Федерация)

Хамид Абдулла Джалаб, доктор наук (информатика и ИТ), университет Малайя (Малайзия)

Егназарян Карен Оникович, доктор технических наук, профессор, Технологический университет Тампере (Финляндия)

Еремеев Виктор Анатольевич, доктор физико-математических наук, профессор, Южный научный центр РАН (Ростов-на-Дону, Российская Федерация)

Заковоротный Вилор Лаврентьевич, доктор технических наук, профессор, Донской государственный технический университет (Ростов-на-Дону, Российская Федерация)

Кавтарадзе Реваз Зурабович, доктор технических наук, профессор, Институт механики машин им. Р. Двали (Грузия)

Козубал Януш Виталис, доктор технических наук, профессор, Вроцлавский технический университет (Польша)

Хосе Карлос Куадрадо, доктор наук (электротехника и компьютеры), Политехнический институт Порту (Португалия)

Кудиш Илья Исидорович, доктор физико-математических наук, Университет Кеттеринга (США)

Кузнецов Гений Владимирович, доктор физико-математических наук, профессор, Томский политехнический университет (Томск, Российская Федерация)

Курейник Виктор Михайлович, доктор технических наук, профессор, Южный федеральный университет (Ростов-на-Дону, Российская Федерация)

Лысак Владимир Ильич, доктор технических наук, профессор, Волгоградский государственный технический университет (Волгоград, Российская Федерация)

Марчук Владимир Иванович, доктор технических наук, профессор, Институт сферы обслуживания и предпринимательства, филиал ДГТУ (Шахты, Российская Федерация)

Владимир Младенович, доктор технических наук, профессор, Крагуевацкий университет (Сербия)

Мукутадзе Мурман Александрович, доктор технических наук, доцент, Ростовский государственный университет путей сообщения (Ростов-на-Дону, Российская Федерация)

Наседкин Андрей Викторович, доктор физико-математических наук, профессор, Южный федеральный университет (Ростов-на-Дону, Российская Федерация)

Натришвили Тамаз Мамиевич, академик, Институт механики машин им. Р. Двали (Грузия)

Нгуен Донг Ань, доктор физико-математических наук, профессор, Институт механики Академии наук и технологий Вьетнама (Вьетнам)

Нгуен Суан Тьем, доктор технических наук, Вьетнамский государственный технический университет им. Ле Куи Дона (Вьетнам)

Паршин Сергей Георгиевич, доктор технических наук, доцент, Санкт-Петербургский политехнический университет (Санкт-Петербург, Российская Федерация)

Подмастерьев Константин Валентинович, доктор технических наук, профессор, Орловский государственный университет им. И.С. Тургенева (Орел, Российская Федерация)

Поляков Роман Николаевич, доктор технических наук, доцент, Орловский государственный университет им. И.С. Тургенева (Орел, Российская Федерация)

Попов Валентин Леонидович, доктор физико-математических наук, профессор, Институт механики Берлинского технического университета (Германия)

Прокопенко Николай Николаевич, доктор технических наук, профессор, Донской государственный технический университет (Ростов-на-Дону, Российская Федерация)

Рыбак Александр Тимофеевич, доктор технических наук, профессор, Донской государственный технический университет (Ростов-на-Дону, Российская Федерация)

Музафер Сарачевич, доктор наук, профессор, Университет Нови-Пазара (Сербия)

Саруханиян Арестак Арамаисович, доктор технических наук, профессор, Национальный университет архитектуры и строительства Армении (Армения)

Сидоров Владимир Николаевич, доктор технических наук, Российский университет транспорта (Москва, Российская Федерация)

Соловьев Аркадий Николаевич, доктор физико-математических наук, профессор, Крымский инженерно-педагогический университет имени Февзи Якубова (Симферополь, Республика Крым)

Сумбатян Межлум Альбертович, доктор физико-математических наук, профессор, Южный федеральный университет (Ростов-на-Дону, Российская Федерация)

Тамаркин Михаил Аркадьевич, доктор технических наук, профессор, Донской государственный технический университет (Ростов-на-Дону, Российская Федерация)

Мурат Тезер, профессор, Ближневосточный университет (Турция)

Бертрам Торстен, доктор технических наук, профессор, Технический университет Дортмунда (Германия)

Турдиалиев Умид Мухтаралиевич, доктор технических наук, профессор, Андижанский машиностроительный институт (Узбекистан)

Ахмет Уюмаз, доктор технических наук, профессор, университет Бурдура Мехмета Акифа Эрсоя (Турция)

Али Маджид Хасан Алвазли, доктор наук (компьютерная инженерия), доцент, Университет Аль-Нахрейн (Ирак)

Цибулин Вячеслав Георгиевич, доктор физико-математических наук, доцент, Южный федеральный университет (Ростов-на-Дону, Российская Федерация)

Чернышев Юрий Олегович, доктор технических наук, профессор, Донской государственный технический университет (Ростов-на-Дону, Российская Федерация)

Хухан Ляо, профессор, научный сотрудник ИААМ Старший член Школы бизнеса IEEE, Университет Сычуань (Китай)

Языев Батыр Меретович, доктор технических наук, профессор, Донской государственный технический университет (Ростов-на-Дону, Российская Федерация)

Contents

MECHANICS

Exact and Approximate Stiffness Matrix and Nodal Load Vector for a Beam Finite Element with Linearly Varying Stiffness along Its Length	275
<i>Nikita Yu. Tsybin</i>	
Iterative Model of Elastic Deformation of a Particle Conglomerate Taking into Account the Compressibility of the Medium during Pressing	290
<i>Ivan K. Andrianov, Sergey N. Ivanov, Elena K. Chepurnova</i>	
Investigation of the Actual Value of the Vacuum Time of a Measuring Vessel by Ejector	300
<i>Sergey I. Savchuk, Ervin D. Umerov</i>	
Optical Method for Material Imperfections Identification in the Resonator Workpiece of Hemispherical Vibratory Gyroscope	311
<i>Sergei A. Shevchenko, Ivan A. Popov, Boris E. Melnikov</i>	
Analysis of Deformation Energy Dissipation in Reinforced-Layer Pavement	324
<i>Artem N. Tiraturyan</i>	

INFORMATION TECHNOLOGY, COMPUTER SCIENCE AND MANAGEMENT

Observer-Based Finite-Time Adaptive Reinforced Super-Twisting Sliding Mode Control for Robotic Manipulators	337
<i>Hoang Duc Long</i>	
Comparative Analysis of Neural Network and Machine Learning Models for Short-Term Traffic Flow Prediction on Shenzhen Expressway	350
<i>Ivan V. Topilin, Mengyi Han, Anastasia A. Feofilova, Nikita A. Beskopylny</i>	
Identification of the Activity Function of Social Network Users in a Linear Diffusion Model	363
<i>Margarita A. Tolstykh, Victor K. Tolstykh</i>	
Concept of a Multilevel Network Infrastructure for Monitoring Agricultural Facilities Based on Wireless Sensor Networks	371
<i>Vladimir V. Samoylenko</i>	

Содержание

МЕХАНИКА

- Точная и приближенная матрица жесткости и вектор узловых нагрузок балочного конечного элемента с линейным законом изменения жесткости по длине** 275
Н.Ю. Цыбин
- Итерационная модель упругого деформирования конгломерата частиц с учетом сжимаемости среды в процессе прессования** 290
И.К. Андрианов, С.Н. Иванов, Е.К. Чепурнова
- Исследование фактического значения времени вакуумирования мерной емкости эжектором** ... 300
С.И. Савчук, Э.Д. Умеров
- Оптический метод идентификации несовершенств материала в заготовке резонатора волнового твердотельного гироскопа** 311
С.А. Шевченко, И.А. Попов, Б.Е. Мельников
- Анализ диссипации энергии деформирования в дорожных одеждах с укрепленными слоями** 324
А.Н. Тиратурян

ИНФОРМАТИКА, ВЫЧИСЛИТЕЛЬНАЯ ТЕХНИКА И УПРАВЛЕНИЕ

- Наблюдательно-адаптивное управление скользящим режимом с конечным временем сходимости на основе усиленного супер-скручивающего алгоритма для роботизированных манипуляторов** 337
Хоанг Дык Лонг
- Сравнительный анализ нейросетевой и машинной моделей для краткосрочного прогнозирования транспортного потока на скоростной автомагистрали Мэйгуан Шэньчжэня..** 350
И.В. Топилин, М. Хань, А.А. Феофилова, Н.А. Бескопыйный
- Идентификация функции активности пользователей социальной сети в линейной диффузионной модели** 363
М.А. Толстых, В.К. Толстых
- Концепция многоуровневой сетевой инфраструктуры мониторинга агропромышленных объектов на основе беспроводных сенсорных сетей** 371
В.В. Самойленко

MECHANICS МЕХАНИКА



UDC 539.3; 624.072.2; 519.624.3

Original Theoretical Research

<https://doi.org/10.23947/2687-1653-2025-25-4-2206>

Exact and Approximate Stiffness Matrix and Nodal Load Vector for a Beam Finite Element with Linearly Varying Stiffness along Its Length

Nikita Yu. Tsybin

Moscow State University of Civil Engineering (National Research University), Moscow, Russian Federation

✉ science@nikitatsybin.ru

EDN: VHVNIF

Abstract

Introduction. Modern trends in construction, related to the optimization of weight and materials, require accurate methods for calculating the stress-strain state, particularly of beams with variable stiffness. Analytical calculation of the stress-strain state for such beams is fraught with considerable difficulties, limiting its practical application. Numerical methods, specifically the Finite Element Method (FEM), are widely used to solve these problems, where the law of stiffness change is typically approximated by a piecewise (discrete) function. This study is aimed at the development of an approach based on piecewise-linear approximation of stiffness. Linear stiffness approximation suggests an optimal balance of accuracy and computational resources. This approach provides significantly higher accuracy compared to the traditional discrete approximation with similar computational complexity, allowing for adequate modeling of both smooth stiffness gradients and its violent changes.

Materials and Methods. A first-approximation stiffness matrix for a one-dimensional beam finite element with linearly varying flexural stiffness was derived on the basis of a variational formulation of the problem. An exact stiffness matrix was obtained by direct integration of the differential equation for beam bending. In the calculation examples, an exact solution was obtained using the Maple software package. The numerical solution using FEM was implemented in the author's program written in Python.

Results. During the study, approximate and exact stiffness matrices of the beam finite element were obtained, as well as the vector of nodal reactions (loads) from distributed loads. The efficiency of the proposed approach was demonstrated by numerical examples. The results obtained by the FEM were verified using analytical calculations. Based on the performed calculations, recommendations and criteria for using the exact or approximate stiffness matrix were developed.

Discussion. Finite elements that account for linear change of stiffness along the length make it possible to increase the accuracy of the results and reduce the degree of discretization of the computational scheme by more than two times. The approximate matrix shows good convergence with a smooth change in stiffness along the length. In such cases, discrete approximation is also acceptable. The exact matrix allows for calculating cases where the stiffness within the beam changes by orders of magnitude with low error. The classical discrete approximation in this case does not ensure high accuracy of the calculation results.

Conclusion. The paper presents stiffness matrices for finite elements that account for linear change of stiffness along the length. Their derivation is performed by two methods: on the basis of a variational formulation of the problem, and by direct integration of the differential equation of bending. The resulting matrices enable more accurate stress-strain analysis of beams with variable stiffness. They have an analytical format that simplifies their integration into existing software systems. Further research will be directed towards applying the obtained matrices to the calculation of reinforced concrete beams, considering physical nonlinearity, as well as to solving problems of stability and dynamics of beams with variable stiffness.

Keywords: finite element method, stiffness matrix, beam element, variable stiffness

Acknowledgements. The author would like to thank the Editorial board and the reviewers for their attentive attitude to the article and for the specified comments that improved the quality of the article.

For Citation. Tsybin NYu. Exact and Approximate Stiffness Matrix and Nodal Load Vector for a Beam Finite Element with Linearly Varying Stiffness along Its Length. *Advanced Engineering Research (Rostov-on-Don)*. 2025;25(4):275–289. <https://doi.org/10.23947/2687-1653-2025-25-4-2206>

Оригинальное теоретическое исследование

Точная и приближенная матрица жесткости и вектор узловых нагрузок балочного конечного элемента с линейным законом изменения жесткости по длине

Н.Ю. Цыбин 

Национальный исследовательский Московский государственный строительный университет, г. Москва, Российская Федерация

✉ science@nikitatsybin.ru

Аннотация

Введение. Современные тенденции в строительстве, связанные с оптимизацией массы и материалов, требуют точных методов расчёта напряжённо-деформированного состояния, в частности для балок переменной жёсткости. Аналитический расчёт напряжённо-деформированного состояния таких балок сопряжён со значительными трудностями, что ограничивает его практическое применение. Для решения подобных задач широко используются численные методы, в частности метод конечных элементов (МКЭ), при этом закон изменения жёсткости обычно аппроксимируется ступенчатой (дискретной) функцией. Цель настоящей работы — разработать подход на основе кусочно-линейной аппроксимации жёсткости. Линейная аппроксимация жёсткости обеспечивает оптимальное соотношение точности, сложности и вычислительных ресурсов. Предлагаемый подход обеспечивает существенно более высокую точность по сравнению с традиционной дискретной аппроксимацией при сопоставимой вычислительной сложности — это позволяет адекватно моделировать как плавные градиенты жёсткости, так и резкие её изменения.

Материалы и методы. В первом приближении матрица жесткости одномерного балочного конечного элемента с линейно изменяющейся изгибной жесткостью получена на основе вариационной формулировки задачи. Точная матрица жесткости — методом непосредственного интегрирования дифференциального уравнения изгиба балки. Точные решения в примерах расчета получены с применением программного комплекса Maple. Численное решение, с использованием метода конечных элементов, реализовано в разработанной автором программе на языке программирования Python.

Результаты исследования. В ходе исследования были получены приближенная и точная матрицы жесткости балочного конечного элемента, а также вектор узловых реакций (нагрузок) от распределенных нагрузок. Эффективность предложенного подхода продемонстрирована на примерах численного расчета. При этом результаты, полученные методом конечных элементов, верифицированы посредством аналитических вычислений. По итогам проведённых расчётов были выработаны рекомендации и критерии для использования точной или приближенной матрицы жесткости.

Обсуждение. Конечные элементы, учитывающие линейное изменение жесткости по длине, позволяют повысить точность получаемых результатов и снизить степень дискретизации расчетной схемы более чем в два раза. Приближенная матрица демонстрирует хорошую сходимость при плавном изменении жесткости по длине. В подобных случаях также допустимо применять дискретную аппроксимацию. Точная матрица позволяет с малой погрешностью рассчитывать ситуации, в которых жесткость в пределах балки изменяется на несколько порядков. Классическая дискретная аппроксимация в таких случаях не обеспечивает высокой точности результатов расчета. **Заключение.** В данной работе были получены матрицы жесткости конечных элементов с учетом линейного изменения жесткости по длине. Их вывод осуществлен двумя методами: на основе вариационной постановки задачи и путём непосредственного интегрирования дифференциального уравнения изгиба. Полученные матрицы позволяют выполнять более точный анализ напряжённо-деформированного состояния балок переменной жесткости. Они обладают аналитическим видом, что упрощает их внедрение в существующие программные комплексы. Дальнейшие исследования будут направлены на применение этих матриц к расчёту железобетонных балок с учетом физической нелинейности, а также на решение задач устойчивости и динамики балок переменной жесткости.

Ключевые слова: метод конечных элементов, матрица жесткости, балочный элемент, переменная жесткость

Благодарность. Автор выражает благодарность редакции и рецензентам за внимательное отношение к статье и указанные замечания, которые позволили повысить ее качество.

Для цитирования. Цыбин Н.Ю. Точная и приближенная матрица жесткости и вектор узловых нагрузок балочного конечного элемента с линейным законом изменения жесткости по длине. *Advanced Engineering Research (Rostov-on-Don)*. 2025;25(4):275–289. <https://doi.org/10.23947/2687-1653-2025-25-4-2206>

Introduction. In modern engineering practice, specifically in the context of sustainable development and resource optimization, structures with variable stiffness — for example, beams with variable cross-sections — are widely used [1]. Such solutions significantly reduce the material consumption and dead weight of structures, which directly improves their cost-effectiveness and environmental friendliness by reducing material consumption [2]. In addition, the mathematical model of a beam of variable stiffness serves as a tool for the qualitative description of the stress-strain state of reinforced concrete elements, in which the change in stiffness occurs due to the nonlinear behavior of the material [3, 4] and the formation of cracks [5, 6].

In statically indeterminate beams, which are common in structural mechanics, the distribution of internal forces depends on the stiffness ratio of the elements. Neglecting the variable nature of stiffness can cause significant errors in determining internal forces and, consequently, the incorrect cross-section selection, which compromises both the reliability and economic viability of the project. Figure 1 shows a clear example: taking into account variable stiffness in a beam (Fig. 1 *b*) has led to a radical change in the bending moment diagram compared to the calculation model of constant stiffness (Fig. 1 *a*).

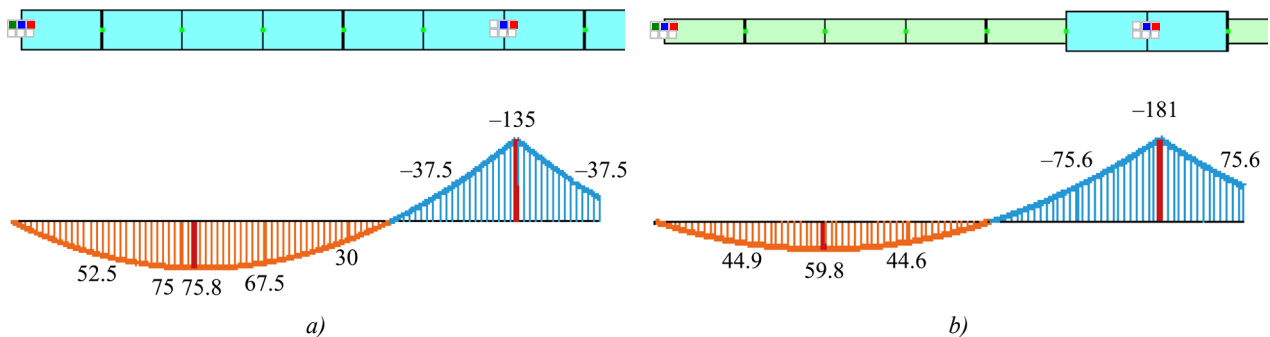


Fig. 1. Results of calculation of statically indeterminate beam:
a — fragment of statically indeterminate beam of constant stiffness and diagram of bending moments in it; *b* — the same for beam of variable stiffness

The analysis of beams with variable cross-sections is traditionally performed using numerical methods, in particular, the finite element method (FEM). Despite the existence of analytical solutions [7], they are often represented as complex series [8] or special functions [9], which complicates their practical implementation in engineering software. Moreover, such solutions often lack universality for arbitrary laws of stiffness change and boundary conditions [10, 11].

The stress-strain state of beams with variable cross-sections has been studied by various authors for a long time. In the context of numerical calculations using FEM, some of the first works [12, 13] can be mentioned. The most common approach to accounting for variable stiffness is a discrete approximation using finite elements of constant stiffness (Fig. 1 *b*), whose value is taken equal to the average in the section [14, 15]. Despite its simplicity, this approach does not always ensure the required accuracy of calculations.

More accurate results are obtained by using a linear approximation of the stiffness within the finite element. This approach is described in this article. At the same time, classical methods for constructing stiffness matrices for elements with variable parameters [16], based on variational approaches [17] or approximations [18], may not provide the exact fulfillment of the differential equations of equilibrium and boundary conditions. This causes errors with significant changes in stiffness along the length of the element or in extreme cases, for example, when modeling zones with a sharp drop in stiffness (formation of cracks, plastic hinge).

Thus, the relevance of this study is determined by the need to develop an efficient and more accurate method for calculating beams with variable stiffness.

The objective of this study is to obtain and verify stiffness matrices for a beam finite element with a piecewise linear law of stiffness change.

To reach this objective, the following tasks were formulated:

1. To obtain an approximate stiffness matrix on the basis of a variational formulation of the problem and a linear approximation of the stiffness within the finite element.
2. To develop an exact stiffness matrix for a beam finite element with linearly varying stiffness using an analytical solution to the differential bending equation.

3. To conduct a comparative analysis of the accuracy of the calculation results using the proposed stiffness matrices and the classical approach with discrete stiffness approximation on a series of test examples; to determine the accuracy by comparing to the results of the analytical solution.

Materials and Methods

Variational Method for Obtaining the Stiffness Matrix. Variational methods [19] are the generally accepted and most versatile methods for obtaining the stiffness matrix of a finite element. The accuracy of the resulting matrix depends on how well the input approximation of the desired function reflects the solution to the differential equation.

For the beam under consideration, the classical Euler-Bernoulli hypotheses are applied. The change in the flexural stiffness of the cross-section D_z along the length of the finite element is assumed to be a linear function:

$$D_z(x) = D_0 \left[\psi_0 + \frac{x}{L}(\psi_1 - \psi_0) \right], \quad D_z(0) = \psi_0 D_0, \quad D_z(L) = \psi_1 D_0, \quad (1)$$

where D_0 — initial stiffness; L — length of the finite element; ψ_0 and ψ_1 — coefficients that take into account the change in initial stiffness D_0 at the beginning and end of the element, respectively. In this case, $\psi_0 \geq 0$ and $\psi_1 \geq 0$.

The finite element method is considered in the form of displacements. The unknowns are the deflection and rotation angle of the section v_i and φ_i (Fig. 2 a) at the beginning $x = 0$ and end $x = L$ of the element.



Fig. 2. Beam finite element:

a — unknowns of the finite element method; b — nodal loads and internal forces

To approximate the displacement function $v(x)$, Hermite polynomials are used [1, 4]:

$$v = v_0 N_1 + \varphi_0 N_2 + v_1 N_3 + \varphi_1 N_4, \quad (2)$$

where N_i — shape functions (Hermite polynomials) written below:

$$N_1 = \frac{2x^3}{L^3} - \frac{3x^2}{L^2} + 1; \quad N_2 = \frac{x^3}{L^2} - \frac{2x^2}{L} + x; \quad N_3 = -\frac{2x^3}{L^3} + \frac{3x^2}{L^2}; \quad N_4 = \frac{x^3}{L^2} - \frac{x^2}{L}. \quad (3)$$

Approximation (2) corresponds to the following boundary conditions:

$$v(0) = v_0; \quad v'(0) = \varphi(0) = \varphi_0; \quad v(L) = v_1; \quad v'(L) = \varphi(L) = \varphi_1. \quad (4)$$

The prime in (4) denotes the derivative of function $v(x)$ in respect to x .

From formulas (3), it follows that classical shape functions do not take into account the distribution of bending stiffness along the length of the element, which, in turn, negatively impacts the accuracy of the calculation results. To improve the accuracy of calculations, when using a variational formulation of the problem, the double approximation method can be applied [20].

The bending moment is associated with the curvature by the relation:

$$\frac{d^2 v}{dx^2} = -\frac{M_z}{D_z}. \quad (5)$$

Here, D_z — bending stiffness of the beam cross-section according to (1).

Taking into account (2) and (3):

$$-\frac{M_z}{D_z} = v_0 \left(\frac{12x}{L^3} - \frac{6}{L^2} \right) + \varphi_0 \left(\frac{6x}{L^2} - \frac{4}{L} \right) + v_1 \left(-\frac{12x}{L^3} + \frac{6}{L^2} \right) + \varphi_1 \left(\frac{6x}{L^2} - \frac{2}{L} \right). \quad (6)$$

The potential energy of bending deformation is determined by the formula:

$$U = \frac{1}{2} \int_0^L D_z \left(\frac{d^2 v}{dx^2} \right)^2 dx. \quad (7)$$

Taking into account (6) and (1), formula (7) takes the form:

$$U \cdot 2L^3 / D_0 = 6(\psi_0 + \psi_1) f_{11} + 4L(2\psi_0 + \psi_1) f_{12} - 12(\psi_0 + \psi_1) f_{13} + 4L(\psi_0 + 2\psi_1) f_{14} + \\ + L^2(3\psi_0 + \psi_1) f_{22} - 4L(2\psi_0 + \psi_1) f_{23} + 2L^2(\psi_0 + \psi_1) f_{24} + \\ + 6(\psi_0 + \psi_1) f_{33} - 4L(\psi_0 + 2\psi_1) f_{34} + L^2(\psi_0 + 3\psi_1) f_{44}, \quad (8)$$

where

$$\begin{aligned} f_{11} &= v_0 v_0; \quad f_{12} = v_0 \varphi_0; \quad f_{13} = v_0 v_1; \quad f_{14} = v_0 \varphi_1; \\ f_{22} &= \varphi_0 \varphi_0; \quad f_{23} = \varphi_0 v_1; \quad f_{24} = \varphi_0 \varphi_1; \quad f_{33} = v_1 v_1; \quad f_{34} = v_1 \varphi_1; \quad f_{44} = \varphi_1 \varphi_1. \end{aligned} \quad (9)$$

If we introduce the vector of unknowns $\bar{u} = [v_0, \varphi_0, v_1, \varphi_1]^T$, then (8) can be rewritten in the following form:

$$U = \frac{1}{2} \bar{u}^T \cdot [K] \cdot \bar{u}. \quad (10)$$

Here, $[K]$ — stiffness matrix of the element, determined taking into account (8) and (9):

$$[K] = \frac{D_0}{L^3} \begin{bmatrix} 6(\psi_0 + \psi_1) & 2L(2\psi_0 + \psi_1) & -6(\psi_0 + \psi_1) & 2L(\psi_0 + 2\psi_1) \\ 2L(2\psi_0 + \psi_1) & L^2(3\psi_0 + \psi_1) & -2L(2\psi_0 + \psi_1) & L^2(\psi_0 + \psi_1) \\ -6(\psi_0 + \psi_1) & -2L(2\psi_0 + \psi_1) & 6(\psi_0 + \psi_1) & -2L(\psi_0 + 2\psi_1) \\ 2L(\psi_0 + 2\psi_1) & L^2(\psi_0 + \psi_1) & -2L(\psi_0 + 2\psi_1) & L^2(\psi_0 + 3\psi_1) \end{bmatrix}. \quad (11)$$

This case $\psi_0 = \psi_1 = 1$ corresponds to the classical beam stiffness matrix.

The positive directions of the nodal loads and internal forces are shown in Figure 2 b, from which it follows:

$$Q_0 = -X_1; \quad M_0 = X_2; \quad Q_1 = X_3; \quad M_1 = -X_4. \quad (12)$$

Let us calculate the work of external forces.

$$\begin{aligned} W &= X_1 v_0 + X_2 \varphi_0 + X_3 v_1 + X_4 \varphi_1 + \int_0^L (qv) dx = \\ &= \left(X_1 + \frac{qL}{2} \right) v_0 + \left(X_2 + \frac{qL^2}{12} \right) \varphi_0 + \left(X_3 + \frac{qL}{2} \right) v_1 + \left(X_4 - \frac{qL^2}{12} \right) \varphi_1. \end{aligned} \quad (13)$$

In matrix form

$$W = \bar{u}^T \cdot (\bar{F} + \bar{F}_q), \quad (14)$$

where \bar{F} — vector of concentrated nodal loads; \bar{F}_q — vector of nodal loads from distributed loads. The components of these vectors have the form (15):

$$\bar{F} = [X_1, X_2, X_3, X_4]^T; \quad \bar{F}_q = [qL/2, qL^2/12, qL/2, -qL^2/12]^T. \quad (15)$$

As we can see, the vector of nodal forces from distributed loads obtained in (15) does not take into account the change in stiffness along the length. This is a drawback of the variational approach in the context of the problem under consideration.

The total energy of the system, taking into account (10) and (14), is determined by the expression:

$$\Pi = U - W = \frac{1}{2} \bar{u}^T \cdot [K] \cdot \bar{u} - \bar{u}^T \cdot (\bar{F} + \bar{F}_q). \quad (16)$$

Applying the principle of minimum potential energy, we obtain the condition for the stationarity of functional (16):

$$\frac{\partial \Pi}{\partial \bar{u}} = \frac{\partial}{\partial \bar{u}} \left\{ \frac{1}{2} \bar{u}^T \cdot [K] \cdot \bar{u} - \bar{u}^T \cdot (\bar{F} + \bar{F}_q) \right\} = [K] \cdot \bar{u} - (\bar{F} + \bar{F}_q) = 0. \quad (17)$$

The basic equation of the finite element method follows from (17):

$$[K] \cdot \bar{u} = \bar{F} + \bar{F}_q. \quad (18)$$

Direct Method for Obtaining the Stiffness Matrix. The resulting stiffness matrix (11) has a significant drawback. If we assume $v_0 = \varphi_0 = 0$, as well as $\psi_0 = 0$ and $\psi_1 = 1$ (which corresponds to zero stiffness at the left clamped edge), the moment at the left edge will be determined by the formula:

$$M_0 = X_2 = K_{2,1} v_0 + K_{2,2} \varphi_0 + K_{2,3} v_1 + K_{2,4} \varphi_1 = \frac{D_0}{L^2} (-2v_1 + \varphi_1 L). \quad (19)$$

Note that (19) considers a limiting case — a mathematical idealization, where the stiffness at the support is not simply small but asymptotically tends to zero. Thus, in accordance with (19), the moment at the left edge does not vanish, which contradicts formula (5). The reason lies in the inaccurate approximation of the deflection function by formula (2). To eliminate this discrepancy, an exact stiffness matrix was found through direct integrating the differential equation for beam bending, taking into account the change in stiffness along the length by formula (1).

A similar approach was used by other authors. In [21], the solution is obtained in the form of power series, therefore, it cannot be considered closed. In [22], a direct integration method is used to obtain the stiffness matrix of an element with a power law of stiffness change for stability problems. In [23], an arbitrary law of stiffness change along the length

is considered. However, for the practical use of the presented results, integration is required. Works [24, 25] are devoted to solving stability problems. In these papers, the law of stiffness change along the length is given in the form of a polynomial of the second and fourth degree, while the vector of nodal forces from distributed loads is not provided. A common drawback of works that take into account second and higher order polynomials in the function of stiffness change along the length is the complexity of calculating the stiffness matrix. For example, according to [26], to obtain the stiffness matrix coefficients, it is required to calculate expressions of the form $\sin[\varepsilon \ln(\lambda)]$ (the original notations are preserved), which complicates the analysis of limiting cases and the implementation of solutions in commercial software packages.

To obtain an accurate stiffness matrix, the differential equation for plane transverse bending of a beam with variable stiffness, known from the course on strength of materials, is considered:

$$\frac{d^2}{dx^2} \left(D_z \frac{d^2 v}{dx^2} \right) = q. \quad (20)$$

Given the form (1), the general solution to the homogeneous equation (20) will contain a logarithm. We eliminate the dimensional quantities under the logarithm sign by replacing the variable using the formula:

$$x = \rho L, \quad 0 \leq \rho \leq 1. \quad (21)$$

Considering (21):

$$\varphi = \frac{dv}{dx} = \frac{1}{L} \frac{dv}{d\rho}. \quad (22)$$

As a result, general solution [27] of equation (20) takes the form:

$$v(\rho) = C_1 + C_2 (\rho - \alpha)^2 + C_3 (\rho - \alpha) + C_4 (\rho - \alpha) \ln|\rho - \alpha| + v^*, \quad (23)$$

where $\alpha = \psi_0 / (\psi_0 - \psi_1)$, v^* — particular solution to the inhomogeneous equation. Due to its cumbersome nature, the particular solution is not given.

Solution (23) is valid for the cases $\psi_0 \neq \psi_1$, $\rho \neq \alpha$, since these cases generate uncertainties that are resolved through limiting in formulas (31), (32) and (33).

The unknown integration constants are determined from the boundary conditions:

$$v(0) = v_0; \quad v'(0) = \varphi_0 L; \quad v(1) = v_1; \quad v'(1) = \varphi_1 L. \quad (24)$$

In (24), the prime denotes the derivative with respect to ρ . Multiplier L at the rotation angles in the boundary conditions (24) is present due to the introduced change of variable (21), which is reflected in (22). After determining the integration constants from (24), the moment and shear force in the beam, taking into account the introduced change of variables, are calculated using the formulas:

$$M = -\frac{D_0 [\psi_0 + \rho(\psi_1 - \psi_0)]}{L^2} \frac{d^2 v(\rho)}{d\rho^2}; \quad Q = -\frac{1}{L^3} \frac{d}{d\rho} \left(D_0 [\psi_0 + \rho(\psi_1 - \psi_0)] \frac{d^2 v(\rho)}{d\rho^2} \right). \quad (25)$$

The coefficients of the stiffness matrix, taking into account (25) and (12), can be found from the expressions:

$$\left. \begin{aligned} X_1 &= -Q(0) = k_{11}v_0 + k_{12}\varphi_0 + k_{13}v_1 + k_{14}\varphi_1 - F_{q,1}; \\ X_2 &= M(0) = k_{21}v_0 + k_{22}\varphi_0 + k_{23}v_1 + k_{24}\varphi_1 - F_{q,2}; \\ X_3 &= Q(1) = k_{31}v_0 + k_{32}\varphi_0 + k_{33}v_1 + k_{34}\varphi_1 - F_{q,3}; \\ X_4 &= -M(1) = k_{41}v_0 + k_{42}\varphi_0 + k_{43}v_1 + k_{44}\varphi_1 - F_{q,4}. \end{aligned} \right\}. \quad (26)$$

Matrix form (26) is equivalent to the one obtained earlier (18). The stiffness matrix in the case under consideration will take the form:

$$[K] = \frac{D_0}{\beta L^3} \begin{bmatrix} 2\xi^2\lambda & 2L\xi\omega_0 & -2\xi^2\lambda & -2L\xi\omega_1 \\ 2L\xi\omega_0 & L^2(2\psi_0\omega_0 - \xi^2) & -2L\xi\omega_0 & -L^2(2\psi_0\omega_1 + \xi^2) \\ -2\xi^2\lambda & -2L\xi\omega_0 & 2\xi^2\lambda & 2L\xi\omega_1 \\ -2L\xi\omega_1 & -L^2(2\psi_0\omega_1 + \xi^2) & 2L\xi\omega_1 & L^2(2\psi_1\omega_1 + \xi^2) \end{bmatrix}. \quad (27)$$

In (27), the following notations are introduced for the sake of compactness:

$$\lambda = \ln(\psi_0 / \psi_1); \quad \xi = \psi_0 - \psi_1; \quad \beta = \lambda(\psi_0 + \psi_1) - 2\xi; \quad \omega_0 = \psi_0\lambda - \xi; \quad \omega_1 = \psi_1\lambda - \xi. \quad (28)$$

To implement the proposed stiffness matrix in software, it is critical to be able to transform distributed loads into a nodal force vector. The exact expressions for vector \bar{F}_q are given below.

$$\bar{F}_q = \begin{bmatrix} \frac{qL \left[2\lambda (2\psi_0^2 + 2\psi_0\psi_1 - \psi_1^2) - 3\xi (3\psi_0 - \psi_1) \right]}{6\beta\xi} \\ \frac{qL^2 \left[2\lambda\psi_0 (\psi_0 + 2\psi_1) - \xi (5\psi_0 + \psi_1) \right]}{12\beta\xi} \\ \frac{qL \left[2\lambda (\psi_0^2 - 2\psi_0\psi_1 - 2\psi_1^2) - 3\xi (\psi_0 - 3\psi_1) \right]}{6\beta\xi} \\ \frac{qL^2 \left[2\lambda\psi_1 (2\psi_0 + \psi_1) - \xi (\psi_0 + 5\psi_1) \right]}{12\beta\xi} \end{bmatrix}. \quad (29)$$

The main advantage of the obtained matrix (27) and vector (29) is the simplicity of implementation, as well as the absence of series and special functions in the calculations.

When solving certain problems, it is more convenient to relate section stiffness coefficients ψ_0 and ψ_1 to the curvature. In this case, it is necessary to know how the curvature is related to the displacements and rotation angles of the nodes of the element. Formula (5) can be used for this. Knowing how the moment is expressed at the beginning and end of the element according to formulas (26), we obtain:

$$\left. \begin{aligned} \frac{d^2v}{dx^2} \Big|_{x=0} &= -\frac{M(0)}{D_z(0)} = -\frac{1}{D_0\psi_0} (k_{21}v_0 + k_{22}\varphi_0 + k_{23}v_1 + k_{24}\varphi_1 - F_{q,2}); \\ \frac{d^2v}{dx^2} \Big|_{x=L} &= -\frac{M(\rho=1)}{D_z(x=L)} = -\frac{1}{D_0\psi_1} (k_{41}v_0 + k_{42}\varphi_0 + k_{43}v_1 + k_{44}\varphi_1 - F_{q,4}). \end{aligned} \right\} \quad (30)$$

Cases $\psi_0 = 0$, $\psi_1 = 0$ and $\psi_0 = \psi_1 = \psi$ generate uncertainties of various types in matrix (27) and vector (29). Let us develop them.

Case $\psi_0 = 0$.

$$[K] = \frac{2D_0\psi_1}{L^3} \begin{bmatrix} 1 & 0 & -1 & L \\ 0 & 0 & 0 & 0 \\ -1 & 0 & 1 & -L \\ L & 0 & -L & L^2 \end{bmatrix}; \quad \bar{F}_q = \begin{bmatrix} qL/3 \\ 0 \\ 2qL/3 \\ -qL^2/6 \end{bmatrix}. \quad (31)$$

Case $\psi_1 = 0$.

$$[K] = \frac{2D_0\psi_0}{L^3} \begin{bmatrix} 1 & L & -1 & 0 \\ L & L^2 & -L & 0 \\ -1 & -L & 1 & 0 \\ 0 & 0 & 0 & 0 \end{bmatrix}; \quad \bar{F}_q = \begin{bmatrix} 2qL/3 \\ qL^2/6 \\ qL/3 \\ 0 \end{bmatrix}. \quad (32)$$

From (31) and (32), it is evident that the columns and rows of the stiffness matrix, as well as the components of the nodal force vector from distributed loads associated with the bending moments at the left and right ends of the finite element, respectively, are set to zero — which corresponds to equation (5). The vanishing of the bending stiffness can occur, for example, when tensile reinforcement breaks, or the compressed zone of a reinforced concrete beam fails in any section. In the case of a statically indeterminate beam, the structure can continue to function during such failures. In commercial software packages, when such situations arise, hinges are typically activated in the calculation model.

Case $\psi_0 = \psi_1 = \psi$. This case corresponds to the classical stiffness matrix.

$$[K] = \frac{D_0\psi}{L^3} \begin{bmatrix} 12 & 6L & -12 & 6L \\ 6L & 4L^2 & -6L & 2L^2 \\ -12 & -6L & 12 & -6L \\ 6L & 2L^2 & -6L & 4L^2 \end{bmatrix}; \quad \bar{F}_q = \begin{bmatrix} qL/2 \\ qL^2/12 \\ qL/2 \\ -qL^2/12 \end{bmatrix}. \quad (33)$$

In practical calculations, to reduce computational errors that may accumulate during the calculation of the stiffness matrix components and factors (28), it is recommended to use formulas (31), (32) and (33) not when strictly reaching the limiting case, but when approaching it. For example, set the threshold conditions for using (27) and (29) in the form $\psi_i > 10^{-4}$ and $|1 - \psi_0 / \psi_1| > 10^{-3}$. The specified values are approximate and depend on the specific implementation features.

Figure 3 shows graphs of three elements of the stiffness matrix, calculated using formulas (11) and (27) for $\psi_1 = D_0 = L = 1$.

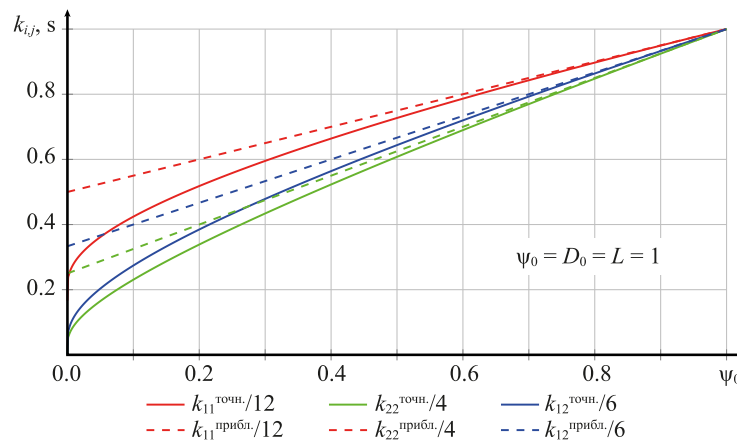


Fig. 3. Dependences k_{11} , k_{22} and k_{12} on ψ_0 . Solid lines are based on exact stiffness matrix (27); dashed lines — on approximate matrix (11)

The results presented in Figure 3 show that, for $\psi_0 = 0$ and the corresponding boundary conditions, the stiffness matrix coefficients associated with the moment at the left edge vanish in the exact matrix (27) — this corresponds to the physical meaning. Approximate stiffness matrix (11) does not have this property. With a significant difference in stiffness, at the beginning and end of the element ($\psi_0 / \psi_1 < 0.2$), values of the coefficients of the exact and approximate matrices can differ by up to 100% (excluding from consideration the limiting case $\psi_0 \rightarrow 0$). In such situations, it is recommended to use exact stiffness matrix (27). Similar conclusions can be drawn for the right edge of the finite element.

Research Results. To demonstrate the results obtained using the proposed stiffness matrices, calculation examples are performed for beams of length $2L$, shown in Figure 4.



Fig. 4. Schematic diagrams for calculation examples:
a — clamped beam of length $2L$, loaded with concentrated force;
b — the same under uniformly distributed load

Due to symmetry with respect to $x = L$, half of the beam is considered in the solution. The boundary conditions under the action of a concentrated force (diagram in Fig. 4 a) are as follows:

$$v(0) = 0; \quad v'(0) = 0; \quad v'(L) = 0; \quad (D_z v'')' \Big|_{x=L} = -P/2. \quad (34)$$

Similarly for the case of distributed load (diagram in Fig. 4 b):

$$v(0) = 0; \quad v'(0) = 0; \quad v'(L) = 0; \quad (D_z v'')' \Big|_{x=L} = 0. \quad (35)$$

The following stiffness distribution function along the beam length is considered:

$$D_z(x) = D_0 \left[s_0 - \frac{x}{L} (3s_0 + s_1 - 4) + \frac{2x^2}{L^2} (s_0 + s_1 - 2) \right], \quad (36)$$

s_0 and s_1 — beam stiffness coefficients at the beginning and middle of the span, that is, $D_z(0) = D_0 s_0$ and $D_z(L) = D_0 s_1$. In this case, $D_z(L/2) = D_0$. It is important to note that (36) determines the law of stiffness change along the length of the beam as a whole, while (1) — along the length of the finite element.

Function (36) is selected on the base of the method of load application and the boundary conditions. In this case, for a beam of constant stiffness, the moments at the support and in the middle of the beam reach maximum values. If the beam material is reinforced concrete, cracks and a decrease in flexural stiffness should be expected at these points [27]. At a quarter span, the moments are close to zero and, consequently, the stiffness is close to the initial $D_z(L/2) = D_0$.

Figure 5 shows the graphs of the stiffness distribution along the length of the beam, as well as the approximation methods under consideration for two alternatives: option 1 — $s_0 = 0.001$, $s_1 = 1.0$; option 2 — $s_0 = 0.6$, $s_1 = 0.2$.

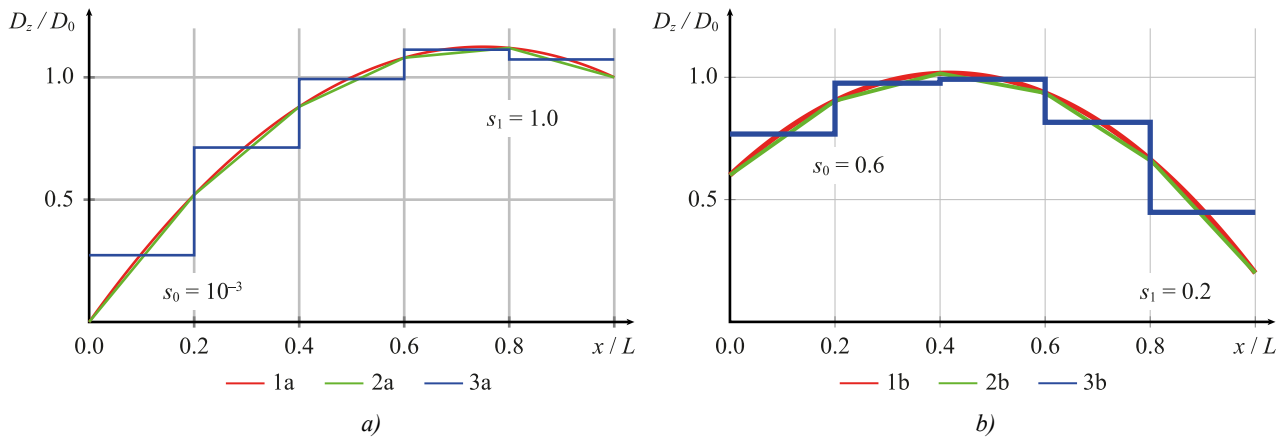


Fig. 5. Stiffness $D_z(x) / D_0$ distribution along the beam length:
 a — option 1 — $s_0 = 0.001$ and $s_1 = 1.0$; b — option 2 — $s_0 = 0.6$ and $s_1 = 0.2$.
 Curves 1 a, 1 b — initial function; 2 a, 2 b — piecewise linear approximation;
 3 a, 3 b — discrete approximation

From the results presented in Figure 5, it is evident that the linear approximation, even with five finite elements, provides satisfactory agreement (the deviation does not exceed 5%) with the initial function of stiffness change along the length for the examples under consideration. High accuracy is maintained when approximating the stiffness with a piecewise linear function for variable cross-sections of complex shape [28]. The value of the average stiffness for discrete approximation was calculated using the formula:

$$D_{z,i} = \frac{1}{x_{i+1} - x_i} \int_{x_i}^{x_{i+1}} D_z(x) dx. \quad (37)$$

The results of calculating the coefficients for the stiffness matrices of finite elements are given in Table 1. For discrete approximation, $\psi_0 = \psi_1 = \psi$.

Table 1

Coefficients of Element Stiffness Matrices

Element		1		2		3		4		5	
x_i	x_{i+1}	0.0	0.6	0.6	1.2	1.2	1.8	1.8	2.4	2.4	3.0
Option 1: $s_0 = 0.001$ and $s_1 = 1.0$											
Coeff. $\psi_{0,1}$		ψ_0	ψ_1	ψ_0	ψ_1	ψ_0	ψ_1	ψ_0	ψ_1	ψ_0	ψ_1
Linear		0.001	0.52	0.52	0.88	0.88	1.08	1.08	1.12	1.12	1.0
Discrete		0.274		0.714		0.993		1.113		1.073	
Option 2: $s_0 = 0.6$ and $s_1 = 0.2$											
Coeff. $\psi_{0,1}$		ψ_0	ψ_1	ψ_0	ψ_1	ψ_0	ψ_1	ψ_0	ψ_1	ψ_0	ψ_1
Linear		0.6	0.904	0.904	1.016	1.016	0.936	0.936	0.664	0.664	0.2
Discrete		0.768		0.976		0.992		0.816		0.448	

Since an elastic problem is being solved, the results of calculating the stress-strain state components depend linearly on the load magnitude and initial stiffness D_0 . Therefore, in the calculation, these quantities are assumed to be equal to unity.

The solution to equation (20) with boundary conditions (34) and the law of stiffness change (36) is found analytically for values s_0 and s_1 under consideration. Due to its cumbersome nature, this solution is not presented here. It was not possible to obtain an analytical solution for arbitrary values s_0 and s_1 .

The results from the obtained analytical solution were then compared to the results of the finite element calculation. In the basic calculation, the beam was divided into five finite elements. To study the effect of the number of finite elements on the accuracy of the results, a series of calculations were performed in which their number varied.

Based on the calculation results, the error value was determined in comparison with the analytical solution. To formulate conclusions regarding the required number of elements, a 5% error threshold was adopted. Conclusions regarding the feasibility of applying this approach in practical calculations were based on the assumption that the threshold accuracy was achieved with fewer than 60 elements — in this case, the finite element length was 50 mm. Using a finer granularity is impractical for calculating beams in building structures — it significantly increases computational costs and calculation time. The maximum number of elements in the calculation examples was set to 400 (with a finite element length of 7.5 mm). With a larger number of finite elements, the solver implemented by the author began to accumulate computational errors.

Example 1. Solution to the problem of bending of a clamped beam loaded at the center with a concentrated force. A sketch of the calculation scheme is shown in Figure 4 *a*. The stiffness distribution is adopted according to option 1: $s_0 = 0.001$ and $s_1 = 1$. The graph of the stiffness function for this option is shown in Figure 5 *a*. Figures 6 and 7 show the results of calculating the deflections and bending moments, as well as the calculation error.

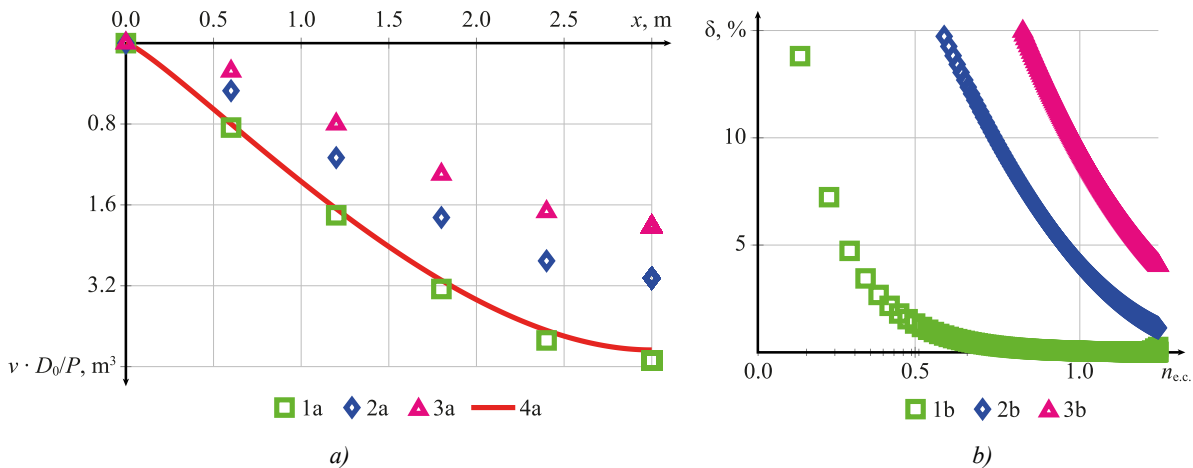


Fig. 6. Results of deflection calculations for the example: *a* — calculation results of deflection v depending on x ; *b* — calculation error depending on the number of finite elements. 1 *a*, 1 *b* — linear approximation and exact stiffness matrix (27); 2 *a*, 2 *b* — linear approximation and approximate stiffness matrix (11); 3 *a*, 3 *b* — discrete approximation; 4 *a* — analytical calculation results

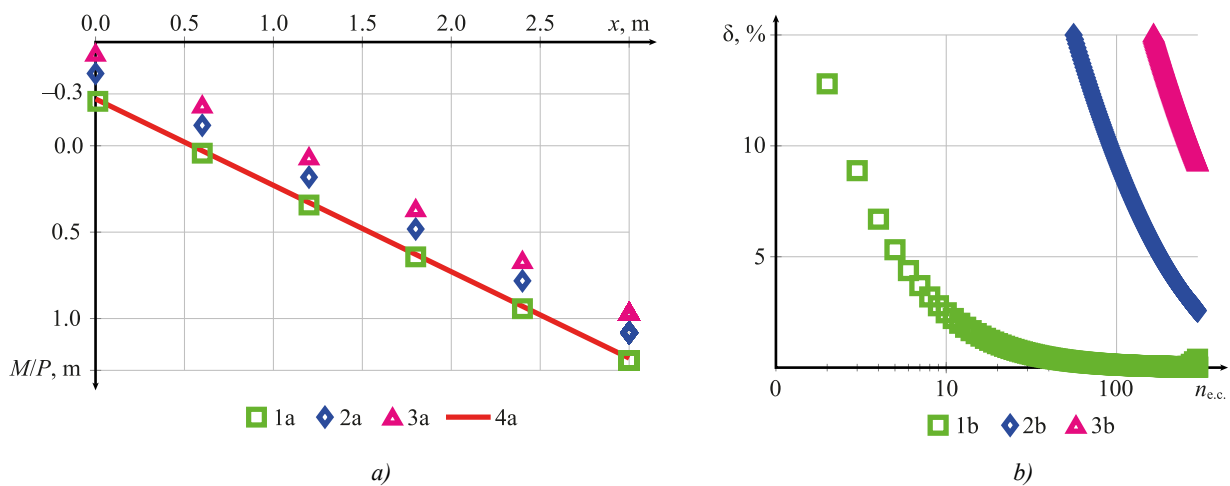


Fig. 7. Results of moment calculations for example 1: *a* — calculation results of bending moment M depending on x ; *b* — calculation error depending on the number of finite elements; 1 *a*, 1 *b* — linear approximation and exact stiffness matrix (27); 2 *a*, 2 *b* — linear approximation and approximate stiffness matrix (11); 3 *a*, 3 *b* — discrete approximation; 4 *a* — analytical calculation results

Example 2. Example 1, considered previously, represents a case close to the limit, since the stiffness at the left edge of the beam tends to zero. For a more objective assessment of the accuracy of the approaches under consideration, a similar series of calculations was performed for the case of a smooth change in stiffness. Figures 8 and 9 present the results for option 2 of the stiffness change, namely for $s_0 = 0.6$ and $s_1 = 0.2$. The graph of the stiffness function for this option is shown in Figure 5 *b*.

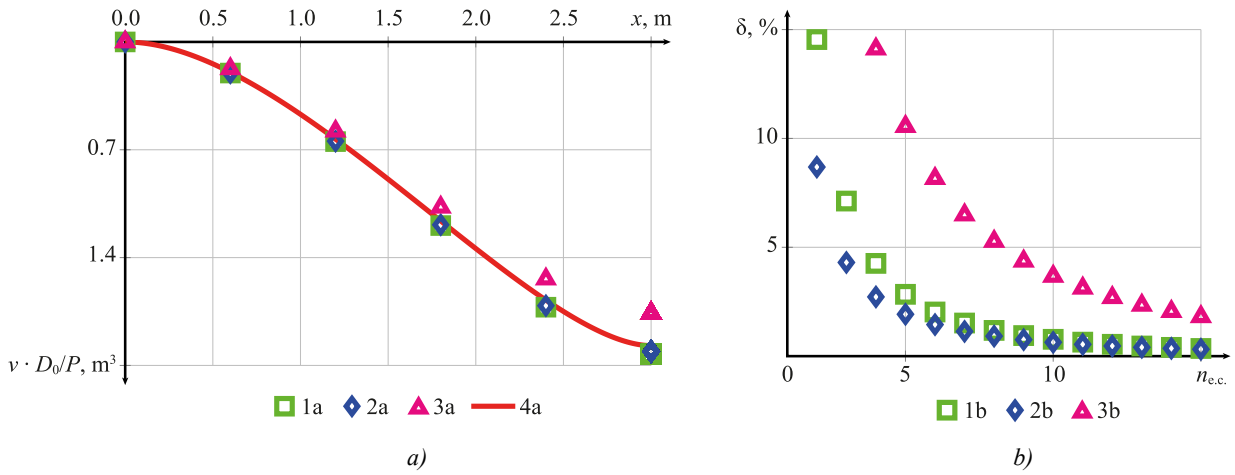


Fig. 8. Results of deflection calculations for example 2: *a* — calculation results of deflections v depending on x ; *b* — calculation error depending on the number of finite elements. 1 *a*, 1 *b* — linear approximation and exact stiffness matrix (27); 2 *a*, 2 *b* — linear approximation and approximate stiffness matrix (11); 3 *a*, 3 *b* — discrete approximation; 4 *a* — analytical calculation results

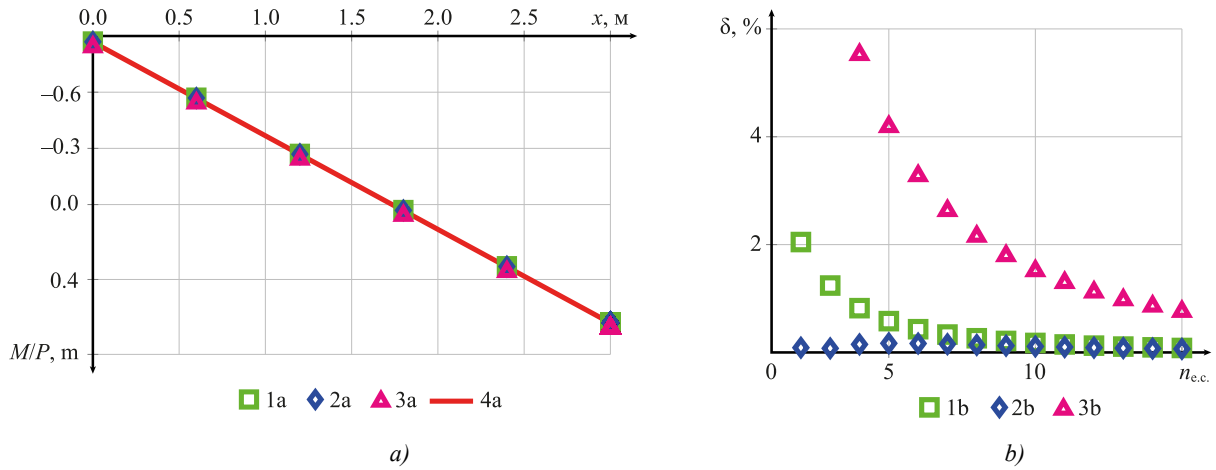


Fig. 9. Results of calculating moments for example 2: *a* — calculation results of bending moments M depending on x ; *b* — calculation error depending on the number of finite elements. 1 *a*, 1 *b* — linear approximation and exact stiffness matrix (27); 2 *a*, 2 *b* — linear approximation and approximate stiffness matrix (11); 3 *a*, 3 *b* — discrete approximation; 4 *a* — analytical calculation results

Example 3. The problem of bending of a clamped beam under a distributed load. The sketch is shown in Figure 4 *b*. The calculation results in Figures 10 and 11 were obtained for option 1 of the stiffness distribution, i.e., for $s_0 = 0.001$ and $s_1 = 1$.

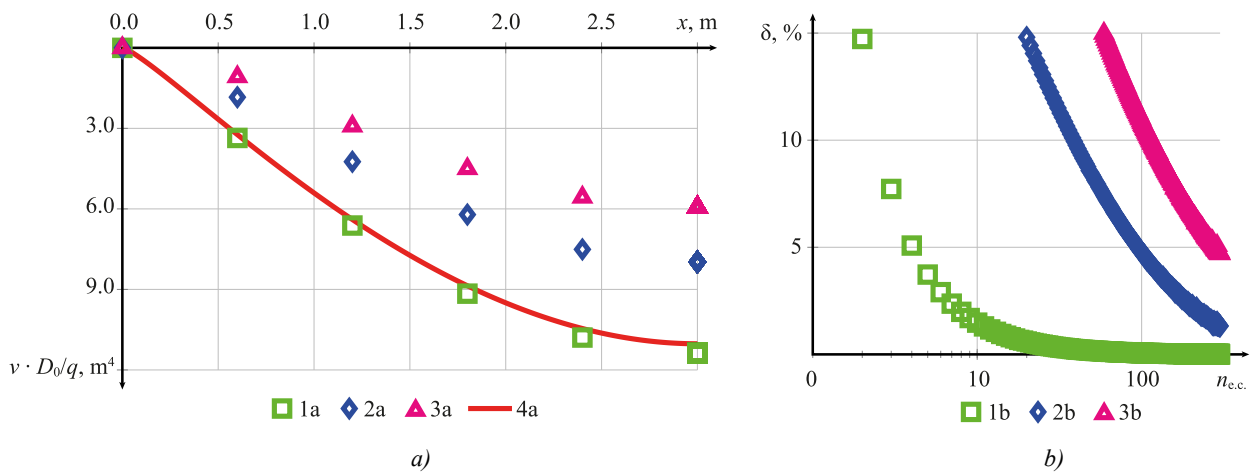


Fig. 10. Results of deflection calculations for example 3: *a* — calculation results of deflections v depending on x ; *b* — calculation error depending on the number of finite elements; 1 *a*, 1 *b* — linear approximation and exact stiffness matrix (27); 2 *a*, 2 *b* — linear approximation and approximate stiffness matrix (11); 3 *a*, 3 *b* — discrete approximation; 4 *a* — analytical calculation results

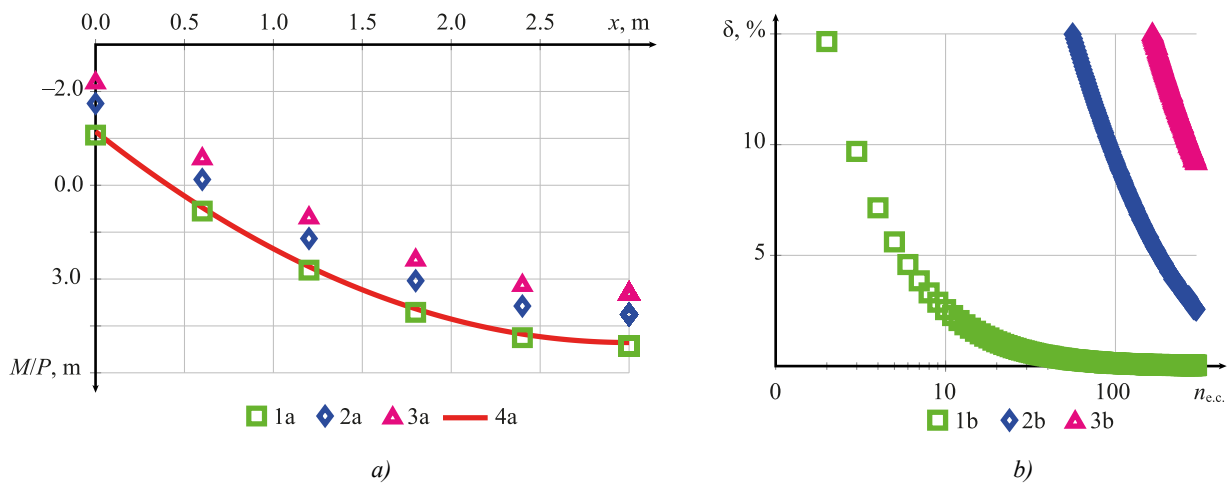


Fig. 11. Results of calculating moments for example 3: *a* — calculation results of bending moments M depending on x ; *b* — calculation error depending on the number of finite elements; 1 *a*, 1 *b* — linear approximation and exact stiffness matrix (27); 2 *a*, 2 *b* — linear approximation and approximate stiffness matrix (11); 3 *a*, 3 *b* — discrete approximation; 4 *a* — analytical calculation results

Discussion. Based on the analysis of the results shown in Figures 6 and 7, the following conclusions were formulated. In cases of significant changes in stiffness, as in Example 1, only the exact stiffness matrix (27) provided obtaining results comparable with an analytical calculation. In this case, the threshold accuracy of 5% was attained with five finite elements for displacements (Fig. 6 *b*) and with six finite elements (Fig. 7 *b*) for bending moments. Using the approximate stiffness matrix (11), similar accuracy was attained only with 90 and 180 finite elements for deflections and moments, respectively. Discrete approximation allowed us to obtain the threshold accuracy for deflections with 220 finite elements. For moments, the required accuracy for discrete approximation was not attained even with 400 elements.

The calculation results for a distributed load, shown in Figures 10 and 11 for Example 3, are similar to those shown in Figures 6 and 7 for Example 1. The key difference is that the accuracy of the results when using the approximate matrix (11) and the discrete approximation has decreased. Thus, it can be concluded that the calculation results are affected not only by the stiffness matrix — exact or approximate — but also by the vector of nodal forces from distributed loads.

Based on the calculation results for a smooth change in stiffness, shown in Figures 8 and 9 for Example 2, the following conclusions were drawn. The approximate (11) and exact (27) finite element stiffness matrices for a smooth change in beam stiffness along its length allowed for comparable results with fewer elements. For example, to attain an error of 5% when calculating deflections using the proposed matrices, no more than four finite elements were required, compared with eight for discrete approximation. Thus, even in the case of a smooth change in stiffness, a linear approximation within a finite element allowed for a two-fold reduction in the degree of discretization of the calculation model, while maintaining comparable calculation accuracy.

The results presented in Figure 8 *b* and Figure 9 *b* have a unique feature. The results obtained by the approximate stiffness matrix (11) with the same number of elements showed a smaller deviation from the analytical solution than the results obtained by the exact matrix (27). This was due to the convexity (Fig. 5) of the stiffness change function along the length. In this case, the area of the figure bounded above by the approximation was smaller than the initial. Consequently, the deflection value obtained by the linear approximation was greater (0 *a*). From the results of calculating the coefficients of the approximate (11) and exact matrix (27), shown in Figure 3, it was clear that the approximate matrix (11) had greater stiffness, which partially compensated for this effect and reduced the total error. Below is matrix $[\Delta K]$, whose coefficients were calculated from the formula where $\Delta K_{ij} = K_{ij}^{\text{приб.}} / K_{ij}^{\text{тозн.}}$ где $K_{ij}^{\text{приб.}}$ — coefficients of matrix (11); $K_{ij}^{\text{тозн.}}$ — coefficients of matrix (27). The calculations were performed for parameters $\psi_0 = 0.664$, $\psi_1 = 0.2$, $D_0 = 1.0$ and $L = 0.6$, which corresponds to the fifth finite element for option 2 of the stiffness distribution.

$$[\Delta K] = \begin{bmatrix} 1.09 & 1.08 & 1.09 & 1.11 \\ 1.08 & 1.06 & 1.08 & 1.14 \\ 1.09 & 1.08 & 1.09 & 1.11 \\ 1.11 & 1.14 & 1.11 & 1.09 \end{bmatrix}. \quad (38)$$

The average value of the coefficients of matrix (38) is 1.098. Therefore, the stiffness of finite element 5 will be approximately 10% higher if the approximate stiffness matrix is used (11).

Conclusion. This paper proposes and verifies an approach to constructing stiffness matrices for beam finite elements with linear stiffness change along their length. Both approximate (based on a variational solution to the problem) and exact (by analytical integration of a differential equation) stiffness matrices and corresponding nodal load vectors are obtained. The key advantages of the resulting matrices are the following.

1. Analytical form of approximate (11) and exact (27) stiffness matrices is presented, as well as approximate (15) and exact (29) vectors of nodal forces from distributed loads, which makes them easily implemented in existing FEM programs — both in the author's implementation in Python and in commercial packages.

2. The presented verification examples (Fig. 6–11) allow us to state that even with a relatively rough discretization (a small number of elements), the linear approximation describes adequately the stress-strain state of beams with both smooth and abrupt changes in stiffness (including modeling of zones of significant decrease in stiffness).

Linear stiffness approximation provides an optimal balance between accuracy, complexity, and computational resources, making the proposed method a practical tool for analyzing real-world structures with variable stiffness. A comparison of calculation results using an approximate and exact stiffness matrix shows that the approximate matrix allows for attaining the required accuracy with high precision and lower computational costs for beams with smoothly varying stiffness along their length. For rapid changes in stiffness along the length, as well as in extreme cases, to obtain significantly higher accuracy while maintaining the same number of elements, it is recommended to use the exact (27) stiffness matrix. Discrete approximation is only applicable in cases of smooth changes in stiffness along the length.

The resulting stiffness matrices open up possibilities for more accurate and efficient analysis of real structures, including reinforced concrete elements, taking into account physical nonlinearity — this determines the direction of further research. It is also planned to obtain a geometric stiffness matrix for solving stability problems and a mass matrix for dynamic analysis.

References

1. Chepurnenko AS, Turina VS, Akopyan VF. Optimization of Rectangular and Box Sections in Oblique Bending and Eccentric Compression. *Construction Materials and Products*. 2023;6(5):1–14. <https://doi.org/10.58224/2618-7183-2023-6-5-2>
2. Sventikov AA, Kuznetsov DN. Strength and Deformability of Steel Beams with a Step-by-Step Change in Wall Thickness. *Russian Journal of Building Construction and Architecture*. 2025;1(77):14–23. <https://doi.org/10.36622/2541-7592.2025.77.1.002>
3. Godínez-Domínguez E, Tena-Colunga A, Velázquez-Gutiérrez I, Silvestre-Pascacio R. Parametric Study of the Bending Stiffness of RC Cracked Building Beams. *Engineering Structures*. 2021;243:112695. <https://doi.org/10.1016/j.engstruct.2021.112695>
4. Abuizeh YQY, Tamov MM, Leonova AN, Mailyan DR, Nikora NI. Numerical Simulation of Nonlinear Bending Behaviour of UHPC Beams. *Construction Materials and Products*. 2025;8(4):6. <https://doi.org/10.58224/2618-7183-2025-8-4-6>
5. Jun Zhao, Yibo Jiang, Gaochuang Cai, Xiangsheng Deng, Amir Si Larbi. Flexural Stiffness of RC Beams with High-Strength Steel Bars after Exposure to Elevated Temperatures. *Structural Concrete*. 2024;25(5):3081–3102. <https://doi.org/10.1002/suco.202300934>
6. Imamović D, Skrinar M. Static Bending Analysis of a Transversely Cracked Strip Tapered Footing on a Two-Parameter Soil Using a New Beam Finite Element. *Continuum Mechanics and Thermodynamics*. 2024;36:571–584. <https://doi.org/10.1007/s00161-024-01283-7>
7. Volkov AV, Golubkin KS. Analysis of Shear Stress Distribution in a Rod with Tapered Cross-Section in Gradient Elasticity Theory. *Mechanics of Composite Materials and Structures*. 2025;31(1):40–56. <https://doi.org/10.33113/mkmk.ras.2025.31.01.04>
8. Rao Hota VS Ganga, Spyarakos CC. Closed Form Series Solutions of Boundary Value Problems with Variable Properties. *Computers & Structures*. 1986;23(2):211–215. [https://doi.org/10.1016/0045-7949\(86\)90213-0](https://doi.org/10.1016/0045-7949(86)90213-0)
9. Banerjee JR, Williams FW. Exact Bernoulli–Euler Static Stiffness Matrix for a Range of Tapered Beams. *International Journal for Numerical Methods in Engineering*. 1986;23(9):1707–1719. <https://doi.org/10.1002/nme.1620230904>
10. Yagofarov AKh. Calculation of a Two-Span Uncut Beam of Variable Rigidity with Equal Spans. *News of Higher Educational Institutions. Construction*. 2021;(754(10)):55–65. <https://doi.org/10.32683/0536-1052-2021-754-10-55-65>

11. Karamysheva AA, Yazyeva SB, Chepurnenko AS. Calculation of Plane Bending Stability of Beams with Variable Stiffness. *Bulletin of Higher Educational Institutions. North Caucasus region. Technical Sciences*. 2016;(186(1)):95–98. <https://doi.org/10.17213/0321-2653-2016-1-95-98>
12. Just DJ. Plane Frameworks of Tapering Box and I-Section. *Journal of the Structural Division*. 1977;103(1):71–86. <https://doi.org/10.1061/jsdeag.0004549>
13. Brown CJ. Approximate Stiffness Matrix for Tapered Beams. *Journal of Structural Engineering (ASCE)*. 1984;110(12):3050–3055. [https://doi.org/10.1061/\(ASCE\)0733-9445\(1984\)110:12\(3050\)](https://doi.org/10.1061/(ASCE)0733-9445(1984)110:12(3050))
14. Cherednichenko AP, Potelzheko EA, Tyufanov VA. Methods for Calculating Beams with Variable Stiffness. In: *Proc. International Student Construction Forum-2017*. Vol. 1. Belgorod: Belgorod State Technological University named after V.G. Shukhov; 2017. P. 249–252.
15. Ziou H, Guenfold M. Simple Incremental Approach for Analysing Optimal Non-Prismatic Functionally Graded Beams. *Advances in Civil and Architectural Engineering*. 2023;14(26):118–137. <https://doi.org/10.13167/2023.26.8>
16. Bui Thi Thu Hoai, Le Cong Ich, Nguyen Dinh Kien. Size-Dependent Nonlinear Bending of Tapered Cantilever Microbeam Based on Modified Couple Stress Theory. *Vietnam Journal of Science and Technology*. 2024;62(6):1196–1209. <https://doi.org/10.15625/2525-2518/19281>
17. Haskul M, Kisa M. Free Vibration of the Double Tapered Cracked Beam. *Inverse Problems in Science and Engineering*. 2021;29(11):1537–1564. <https://doi.org/10.1080/17415977.2020.1870971>
18. Hosseini N, Attarnejad R. A Novel Finite Element for the Vibration Analysis of Tapered Laminated Plates. *Polymer Composites*. 2024;45(10):8732–8743. <https://doi.org/10.1002/pc.28372>
19. Nesterov VA. Stiffness Matrix of the Tridimensional Beam Finite Element with Low Transverse Shear Stiffness. *Siberian Aerospace Journal*. 2010;29(3):71–75.
20. Gaidzhurov PP, Saveleva NA. Application of the Double Approximation Method for Constructing Stiffness Matrices of Volumetric Finite Elements. *Advanced Engineering Research (Rostov-on-Don)*. 2023;23(4):365–375. <https://doi.org/10.23947/2687-1653-2023-23-4-365-375>
21. Zeinali Y, Jamali M, Musciani S. General Form of the Stiffness Matrix of a Tapered Beam-column. *International Journal of Mining, Metallurgy & Mechanical Engineering (IJMMME)*. 2013;1(3):149–153.
22. Peng He, Zhansheng Liu, Chun Li. An Improved Beam Element for Beams with Variable Axial Parameters. *Shock and Vibration*. 2013;20(4):601–617. <https://doi.org/10.3233/SAV-130771>
23. Ceba AI. Stiffness Matrix for Bars with Variable Section or Inertia. *International Journal of Materials Science and Applications*. 2025;14(1):13–28. <https://doi.org/10.11648/j.ijmsa.20251401.12>
24. Rezaiee-Pajand M, Masoodi AR, Bambaeechee MT. Tapered Beam–Column Analysis by Analytical Solution. *Proceedings of the Institution of Civil Engineers — Structures and Buildings*. 2019;172(11):789–804. <https://doi.org/10.1680/jstbu.18.00062>
25. Li Xia Meng, Nian Li Lu, Shi Ming Liu. Exact Expression of Element Stiffness Matrix for a Tapered Beam and Its Application in Stability Analysis. *Advanced Materials Research*. 2011;255–260:1968–1973. <https://doi.org/10.4028/www.scientific.net/AMR.255-260.1968>
26. Fedorinin NI, Solomonov KN, Tishchuk LI. Universal Equation of Elastic Line of a Beam of Linear Rigidity. *News of Tula State University. Technical Sciences*. 2022;(9):517–521. <https://doi.org/10.24412/2071-6168-2022-9-517-521>
27. Ksenofontova TK, Mareeva OV, Verkhoglyadova AS. Calculation of Monolithic Buildings Structures Taking into Account the Nonlinear Operation of Reinforced Concrete. *Construction Materials and Products*. 2024;7(1):1–8. <https://doi.org/10.58224/2618-7183-2024-7-1-4>
28. Deryugin EE. Simplified Calculation of the Inertia Moment of the Cross Section of the Console under Loading. *Advanced Engineering Research (Rostov-on-Don)*. 2024;24(2):159–169. <https://doi.org/10.23947/2687-1653-2024-24-2-159-169>

About the Author:

Nikita Yu. Tsybin, Cand.Sci. (Eng.), Associate Professor of the Department of Strength of Materials, Moscow State University of Civil Engineering (National Research University) (26, Yaroslavskoye Shosse, Moscow, 129337, Russian Federation), [SPIN-code](#), [ORCID](#), [ResearchGate](#), [ScopusID](#), [ResearcherID](#), science@nikitatsybin.ru

Conflict of Interest Statement: the author declares no conflict of interest.

The author has read and approved the final version of manuscript.

Об авторе:

Никита Юрьевич Цыбин, кандидат технических наук, доцент кафедры «Сопротивление материалов» Национального исследовательского Московского государственного строительного университета (129337, Российская Федерация, г. Москва, Ярославское шоссе, дом 26), [SPIN-код](#), [ORCID](#), [ResearchGate](#), [ScopusID](#), [ResearcherID](#), science@nikitasybin.ru

Конфликт интересов: автор заявляет об отсутствии конфликта интересов.

Автор прочитал и одобрил окончательный вариант рукописи.

Received / Поступила в редакцию 02.09.2025

Reviewed / Поступила после рецензирования 22.09.2025

Accepted / Принята к публикации 06.10.2025

MECHANICS МЕХАНИКА



UDC 539.3

Original Theoretical Research

<https://doi.org/10.23947/2687-1653-2025-25-4-2218>

Iterative Model of Elastic Deformation of a Particle Conglomerate Taking into Account the Compressibility of the Medium during Pressing

Ivan K. Andrianov , Sergey N. Ivanov , Elena K. Chepuranova

Komsomolsk-na-Amure State University, Komsomolsk-on-Amur, Russian Federation

✉ ivan_andrianov_90@mail.ru

EDN: XHHEDX

Abstract

Introduction. Briquetting and pressing of wood and other powdered materials are becoming key processes in the circular economy and recycling of wood processing waste. Accurate calculation of compaction pressure is essential for equipment selection and optimization, making the task of modeling the deformation of conglomerates both practical and economically significant. The literature addresses the mechanics of powder media, porous materials, and the modeling of elastic-plastic deformations of granular conglomerates. However, most models assume fixed mechanical characteristics or approximations that do not account for the dependence of strength and elastic properties on changing density under compression. This leaves a gap in theoretical and applied approaches to adequately calculating pressure for materials with variable density. Therefore, the objective of this work is to develop an approach for calculating the compaction pressure of a particle conglomerate as a function of the degree of elastic compression, taking into account changes in the mechanical characteristics of the medium.

Materials and Methods. In the mathematical description of the research problem, the provisions of the theory of elasticity were used. Based on the principle of superposition, the process of medium deformation was divided into a number of stages, within which the particle conglomerate received a small increment in height, and the mechanical characteristics assumed a constant value. The proposed approach for determining the compaction pressure was based on the solution to a series of inverse elastic problems in which the displacement of the upper boundary of a conglomerate of rectangular particles was specified, and the normal stress that caused this increment was sought. To account for changes in the density of the medium during deformation, the method of sequential loads was used, within each of them, the density was taken to be constant and was determined depending on the magnitude of the total compressive deformation. The Hencky strain, which has the property of additivity, was used as a measure of deformation.

Results. As part of the study, an iterative model was constructed for calculating the compaction pressure of a particle conglomerate when the mechanical characteristics change depending on the degree of elastic compression. Series of test calculations were conducted using a conglomerate of wood particles, whose Young's modulus is described by a power-law density function. At each stage of deformation, the elastic constants of the material were assumed to be constant, depending on the density of the medium. Using the equilibrium equation and the superposition principle, based on the results of solving elastic deformation problems, the compaction pressure was calculated at each loading stage, and the dependence of the compaction pressure on the magnitude of the compressive deformation and the degree of compaction was constructed.

Discussion. The obtained results of deformation of the medium taking into account the change in mechanical characteristics depending on the degree of compression showed a clearly expressed nonlinearity of the curve of dependence of the compaction pressure on the compression deformation — with an increase in pressure, both the degree of compaction of the medium and the compression deformation increase. A comparative analysis of calculations using the example of a conglomerate of wood particles under the condition of a constant density of the medium and taking into account the change in density during the deformation process revealed a significant error in estimating the compaction pressure when averaging the density or when using constant density values corresponding to the initial (undeformed) or final state.

Conclusion. The constructed iterative model allows for calculating the compaction pressure of a particle conglomerate, taking into account changes in mechanical properties under elastic compression. The proposed approach accounts for the nonlinearity of the compaction pressure dependence on the degree of compaction of the medium and can be applied to briquetting processes for wood waste.

Keywords: pressing, compressibility, density, particle conglomerate, sequential loading, stress-strain state

Acknowledgements. The authors would like to thank the Editorial board of the Journal and the reviewer for their professional analysis of the article and recommendations for its correction.

Funding Information. The research is done with the financial support from the Russian Science Foundation (grant no. 24-29-00089), <https://rscf.ru/project/24-29-00089/>

For Citation. Andrianov IK, Ivanov SN, Chepurnova EK. Iterative Model of Elastic Deformation of a Particle Conglomerate Taking into Account the Compressibility of the Medium during Pressing. *Advanced Engineering Research (Rostov-on-Don)*. 2025;25(4):290–299. <https://doi.org/10.23947/2687-1653-2025-25-4-2218>

Оригинальное теоретическое исследование

Итерационная модель упругого деформирования конгломерата частиц с учетом сжимаемости среды в процессе прессования

И.К. Андрианов , С.Н. Иванов , Е.К. Чепурнова 

Комсомольский-на-Амуре государственный университет, г. Комсомольск-на-Амуре, Российская Федерация

✉ ivan_andrianov_90@mail.ru

Аннотация

Введение. Процессы брикетирования и прессования древесных и других порошкообразных материалов становятся ключевыми в круговой экономике и утилизации отходов деревообработки. Точный расчет давления прессования необходим для выбора оборудования и оптимизации режимов, что делает задачу моделирования деформирования конгломератов практически и экономически значимой. В литературе рассматриваются механика порошковых сред, пористых материалов и моделирование упругопластических деформаций гранулярных конгломератов; однако большинство моделей предполагает фиксированные механические характеристики или аппроксимации, не учитывающие зависимость прочности и упругих свойств от изменяющейся плотности при сжатии. Это оставляет пробел в теоретических и прикладных подходах к адекватному расчету давления для материалов с переменной плотностью. Поэтому целью данной работы является разработка подхода для расчета давления прессования конгломерата частиц как функцию степени упругого сжатия с учетом изменения механических характеристик среды.

Материалы и методы. При математическом описании исследуемой задачи использовались положения теории упругости. На основании принципа суперпозиции процесс деформирования среды разбивался на несколько этапов, в каждом из которых среда получала малое приращение по высоте, а механические характеристики оставались постоянными. Предложенный метод определения давления прессования опирался на решение серии обратных упругих задач, в которых задавалось перемещение верхней границы конгломерата прямоугольных частиц и искалось нормальное напряжение, вызвавшее это приращение. Для учёта изменения плотности среды в процессе деформирования применялся метод последовательных нагружений — в пределах каждого из них плотность принималась постоянной и определялась в зависимости от величины суммарной деформации сжатия. В качестве меры деформации использовалась деформация Генки, обладающая свойством аддитивности.

Результаты исследования. В рамках исследования построена итерационная модель расчёта давления прессования конгломерата частиц при изменении механических характеристик в зависимости от степени упругого сжатия. Проведены серии тестовых расчётов на примере конгломерата древесных частиц, у которых модуль Юнга описывается степенной функцией плотности. На каждом этапе деформирования упругие константы материала принимались постоянными в зависимости от плотности среды. С использованием уравнения равновесия и принципа суперпозиции по результатам решения задач упругого деформирования было вычислено давление прессования на каждом этапе нагружения, а также построена зависимость давления прессования от величины деформации сжатия и степени уплотнения.

Обсуждение. Полученные результаты деформирования среды с учётом изменения механических характеристик в зависимости от степени сжатия показали явно выраженную нелинейность кривой зависимости давления прессования от деформации сжатия — при возрастании давления увеличиваются как степень уплотнения среды, так и деформация сжатия. Сравнительный анализ расчётов на примере конгломерата древесных частиц при условии постоянной плотности среды и с учётом изменения плотности в процессе деформирования выявил значительную погрешность оценки давления прессования при усреднении плотности либо при использовании постоянных значений плотности, соответствующих начальному (недеформированному) или конечному состоянию.

Заключение. Построенная итерационная модель позволяет рассчитать давление прессования конгломерата частиц с учётом изменения механических характеристик при упругом сжатии. Предложенный подход учитывает нелинейность зависимости давления прессования от степени уплотнения среды и может быть применён в процессах брикетирования отходов деревообработки.

Ключевые слова: прессование, сжимаемость, плотность, конгломерат частиц, последовательное нагружение, напряженно-деформированное состояние

Благодарности. Авторы выражают благодарность редакционной коллегии журнала и рецензенту за профессиональный анализ статьи и рекомендации для ее корректировки.

Финансирование. Исследование выполнено за счет гранта Российского научного фонда № 24-29-00089 <https://rscf.ru/project/24-29-00089/>

Для цитирования. Андрианов И.К., Иванов С.Н., Чепурнова Е.К. Итерационная модель упругого деформирования конгломерата частиц с учетом сжимаемости среды в процессе прессования. *Advanced Engineering Research (Rostov-on-Don)*. 2025;25(4):290–299. <https://doi.org/10.23947/2687-1653-2025-25-4-2218>

Introduction. Materials with density-dependent mechanical properties are found in various industrial applications. These include granular media, wood particle aggregates, composite materials, and others. The behavior of such materials can differ significantly from the classic case, where properties remain constant and are independent of density. Some issues related to assessing the strength and stiffness of granular media are discussed in [1], and for sand molds — in [2].

Currently, briquetting processes of wood particle conglomerates are widely used in the woodworking waste [3]. Therefore, it is important to describe the behavior of particles during the compacting process. The issues of assessing the compaction pressure were discussed in [4]; mechanical and thermal analysis of the characteristics of pressed blocks with wood inclusions — in [5]; assessment of the strength of wood conglomerate — in [6]. Wood sawdust is widely used in the production of building materials, processing into fuel, and briquetting. The pressing process is affected by various factors [7]: for example, storage humidity is described in [8], and the effect of temperature is specified in [9]. In addition, wood particles are used in composite materials, in particular in the production of biocomposites [10], polymeric materials [11], and multilayer composites [12].

One of the key tasks in particle deformation modeling is the selection of pressing equipment. Paper [13] is devoted to the selection of pressing machines for producing solid biofuel through granulating, briquetting, and mechanically processing biomass. When applying the conglomerate pressing procedure, it is important to model the stress-strain state during the compression process, taking into account the compaction of the medium. A change in density entails a change in the mechanical properties of the medium, which affects the accuracy of calculating the required deforming force and the selection of equipment. The development of more accurate methods for calculating compaction pressure, taking into account the compressibility of the medium, is important for creating new, efficient technologies and improving existing ones. Some aspects of the mathematical description of an elastic-plastic problem under compression for the case of constant mechanical properties are discussed in [14].

An analysis of the current state of the art shows that not all software packages are capable of accounting for changes in density and mechanical properties under deformation. Most CAE systems perform engineering calculations with given constant values of physical and mechanical properties. Therefore, the development of effective models and methods for assessing the stress-strain state of media under pressing, taking into account compressibility and changes in characteristics, is a challenge.

The objective of this study is to develop an approach for calculating the compaction pressure required to compress a particle conglomerate to a given geometry, taking into account the effect of the compaction degree on the mechanical properties of the medium. In accordance with this objective, the following tasks are set:

- to conduct a mathematical formulation of the elastic compression problem for a particle conglomerate, taking into account the compressibility of the medium;
- to build an iterative model for calculating the stress-strain state of the medium based on solving a series of inverse problems using sequential loading;

- to perform test calculations of the stress-strain state of a particle conglomerate and plot the dependence of compaction pressure on the compressive strain of the medium;
- to estimate the error in calculating compaction pressure when ignoring changes in the density of the medium during deformation.

Research Methods. We construct a calculation method for the process of deformation of a particle conglomerate taking into account the compressibility of the medium under the following assumptions:

- since the study examines the compression of the medium, the condition of continuity is assumed, meaning the particle conglomerate uniformly fills the volume under consideration;
- the mass of the medium remains constant throughout the entire pressing process;
- the compression process of the medium is considered within the limits of elastic deformation;
- the principle of superposition is observed — independently accumulated deformations at each loading stage;
- pressing is performed in an absolutely rigid matrix using an absolutely rigid friction-free punch; the layers move uniformly along the height, eliminating shear;
- the viscosity of the medium is neglected, and the pressing temperature remains constant;
- the variable mechanical characteristics dependent on the density of the medium are Young's modulus and Poisson's ratio;
- the density of the medium is a function of the compressive strain.

The geometric model of a particle conglomerate (Fig. 1) has the shape of a parallelepiped with height h and a constant square base with area S . Due to the rectangular shape of the particle conglomerate, the model is considered in a Cartesian coordinate system, where axis $0x_3$ is directed along the height of the parallelepiped, and axes $0x_1$ and $0x_2$ lie in the plane of the parallelepiped base.

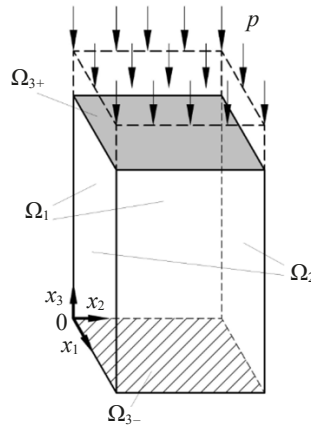


Fig. 1. Scheme of deformation of a particle conglomerate

Since the axial compressive strain increases in absolute value during compacting under pressure p , the density of the medium and, consequently, its elastic constants change. Accordingly, Young's modulus E and Poisson's ratio μ are functions of density ρ : $E = E(\rho)$, $\mu = \mu(\rho)$. We use the Hencky strain as a measure of deformation.

We divide the entire process of medium deformation into a series of loading stages, within each of which a kinematic condition in the form of a small increment of the upper boundary of the medium $\Delta h = \Delta h^*$ in height is specified. At each loading stage, we assume that the density of the medium remains constant and the mechanical properties — Young's modulus and Poisson's ratio — do not change. At subsequent loading stages, the density of the medium and the mechanical properties also remain constant within each stage, but change depending on the magnitude of the total deformation over all previous loading stages.

We consider the solution to the inverse problem, taking the pressure increment at each loading stage Δp as the unknown value. Then, the mathematical formulation of the research problem in accordance with the accepted assumptions will include the following system of equations:

- static equations:

$$\partial \Delta \sigma_{11} / \partial x_1 = 0, \quad \partial \Delta \sigma_{22} / \partial x_2 = 0, \quad \partial \Delta \sigma_{33} / \partial x_3 = 0, \quad (1)$$

- physical equations:

$$\Delta e_{11} = \frac{1}{E(\rho)} \Delta \sigma_{11} - \frac{\mu(\rho)}{E(\rho)} (\Delta \sigma_{22} + \Delta \sigma_{33}), \quad (2)$$

$$\Delta e_{22} = \frac{1}{E(\rho)} \Delta \sigma_{22} - \frac{\mu(\rho)}{E(\rho)} (\Delta \sigma_{33} + \Delta \sigma_{11}), \quad (3)$$

$$\Delta e_{33} = \frac{1}{E(\rho)} \Delta \sigma_{33} - \frac{\mu(\rho)}{E(\rho)} (\Delta \sigma_{11} + \Delta \sigma_{22}), \quad (4)$$

– geometric relationships:

$$\Delta e_{11} = \Delta e_{22} = 0, \quad \Delta e_{33} = \ln(1 + \Delta h / h), \quad (5)$$

– boundary conditions:

$$\begin{aligned} u_1|_{\Omega_1, \Omega_2} = u_2|_{\Omega_1, \Omega_2} &= 0, \\ u_1|_{\Omega_{3-}} = u_2|_{\Omega_{3-}} = u_3|_{\Omega_{3-}} &= 0, \\ u_3|_{\Omega_{3+}} &= -\Delta h, \\ \Delta \sigma_{33}|_{\Omega_{3+}} &= -\Delta p. \end{aligned} \quad (6)$$

where $\Delta \sigma_{11}$, $\Delta \sigma_{22}$, $\Delta \sigma_{33}$ — stress increments; Δe_{11} , Δe_{22} , Δe_{33} — increment of elastic deformations; $u_i, i = \overline{1, 3}$ — displacement components.

Based on differential equations (1) and condition (6), we arrive at the relations: $\Delta \sigma_{11} = \text{const}$; $\Delta \sigma_{22} = \text{const}$; $\Delta \sigma_{33} = -\Delta p$.

Considering that there are no displacements in the plane $0x_1x_2$, according to relations (3), (5), the system of equations (2), (3) can be written as:

$$\Delta \sigma_{11} = \Delta \sigma_{22} = -\frac{\mu(\rho)}{1 - \mu(\rho)} \Delta p. \quad (7)$$

Substituting relations (5) and (7) into equation (4), we express the pressure increment in the following form:

$$\Delta p = -\frac{E(\rho)(1 - \mu(\rho))}{(1 + \mu(\rho))(1 - 2\mu(\rho))} \ln\left(1 + \frac{\Delta h}{h}\right).$$

Thus, when constructing the calculation algorithm, we specify a discrete change in the height of the conglomerate depending on the loading stage:

$$h = \{h^{(0)} = h_0, \dots, h^{(j)} = h_0 - j\Delta h, j = \overline{1, n}, \dots, h^{(n)} = h_{\text{end}}\},$$

where h_0 — initial height corresponding to the undeformed state of the conglomerate; h_{end} — final height of the conglomerate after all stages of loading; j — loading stage.

Since the change in the height of the conglomerate is known, it is possible to determine the increment of deformation in height within each loading stage:

$$\Delta e_{33}^{(j)} = \ln\left(\frac{h^{(j)}}{h^{(j-1)}}\right), \quad j = \overline{1, n}.$$

The total deformation at the current stage of loading is determined according to the superposition principle:

$$e_{33}^{(j)} = \sum_{i=1}^j \Delta e_{33}^{(i)}.$$

It should be noted that the selection of the Hencky strain as a measure of deformation is due to its additivity, unlike relative strain, which allows for the summation of deformations at individual loading stages. Moreover, the Hencky strain allows for calculations at large deformations.

Considering that the mass of the conglomerate and the base area remain constant: $m = \text{const}$, $S = \text{const}$, we proceed to the continuity condition in the form: $\rho_0 h_0 = \rho h$, from which the density of the medium is determined depending on the magnitude of the compressive strain $\Delta e_{33}^{(j)}$ at a given loading stage according to the relationship:

$$\rho^{(j)} = \rho^{(j-1)} / \exp \Delta e_{33}^{(j)}.$$

Knowing the density of the medium at the current stage of loading, Young's modulus and Poisson's ratio at each stage of loading are determined in accordance with the degree of compaction by a certain function:

$$E^{(j)} = E(\rho)|_{\rho=\rho^{(j)}}, \quad \mu^{(j)} = \mu(\rho)|_{\rho=\rho^{(j)}}.$$

Then the increase in compaction pressure is determined as:

$$\Delta p^{(j)} = - \frac{E(\rho^{(j)})(1 - \mu(\rho^{(j)}))}{(1 + \mu(\rho^{(j)}))(1 - 2\mu(\rho^{(j)}))} \ln \left(\frac{h^{(j)}}{h^{(j-1)}} \right).$$

According to the principle of superposition, the components of the stress tensor at the current stage of loading are determined as:

$$\sigma_{11}^{(j)} = \sum_{i=1}^j \Delta \sigma_{11}^{(i)}, \quad \sigma_{22}^{(j)} = \sum_{i=1}^j \Delta \sigma_{22}^{(i)}, \quad \sigma_{33}^{(j)} = \sum_{i=1}^j \Delta \sigma_{33}^{(i)},$$

where the voltage increments at each stage are determined by the dependences:

$$\Delta \sigma_{11}^{(j)} = \Delta \sigma_{22}^{(j)} = - \frac{E(\rho^{(j)})\mu(\rho^{(j)})}{(1 + \mu(\rho^{(j)}))(1 - 2\mu(\rho^{(j)}))} \ln \left(\frac{h^{(j)}}{h^{(j-1)}} \right), \quad \Delta \sigma_{33}^{(j)} = \Delta p^{(j)}.$$

Thus, the process of compacting a particle conglomerate is represented by a series of loading stages, within each of which the medium density and elastic constants are assumed constant. At each stage, an inverse elastic problem of medium compression is solved. The input data for this problem are the density, Young's modulus, and Poisson's ratio, whose values are determined by the total compressive strain accumulated during the previous and current loading stages. This results in a sequence of inverse problems based on data on the change in the height of the particle conglomerate, which is used to calculate the change in compaction pressure depending on the degree of compaction of the medium.

Research Results. Based on the developed approach, a series of calculations are performed for the deformation of a particle conglomerate using sawdust as an example. Young's modulus (MPa) is described by the density function (g/cm^3): $E(\rho) = a\rho^b$, $a = 6500$, $b = 3.5$ [15]. The selection of a power-law dependence is due to the fact that it describes the behavior of a conglomerate of wood particles quite well, according to [15]. Poisson's ratio $\mu = 0.32$ takes a constant value, since it is less sensitive to changes in the density of the conglomerate, as noted in [16]. Moreover, according to experimental studies [17, 18], the greatest change in Poisson's ratio occurs at low values of compression, and at pressure values above 20 MPa, Poisson's ratio asymptotically approaches a constant value. The initial density of the conglomerate of wood particles in the undeformed state is taken to be: $\rho_0 = 0.2 \text{ g/cm}^3$. Ten loading stages were selected for the test calculation. At each stage, the upper boundary of the conglomerate was displaced by value $\Delta h = 10 \text{ mm}$, resulting in a discrete change in the height of the conglomerate: $h = \{200, 190, \dots, 110\} \text{ mm}$. At the final loading stage, at $h = 110 \text{ mm}$, the maximum compaction pressure was 112 MPa, and the density of the medium — 0.4 g/cm^3 .

Based on the results of the calculations, the dependence of compaction pressure on changes in compression strains (Fig. 2) and on changes in the density of the conglomerate of wood particles (Fig. 3) was plotted. For the comparative analysis, a series of calculations were also performed at a constant density and a constant Young's modulus for two extreme cases: with $\rho = \rho_0 = \text{const}$ and with $\rho = \rho_{\text{end}} = \rho|_{h=100 \text{ mm}} = \text{const}$, that is, when the density of the medium corresponds to the initial undeformed state and the final deformed state at the last stage of loading; and also for the case of averaging the density of the medium: with $\rho = (\rho_0 + \rho_{\text{end}}) / 2 = \text{const}$. The results of calculations at constant values of density and elastic constants are presented in Figure 2.

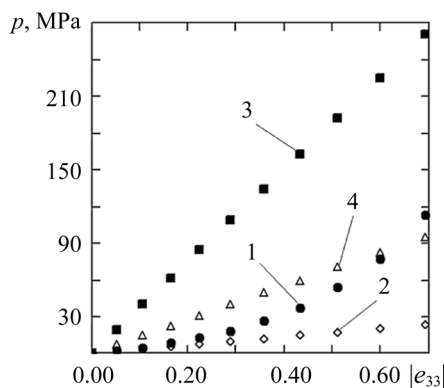


Fig. 2. Dependence of compaction pressure on compressive strain:

1 — at $\rho = \rho(e)$; 2 — at $\rho = \rho_0$;
3 — at $\rho = \rho_{\text{end}}$; 4 — at $\rho = (\rho_0 + \rho_{\text{end}}) / 2$

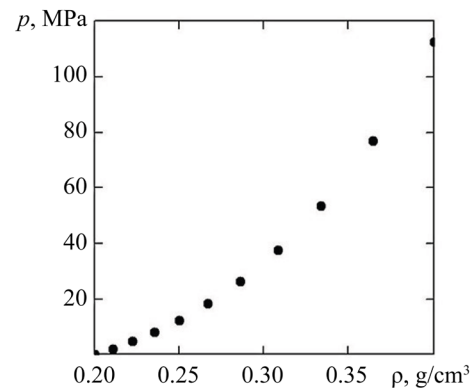


Fig. 3. Dependence of compaction pressure on the density of the medium

According to the results of solving the inverse problem of elastic compression, for the first stage of loading with a given displacement of the upper boundary of the medium $h^{(1)} = 10$ mm, the increments of deformations, stresses and the required pressure were: $\Delta e_{33}^{(1)} = -0.051$, $\Delta \sigma_{33}^{(1)} = \Delta p^{(1)} = 2.041$ MPa. To assess the adequacy of the constructed model, a finite element calculation of the direct loading problem was performed in the ANSYS software package at a given external pressure $\Delta p^{(1)} = 2.041$. Since the software package requires the specification of constant characteristics of the medium, the finite element calculation was performed only for the first stage of loading [19]. The calculation results of the stress-strain state under elastic compression of the medium for the first stage of loading are presented in Figure 4.

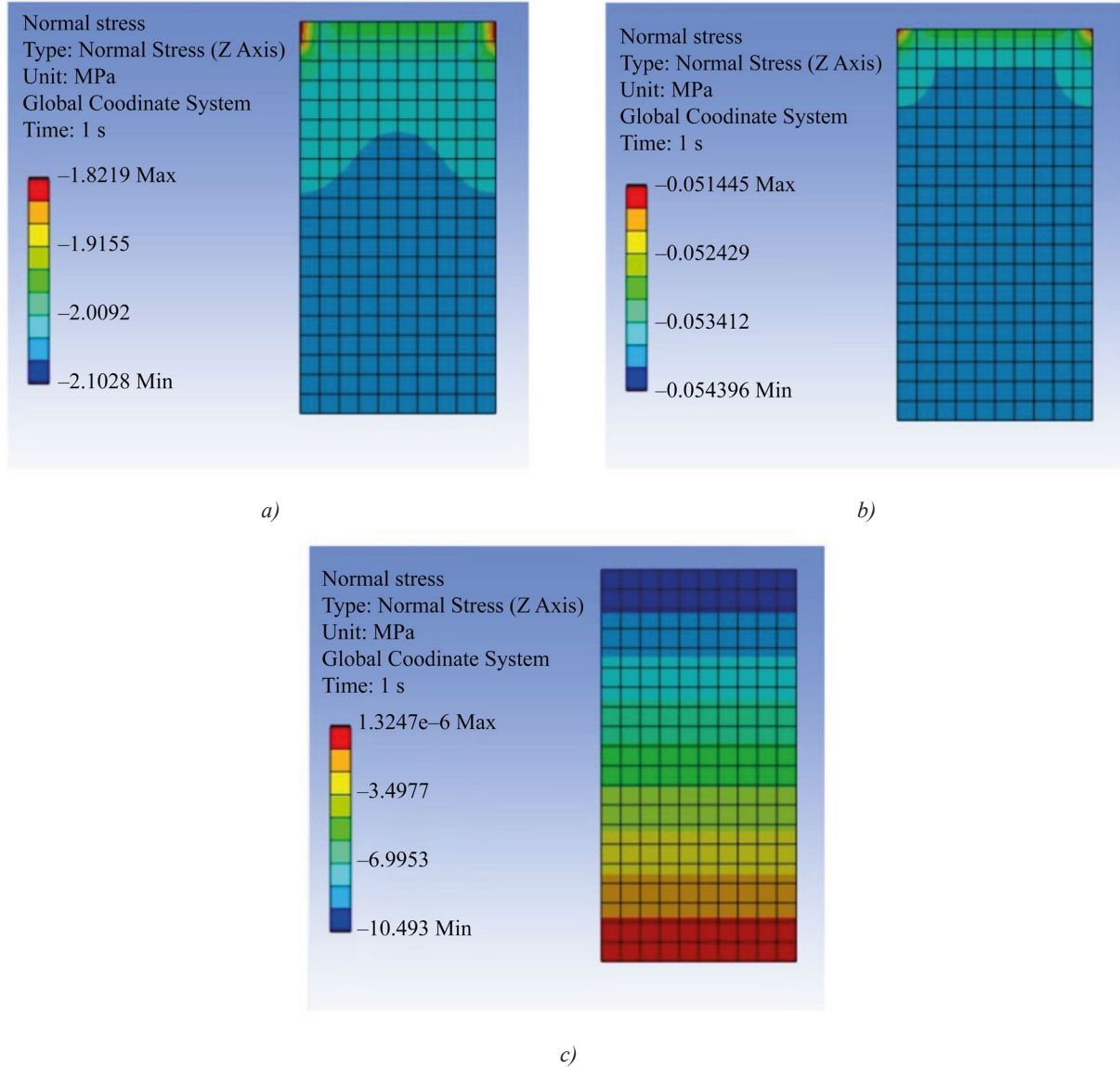


Fig. 4. Results of finite element calculation of the direct problem for the first stage of elastic compression:

a — stress distribution $\Delta \sigma_{33}^{(1)}$ MPa; *b* — strain distribution $\Delta e_{33}^{(1)}$; *c* — displacement distribution $u_3^{(1)}$ (mm)

Discussion of Results. According to the calculation results (Fig. 2 and 3), as the magnitude of the compressive strain increases, the required compaction pressure and the degree of compaction of the particle conglomerate rise. The dependence of the compaction pressure on the degree of compaction is clearly nonlinear. The dependence of the compaction pressure on the longitudinal compressive strain (Fig. 2, curve 1) is also described by a nonlinear function, whose behavior is quite adequately approximated by a third-order polynomial function. Figure 2 shows that, at a constant density of the wood particle conglomerate, the curves for the dependence of the compaction pressure on the magnitude of the compressive strain exhibit a weakly nonlinear character. Accordingly, at a fixed density of the medium, the curves for the change in compaction pressure can be approximated by linear functions.

According to the comparative analysis, the simplification of using the density value as a constant characteristic in cases where the density of the medium changes drastically during deformation can cause significant errors. In particular, when using a constant particle conglomerate density $\rho = \rho_0$, corresponding to the initial state, the error in calculating the compaction pressure increases to 80%, with the greatest error being attained at the maximum compaction pressure. For a constant density value $\rho = \rho_{\text{end}}$, corresponding to the final state of the medium, the calculation results at some loading stages differ by more than 9.4 times, and for an average density value $\rho = (\rho_0 + \rho_{\text{end}}) / 2$ — by more than 3.4 times.

According to the data in Figure 4, the results obtained by the finite element method in solving the direct problem of the first loading stage are consistent with the results obtained in solving the inverse problem, according to the approach proposed in this study. The results presented in Figure 4 clearly demonstrate that the normal stresses and strains along the height are practically the same at each point of the body, which confirms the uniformity of their distribution along the height of the conglomerate under the action of uniform pressure at the upper boundary. It should be noted that in Figure 4 *a, b* there is a gradient of stresses and strains along the longitudinal axis, which is most likely a consequence of singularity (specifically in the areas highlighted in red) — one of the shortcomings of the finite element method, when there is an incorrect distribution of stresses and strains in the area of corners, with rigid fastenings, etc.

Conclusion. Based on the research results, an iterative model was developed for calculating the compaction pressure of a particle conglomerate whose mechanical characteristics depend on the degree of compaction under elastic compression. By performing iterative calculations, increasing the number of loading stages and decreasing the incremental step of the upper boundary of the conglomerate, a discrete dependence of the compaction pressure on the degree of medium compression can be constructed, which can then be approximated by a smooth curve. A series of calculations using the example of an elastic problem of pressing a wood particle conglomerate, taking into account changes in Young's modulus and the density of the medium, has revealed a nonlinear relationship between the compaction pressure and the degree of compaction of the medium and the compressive strain during compression. According to the constructed graphical dependences, the consideration of the compressibility of the particle conglomerate affects significantly the nonlinearity of the change in pressing pressure as a function of the density of the medium during deformation. The comparative analysis has shown that the calculation of the stress-strain state of media, whose density changes significantly during compaction and affects their mechanical properties, cannot be performed at constant density values due to significant errors. This allows us to conclude that the compressibility of the medium, associated with changes in the density of the particle conglomerate during compression, affects significantly the estimation of the compaction pressure. The constructed iterative model will provide a practical estimation of the maximum compaction pressure required to ensure elastic compression of the particle conglomerate to a given geometry, taking into account the dependence of mechanical properties on the density of the medium. The proposed approach can find practical application in selecting equipment for briquetting wood particles for recycling wood waste. Further research focuses on developing mathematical models for calculating the stress-strain state and compaction pressure during the deformation of particle conglomerates using complex-geometry molds.

References

1. Nazarenko VA, Pushkarev OI, Goncharova AV. Monitoring the Quality of Grinding Materials on the Basis of Their Granular Strength. *Russian Engineering Research*. 2009;29(10):1056–1058. <https://doi.org/10.3103/S1068798X09100219>
2. Mambetaliev TS. One-Dimensional Model of the Process of Pulsed Compaction of Sand Forms. *Izvestiya VUZov Kyrgyzstana*. 2015;(7):20–23. (In Russ.)
3. Mikheevskaya MA, Burmistrova DD, Storodubtseva TN. Theoretical Study of Wood Waste Briquetting Taking into Account Nonlinear Strengthening of the Raw Materials. *Proceedings of the St. Petersburg Forestry Academy*. 2022;(240):175–185. <https://doi.org/10.21266/2079-4304.2022.240.175-185>
4. Chibirev OV, Kunitskaya OA, Grigoriev MF. Calculation of Needed Pressure for Sawdust Pressing during Briquetting. *Repair, Reconditioning, Modernization*. 2019;(2):22–25. <https://doi.org/10.31044/1684-2561-2019-0-2-22-25>
5. Bouzouidja R, Tingting Vogt Wu, Sbartaï M. Mechanical and Thermal Analysis of Performance of Compressed Earth Blocks with Sawdust Material Stabilized with Cement. In book: Amziane S, Merta I, Page J (eds). *Bio-Based Building Materials*. Cham: Springer; 2023. P. 324–332. https://doi.org/10.1007/978-3-031-33465-8_26
6. Rudenko BD, Kulak VV. Description of the Strength of a Cement-Wood Conglomerate Made of Cavitated Wood Particles. *Trends in the Development of Science and Education*. 2019;57(1):30–33. (In Russ.) <https://doi.org/10.18411/jj-12-2019-08>
7. Bereziuk O, Petrov O, Vishtak I. The Impact of the Parameters of the Briquetting Process Using a Hydraulic Press on the Density Briquettes of Plant Waste. In book: Campilho RD, Ivanov V, Pinto GF, Baptista A, Silva FJG (eds). *Advances in Design, Simulation and Manufacturing VIII. Lecture Notes in Mechanical Engineering*. Cham: Springer; 2025. P. 83–97. https://doi.org/10.1007/978-3-031-95218-0_8

8. Shengnan Zhao, Lujia Han, Bing Gao, Pengfei Wu and Xian Liu. Effects of Wet Storage on Compression Molding of Sawdust and Mechanism Analysis. *IOP Conference Series: Earth and Environmental Science*. 2019;227(2):022024. <https://doi.org/10.1088/1755-1315/227/2/022024>
9. Halimatuddahlia Nasution, Hamidah Harahap, Retno Riani, AI Pelawi. Effect of Pressing Temperature on the Mechanical Properties of Waste Styrofoam Filled Sawdust Composite. *IOP Conference Series: Materials Science and Engineering*. 2018;309(1):012034. <https://doi.org/10.1088/1757-899X/309/1/012034>
10. Rahmani H, Algirdas A, Shestavetska A, Vaiciukyniene D. Preparation and Mechanical Characterization of Pressed Carbonized Wood Sawdust Bio-Composite. *Scientific Reports*. 2025;15:14981. <https://doi.org/10.1038/s41598-025-98658-w>
11. Camilo Oliveros-Gaviria, Edwin Cumbalaza, Jose Hermisul Mina-Hernandez, Mayra Eliana Valencia-Zapata, Juan Nicolas Suarez-Bonilla, Nicolas Martinez-Mera. Wood Plastic Composite Based on Recycled High-Density Polyethylene and Wood Waste (Sawdust). *Polymers*. 2024;16(22):3136. <https://doi.org/10.3390/polym16223136>
12. Adole AM, Anum I, Jamaludin MY, Suhaimi AR. Mechanical Characterization of Green Sandwich Composites from Kenaf Fiber Skins and Sawdust Core. *Discover Civil Engineering*. 2025;2:76. <https://doi.org/10.1007/s44290-025-00241-9>
13. Križan P. Construction and Types of Pressing Machines. In book: *Biomass Compaction*. Cham: Springer; 2022. P. 5–19. https://doi.org/10.1007/978-3-030-89956-1_2
14. Manakhov PV, Fedoseev OB. Elastoplastic Compression of a Rectangular Body: An Alternative Approach. *Russian Engineering Research*. 2009;29(1):20–23. <https://doi.org/10.3103/S1068798X09010067>
15. Vlasov YuN. Theoretical Study of the Effect of Pressing Time and Moulding Speed on Density of Sawdust Briquettes. *Proceedings of the St. Petersburg Forestry Academy*. 2019;(227):188–198. <https://doi.org/10.21266/2079-4304.2019.227.188-198>
16. Chibirev OV, Vlasov YuN, Kucher SV, Kunitskaya OA. Evaluation of Elastic Properties of Wood Particles Conglomerate. *Systems. Methods. Technologies*. 2017;(1(33)):140–146. <https://doi.org/10.18324/2077-5415-2017-1-140-146>
17. Myuller OD, V.I. Melekhov VI, Lyubov VK, Malygin VI. The Effect of Compacting Pressure on the Side Pressure Coefficient of Wood Pellets. *Russian Forestry Journal*. 2013;(3):97–102. URL: https://lesnoizhurnal.ru/issuesarchive/?ELEMENT_ID=56317&ysclid=mh4hl9lx33532851616 (accessed: 10.09.2025).
18. Feoktistov SI, Andrianov IK. Construction of Forming Limit Diagram for Sheet Blanks from Aviation Aluminum Alloys. *Advanced Engineering Research (Rostov-on-Don)*. 2023;23(1):7–16. <https://doi.org/10.23947/2687-1653-2023-23-1-7-16>
19. Shlyakhin DA, Savinova EV. Coupled Axisymmetric Thermoelastostaticity Problem for a Round Rigidly Fixed Plate. *Advanced Engineering Research (Rostov-on-Don)*. 2024;24(1):23–35. <https://doi.org/10.23947/2687-1653-2024-24-1-23-35>

About the Authors:

Ivan K. Andrianov, Cand.Sci. (Eng.), Associate Professor of the Department of Aircraft Engineering and Computer-Aided Design, Komsomolsk-na-Amure State University (27, Lenin Prospect, Komsomolsk-on-Amur, 681013, Russian Federation), [SPIN-code](#), [ORCID](#), [ScopusID](#), [ResearcherID](#), ivan_andrianov_90@mail.ru

Sergey N. Ivanov, Dr.Sci. (Eng.), Associate Professor, Professor of the Electrical Engineering Department, Komsomolsk-na-Amure State University (27, Lenin Prospect, Komsomolsk-on-Amur, 681013, Russian Federation), [SPIN-code](#), [ORCID](#), [ScopusID](#), [ResearcherID](#), snivanov57@mail.ru

Elena K. Chepurnova, research laboratory assistant of the Department of Aircraft Engineering and Computer-Aided Design, Komsomolsk-na-Amure State University (27, Lenin Prospect, Komsomolsk-on-Amur, 681013, Russian Federation), [SPIN-code](#), [ORCID](#), [ScopusID](#), [ResearcherID](#), el.chep@bk.ru

Claimed Contributorship:

IK Andrianov: investigation, software.

SN Ivanov: conceptualization, writing – review & editing.

EK Chepurnova: investigation.

Conflict of Interest Statement: the authors declare no conflict of interest.

All authors have read and approved the final version of manuscript.

Об авторах:

Иван Константинович Андрианов, кандидат технических наук, доцент кафедры «Авиационное и компьютерное проектирование» Комсомольского-на-Амуре государственного университета, (681013, Российская Федерация, г. Комсомольск-на-Амуре, пр. Ленина, 27), [SPIN-код](#), [ORCID](#), [ScopusID](#), [ResearcherID](#), ivan_andrianov_90@mail.ru

Сергей Николаевич Иванов, доктор технических наук, доцент, профессор кафедры «Электромеханика» Комсомольского-на-Амуре государственного университета (681013, Российская Федерация, г. Комсомольск-на-Амуре, пр. Ленина, 27), [SPIN-код](#), [ORCID](#), [ScopusID](#), [ResearcherID](#), snivanov57@mail.ru

Елена Константиновна Чепурнова, лаборант-исследователь, кафедра «Авиационное и компьютерное проектирование» Комсомольского-на-Амуре государственного университета (681013, Российская Федерация, г. Комсомольск-на-Амуре, пр. Ленина, 27), [SPIN-код](#), [ORCID](#), [ScopusID](#), [ResearcherID](#), el.chep@bk.ru

Заявленный вклад авторов:

И.К. Андрианов: проведение исследования, разработка программного обеспечения.

С.Н. Иванов: разработка концепции, написание рукописи – рецензирование и редактирование.

Е.К. Чепурнова: проведение исследования.

Конфликт интересов: авторы заявляют об отсутствии конфликта интересов.

Все авторы прочитали и одобрили окончательный вариант рукописи.

Received / Поступила в редакцию 02.09.2025

Reviewed / Поступила после рецензирования 26.09.2025

Accepted / Принята к публикации 06.10.2025

MECHANICS МЕХАНИКА



UDC 531.788

Original Empirical Research

<https://doi.org/10.23947/2687-1653-2025-25-4-2156>

Investigation of the Actual Value of the Vacuum Time of a Measuring Vessel by Ejector

Sergey I. Savchuk , Ervin D. Umerov

Crimean Engineering and Pedagogical University named after Fevzi Yakubov, Simferopol, Republic of Crimea

Ervin777@yandex.ru

EDN: XOCYKW

Abstract

Introduction. In industry, the process of obtaining technological vacuum using ejectors that utilize the kinetic energy of a jet of compressed air is widely used. The selection of the required ejector model, as well as their number (when creating a field of ejectors), is performed proceeding from the compliance of the ejector characteristics with the key parameters of the designed process technology. One of the most important characteristics of an ejector, significantly affecting the overall performance of the vacuum system, is the evacuation time of the graduated (calibrated) container. However, in technical literature, this parameter is not specified for the maximum vacuum depth produced by the ejector, nor for the corresponding supply pressure, but for certain, less-defined parameters, referred to as optimal by ejector manufacturers. In such cases, it is impossible to accurately estimate the actual value of an important criterion. Therefore, the objective of this work is to experimentally determine the actual value of the vacuum time of a graduated (calibrated) vessel for various types of ejectors.

Materials and Methods. Experimental studies were performed on a stand specifically designed and manufactured by the authors, which made it possible to study various parameters of vacuum ejectors. In particular, the stand provided establishing the exact time of vacuuming a measuring vessel using ejectors with a nozzle diameter from 0.1 to 4.0 mm at a supply pressure value that induced the maximum vacuum depth for each model under study. The research was carried out using the most popular vacuum ejectors of the VEB, VEBL, VED and VEDL families manufactured by Camozzi at a pre-determined, precisely set input supply pressure for each ejector size. The actual values of the vacuum time at the highest vacuum depth for each ejector were experimentally determined.

Results. It has been established that the performance of VEB, VEBL, VEDL, and VED series ejectors differs from that stated in the manufacturer's catalog. The time required to reach maximum vacuum for each ejector exceeds the manufacturer's specifications by 25–40%, which impacts the performance of the vacuum system.

Discussion. The experimental data have shown that the actual values of the vacuum time of the measuring vessel differ from the values given in the catalogs of manufacturers of ejectors. This difference is explained by the fact that when conducting appropriate tests, manufacturers are guided not by the maximum vacuum depth created by the ejector, but by the vacuum depth created by a certain “optimal” (the wording of the ejector manufacturer) value of the supply pressure. In almost all the cases considered by us, this “optimal” supply pressure produced a vacuum, whose depth differed from the maximum. In this regard, it seems advisable to adjust the value of the inlet supply pressure to attain the maximum vacuum depth for each type of ejector.

Conclusions. The results of the obtained values of the vacuum creation time in one liter of volume at the maximum depth of the vacuum produced by the ejector provide a more accurate selection of vacuum ejectors depending on the required process tasks, ensure the greatest efficiency and cost-effectiveness of automated vacuum systems. The research results can be used by all ejector manufacturers to adjust their basic catalogs and appropriate recommendations for the use of these products. Further research will be conducted to study the accuracy of the geometric shapes of the surface of the ejector channel, the purity of processing, and their production technology, which affect the passage of air flow.

Keywords: vacuum depth, vacuum ejector, measuring vessel, ejector supply pressure

Acknowledgements. The authors would like to thank the reviewers and the Editorial board of the Journal for their attentive attitude towards the article and the comments indicated, the elimination of which allowed us to improve the quality of the article.

For Citation. Savchuk SI, Umerov ED. Investigation of the Actual Value of the Vacuum Time of a Measuring Vessel by Ejector. *Advanced Engineering Research (Rostov-on-Don)*. 2025;25(4):300–310. <https://doi.org/10.23947/2687-1653-2025-25-4-2156>

Оригинальное эмпирическое исследование

Исследование фактического значения времени вакуумирования мерной емкости эжектором

С.И. Савчук^{ID}, Э.Д. Умеров^{ID}✉

Крымский инженерно-педагогический университет имени Февзи Якубова, г. Симферополь

✉ Ervin777@yandex.ru

Аннотация

Введение. В промышленности широко распространен процесс получения технологического вакуума с помощью эжекторов, использующих кинетическую энергию струи сжатого воздуха. Выбор необходимой модели эжектора, а при создании поля эжекторов также и их количества, осуществляется исходя из соответствия характеристик эжектора основным параметрам проектируемого технологического процесса. Одной из важных характеристик эжектора, существенно влияющих на повышение производительности всей вакуумной системы в целом, является время вакуумирования мерной (тарированной) емкости. При этом в технической литературе данный параметр приводится не при максимальной глубине вакуума, производимого эжектором, и не при соответствующей этому значению величине питающего давления, а при некоторых, не вполне определенных параметрах, называемых изготовителями эжекторов оптимальными. В таких случаях невозможно точно оценить фактическое значение важного критерия. В связи с этим цель данной работы — путем экспериментальных исследований установить фактическое значение времени вакуумирования мерной (тарированной) емкости для различных типов эжекторов.

Материалы и методы. Экспериментальные исследования проводились на специально спроектированном и изготовленном авторами стенде, позволяющем изучать различные параметры вакуумных эжекторов. В частности, стенд дает возможность установить точное время вакуумирования мерной емкости эжекторами, имеющими диаметр сопла от 0,1 до 4,0 мм при величине питающего давления, обеспечивающего максимальную глубину вакуума для каждой исследуемой модели. Исследования проводились с использованием наиболее популярных вакуумных эжекторов семейств VEB, VEBL, VED и VEDL производства Camozzi при заранее определенной, точно заданной величине входного питающего давления для каждого типоразмера эжектора. Фактические значения времени вакуумирования при наибольшей глубине вакуума для каждого эжектора определялись экспериментально.

Результаты исследования. Установлено, что производительность эжекторов серий VEB, VEBL, VEDL и VED отличается от данных, приведенных в каталоге фирмы-изготовителя. Необходимое время для достижения максимальной глубины вакуума каждого из эжекторов превышает на 25–40 % приведенные производителем данные, и эта «погрешность» сказывается в итоге на производительности вакуумной системы.

Обсуждение. Экспериментальные данные показали, что отличие действительных значений времени вакуумирования мерной емкости от значений, приведенных в каталогах фирмы-изготовителя эжекторов, объясняется тем, что при проведении соответствующих испытаний изготовитель ориентируется не на максимальную глубину вакуума, создаваемую эжектором, а на глубину вакуума, создаваемую неким «оптимальным» (формулировка изготовителя) значением питающего давления. Практически во всех рассмотренных авторами статьи случаях это «оптимальное» питающее давление производило вакуум, глубина которого отличалась от максимальной. В этой связи представляется целесообразным вводить корректировку величины входного питающего давления для достижения максимальной глубины вакуума для каждого типа эжектора.

Заключение. Полученные значения времени создания вакуума в одном литре объема при максимальной глубине вакуума, производимого эжектором, позволяют осуществлять более точный выбор вакуумных эжекторов в зависимости от решаемых технологических задач, обеспечить наибольшую эффективность и экономичность автоматизированных вакуумных систем. Результаты исследований могут быть использованы всеми фирмами-изготовителями эжекторов для корректировки их базовых каталогов и соответствующих рекомендаций по применению этих изделий. Дальнейшие исследования в этой области будут направлены на изучение точности геометрических форм поверхности канала эжектора, чистоты обработки и технологии их производства, влияющие на прохождение воздушного потока.

Ключевые слова: глубина вакуума, вакуумный эжектор, мерная емкость, питающее давление эжекторов

Благодарности. Авторы выражают глубокую благодарность рецензентам и редколлегии журнала за внимательное отношение к статье и указанные замечания, устранение которых позволило улучшить качество статьи.

Для цитирования. Савчук С.И., Умеров Э.Д. Исследование фактического значения времени вакуумирования мерной емкости эжектором. *Advanced Engineering Research (Rostov-on-Don)*. 2025;25(4):300–310. <https://doi.org/10.23947/2687-1653-2025-25-4-2156>

Introduction. Industrial development, continuous improvement of processing, and the introduction of innovations in production bring about the ever-growing use of vacuum for moving parts by robots and manipulators in assembly areas, conveyor lines, metal spraying in a vacuum environment, etc. Moving and positioning complex-shaped parts, especially those such as foil or paper, is not possible without the use of vacuum suction cups.

The key parameter of a vacuum ejector is the supply pressure. Its optimal value provides a deep vacuum, which creates the conditions for attaining maximum efficiency. This provides high performance of the vacuum suction cup, a key element of the vacuum system, while minimizing energy costs.

In [1], a group of authors examined vacuum ejectors with various design features. A special-purpose vacuum stand was used for the experiments, measuring the magnitude of the generated vacuum as a function of the feed pressure at the inlet. It was found that the recommended feed pressure values provided in the ejector manufacturers' catalogs differed from the actual values obtained experimentally.

Typically, the supply pressure values recommended by ejector manufacturers do not allow for the full utilization of the ejectors they manufacture. That is, the “optimal” supply pressure values recommended in catalogs do not provide the maximum vacuum depth that each ejector in question can create. This reduces the device performance and, consequently, the efficiency of its actuator — the suction cup. The vacuum depth created by the ejector impacts significantly the cycle time. The deeper the vacuum created by the ejector, the shorter the suction cup response time, and the faster the vacuum-equipped section operates. This discovery is the occasion for further experimental research to determine the time it takes to create vacuums of varying depths in a liter of measuring vessel volume at a given supply pressure. This parameter can be considered as the ejector operating speed, reflecting the response speed of the ejector-suction cup system and directly affecting the operating time of this pair. It is also listed in the manufacturers' catalogs and directly impacts the operation of the vacuum suction cup and the guaranteed holding force.

It should be noted that the experiments to determine the vacuum time of the measuring vessel were carried out at a pre-determined supply pressure value [1], which provided the maximum vacuum depth produced by the ejector. This supply pressure value was set at the ejector inlet at the start of the experiment.

Currently, various types of ejectors, which are used in supersonic [2], steam [3], refrigeration [4] and other systems, are known. There are also two-stage ejectors used in hydrodynamics [5] and cooling systems [6]. They allow for the dynamic pressure control, which increases the efficiency of the performance.

Previously conducted studies made it possible to develop an analytical method for predicting the air flow in a supersonic air ejector [7]. A theory about its speed was put forward, a numerical analysis of the ejector operation was made [8], the results of its performance were obtained experimentally [9], the effect of the primary nozzle deflection on the ejector performance was studied using computational fluid dynamics [10], the effect of the Mach wave on the formation of the boundary of the moving flow in the device was considered [11], a theory of flow mixing was formulated [12], etc.

There is a large amount of research that demonstrates the use of various types of both vacuum ejectors [13], and vacuum technology [14]. In [15], the authors disclosed the theoretical foundations of vacuum and their physical essence [16]. However, very little attention was paid to the practical possibilities of using vacuum.

In [17], the author examines the application features of compressed air in pneumatic elements. In [18], the results of experimental studies with improved characteristics of the ejector nozzle are presented. And in [19], the process of air flow modeling is described. However, the issues related to the study of the parameters of vacuum ejectors receive almost no attention in modern scientific and technical literature. Basically, information about their parameters is contained only in specialized publications, for example, in the catalogs of companies engaged in the production of vacuum equipment, such as Schmalz, Festo, Camozzi, SMC, and others.

Taking into account all of the above, the authors aimed at establishing the actual value of the vacuuming time of a measuring (calibrated) vessel for various types of ejectors through experimental research.

Materials and Methods. Previously, the authors studied vacuum ejectors at various inlet supply pressures [1], recording the vacuum depth reached. After establishing the maximum vacuum at a given supply pressure, the time it took to attain vacuum in a volume equal to one liter was measured. The data obtained can be used to optimize the vacuum system parameters and improve its performance.

A specifically designed stand [20] was used for the experimental studies. Its photograph is shown in Figure 1.

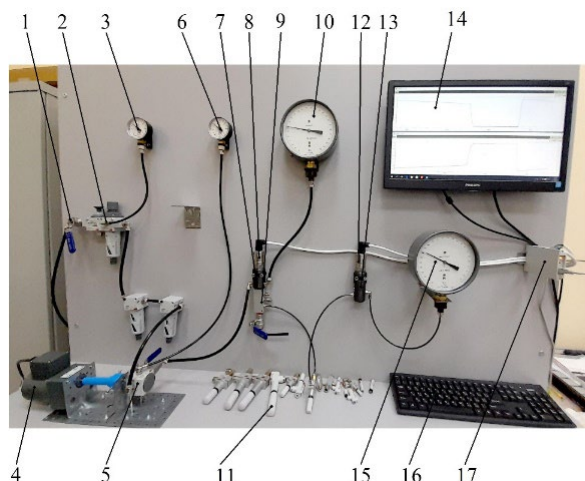


Fig. 1. Experimental stand:

- 1 — ball valve; 2 — air preparation unit; 3 — inlet control pressure gauge;
 4 — electronically controlled motor gear; 5 — pressure regulator with shutoff valve; 6 — control pressure gauge;
 7, 13 — pneumatic tees; 8 — MIDA-DI-15 excess pressure sensor; 9 — distribution block manifold; 10 — standard deformation pressure gauge; 11 — test vacuum ejector; 12 — MIDA-DA-15 absolute pressure sensor; 14 — monitor; 15 — standard deformation vacuum gauge (accuracy class 0.4); 16 — computer keyboard; 17 — MIDA-US-410 communication device

In the course of studies [1], the maximum vacuum depth created by the ejector was recorded depending on the inlet supply pressure. These parameters were subsequently used as reference values for a series of experiments aimed at establishing the time interval for creating a vacuum in a volume equal to one liter.

To conduct this part of the experiment, a special sealed vessel (Fig. 2) was designed and manufactured. It was equipped with fittings and shutoff valves to allow for the connection to the test stand and the ejectors being tested. The vessel volume was carefully measured with certified measuring instruments and found to be 1000.03 ml.

Before each experiment, the input supply pressure for all ejectors was set to provide the maximum vacuum depth. The value of this pressure corresponded to the experimental data given in [1] and was set using the control pressure gauge 10 and the pressure sensor 8 (Fig. 1).

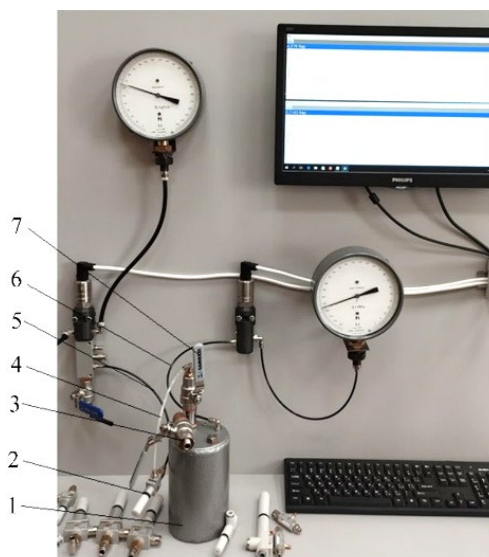


Fig. 2. Measuring vessel:

- 1 — measuring vessel; 2 — vacuum ejector under test; 3 — ball valve;
 4 — ejector vacuum line; 5 — ejector inlet pressure line;
 6 — vessel vacuum line; 7 — shutoff ball valve

Measuring vessel 1 can be linked with any ejectors that are connected to the process equipment through PVC tubing with a diameter of 4 to 10 mm. Ejectors 2 under study are connected to the distribution manifold 8 via the inlet supply pressure line 5 (Fig. 1). The ejectors under study are connected to the shutoff valve 7 installed directly on measuring vessel 1 via the vacuum line 4. Measuring vessel 1 is connected via the vacuum line 6 to tee 13 (Fig. 1). Air valve 3 connects the measuring vessel to the atmosphere.

The experiment was conducted in the following order. Air valve 3 and shutoff valve 7 were closed. The ejector under study was then connected to a specialized test stand, where the supply pressure at the inlet was adjusted to a value that provided the greatest vacuum depth. Shutoff valve 7 was then opened, and the emptying of the measuring vessel started. A sign of complete emptying was the achievement of a stable vacuum depth, which was recorded by vacuum gauge 12 and absolute pressure sensor 15 (Fig. 1). After recording the instrument readings, the measuring vessel was refilled with air at atmospheric pressure, for which purpose shutoff valve 7 was closed and air valve 3 was opened.

Research Results. Figures 3–6 show diagrams of the dependence of the time to reach the vacuum depth in one liter of volume on the supply pressure for different types of ejectors. Tables 1–4 present the supply pressure and vacuum depth data obtained experimentally and provided in the manufacturer's catalog.

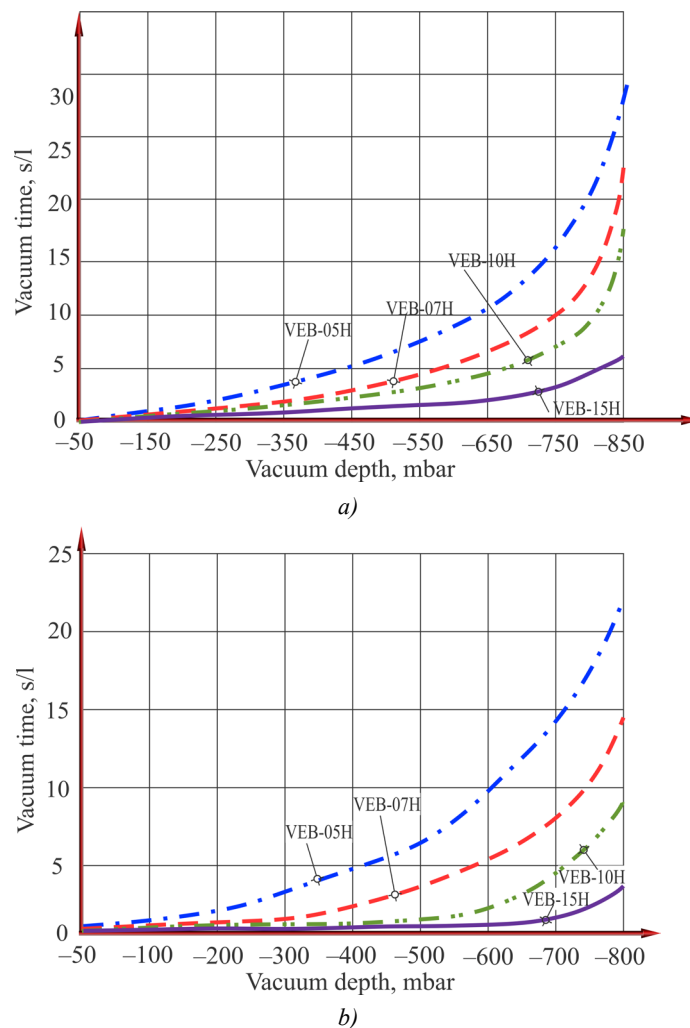


Fig. 3. Vacuum creation time diagrams for one liter of volume for VEB series ejectors:
a — according to the authors' data; *b* — according to the company catalog

Figure 3 shows the diagrams of the dependence of the vacuum time of the measuring vessel for the VEB series ejectors, obtained by the authors (left) and contained in the manufacturer's catalog (right). Table 1 shows the supply pressure values at which the optimal vacuum depth values were obtained, as well as the manufacturer's recommended values for the optimal supply pressure and the expected vacuum depth at these values.

Table 1

Comparative Data on Supply Pressure and Vacuum Level for VEB Series Ejectors

Ejector model	Manufacturer's data			Experimental data		
	Ø nozzle, mm	Vacuum depth, mbar	Optimal working pressure, bar	Maximum vacuum depth, mbar	Feed pressure, bar	Vacuum depth at recommended pressure, mbar
VEB-05H	0.5	182	4.5	96	4.73	115
VEB-07H	0.7	152	4.5	108	4.07	115
VEB-10H	1.0	152	5.0	132	4.90	133
VEB-15H	1.5	152	4.5	109	4.75	145

The analysis of the diagrams and tables shows that the curve patterns and measuring vessel vacuum time for the VEB series ejectors are similar to those provided in the manufacturer's catalog. It has been established that the ejectors reach significantly greater vacuum depth at lower supply pressures. This means that the desired effect is attained at lower supply pressures than those recommended by the ejector manufacturer, which is undoubtedly safer and more efficient. Moreover, even with a feed pressure at the ejector inlet equal to the manufacturer's recommended "optimal" pressure, the vacuum depth is still greater than stated in the manufacturer's catalog (Table 1). The authors have also found that for the VEB-15H ejector, even when reaching maximum vacuum depth, the time required to empty the measuring vessel is 70% longer than stated in the manufacturer's catalog.

Figure 4 shows the diagrams of the dependence of the vacuum time of the measuring vessel for the VEBL series ejectors, obtained by the authors (left) and given in the manufacturer's catalog (right). Table 2 presents the supply pressure values at which the authors obtained the best (optimal) vacuum depth values. It also lists the manufacturers' recommended optimal supply pressure values and the expected vacuum depth at these values.

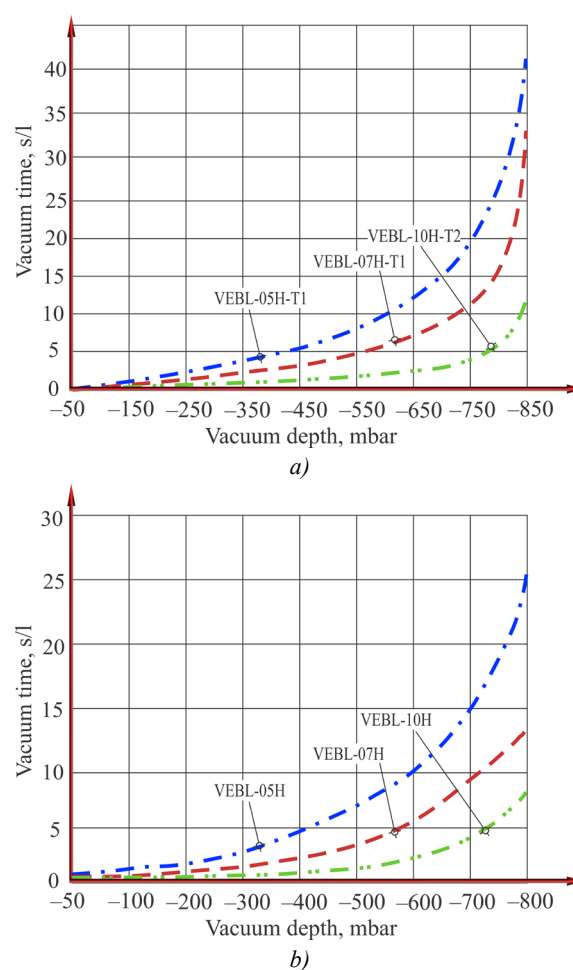


Fig. 4. Vacuum creation time diagrams for one liter of volume for the VEBL series ejectors:
a — according to the authors' data; b — according to the company's catalogue

Table 2

Comparative Data on Supply Pressure and Vacuum Level for VEBL Series Ejectors

Ejector model	Manufacturer's data			Experimental data		
	Ø nozzle, mm	Vacuum depth, mbar	Optimal working pressure, bar	Maximum vacuum depth, mbar	Feed pressure, bar	Vacuum depth at recommended pressure, mbar
VEBL-05H-T1	0.5	160	4.5	121	4.20	127
VEBL-07H-T1	0.7	150	4.5	133	4.10	142

The diagrams and table show that the curves and measuring vessel evacuation times for the VEBL series ejectors are similar to those provided in the manufacturer's catalog. However, since the ejectors reach significantly greater vacuum depths at lower supply pressures, the desired effect is attained at lower supply pressures than recommended by the ejector manufacturer, which is undoubtedly safer and more efficient. Moreover, even if the feed pressure at the ejector inlet is set to the manufacturer's recommended "optimal" pressure, the vacuum depth is still greater than that specified in the manufacturer's catalog (Table 2). The authors have also found that for the VEBL-10H ejector, even when the maximum vacuum depth is reached, the time required to empty the measuring tank is 40% longer than that specified in the manufacturer's catalog.

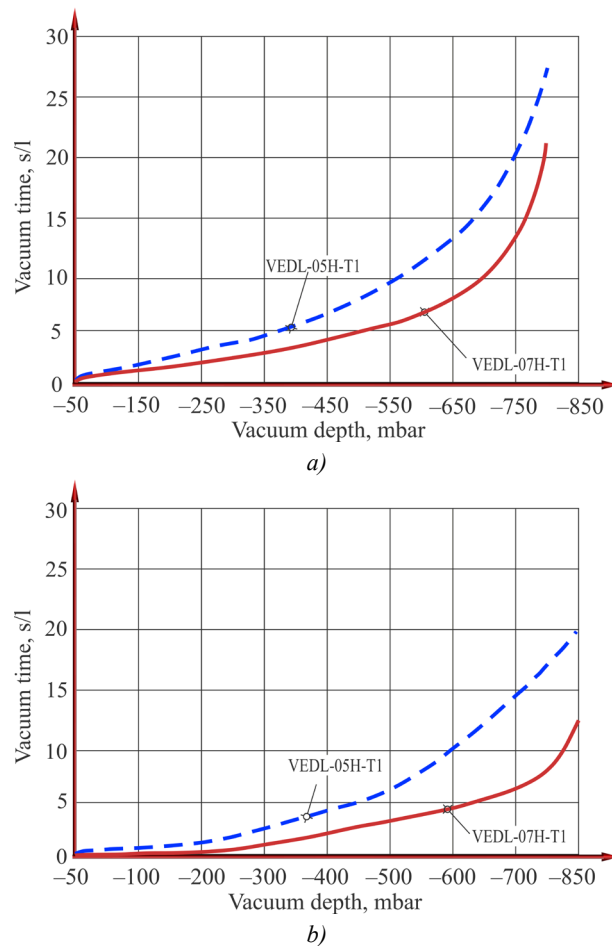


Fig. 5. Vacuum creation time diagrams for one liter of volume for the VEBL series ejectors:
a — according to the authors' data; *b* — according to the company's catalogue

Figure 5 shows the diagrams of the dependence of the vacuum time of the measuring vessel for the VEDL series ejectors, obtained by the authors (left) and given in the manufacturer's catalog (right). Table 3 presents the supply pressure values at which the best (optimal) vacuum depth values were obtained, as well as the recommended optimal supply pressure values by the manufacturers, and the expected vacuum depth at these values.

Table 3

Comparative Data on Supply Pressure and Vacuum Level for VEBL Series Ejectors

Ejector model	Manufacturer's data			Experimental data		
	\varnothing nozzle, mm	Vacuum depth, mbar	Optimal working pressure, bar	Maximum vacuum depth, mbar	Feed pressure, bar	Vacuum depth at recommended pressure, mbar
VEDL-05H-T1	0.5	170	4.5	130	4.00	142
VEDL-07H-T1	0.7	150	4.5	207	3.40	256

Judging by the diagrams and data in the table, the nature of the curves and the vacuum time of the measuring vessel for the VEDL series ejectors are similar to the data given in the manufacturer's catalog.

The authors have found that the performance data for the VEDL series ejectors differs from that provided in the manufacturer's catalog. Specifically, for the VEDL-05N-T1 ejector, the time required to reach maximum emptying of the measuring vessel (-800 mbar) was 27 seconds (the time provided in the catalog is 19 seconds), which is 40% longer. Similarly, for the VEDL-07N-T1 ejector, the time required to attain maximum emptying of the measuring vessel (-800 mbar) was 20 seconds (the time provided in the catalog is 11 seconds), which is 81% longer.

Figure 6 shows the diagrams of the dependence of the vacuum time of the measuring vessel for the VED series ejectors, obtained by the authors (left) and given in the manufacturer's catalog (right). Table 4 shows the supply pressure values at which the best vacuum depth values were reached, as well as the manufacturer's recommended optimal supply pressure values and the expected vacuum depth at these values.

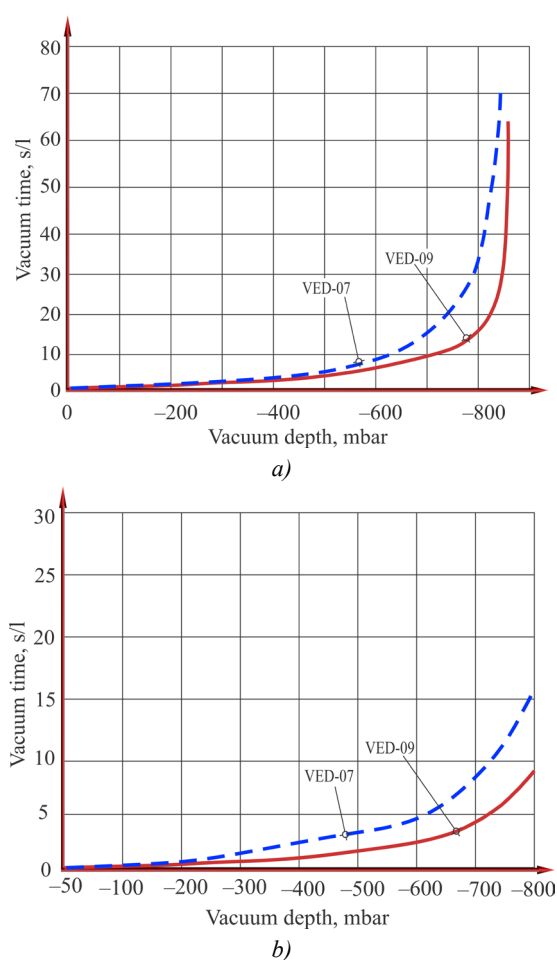


Fig. 6. Vacuum creation time diagrams for one liter of volume for VEB series ejectors:
a — according to the authors' data; *b* — according to the company catalog

Table 4

Comparative Data on Supply Pressure and Vacuum Level for VEB Series Ejectors

Ejector model	Manufacturer's data			Experimental data		
	Ø nozzle, mm	Vacuum depth, mbar	Optimal working pressure, bar	Maximum vacuum depth, mbar	Feed pressure, bar	Vacuum depth at recommended pressure, mbar
VED-07	0.7	101	5.0	405	4.70	409
VED-09	0.9	111	5.0	120	4.20	133

The analysis of the experimental data shows that the nature of the curves and the vacuum time of the measuring vessel for the VED series ejectors are similar to the curves given in the manufacturer's catalog.

The authors also found that the performance of the VED series ejectors differed from that listed in the manufacturer's catalog. Specifically, for the VED-07 ejector, the time required to reach maximum emptying of the measuring vessel (–800 mbar) was 20 seconds (versus 15 seconds listed in the catalog), a 33% increase. For the VED-09 ejector, the time required to achieve maximum emptying of the measuring vessel (–800 mbar) was 10 seconds (versus 8 seconds listed in the catalog), a 25% increase.

Discussion. The experimentally obtained data on the actual time of vacuuming the measuring vessel by ejectors differ from the data given in the catalogs of the manufacturers. A positive aspect here is that the vacuum depth values stated by the manufacturer are reached at much lower supply pressures than those presented in the catalogs. Furthermore, the actual vacuum depth is significantly more efficient than described by the manufacturer. However, the actual time to empty the measuring vessel turned out to be longer than the manufacturers stated in their catalogs. Sometimes, this time was significantly exceeded.

This fact can be of vital importance for designing the process cycle of equipment operation, as it reflects the actual capabilities of certain types of ejectors in terms of vacuum creation rates. This emphasizes the significance of such a parameter as the vacuum time of the measuring vessel when selecting ejectors. This property is critically important for calculating the required amount of time when constructing an ejector field to maintain the required vacuum depth.

Conclusion. The analysis of the data obtained during the experiment shows that the nature of the curves during evacuation of the measuring vessel for ejectors of the VEB, VEBL, VEDL and VED series is similar to the data given in the manufacturer's catalog. However, the time required for each of the ejectors to reach maximum vacuum depth differs. It exceeds the time specified by the manufacturers by 25–40%. This fact affects the performance of both the ejector itself and the vacuum system as a whole. In this regard, when solving process tasks in production, it is required to carefully select vacuum ejectors in order to provide the greatest efficiency and cost-effectiveness of automated vacuum systems.

The research results can be used as recommendations for the utilization of ejectors and for adjusting catalogs of manufacturing companies.

Further research in this area will be aimed at studying the accuracy of the geometric shapes of the surface of the ejector channel, the cleanliness of processing and their production technology, which affect the passage of air flow.

References

1. Savchuk SI, Umerov ED, Abdulgazis AU. Investigation of the Optimal Vacuum Depth Created by the Ejector Depending on the Value of the Supply Pressure. *Advanced Engineering Research (Rostov-on-Don)*. 2025;25(1):43–51. <https://doi.org/10.23947/2687-1653-2025-25-1-43-51>
2. Xinyue Hao, Jiwei Yan, Neng Gao, Volovyk O, Yifan Zhou, Guangming Chen. Experimental Investigation of an Improved Ejector with Optimal Flow Profile. *Case Studies in Thermal Engineering*. 2023;47:103089. <https://doi.org/10.1016/j.csite.2023.103089>
3. Yongzhi Tang, Zhongliang Liu, Can Shi, Yanxia Li. A Novel Steam Ejector with Pressure Regulation to Optimize the Entrained Flow Passage for Performance Improvement in MED-TVC Desalination System. *Energy Conversion and Management*. 2018;172(8):237–247. <https://doi.org/10.1016/j.enconman.2018.07.022>
4. Tashtoush BM, Al-Nimr MA, Khasawneh MA. A Comprehensive Review of Ejector Design, Performance, and Applications. *Applied Energy*. 2019;240:138–172. <https://doi.org/10.1016/j.apenergy.2019.01.185>
5. Elhub B, Mat S, Sopian K, Elbreki AM, Ruslan MH, Ammar AA. Performance Evaluation and Parametric Studies on Variable Nozzle Ejector Using R134A. *Case Studies in Thermal Engineering*. 2018;12:258–270. <https://doi.org/10.1016/j.csite.2018.04.006>

6. Tao Hai, Masood Ashraf Ali, Dhahad HA, Alizadeh A, Sharma K, Sattam Fahad Almojil, et al. A Novel Bi-Evaporator Cooling System via Integration of Absorption Refrigeration Cycle for Waste Energy Recovery from an Ejector-Expansion Trans-Critical CO₂ (EETRCC) Cycle: Proposal and Optimization with Environmental Considerations. *Sustainable Energy Technologies and Assessments*. 2023;57(12):103118. <http://doi.org/10.1016/j.seta.2023.103118>
7. Arvind Kumar, Surendra Yadav, Virendra Kumar, Abhishek Kulkarni. A Comprehensive Exploration of Ejector Design, Operational Factors, Performance Metrics, and Practical Applications. *Journal of the Brazilian Society of Mechanical Sciences and Engineering*. 2024;46:39. <https://doi.org/10.1007/s40430-023-04618-8>
8. Mazzelli F, Little AB, Garimella S, Bartosiewicz Y. Computational and Experimental Analysis of Supersonic Air Ejector: Turbulence Modeling and Assessment of 3D Effects. *International Journal of Heat and Fluid Flow*. 2015;56:305–316. <https://doi.org/10.1016/j.ijheatfluidflow.2015.08.003>
9. Yin-Hai Zhu, Yanzhong Li. Novel Ejector Model for Performance Evaluation on Both Dry and Wet Vapors Ejectors. *International Journal of Refrigeration*. 2009;32(1):21–31. <https://doi.org/10.1016/j.ijrefrig.2008.08.003>
10. Yuyan Hou, Fengwu Chen, Sheng Zhang, Weixiong Chen, Jiantao Zheng, Daotong Chong, et al. Numerical Simulation Study on the Influence of Primary Nozzle Deviation on the Steam Ejector Performance. *International Journal of Thermal Sciences*. 2022;17:107633. <https://doi.org/10.1016/j.ijthermalsci.2022.107633>
11. Zuozhou Chen, Chaobin Dang, Eiji Hihara. Investigations on Driving Flow Expansion Characteristics inside Ejectors. *International Journal of Heat and Mass Transfer*. 2015;108(A):490–500. <https://doi.org/10.1016/j.ijheatmasstransfer.2016.12.040>
12. Sunghoon Baek, Seungbin Ko, Simon Song, Sungmin Ryu. Numerical Study of High-Speed Two-Phase Ejector Performance with R134a Refrigerant. *International Journal of Heat and Mass Transfer*. 2018;126(A):1071–1082. <http://doi.org/10.1016/j.ijheatmasstransfer.2018.05.053>
13. Levchenko DA, Meleychuk SS, Arseniev VM. Substantive Provision of a Method of Calculation Vortical Ejector Stage of the Vacuum Unit. *Procedia Engineering*. 2012;39:28–34. <https://doi.org/10.1016/j.proeng.2012.07.004>
14. Kumar V, Sachdeva G. 1-D Model for Finding Geometry of a Single Phase Ejector. *Energy*. 2018;165(A):75–92. <https://doi.org/10.1016/j.energy.2018.09.071>
15. Arun Kumar R, Rajesh G. Physics of Vacuum Generation in Zero-Secondary Flow Ejectors. *Physics of Fluids*. 2018;30(6):066102. <https://doi.org/10.1063/1.5030073>
16. Karthick SK, Rao SM, Jagadeesh G, Reddy KP. Parametric Experimental Studies on Mixing Characteristics within a Low Area Ratio Rectangular Supersonic Gaseous Ejector. *Physics of Fluids*. 2016;28(7):076101. <https://doi.org/10.1063/1.4954669>
17. Hesse S. *Compressed Air as an Energy Carrier*. Moscow: Festo; 2004. 128 p. (In Russ.)
18. Goodman N, Leege BJ, Johnson PE. An Improved de Laval Nozzle Experiment. *International Journal of Mechanical Engineering Education*. 2021;50(2):513–537. <https://doi.org/10.1177/03064190211034165>
19. Moukalled F, Mangani L, Darwish M. *The Finite Volume Method in Computational Fluid Dynamics*. Berlin, Heidelberg: Springer; 2016. 113 p. <https://doi.org/10.1007/978-3-319-16874-6>
20. Savchuk SI, Umerov ED, Abdulgazis UA. Stand for Assessing the Depth of Vacuum Supplied to Specialized Suction Cups Used in Technological Processes of Service during Operation and Production of Cars. *Scientific Notes of the Crimean Engineering and Pedagogical University*. 2023;82(4):225–230. <https://doi.org/10.34771/UZCEPU.2023.82.4.043>

About the Authors:

Sergey I. Savchuk, Cand.Sci. (Eng.), Associate Professor of the Department of Automobile Transport and Traffic Management, Crimean Engineering and Pedagogical University named after Fevzi Yakubov (8, Uchebnyi Lane, Simferopol, 295015, Republic of Crimea), [ORCID](https://orcid.org/0000-0001-9151-1000), ofelos@outlook.com

Ervin D. Umerov, Cand.Sci. (Eng.), Associate Professor of the Department of Automobile Transport and Traffic Management, Crimean Engineering and Pedagogical University named after Fevzi Yakubov (8, Uchebnyi Lane, Simferopol, 295015, Republic of Crimea), [SPIN-код](https://orcid.org/0000-0001-9151-1000), [ORCID](https://orcid.org/0000-0001-9151-1000), [ScopusID](https://orcid.org/0000-0001-9151-1000), Ervin777@yandex.ru

Claimed Contributorship:

SI Savchuk: conceptualization, investigation.

ED Umerov: validation, writing – review & editing.

Conflict of Interest Statement: the authors declare no conflict of interest.

All authors have read and approved the final manuscript.

Об авторах:

Сергей Игоревич Савчук, кандидат технических наук, доцент кафедры «Автомобильный транспорт и организация дорожного движения» Крымского инженерно-педагогического университета имени Февзи Якубова (295015, Республика Крым, г. Симферополь, пер. Учебный, 8), [ORCID](#), ofelos@outlook.com

Эрвин Джеватович Умеров, кандидат технических наук, доцент кафедры «Автомобильный транспорт и организация дорожного движения» Крымского инженерно-педагогического университета имени Февзи Якубова (295015, Республика Крым, г. Симферополь, пер. Учебный, 8), [SPIN-код](#), [ORCID](#), [ScopusID](#), Ervin777@yandex.ru

Заявленный вклад авторов:

С.И. Савчук: разработка концепции, проведение исследования.

Э.Д. Умеров: валидация результатов, написание рукописи, рецензирование и редактирование.

Конфликт интересов: авторы заявляют об отсутствии конфликта интересов.

Все авторы прочитали и одобрили окончательный вариант рукописи.

Received / Поступила в редакцию 04.09.2025

Reviewed / Поступила после рецензирования 29.09.2025

Accepted / Принята к публикации 06.10.2025

MECHANICS МЕХАНИКА



UDC 531.383

Original Theoretical Research

<https://doi.org/10.23947/2687-1653-2025-25-4-2202>

Optical Method for Material Imperfections Identification in the Resonator Workpiece of Hemispherical Vibratory Gyroscope

Sergei A. Shevchenko , Ivan A. Popov , Boris E. Melnikov 

Peter the Great St. Petersburg Polytechnic University, St. Petersburg, Russian Federation

✉ shevchenko.sergei.a@yandex.ru

EDN: TVJRQI

Abstract

Introduction. The implementation of high-precision attitude control systems of a new generation with improved technical characteristics remains a key task in precision instrumentation — this is required for the reliable operation of moving objects with a long service life. One of the promising ways is the use of sensors based on the Bryan effect (hemispherical resonator gyroscopes, HRG), which show significant advantages in stability of characteristics under external factors. Over the past 10 years, foreign and domestic research has reached noticeable success in increasing the target parameters of HRG, however, certain improvement problems remain open. Thus, in the literature, attention is paid to reducing the errors in measuring the HRG through compensating for the impact of imperfections of the resonator, but more often these methods are applicable at stages after geometry generation. Methods for early identification of material inhomogeneities (density variation) during workpiece inspection are insufficiently developed, creating a gap in the process chain and reducing the efficiency of subsequent balancing and calibration. The objective of this study is to develop a method for identifying resonator density variations at an early stage of the process — during workpiece inspection.

Materials and Methods. An optically transparent material is considered – fused quartz glass, which is the most common material for making a HRG resonator, in particular, the KU-1 brand (foreign analogs — Corning HPFS 7980, JGS1). The identification method is based on the relationship of the optical properties of quartz glass (absorption coefficient) with the desired density distribution over the volume of the workpiece. A virtual experiment was conducted, which consisted in the formation and resolution of a system of linear algebraic equations (SLAE) based on the measurements series results of a light beam intensity passing through a workpiece. A polynomial approximation was used to describe the density distribution in order to increase the robustness of the method. The SLAE roots were obtained through finding a pseudosolution by the least square method based on the singular value decomposition.

Results. A method for identifying the density variation of quartz glass at the stage of quality control of the technological workpiece of the HRG resonator was developed. The desired density distribution of quartz glass over the volume of the workpiece was obtained, coinciding with the “true” one — the difference was no more than 5%. The sensitivity of the method to the presence of macrodefects in the volume of the workpiece (pores, bubbles, etc.) was assessed.

Discussion. The results show that the proposed method can effectively control the density variation of the workpieces and optimize the resonator production, thereby improving the efficiency of the processes and minimizing the impact of imperfections on their characteristics. Virtual experiments have demonstrated that measuring the light beam intensity passing through the workpiece allows for the accurate reconstruction of the absorption coefficient and density distribution with an accuracy of at least 0.005%. The developed system of linear algebraic equations (SLAE) makes it possible to determine these parameters by volume. The paper highlights some features related to solving uncertain SLAE. Particular attention is paid to the need to control the ratio between the number of roots and unknowns to obtain a stable solution.

Conclusion. The proposed method for identifying the density variation of quartz glass at the stage of workpiece quality control in the production of HRG resonators demonstrates high efficiency and accuracy. The presented method has high accuracy for describing the distribution function, and is also flexible in terms of obtaining the optimal dimension of the SLAE, which is directly related to the number of experiments performed. The obtained results confirm the applicability of the material optical properties for controlling the density distribution over the volume, which allows for improved

control of workpieces and optimization of production processes. The required measurement accuracy, determined by the level of density variation that affects the HRG characteristics, is practically achievable, which indicates that the method can be used in the manufacturing process. This approach can be applied in future research and development of high-precision systems, which will contribute to progress in the precision instrumentation industry and improve the quality of manufactured products.

Keywords: HRG, hemispherical resonator, identification, frequency splitting, imperfections, optics, least squares method

Acknowledgements. The authors would like to thank A.V. Lukin, Cand.Sci. (Phys.-Math.), Associate Professor at the Higher School of Mechanics and Control Processes, SPbPU, and A.N. Belyaev, Senior Lecturer of Department of Deformable Solid Mechanics, BSTU “VOENMEKH” named after D.F. Ustinov, who conducted expert interviews together with the authors of the article.

Funding Information. The research was supported by the Russian Science Foundation (grant no. 25-21-00278), <https://rscf.ru/project/25-21-00278/>

For Citation. Shevchenko SA, Popov IA, Melnikov BE. Optical Method for Material Imperfections Identification in the Resonator Workpiece of Hemispherical Vibratory Gyroscope. *Advanced Engineering Research (Rostov-on-Don)*. 2025;25(4):311–323. <https://doi.org/10.23947/2687-1653-2025-25-4-2202>

Оригинальное теоретическое исследование

Оптический метод идентификации несовершенств материала в заготовке резонатора волнового твердотельного гироскопа

С.А. Шевченко , И.А. Попов , Б.Е. Мельников 

Санкт-Петербургский политехнический университет Петра Великого, г. Санкт-Петербург, Российская Федерация

✉ shevchenko.sergei.a@yandex.ru

Аннотация

Введение. Создание высокоточных систем ориентации нового поколения с улучшенными техническими характеристиками остаётся ключевой задачей точного приборостроения — это необходимо для надёжной работы подвижных объектов длительного срока эксплуатации. Одним из перспективных путей является применение датчиков, основанных на эффекте Брайана (волновой твердотельный гироскоп, ВТГ), которые показывают существенные преимущества по стабильности характеристик в условиях внешних факторов. За последние 10 лет зарубежные и отечественные исследования достигли заметных успехов в повышении целевых параметров ВТГ, однако определенные проблемы совершенствования остаются открытыми. Так, в литературе уделяется внимание снижению погрешностей измерения ВТГ за счёт компенсации влияния несовершенств резонатора, но чаще эти методы применимы на стадиях после формообразования. Недостаточно разработаны методы ранней идентификации неоднородностей материала (разноплотности) на этапе контроля заготовок, что создаёт пробел в технологической цепочке и снижает эффективность последующей балансировки и калибровки. Цель работы — разработать метод идентификации разноплотности резонатора на ранней технологической стадии — на этапе контроля заготовки.

Материалы и методы. Рассматривается оптически прозрачный материал — кварцевое стекло, являющееся наиболее распространённым материалом для изготовления резонаторов ВТГ, в частности марка КУ-1. Метод идентификации основан на связи оптических свойств кварцевого стекла (коэффициента поглощения) с искомым объёмным распределением плотности заготовки. Проведён виртуальный эксперимент, включающий формирование и решение системы линейных алгебраических уравнений (СЛАУ) по результатам серии измерений интенсивности светового пучка, прошедшего через заготовку. Для описания распределения плотности использована полиномиальная аппроксимация, что повышает робастность метода. Решение СЛАУ получено через поиск псевдорешения методом наименьших квадратов на базе сингулярного разложения.

Результаты исследования. Разработан метод идентификации разноплотности кварцевого стекла на этапе контроля качества технологической заготовки резонатора ВТГ. Получено искомое распределение плотности кварцевого стекла по объёму заготовки, совпадающее с «истинным» — отклонение не превышает 5 %. Оценена чувствительность метода к наличию макродефектов в объёме заготовки — пор, пузырьков и пр.

Обсуждение. Результаты показывают, что применение предложенного метода позволяет эффективно контролировать разноплотность заготовок и оптимизировать технологию производства резонаторов, обеспечивая повышение результативности процессов минимизации влияния несовершенств на их характеристики. Виртуальные эксперименты продемонстрировали, что измерение интенсивности светового луча, прошедшего через заготовку,

позволяет восстановить распределение коэффициента поглощения и плотности с точностью не менее 0,005 %. Созданная система линейных алгебраических уравнений обеспечила возможность определения этих параметров по объему. Подчеркнуты некоторые особенности, касающиеся решения неопределенных систем линейных алгебраических уравнений (СЛАУ). Пристальное внимание уделено необходимости контроля соотношения между количеством корней и неизвестных для получения устойчивого решения.

Заключение. Предложенный метод идентификации разноплотности кварцевого стекла на этапе контроля качества заготовки при производстве резонаторов ВТГ показывает высокую эффективность и точность. Метод позволяет адекватно описывать функцию распределения и гибко настраивать оптимальную размерность СЛАУ, напрямую связанную с объемом проводимых экспериментов. Полученные результаты подтверждают применимость оптических характеристик материала для контроля объемного распределения плотности, что даёт возможность улучшить контроль заготовок и оптимизировать производственные процессы. Требуемая точность измерений, обусловленная уровнем разноплотности, влияющим на характеристики ВТГ, практически достижима, что свидетельствует о реальной возможности внедрения метода в производстве. Данный подход может быть использован в последующих исследованиях и разработках высокоточных систем, способствуя прогрессу в точном приборостроении и повышению качества выпускаемой продукции.

Ключевые слова: ВТГ, полусферический резонатор, идентификация, расщепление частоты, несовершенства, оптика, метод наименьших квадратов

Благодарности. Авторы благодарят А.В. Лукина, кандидата физико-математических наук, доцента ВШ МПУ СПбПУ и А.Н. Беляева, старшего преподавателя БГТУ «ВОЕНМЕХ» им. Д.Ф. Устинова, проводивших экспертные интервью совместно с авторами статьи.

Финансирование. Исследование выполнено за счет гранта Российского научного фонда №25-21-00278, <https://rscf.ru/project/25-21-00278/>

Для цитирования. Шевченко С.А., Попов И.А., Мельников Б.Е. Оптический метод идентификации несовершенств материала в заготовке резонатора волнового твердотельного гироскопа. *Advanced Engineering Research (Rostov-on-Don)*. 2025;25(4):311–323. <https://doi.org/10.23947/2687-1653-2025-25-4-2202>

Introduction. Currently, the development of high-precision spatial position-determining systems (attitude control systems, ACS) based on sensors (hemispherical resonator gyroscopes, HRG), whose operating principle is linked to the elastic wave precession effect (the Bryan effect), remains relevant [1, 2]. The urgency of using HRG to construct ACS for various purposes is primarily due to the obvious advantages of such devices compared to devices using other physical principles: better weight and size characteristics, resistance to mechanical stress, energy efficiency, longer service life and readiness time, etc. [3]. In the context of the tendency to increase the required assigned resource when creating new mobile objects, the listed advantages make it possible to increase the payload mass, optimize the layout and, more importantly, reduce the accumulated error of the ACS and the load on the energy systems.

With the development of design and modeling methods, as well as manufacturing technologies for HRG, their technical characteristics are also improving, which makes it possible to create ACS of various accuracy classes and, accordingly, apply them in a wide range of fields of science and technology, including space instrumentation [4]. A large number of works published by leading domestic research teams are devoted to the development, design and manufacturing technology of HRG [5]. This is stimulated both by the achievements of foreign companies in terms of the implemented technical indicators of HRG [6], and by the creation of ACS based on them [7].

Despite the fundamental research and advanced results of our compatriots and their students — Academicians V.F. Zhuravlev and D.M. Klimov [8], Professors B.S. Lunin, M.A. Basarab and V.A. Matveyev [9], I.V. Merkuriev [10], K.V. Shishakov [4] — as well as the achievements of foreign groups of D.D. Lynch [11], D. Roselle [12], B.J. Shaw [13], S. Zotov, A. Trusov and A. Shkel [14] — there remain directions and methods for further improvement of the HRG. This allows us to follow the advanced trend of modern precision instrument making — the development of high-precision ACS, based on various sensitive elements [1], [15], including on the basis of the HRG [16].

One of the directions is the minimization of the impact of imperfections in the main sensitive element of the HRG — the resonator [8] — on the key parameters of the product, in particular on the splitting of its operating natural frequency [9]. When discussing the impact of imperfections, the question arises of how to identify them. Most existing works and studies [3], [5] are devoted to assessing the level of imperfection and its compensation at the stages of mechanical and electrical balancing. However, there are practically no studies proposing an identification method at earlier stages of

production, for example, during quality control of a workpiece. The ability to determine the distribution function of material properties (for example, density) by volume at the stage of choosing workpieces allows for a reduction in production costs through the selection based on the criterion of the permissible magnitude of the imperfection amplitude and the choice of the optimal direction of shaping. This, in turn, reduces the duration of the mechanical balancing process cycle and, consequently, reduces operating frequency splitting. The need to monitor inhomogeneity is further dictated by existing methods for assessing material quality, which are focused on its primary application — quartz glass is predominantly considered an optical material; therefore, the focus of monitoring is shifted toward the corresponding parameters.¹ However, when considering quartz glass as the material for the sensing element of a HVG, it is advisable to control the properties and their distribution throughout the volume, which determine the dynamic characteristics (density, elastic modulus, etc.). In this regard, this paper proposes a method for identifying inhomogeneity that has not previously been used.

The objective of this study is to develop a method for identifying imperfections of the “inhomogeneity” type based on measuring the optical properties of a HVG resonator material, intended for use in the quality control stage of a resonator workpiece. This study tests the feasibility of determining the volumetric density distribution function by directly measuring the intensity of a light beam transmitted through the workpiece, given the existing relationship between density and the optical properties of quartz glass.

Materials and Methods. A KU-1 quartz glass cube with a 30 mm edge length was used as the test object (as part of a virtual experiment). Inhomogeneity across the volume of the cube was determined through a series of experiments measuring the intensity of a light beam passing through the cube. In this case, for simplicity, the transmission of a beam in the cross-section of the workpiece was considered (that is, a plane problem). Figure 1 shows the computational and experimental setup used to identify the imperfection in the form of inhomogeneity.

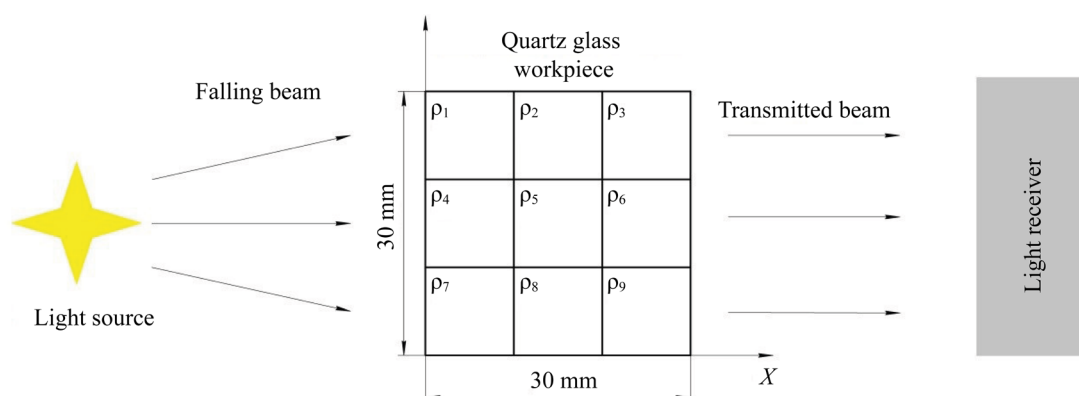


Fig. 1. Calculation and experimental scheme for identifying inhomogeneity

The method involved discretizing the workpiece cross-section into q elements, each of which had its own density value within a specified tolerance characteristic of the material. The minimum element size was determined by the minimum diameter of the light beam generated by the light source. To simplify the calculations, in each of the measurements it was assumed that the light beam fell along the normal to the surface of the workpiece. By generating a light beam of constant frequency (wavelength) and specified intensity, the transmitted light intensity was measured, which made it possible to determine the absorption capacity of the material. The wavelength was selected away from optical resonance to maintain the validity of the previously presented relationships for the non-resonant section [17]. The absorption coefficient value took into account the dimensions of the workpiece, which made it possible to record changes in the intensity of the light beam. As a result of measurements of the intensity of light transmitted through the workpiece, a system of linear algebraic equations (SLAE) was formed on the basis of Bouguer's law, whose solution provided obtaining the desired density distribution of the material.

¹ GOST 15130–86. *Silica Optical Glass. General Specifications*. Electronic Fund of Legal and Regulatory Documents. URL: <https://docs.cntd.ru/document/1200023786> (accessed: 31.10.2025).

It is known that within the framework of electromagnetic optics [18], the intensity of a light beam passing through a continuous medium can be described by the Bouguer-Lambert-Beer law (in the Gaussian system of units) [19]:

$$I = I_0 \exp(-\delta z),$$

where δ — absorption coefficient; z — distance traveled by the light beam. Taking into account the dispersion of light — the dependence of the optical properties of a medium on the frequency of the transmitted electromagnetic wave — and using the Lorentz dispersion model, based on the oscillatory model of the atom, it is possible to determine the relationship between density and absorption coefficient:

$$\delta(\omega) = \frac{\pi N e^2}{m c} \frac{\Gamma}{(\omega_0 - \omega)^2 + \frac{\Gamma^2}{4}},$$

where m and e — mass and charge of an electron excited by a light wave; c — lightspeed; ω_0 — resonant frequency of the electron oscillations; ω — frequency of the light wave (excitation); Γ — damping coefficient of the oscillations; $N = \frac{N_a \rho}{M}$ — number of atoms per unit volume (N_a — Avogadro's number; M — molar mass; ρ — density of the medium).

Due to the directly proportional dependence of the absorption coefficient on density, its distribution by volume was subsequently considered, implying that the change in density could also be found.

To ensure the formation of SLAE, Bouguer's law is represented as:

$$\sum_{h=1}^{u/2} \left(\frac{z}{\ln\left(\frac{I_u}{I_0}\right)} \cdot \frac{\delta_h}{u/2} \right) = -1,$$

where I_u, δ_h — intensity of the beam transmitted through the workpiece for the u -th experiment and the average value of the absorption coefficient for the h -th element in the u -th experiment, respectively; $z = \text{const}$ — dimensions of the workpiece; $I_0 = \text{const}$ — intensity of the generated light beam. Note that a system of q elements with an equal number of elements on the edge was considered, from which it follows that the number of equations $u = 2 \cdot \sqrt{q}$ with the number of unknowns $l = h = q$. Writing the SLAE in matrix form, we obtain:

$$A \cdot x = b,$$

where $A_{u \times l}$ — main matrix of the system; x_l — vector of unknowns; b_u — vector of free terms.

Assuming a continuous and smooth density distribution over the volume, the absorption coefficient distribution is represented as a two-dimensional polynomial of p -th degree. In this case, the number of unknowns will be independent of the number of elements and will be $l = (p + 1)^2$. Conversely, the degree of system discretization and the number of elements will be determined by the steady-state solution to the SLAE and the corresponding required polynomial degree. In other words, it becomes possible to manipulate the data for solving an indefinite SLAE, which is important for analyzing the obtained results to provide finding an approximate solution.

Writing the Legendre polynomial using the Rodrigues formula [20] for each of the coordinates (x, y):

$$P^v = P(x) = CV_t \cdot \frac{1}{2^t \cdot t!} \cdot \frac{d^t}{dx^t} (x^2 - 1)^t,$$

$$P^w = P(y) = CW_t \cdot \frac{1}{2^t \cdot t!} \cdot \frac{d^t}{dy^t} (y^2 - 1)^t,$$

where $t = (0, \dots, p)$ — constant; P^v, P^w — tensors of the first kind ($v = w = (1, \dots, t + 1)$); CV_p, CW_p — unknown coefficients of the polynomial; $x(x_h), y(y_h)$ — coordinates of the h -th element, the desired distribution of the absorption coefficient is represented through the elementwise sum of the corresponding second-rank tensor:

$$\delta_h = \text{sum}(P^v \otimes P^w) = \text{sum}(\Delta) = \sum_{v=1}^p \sum_{w=1}^p \Delta^{vw}.$$

A pseudosolution (approximate solution) of the resulting uncertain system of equations can be found by the least squares method [21]:

$$x = A^+ b = V \Sigma^+ U^* b,$$

where A^+ — Moore-Penrose pseudoinverse matrix, determined by the singular value decomposition (SVD) [21] of the underlying matrix A .

It should be noted that when finding δ_h , due to the properties of the Legendre polynomial used, in particular its orthogonality on the interval $[-1, 1]$, the origin of the coordinate system (X, Y) was determined at the geometric center of the workpiece, and the solution was found in dimensionless form by coordinate:

$$x = \frac{2 \cdot x_h}{z}; y = \frac{2 \cdot y_h}{z}.$$

The computational assessment of the density distribution across the workpiece volume (virtual experiment) was conducted in the MATLAB software package. The results of solving SLAE of various dimensions are presented for the initial data shown in Table 1.

Table 1

Initial Data for Calculation

z , [m]	I_0 , [W/m ²]	λ , [nm]	$\kappa_{\min} / \kappa_{\max}$
0.03	1000	200	$5.768 \cdot 10^{-9} / 5.432 \cdot 10^{-9}$

Note: Values $\kappa_{\min} / \kappa_{\max}$ are given in accordance with the nominal value for quartz glass² and taking into account the results [22].

As the results of the experiment, and also for the possibility of monitoring the reliability of the sought solution, an array of data for I_i (intensity of the beam transmitting through the workpiece) was used, obtained for the following distribution of the absorption coefficient:

$$\delta(x, y) = \frac{\delta_{\min} + \delta_{\max}}{2} + \left(\frac{\delta_{\max} - \delta_{\min}}{2} \right) \cdot \sin(4 \cdot x) \cdot \cos(4 \cdot y).$$

The distribution option selected for the example is due to the greatest impact of the 4th harmonic of the disturbance (inhomogeneity) on the splitting of the operating frequency of the HRG resonator [9].

Research Results. Figures 2–5 show comparison graphs of the obtained solutions to uncertain SLAE of different dimensions. In each figure (here and below for similar figures), the absorption coefficient distribution based on the experimental points (linearly connected) and associated with the discretization in the X -axis direction for the Y value is shown in green. The result of the SLAE solution, that is, a polynomial approximation, which is also true for distribution surfaces, is shown in blue. Index i at y in the figure captions denotes the i -th coordinate along axis y .

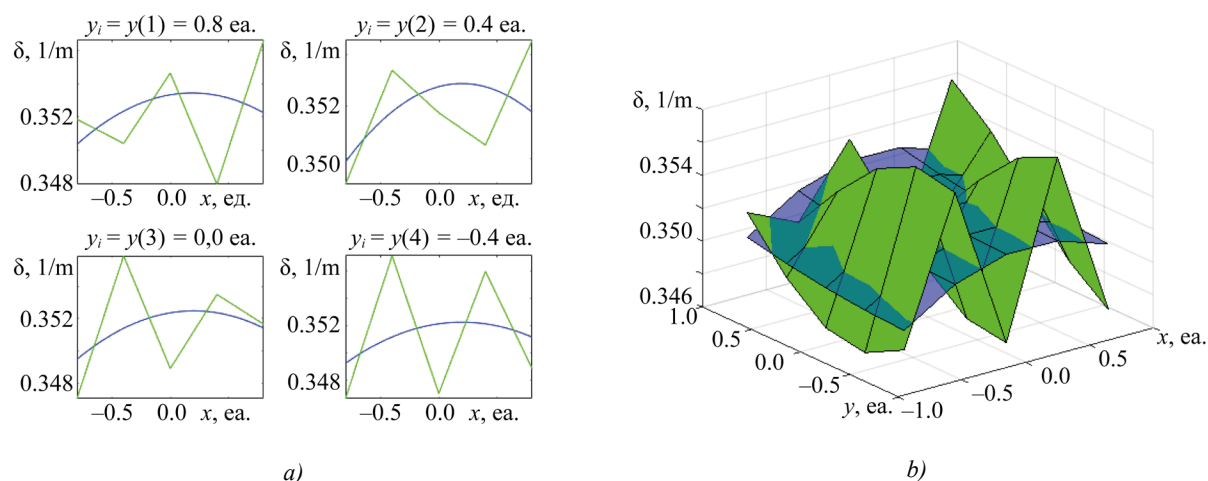


Fig. 2. Result of solving rectangular SLAE ($p = 2$; $q = 25$), dimension of matrix A — $[10 \times 9]$;

a — two-dimensional slice of the absorption coefficient distribution along x ;

b — three-dimensional representation of the distribution of the absorption coefficient along x, y

² GOST 15130–86. Silica Optical Glass. General Specifications. Electronic Fund of Legal and Regulatory Documents. URL: <https://docs.cntd.ru/document/1200023786> (accessed: 10.10.2025).

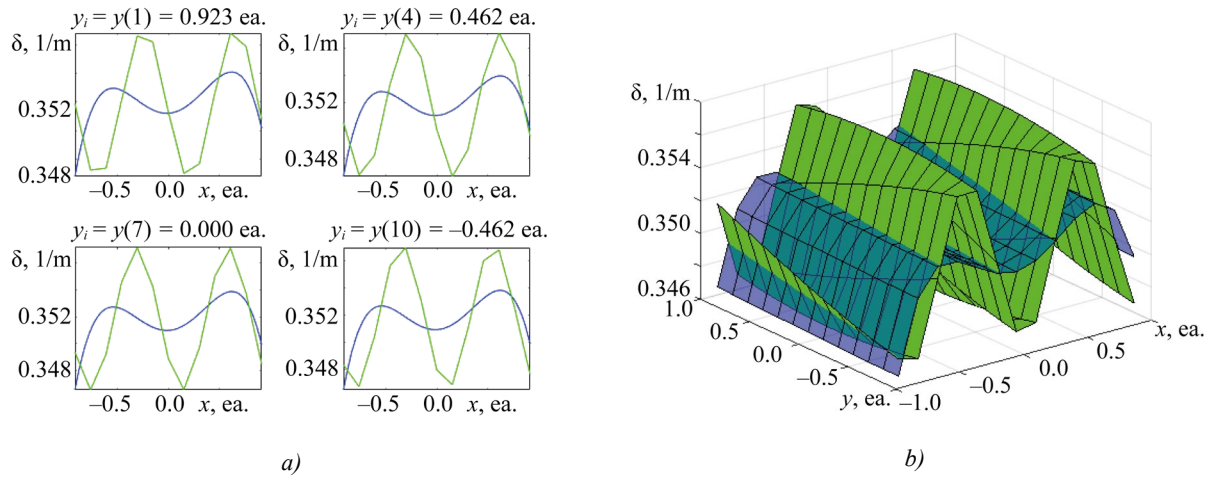


Fig. 3. Result of solving rectangular SLAE ($p = 4$; $q = 169$), dimension of matrix A — $[26 \times 25]$;
 a — two-dimensional slice of the absorption coefficient distribution along x ;
 b — three-dimensional representation of the distribution of the absorption coefficient along x, y

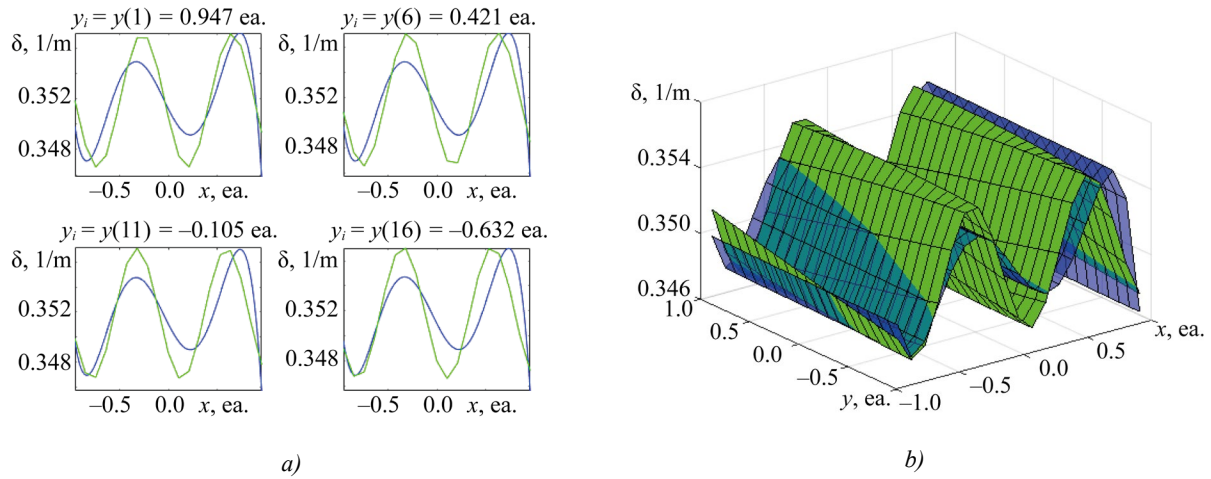


Fig. 4. Result of solving rectangular SLAE ($p = 5$; $q = 361$), dimension of matrix A — $[38 \times 36]$;
 a — two-dimensional slice of the absorption coefficient distribution along x ;
 b — three-dimensional representation of the distribution of the absorption coefficient along x, y

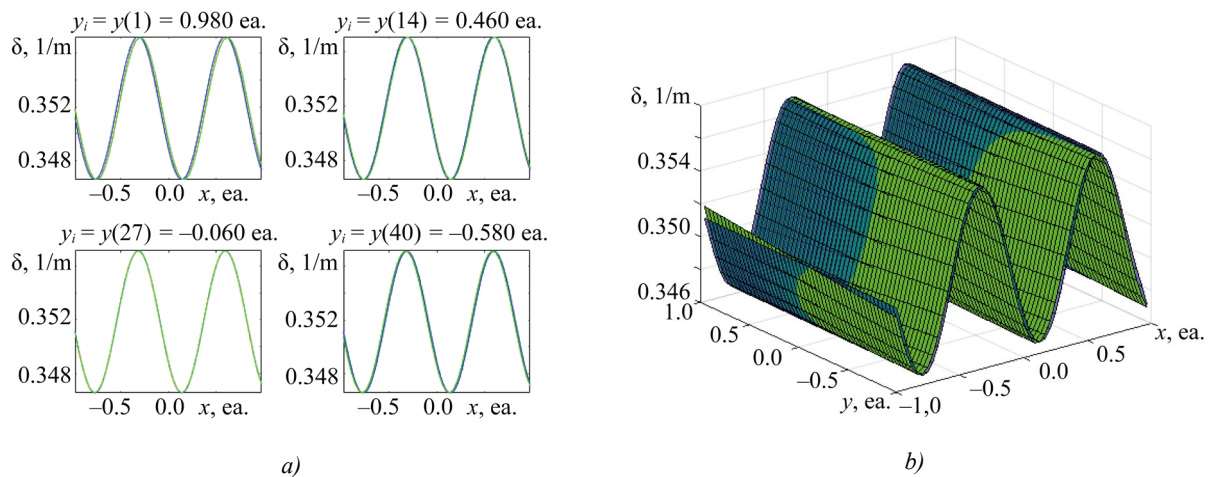


Fig. 5. Result of solving square SLAE ($p = 9$; $q = 2500$), dimension of matrix A — $[100 \times 100]$;
 a — two-dimensional slice of the absorption coefficient distribution along x ;
 b — three-dimensional representation of the distribution of the absorption coefficient along x, y

In addition, Figures 6–9 present supplementary calculation cases for discussing the issue of solvability of indefinite SLAE, as well as the application of the proposed method in the presence of macrodefects of the workpiece.

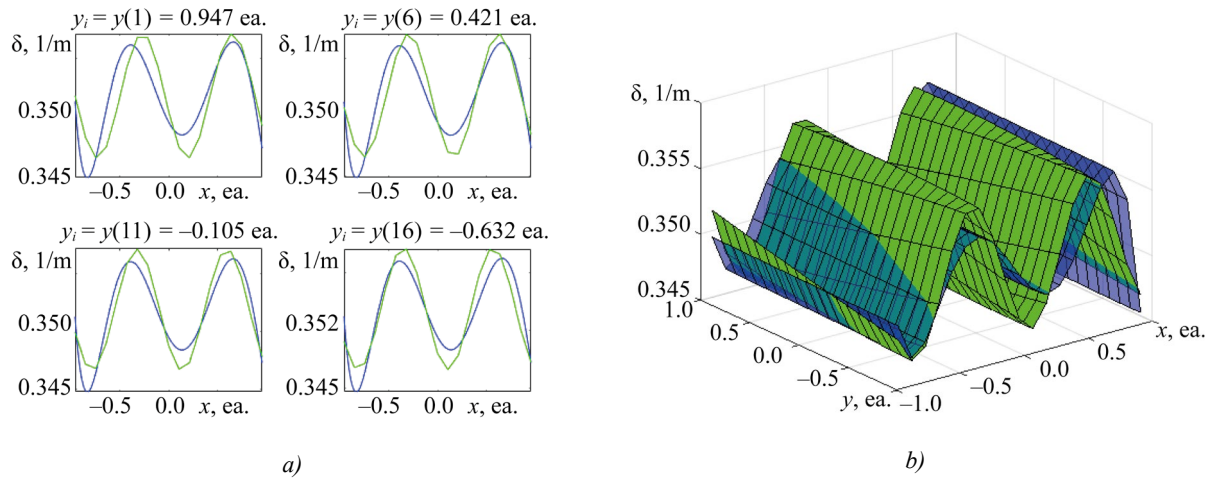


Fig. 6. Result of solving rectangular SLAE ($p = 6$; $q = 361$), dimension of matrix A — $[38 \times 49]$;
a — two-dimensional slice of the absorption coefficient distribution along x ;
b — three-dimensional representation of the distribution of the absorption coefficient along x, y

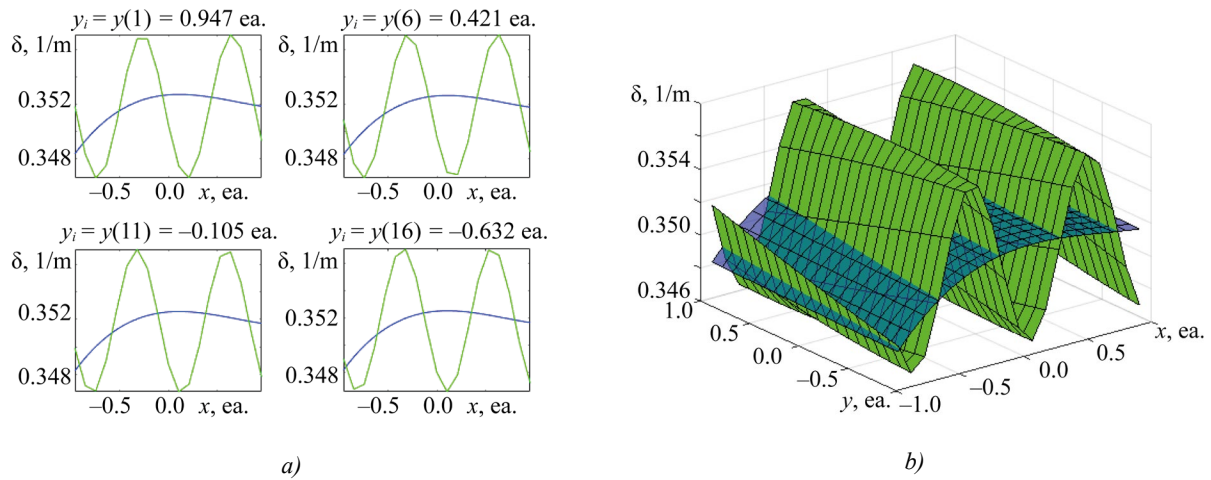


Fig. 7. Result of solving rectangular SLAE ($p = 3$; $q = 361$), dimension of matrix A — $[38 \times 16]$;
a — two-dimensional slice of the absorption coefficient distribution along x ;
b — three-dimensional representation of the distribution of the absorption coefficient along x, y

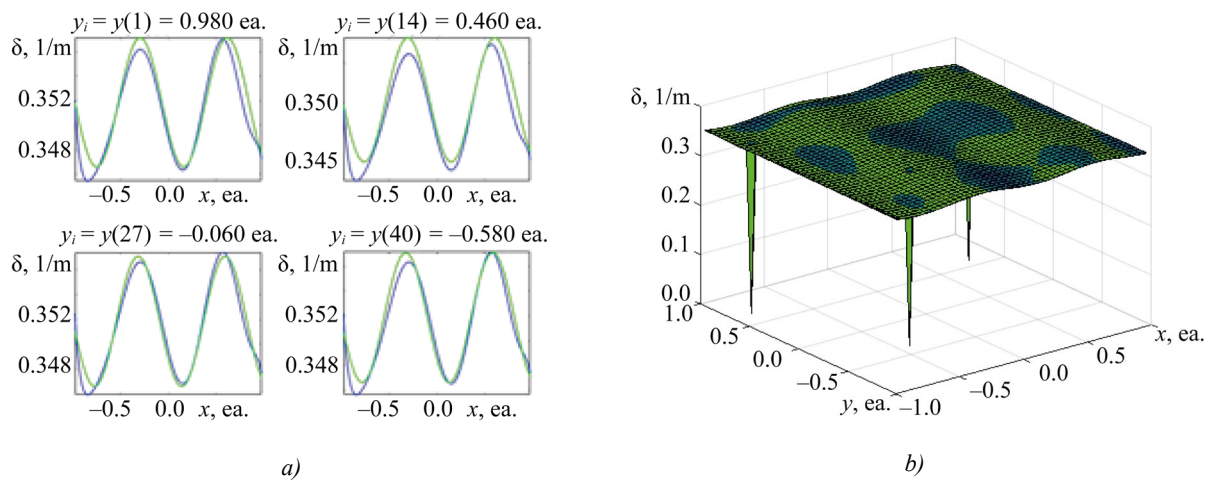


Fig. 8. Result of solving square SLAE ($p = 9$; $q = 2500$), dimension of matrix A — $[100 \times 100]$;
a — two-dimensional slice of the absorption coefficient distribution along x ;
b — three-dimensional representation of the distribution of the absorption coefficient along x, y

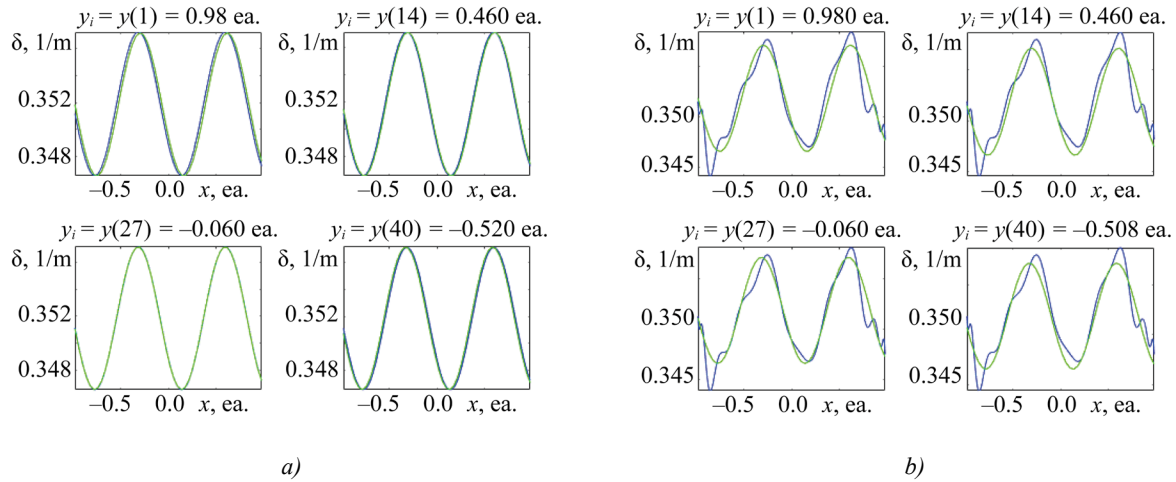


Fig. 9. Result of solving square SLAE ($p = 20$; $q = 2500$), dimension of matrix A — $[100 \times 441]$;
a — two-dimensional slice of the absorption coefficient distribution along x for a defect-free solution;
b — two-dimensional slice of the absorption coefficient distribution along x for a solution with defects

Figure 10 shows the differences in the distribution of the desired value from the distribution obtained on the basis of the results of solving the SLAE.

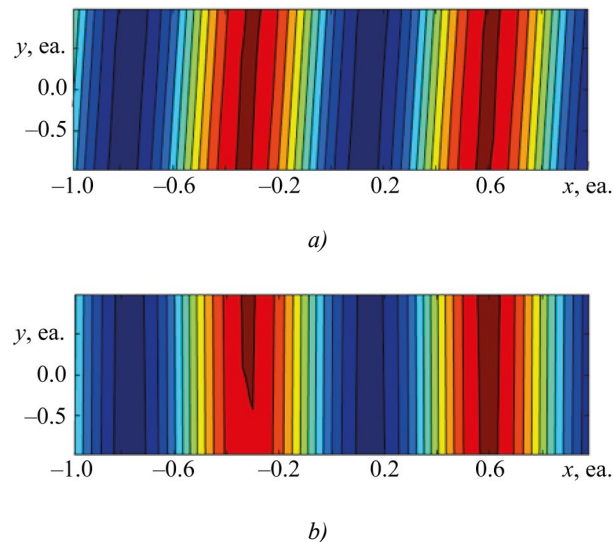


Fig. 10. Result of solving square SLAE ($p = 9$; $q = 2500$), dimension of matrix A — $[100 \times 100]$;
a — distribution of the desired value according to experimental data;
b — distribution of the desired value based on the results of solving the SLAE

Discussion. Analyzing the data obtained by the proposed identification method (Figs. 2–5), it can be noted that with a sufficient number of measurements (system discretization), it is possible to obtain a solution to an uncertain system with the required accuracy. The results for overdetermined systems turned out to be comparable to the results of underdetermined systems [23], although in some cases, the values were inferior in accuracy. For example, the data presented in Figure 4 demonstrated lower accuracy compared to the results for the matrix dimension A — $[38 \times 49]$, obtained by the 6th-degree polynomial (Fig. 6).

In case of significant imbalance between the number of equations and unknowns (for example, for the case of severe overdetermination — Fig. 7), a satisfactory solution could not be found within the presented calculations. Even when obtaining an approximate solution with minimal error, some differences between the reconstructed distribution and the experimental one were still present. This may be due to the features of the proposed method, which requires separate study. For clarity, Figure 10 shows a comparison of the distributions in a color gradient.

At the same time, it was established that the proposed method is sensitive to the presence of macrodefects (pores, bubbles) in the workpiece. Figure 8 shows the result obtained on the basis of the experimental data with three point defects, which correspond to a zero absorption coefficient. When compared to Figure 5 (which presents the results with the highest accuracy), it is evident that the distribution is distorted, and an additional low-frequency harmonic appears on the graph, indicating possible defects. As the degree of the polynomial increases, the solution continues to change, describing a more complex distribution (Fig. 9).

It should be noted that in the case of physical measurements, the presence of macrodefects can significantly affect the results, as this violates the assumption of normal beam incidence on the interface of optically transparent media (pores and bubbles often have curved surfaces). Despite this, the presented method can be improved by taking these aspects into account.

The use of a polynomial increased the stability of the solution to rectangular SLAE. However, it should be remembered that real systems constructed on the basis of experimental data with certain measurement errors create additional complexities that require the use of other methods for calculating SLAE, for example, with solution regularization [24]. Therefore, it is advisable to avoid significant underdetermination and overdetermination of the system. In defense of the method used to solve SLAE, it should be noted that optimization of the relationship between the polynomial degree and the discretization level is required to find an approximate solution with minimal effort. The analysis of the resulting system of equations shows that even for the two-dimensional case, as the element size decreases, the system remains rectangular and becomes increasingly underdetermined — in such systems, the number of equations (u) is less than the number of unknowns (1). Such SLAE have more than one solution and are characterized by a high condition number of the fundamental matrix (matrix A) of the system, which can cause significant difficulties in finding the roots. Taking this into account, in order to control the ratio of the number of equations and unknowns, an assumption was made about the smoothness and continuity of the distribution of the sought quantity over the volume. This assumption is based on the use of the highest quality quartz glass for the manufacture of the HRG resonator, in which the presence of macrodefects³ (bubbles, cavities, cracks) is not allowed [25]. This assumption is consistent with the constitutive relations that are valid both for a constant value of the refractive index and for a slowly varying, continuous function in an optical medium [19].

When discussing practical feasibility, it is necessary to estimate the required measurement error. As noted previously [22], the maximum density spread for quartz glass over the volume of the workpiece (resonator), due to the imperfect geometric parameters of the periodicity cell element, is $\pm 3\%$ of the nominal value. Due to the proportional dependence of the absorption coefficient on density, the spread of the absorption coefficient over the volume will be similar. In this case, the degree of impact of the spread of the absorption coefficient on the intensity of the light beam passing through the workpiece can be estimated at the level of 0.03%. Consequently, the measurement accuracy must be at least 0.005%. Reaching this level of accuracy requires a certain approach to organizing the field experiment, specifically the use of stable light sources (lasers) with active feedback for thermal and current stabilization, light receivers (photodetectors) with low dark current, and noise suppression from various sources (temperature fluctuations, vibration, electromagnetic interference, etc.). This ultimately allows for an accuracy of approximately 0.001%.

Conclusion. Thus, in this study, we proposed and tested a method for identifying imperfections in the form of inhomogeneity in quartz glass at the preform stage, intended for the fabrication of a resonator, a sensitive element of the HRG. The identification was based on the optical properties of quartz glass, specifically its complex refractive index, whose imaginary part is related to the absorption coefficient and, consequently, to the density of the material. It has been demonstrated that, by conducting a series of experiments measuring the intensity of a light beam transmitted through a workpiece, it is possible to reconstruct the unknown distribution of the absorption coefficient and density over the volume with high accuracy (at least 0.005% of the measured value). Here, the distribution is represented through an orthogonal Legendre polynomial of sufficient degree, maintaining an optimal ratio between the number of polynomial coefficients and the degree of system discretization, determined by the magnitude of the harmonic of the imperfection distribution. It

³ GOST 15130–86. *Silica Optical Glass. General Specifications*. Electronic Fund of Legal and Regulatory Documents. URL: <https://docs.cntd.ru/document/1200023786> (accessed: 31.10.2025).

has been established that a ninth-degree polynomial can be used to identify the fourth harmonic of density variation (as a key parameter) with 100 tests. It is important to emphasize that conducting such work at the early stages of production can optimize the shaping process, allowing for the selection of the most effective directions of density distribution throughout the volume to minimize the impact on the splitting of the operating frequency of the resonator.

References

1. Peshekhonov VG. The Outlook for Gyroscopy. *Gyroscopy and Navigation*. 2020;11:193–197. <https://doi.org/10.1134/S2075108720030062>
2. Perelyaev SE. Current State of Wave Solid-State Gyroscopes. Development Prospects in Applied Gyroscopy. In: *Proc. XXX Anniversary St. Petersburg International Conference on Integrated Navigation Systems*. St. Petersburg: Central Scientific Research Institute “Elektropribor”; 2023. p. 431–435. (In Russ.)
3. Volchikhin AI, Volchikhin DM, Malyutin DM, Matveev VV, Raspopov VYa, Telukhin SV, et al. Wave Solid-State Gyroscopes (Analytical Review). *News of Tula State University. Technical Sciences*. 2017;(9–2):59–78.
4. Shishakov KV, Khvorenkov VV. *Solid-State Wave Gyroscopes: Wave Processes, Control, System Integration*. Monograph. Izhevsk: Kalashnikov Izhevsk State Technical University; 2018. 264 p. (In Russ.)
5. Maslov AA, Maslov DA, Ninalalov IG, Merkuryev IV. Hemispherical Resonator Gyros (An Overview of Publications). *Gyroscopy and Navigation*. 2023;14(1):3–25. <https://doi.org/10.1134/S2075108723010054>
6. Delhay F. HRG by Safran: The Game-Changing Technology. In: *Proc. IEEE International Symposium on Inertial Sensors and Systems (INERTIAL)*. New York City: IEEE; 2018. P. 173–177. <https://doi.org/10.1109/ISISS.2018.8358163>
7. Perelyaev SE. Current State and Scientific and Technical Forecast of the Perspectives of Application of Foreign Hemispherical Resonator Gyros (Analytical Review of Foreign Materials). *Navigation News*. 2020;(3):14–28.
8. Klimov DM, Zhuravlev VF, Zhbanov YuK. *Quartz Hemispherical Resonator (Solid-State Wave Gyroscope)*. Monograph. Moscow: Kim L.A.; 2017. 193 p. (In Russ.)
9. Lunin BS, Matveev VA, Basarab MA. *Wave Solid-State Gyroscopes: Theory and Technology*. Moscow: Radiotekhnika; 2014. 176 p. (In Russ.)
10. Merkuryev IV, Podalkov VV. *Micromechanical and Wave Solid-State Gyroscopes Dynamics*. Moscow: Fizmatlit; 2009. 226 p. (In Russ.)
11. Lynch DD. Vibratory Gyro Analysis by The Method of Averaging. In: *Proc. 2nd St. Petersburg Int. Conf. on Gyroscopic Technology and Navigation*. St. Petersburg: Centr. Sci.-Res. Inst. “Elektropribor”; 1995. P. 26–34.
12. Rozelle D. The Hemispherical Resonator Gyro: From Wineglass to the Planets. *Advances in the Astronautical Sciences*. 2009;134:1157–1178.
13. Polunin PM, Shaw SW. Self-Induced Parametric Amplification in Ring Resonating Gyroscopes. *International Journal of Non-Linear Mechanics*. 2017;94:300–308. <https://doi.org/10.1016/j.ijnonlinmec.2017.01.011>
14. Zotov SA, Trusov AA, Shkel AM. Three-Dimensional Spherical Shell Resonator Gyroscopes Fabricated Using Wafer-Scale Glassblowing. *Journal of Microelectromechanical Systems*. 2012;21(3):509–510. <https://doi.org/10.1109/JMEMS.2012.2189364>
15. Saypulaev MR, Merkuryev IV, Solovyev AV, Tarasov AN. Study on Free Oscillations of a Micromechanical Gyroscope taking into Account the Nonorthogonality of the Torsion Axes. *Advanced Engineering Research (Rostov-on-Don)*. 2021;21(3):231–238. <https://doi.org/10.23947/2687-1653-2021-21-3-231-238>
16. El-Sheimy N, Youssef A. Inertial Sensors Technologies for Navigation Applications: State of the Art and Future Trends. *Satellite Navigation*. 2020;1(2):1–22. <https://doi.org/10.1186/s43020-019-0001-5>
17. Saleh B, Teich M. *Optics and Photonics: Principles and Applications*, 2nd ed. In 2 vol. Vol. 2. Dolgoprudnyi: Intellect; 2012. 760 p. (In Russ.)
18. Born M, Wolf E. *Principles of Optics: 60th Anniversary Edition*, Cambridge: Cambridge University Press; 2019. 992 p.
19. Akhmanov SA, Nikitin SYu. *Physical Optics*. 2nd ed. Moscow: Nauka; 2004. 654 p. (In Russ.)

20. Korn GA, Korn Th. *Mathematical Handbook for Scientists and Engineers: Definitions. Theorems. Formulas*, 6th ed. St. Petersburg: Lan'; 2003. 831 p. (In Russ.)
21. Demmel JW. *Computational Linear Algebra. Theory and Applications*. Moscow: Mir; 2001. 430 p. (In Russ.)
22. Shevchenko SA, Melnikov BE. Fused Quartz Imperfections and Their Influence on the CVG Resonator Dynamics. *Izvestiya of Saratov University. Mathematics. Mechanics. Informatics*. 2024;24(4):611–618. <https://doi.org/10.18500/1816-9791-2024-24-4-611-618>
23. Björck Å. *Numerical Methods in Matrix Computations*. New York, NY: Springer; 2015. 800 p.
24. Buccini A, Gazzola S, Onisk L, Pasha M, Reichel L. Projected Iterated Tikhonov in General Form with Adaptive Choice of the Regularization Parameter. *Numerical Algorithms*. 2025;100:1617–1637. <https://doi.org/10.1007/s11075-025-02072-2>
25. Bubis Iya, Weidenbach VA, Dukhoped II, Kuznetsova SM (ed), Okatova MA (ed). *Handbook of an Optical Technologist*. Leningrad: Mashinostroenie; 2009. 244 p. (In Russ.)

About the Authors:

Sergei A. Shevchenko, Engineer of the Higher School of Mechanics and Control Processes, Institute of Physics and Mechanics, Peter the Great St. Petersburg Polytechnic University (29 B, Polytechnicheskaya Str., St. Petersburg, 195251, Russian Federation), [SPIN-code](#), [ResearchGate](#), [ORCID](#), [ScopusID](#), shevchenko.sergei.a@yandex.ru

Ivan A. Popov, Senior Lecturer at the Advanced Engineering Technology School, Advanced Engineering School “Digital Engineering”, Peter the Great St. Petersburg Polytechnic University (29 B, Polytechnicheskaya Str., St. Petersburg, 195251, Russian Federation), [SPIN-code](#), [ResearchGate](#), [ORCID](#), popov_ia@spbstu.ru

Boris E. Melnikov, Dr.Sci (Eng.), Professor of the Higher School of Mechanics and Control Processes, Institute of Physics and Mechanics, Peter the Great St. Petersburg Polytechnic University (29 B, Polytechnicheskaya Str., St. Petersburg, 195251, Russian Federation), [SPIN-code](#), [ResearchGate](#), [ORCID](#), melnikov_be@spbstu.ru

Claimed Contributorship:

SA Shevchenko: conceptualization, investigation.

IA Popov: software.

BE Melnikov: supervision.

Conflict of Interest Statement: the authors declare no conflict of interest.

All authors have read and approved the final version of manuscript.

Об авторах:

Сергей Александрович Шевченко, инженер, «Высшая школа механики и процессов управления. Физико-механический институт» Санкт-Петербургского политехнического университета Петра Великого (195251, Российская Федерация, г. Санкт-Петербург, ул. Политехническая, д. 29 Б), [SPIN-код](#), [ResearchGate](#), [ORCID](#), [ScopusID](#), shevchenko.sergei.a@yandex.ru

Иван Алексеевич Попов, старший преподаватель, «Высшая школа передовых инженерных технологий передовой инженерной школы «Цифровой инжиниринг» Санкт-Петербургского политехнического университета Петра Великого (195251, Российская Федерация, г. Санкт-Петербург, ул. Политехническая, д. 29 Б), [SPIN-код](#), [ResearchGate](#), [ORCID](#), popov_ia@spbstu.ru

Борис Евгеньевич Мельников, доктор технических наук, профессор, «Высшая школа механики и процессов управления. Физико-механический институт» Санкт-Петербургского политехнического университета Петра Великого (195251, Российская Федерация, г. Санкт-Петербург, ул. Политехническая, д. 29 Б), [SPIN-код](#), [ResearchGate](#), [ORCID](#), melnikov_be@spbstu.ru

Заявленный вклад авторов:

С.А. Шевченко: разработка концепции, проведение исследования.

И.А. Попов: разработка программного обеспечения.

Б.Е. Мельников: научное руководство.

Конфликт интересов: авторы заявляют об отсутствии конфликта интересов.

Все авторы прочитали и одобрили окончательный вариант рукописи.

Received / Поступила в редакцию 04.08.2025

Reviewed / Поступила после рецензирования 01.09.2025

Accepted / Принята к публикации 12.09.2025

MECHANICS МЕХАНИКА



UDC 539.3

Original Theoretical Research

<https://doi.org/10.23947/2687-1653-2025-25-4-2184>

Analysis of Deformation Energy Dissipation in Reinforced-Layer Pavement

Artem N. Tiraturyan

Don State Technical University, Rostov-on-Don, Russian Federation

✉ tiraturjan@list.ru

EDN: JZUDVV

Abstract

Introduction. The design of road pavements for highways is a key stage of project development, directly impacting their durability and operational costs. In recent years, in the context of increasing traffic intensity and dynamic loads, technologies for strengthening roadbeds and bases, such as geosynthetic reinforcement and stabilized layers, have become widespread, making the study on their efficiency a challenge. Literature notes the practical advantages of reinforced layers — increased load-bearing capacity and reduced deformation. However, models for energy dissipation under dynamic impacts in structures with such layers are underdeveloped. Theoretical approaches to analyzing energy dissipation, including linear-elastic and viscoelastic models and finite element methods, have been primarily applied to traditional structures. Their adaptation to reinforced and stabilized layers requires further development, as there remain gaps in the quantitative comparison of efficiency by location and rigidity of reinforcements. The objective of the presented work is to analyze the dissipation of deformation energy in the structure of road pavements with different options for the arrangement of reinforced layers, and to determine optimal design solutions that contribute to increasing the durability of road pavements. To achieve this, it is required to formalize an energy dissipation model for structures with reinforcements, conduct a comparative analysis of different locations and rigidity levels of the layers.

Materials and Methods. The research utilized a comprehensive approach to the analysis of deformation processes in layered media using road pavements as an example, involving both a calculation tool and modern experimental equipment. As a calculation tool, a mathematical model of a layered half-space in an axisymmetric formulation in a cylindrical coordinate system was used. It was based on the solution to the system of dynamic Lamé equations and allowed for the construction of amplitude-time characteristics of vertical displacements and impact loading impulse, on the basis of which it was possible to construct dynamic hysteresis loops. The FWD PRIMAX 1500 shock loading unit was used as experimental equipment, which made it possible to register similar characteristics of the road pavement response under field conditions at a load equivalent to the calculated one.

Results. The study involved numerical modeling of road pavement structures traditionally used in the Russian Federation and so-called full-depth road pavements, which were composed almost entirely of materials reinforced with binders. Dynamic hysteresis loops were constructed, and a comparative analysis of the results was provided. A numerical experiment revealed that strengthening only the subgrade layer, even without installing a reinforced base layer beneath the asphalt concrete, reduced the amount of dissipated deformation energy. It was also concluded that the elastic modulus of the underlying half-space simulating the subgrade had the greatest impact on the amount of dissipated energy.

Discussion. The greatest effect, both technical and economic, can be reached by strengthening the top of the roadbed while preserving the loose layers in the base of the road structure. This solution will bring the functioning of the road surface closer to the elastic stage and at the same time reduce the risk of cracks appearing on the surface of the pavement due to an excessively rigid layer of reinforced base.

Conclusion. On the basis of the constructed dynamic hysteresis loops, it is shown that a reduction in the magnitude of deformation energy can be obtained both by installing reinforced layers of the road surface throughout its entire depth, and by locally strengthening the underlying half-space layer and an additional base layer made of sand. The numerical experiment demonstrated that the use of reinforced base layers reduced the amount of deformation energy dissipation in the pavement structure by more than 2–3 times. Qualitative agreement between the experimental results and the numerical simulation results was shown.

Keywords: road pavements, energy dissipation, shock loading unit, dynamic hysteresis loops

Funding Information. The research was done with the financial support from the Russian Science Foundation (grant no. 24-29-00110), <https://rscf.ru/project/24-29-00110/>

Acknowledgements. The author would like to thank the Editorial board of the Journal and the reviewers for their professional analysis of the article and recommendations for its correction.

For Citation. Tiraturyan AN. Analysis of Deformation Energy Dissipation in Reinforced-Layer Pavement. *Advanced Engineering Research (Rostov-on-Don)*. 2025;25(4):324–336. <https://doi.org/10.23947/2687-1653-2025-25-4-2184>

Оригинальное теоретическое исследование

Анализ диссипации энергии деформирования в дорожных одеждах с укрепленными слоями

А.Н. Тиратурян 

Донской государственный технический университет, г. Ростов-на-Дону, Российская Федерация

✉ tiraturjan@list.ru

Аннотация

Введение. Конструирование дорожных одежд автомобильных дорог — ключевой этап проектирования, напрямую влияющий на их долговечность и эксплуатационные расходы. В последние годы в условиях роста интенсивности и динамической нагрузки транспорта получили распространение такие технологии укрепления земляного полотна и оснований, как геосинтетические армирования и стабилизированные слои, что делает изучение их эффективности особенно актуальным. В литературе отмечаются практические преимущества укрепленных слоёв — повышение несущей способности и снижение деформаций. Однако недостаточно разработаны модели диссипации энергии при динамических воздействиях в конструкциях с такими слоями. Теоретические подходы к анализу рассеяния энергии, включая линейно-упругие и вязкоупругие модели и методы конечных элементов, в основном применялись к традиционным конструкциям, их адаптация для армированных и стабилизированных слоёв требует доработки, поскольку остаются пробелы в количественном сравнении эффективности по местоположению и жёсткости укреплений. Цель представленной работы — анализ диссипации энергии деформирования в структуре дорожных одежд с различными вариантами расположения укрепленных слоев и определение оптимальных конструктивных решений, способствующих повышению долговечности дорожных покрытий. Для ее достижения необходимо было формализовать модель диссипации энергии для конструкций с укреплениями, провести сравнительный анализ вариантов расположения и жёсткости слоёв.

Материалы и методы. В рамках исследования применен комплексный подход к анализу процессов деформирования слоистых сред на примере дорожных одежд, предполагающий применение как расчетного аппарата, так и современного экспериментального оборудования. В качестве расчетного аппарата использовалась математическая модель слоистого полупространства в осесимметричной постановке в цилиндрической системе координат, базирующаяся на решении системы динамических уравнений Ламе и позволяющая строить амплитудно-временные характеристики вертикальных перемещений и импульса ударного нагружения, на основе которых возможно построение динамических петель гистерезиса. В качестве экспериментального оборудования применена установка ударного нагружения FWD PRIMAX 1500, позволяющая регистрировать аналогичные характеристики отклика дорожной одежды в натуральных условиях при нагружении, эквивалентном расчетному.

Результаты исследования. В ходе исследования выполнено численное моделирование конструкций дорожных одежд, традиционно используемых в Российской Федерации, и так называемых полноглубинных дорожных одежд, состоящих практически полностью из материалов, укрепленных вяжущими. Построены динамические петли гистерезиса и дано сравнительное описание полученных результатов. В ходе численного эксперимента установлено, что укрепление только слоя земляного полотна даже без устройства укрепленного слоя основания под асфальтобетоном позволяет снизить величину рассеиваемой энергии деформирования. Также сделан вывод о том, что в наибольшей степени влияние на величину рассеиваемой энергии оказывает именно модуль упругости подстилающего полупространства, моделирующего земляное полотно.

Обсуждение. Наибольший эффект, как технический, так и экономический, может быть достигнут путем укрепления верха земляного полотна с сохранением несвязных слоев в основании дорожной конструкции. Это решение позволит приблизить функционирование дорожной одежды к упругой стадии и вместе с тем снизить риски появления трещин на поверхности покрытия из-за излишне жесткого слоя укрепленного основания.

Заключение. На основании построенных динамических петель гистерезиса показано, что снижение величины энергии деформирования может быть достигнуто как устройством укрепленных слоев дорожной одежды по всей ее глубине, так и локальным укреплением слоя подстилающего полупространства и дополнительного слоя основания из песка. В ходе численного эксперимента доказано, что устройство укрепленных слоев оснований более чем в 2–3 раза снижает величину диссипации энергии деформирования в структуре дорожной одежды. Продемонстрировано качественное совпадение результатов экспериментальных исследований и результатов численного моделирования.

Ключевые слова: дорожные одежды, диссипация энергии, установка ударного нагружения, петли динамического гистерезиса

Благодарности. Автор выражает благодарность редакционной коллегии журнала и рецензентам за профессиональный анализ статьи и рекомендации для ее корректировки.

Финансирование. Исследование выполнено при финансовой поддержке Российского научного фонда (грант № 24-29-00110), <https://rscf.ru/project/24-29-00110/>

Для цитирования. Тиратурия А.Н. Анализ диссипации энергии деформирования в дорожных одеждах с укрепленными слоями. *Advanced Engineering Research*. 2025;25(4):324–336. <https://doi.org/10.23947/2687-1653-2025-25-4-2184>

Introduction. One of the most important challenges facing the Russian road industry is providing a 24-year interrepair life for road pavement. One of the key approaches to solving this is improving approaches to pavement design. In the practice of the Russian Federation, it is common to design road pavement so that the rigidity of the layers increases from bottom to top, which stems from both historical design approaches and certain specific features of stress-strain state calculations using engineering methods and specialized nomograms. However, this approach does not fully reflect the efficiency of reinforced layers, such as subgrades or pavement bases.

In recent years, significant changes have occurred in the technologies and methods for calculating road pavement, associated with the introduction of software packages that implement both accurate and numerical schemes for the direct calculation of layered media [1]. In numerical methods, the most widespread are both classical finite element approaches [2], and more modern methods based on the use of spectral elements [3].

The finite element method is widely used in modeling the stress-strain state of asphalt concrete and cement concrete samples applied for the construction of road pavement and bases [4], as well as in calculating objects of limited size, typical for the practice of road and industrial-civil construction [5]. However, most of the aforementioned software packages implement a predominantly linear-elastic static formulation of the problem of determining the stress-strain state of road pavement. The wider adoption of numerical methods is constrained by the difficulty of their application to environments of unlimited volume [6]. At the same time, the actual deformation of road pavement layers is most accurately described by viscoelastic models or models that take into account the outflow of volumetric waves into infinite space [7].

As a rule, when solving problems in a viscoelastic dynamic formulation, the response of the road structure is considered either to an impact equivalent to the dynamic impact of the calculated load [8], or directly to the load from a wheel moving on the surface of the road pavement [9].

One of the most common modern solutions to this problem is the design of so-called full-depth road pavement structures, consisting entirely of layers reinforced with mineral and complex binders [10]. This approach has a number of advantages and disadvantages. The undoubted advantages include the overall high rigidity of the structures and the possibility of using recycled materials for the construction of base layers and their additional layers [11]. A number of scientific papers devoted to this topic note the good resistance of such structures to the accumulation of plastic deformations [12], the possibility of use under various natural and climatic conditions [13], and high manufacturability [14]. Disadvantages include high cost and, often with excessively increased rigidity of the base layers, a strong probability of cracking [15]. One of the most common types of crack formation for such structures is reflective cracking [16]. Some authors also note the need to take into account the specific properties of such structures in cold areas [17], and the influence of various types of defects on changes in the service life of the coating [18].

The concept of “perpetual” road pavement is well known. It involves increasing the rigidity of the structural layers of the road pavement from top to bottom, that is, when materials with a higher modulus of elasticity than asphalt concrete pavement layers are used as the base layer [19]. Such structures do provide extremely long interrepair life, which allows for the replacement of only the upper wear layers [20]. However, it is obvious that the cost and reliability of such structures are undoubtedly extremely high and often not reasonable [21]. Moreover, issues of providing proper adhesion between structural layers of different rigidity require additional research [22].

Thus, it can be argued that there are numerous approaches to pavement design, which, on the one hand, emphasizes the efficiency of such structures, but on the other, still leaves numerous questions unanswered. One of these is the study on deformation energy dissipation processes in layered media with reinforced layers, and, as a result, an assessment of the possibility of shifting deformation mechanisms to the elastic stage. The amount of energy dissipation is the most complete and physically-based characteristic reflecting the mechanisms of deformation in the structure of a multilayer medium, which can be measured and quantitatively assessed both by mathematical modeling tools and modern measuring equipment. Moreover, the use of this indicator is promising in the context of such a relevant area as the analysis of the life cycle of construction projects [23] and its implementation in information modeling technologies for monitoring the remaining useful life [24]. Thus, the objective of this work is to analyze the dissipation of deformation energy in the structure of road pavement with different options for the arrangement of reinforced layers and to evaluate optimal design solutions that contribute to increasing the durability of the road pavement.

Materials and Methods. The study utilized theoretical and experimental approaches to assess the deformation of the layered pavement environment. The research methodology is presented in Figure 1.

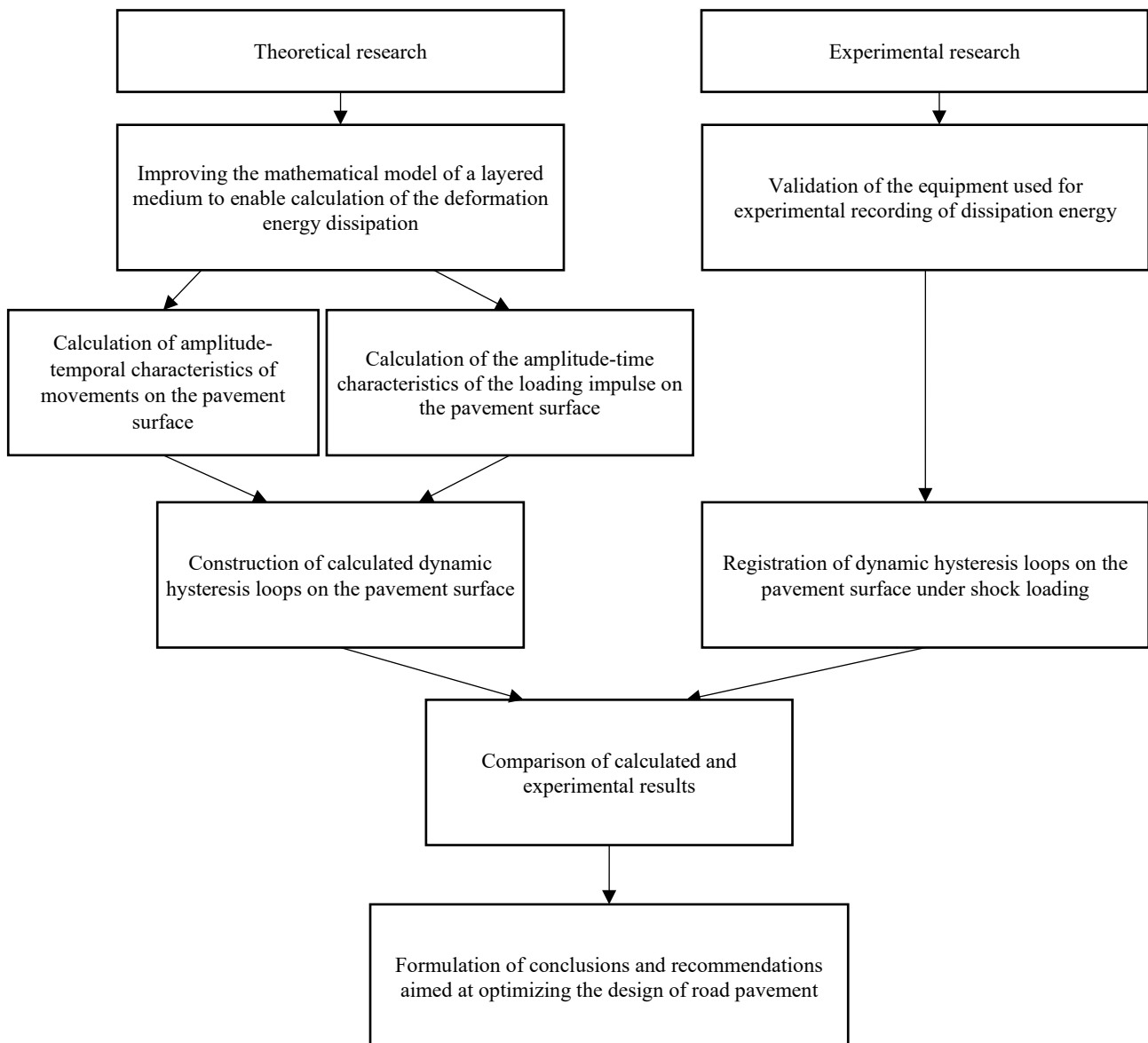


Fig. 1. Research methodology

The following road pavement designs are considered during the numerical and experimental studies. Design 1 represents a standard road pavement design in accordance with the current requirements of GOST R 71404: layer 1 is constructed of asphalt concrete, layer 2 is constructed of a crushed stone-sand mixture reinforced with a complex binder, layers 3 and 4 — dry bound macadam, and an antifrost capillary-breaking layer, respectively.

Structure 2 is an example of a full-depth road structure in which all layers are reinforced with organic or complex binders, which inevitably increases their elastic modulus. However, due to the use of expensive stabilizing and strengthening additives, as well as the inability to reduce the thickness of the structural layers within the current regulatory framework, the cost of this structure will significantly exceed that of Structure 1, which contains layers untreated with binders. Structure 3 is similar in its parameters to Structure 1, but layers 2 and 5 (subgrade soil) are reinforced with a complex binder. Structure 4 involves strengthening only the subgrade soil with a binder. The structures under consideration are shown schematically in Figure 2.

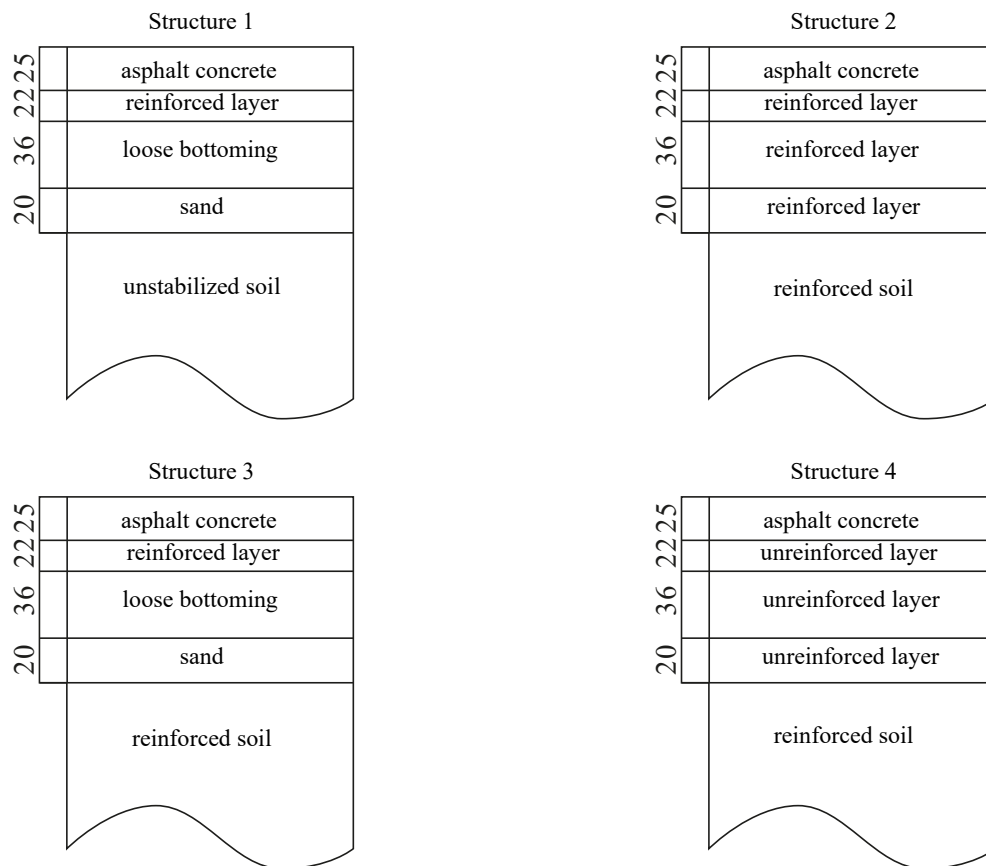


Fig. 2. Designs of simulated pavement

The theoretical approach consists in determining the stress-strain state of a layered medium under the impact of a dynamic load from a falling weight in an axisymmetric setting (Fig. 3).

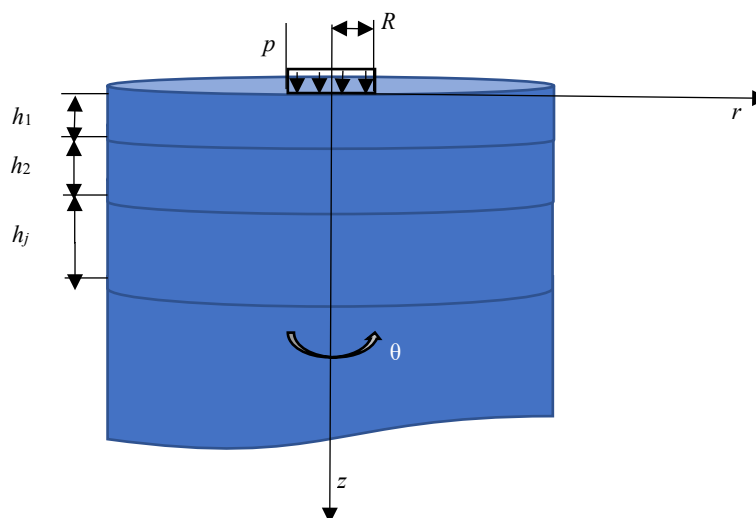


Fig. 3. Multilayer half-space

The equations of motion are as follows: [25, 26]:

$$(\lambda + \mu) \frac{\partial \theta}{\partial r} + \mu \Delta u_r - \frac{\mu}{r^2} u_r = \rho \frac{\partial^2 u_r}{\partial t^2}, \quad (1)$$

$$(\lambda + \mu) \frac{\partial \theta}{\partial z} + \mu \Delta u_z = \rho \frac{\partial^2 u_z}{\partial t^2},$$

where λ, μ — Lamé coefficients; u_r, u_z — radial and vertical components of the displacement vector; ρ — density of the material.

$$\theta = \frac{1}{r} \frac{\partial(r u_r)}{\partial r} + \frac{\partial u_z}{\partial z}, \quad (2)$$

where r — radial coordinate of the point at which the displacement is found.

The Fourier transformed system of equations (1) takes the form [27]:

$$\text{grad div } \mathbf{u}^j(r) - \frac{c_{j1}^2}{c_{j2}^2} \text{rot rot } \mathbf{u}^j(r) + c_{j1}^2 \mathbf{u}^j(r) = 0, \quad (3)$$

where c_{j1}, c_{j2} — reduced frequencies of oscillations.

$$c_{j1}^2 = \frac{\omega^2 R^2}{V_{pj}^2}; \quad (4)$$

$$c_{j2}^2 = \frac{\omega^2 R^2}{V_{sj}^2};$$

where ω — oscillation frequency, rad/s; R — radius of the loading area; V_{pj}, V_{sj} — velocities of longitudinal and transverse waves in the body.

This form of recording allows using the principle of elastic-viscoelastic correspondence, according to which the Lamé coefficients become complex, which, in turn, leads to the complex-valued nature of the reduced frequencies c_{j1}, c_{j2} .

Since the displacement u can be expressed through the scalar φ and vector (vortex) ψ components, the solution will be further considered in the form of the Lamé representation as:

$$\Delta \varphi + c_{j1}^2 \varphi = 0, \quad (5)$$

$$\Delta \psi + c_{j2}^2 \psi = 0$$

The boundary conditions of this problem in stresses are formulated as follows:

$$\begin{cases} \sigma_z(r, z, t)|_{z=0} = \begin{cases} p(t), r \in [0, R] \\ 0, r > R \end{cases} \\ \tau_{rz}(r, z, t)|_{z=0} \equiv 0 \end{cases} \quad (6)$$

At the boundaries of the layers, conditions of rigid adhesion are set, requiring the continuity of displacements $u_r(r, z, t)$ and $u_z(r, z, t)$, and stresses $\sigma_z(r, z, t), \tau_{rz}(r, z, t)$.

At infinity, the conditions for all stress and displacement components to tend to zero are satisfied. The initial conditions of this problem are defined as follows:

$$u_{r,z}(r, z, t)|_{t=0} = 0; \quad \frac{\partial u_{r,z}(r, z, t)}{\partial t}|_{t=0} = 0. \quad (7)$$

The further solution is constructed through applying the properties of the Hankel and Fourier integral transforms to the system of equations (3) and is presented in [28]. Since the solution to a non-stationary problem is considered, the method of discrete harmonic analysis is applied [29].

Experimental approach to assessing the deformation of layered road surfaces involves instrumental measurements of road pavement deformation parameters. The FWD PRIMAX 1500 shock loading unit is used for these measurements [30, 31] (Fig. 4). This unit consists of a trailer with a shock loading mechanism and a measuring beam mounted on it. This beam records the vertical component of the displacement speed, which is subsequently converted into absolute values of vertical displacement. Deformation characteristics are recorded by measuring sensors. Figure 5 shows the distances from them to the dynamic loading stamp of the unit. For this study, only sensor D1, located in the center of the stamp, is used. However, in the future, other sensors could be used to evaluate deformation energy distribution processes.

The difference between FWD and other shock loading units is the possibility of practically continuous recording, with a sampling spacing of 0.002 s, of the amplitude-time characteristics of displacements on the coating surface and the amplitude-time characteristics of the shock loading pulse, based on which it is possible to construct an experimental hysteresis loop.



Fig. 4. FWD for recording vertical displacements on a layer of organomineral mixture

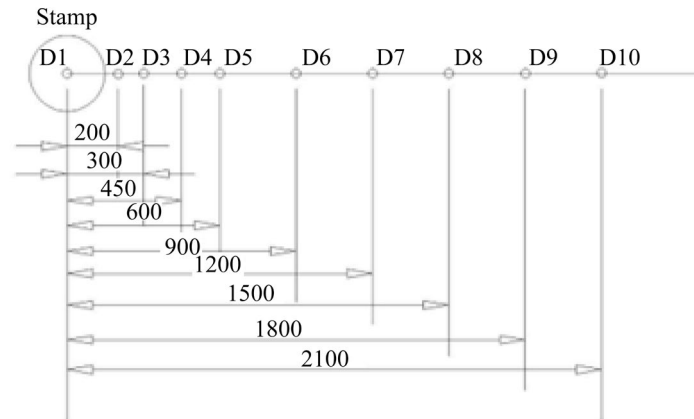


Fig. 5. Measurement design using the FWD (distances are given in mm)

This study examines road pavement structures with different rigidity ratios of the structural layers. The mechanical parameters are presented in Table 1.

Table 1

Road Pavement Designs for Modeling

Layers	Structure 1					Structure 2				
	E , MPa	ν	$tg\gamma$	h , cm	ρ , kg/m ³	E , MPa	ν	$tg\gamma$	h , cm	ρ , kg/m ³
1	3500	0.30	0.25	25	2400	3500	0.30	0.25	25	2400
2	1000	0.25	0.15	22	2400	1000	0.25	0.15	22	2400
3	450	0.25	–	36	1600	1000	0.25	0.15	36	2400
4	120	0.25	–	20	1900	500	0.25	–	20	2200
5	43	0.3	–	–	1900	400	0.3	–	–	2200
Structure 3					Structure 4					
E , MPa	ν	$tg\gamma$	h , cm	ρ , kg/m ³	E , MPa	ν	$tg\gamma$	h , cm	ρ , kg/m ³	E , MPa
3500	0.30	0.25	25	2400	3500	0.30	0.25	25	2400	3500
1000	0.25	0.15	22	2400	450	0.25	–	22	1600	1000
450	0.25	–	36	1600	450	0.25	–	36	1600	450
120	0.25	–	20	1900	120	0.25	–	20	1900	120
400	0.3	–	–	2200	400	0.3	–	–	2200	400

Research Results. The problem of determining the dynamic stress-strain state is solved and hysteresis loops are constructed on the surface of each of them using mathematical modeling for the above structures. The solution to the problem for a layered medium allows specifying the amplitude-time characteristics of the displacements $u(t)$ on the surface of the layered medium, and the amplitude-time characteristic of the impulse $F(t)$, from which the dynamic hysteresis loop, whose area determines the energy irreversibly dissipated in the medium, can be reconstructed [32, 33]. This curve is specified parametrically in accordance with dependence (8):

$$W = \int_0^t u(t) F(t) dt. \quad (8)$$

In the case of setting the dynamic hysteresis loop in the form of a data series containing information on discrete values of the actual load (F_i) and vertical displacements (u_i), corresponding to a given load, the area of the hysteresis curve is determined in accordance with (9):

$$W = \frac{1}{2} \left| \sum_{i=1}^{n-1} u_i F_{i+1} + u_n F_1 - \sum_{i=1}^{n-1} u_{i+1} F_i - u_1 F_n \right|. \quad (9)$$

Function $F(t)$ is described by the equation:

$$F(t) = F \sin\left(\frac{\pi t}{t_{\text{umn}}}\right) \quad (10)$$

where F — design load (taken equal to 57.5 kN); t — time of observation of the object deformation ($t = 0.1$ s); t_{umn} — pulse time ($t_{\text{umn}} = 0.03$ s).

The possibility of constructing the amplitude-time characteristic of a sawtooth pulse and a triangular pulse, which are often used to approximate the impact loading reproduced by FWD, is also implemented.

The design load for the simulation was a 57.5 kN drop load distributed over a 30 cm diameter area, which complied with road industry regulatory requirements. The deformation energy dissipation (W) was calculated at the impact point.

Taking into account the assumption of the need for the road pavement to operate in the elastic stage, allowed in domestic regulatory documents, as well as the fact that the energy value W is essentially a function of both the mechanical and geometric parameters of the studied medium, the problem of optimal design can be reduced to the equation:

$$W(E_j, h_j, \tan \gamma_j, \nu_j) \rightarrow \min, \quad (11)$$

where E_j — elastic moduli of the materials of the pavement layers; h_j — thickness of the pavement layers; γ_j — loss angles or other viscosity characteristics of the material of the layers; ν_j — Poisson's ratios of the materials of the layers.

The damping properties of individual layers are taken into account through introducing the loss tangent $\tan \gamma$, determined on the basis of the given oscillation frequencies:

$$\tan \gamma_j = \frac{\text{Im } c_j^2}{\text{Re } c_j^2}.$$

Figure 6 shows the calculated amplitude-time characteristics of the displacements on the surface of the simulated road pavements. Figure 7 presents various shock loading pulse shapes, in particular, sinusoidal, sawtooth, and triangular, corresponding to different shock load application scenarios. In this study, the sinusoidal shape is considered, as it best corresponds to the experimental loading reproduced by the FWD.

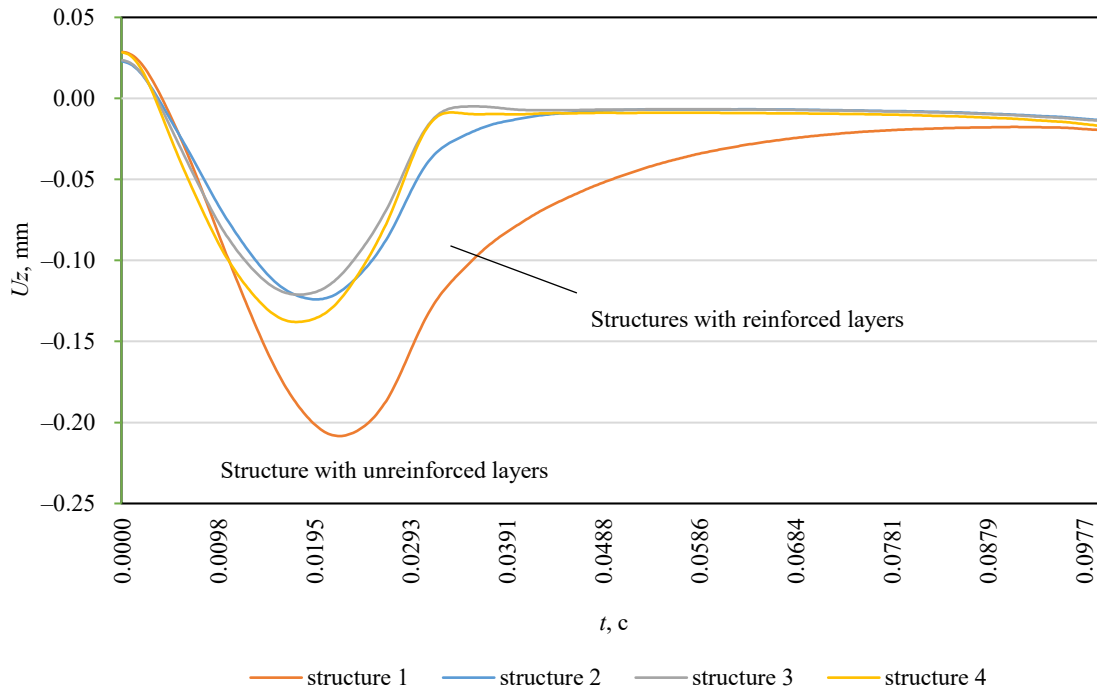


Fig. 6. Calculated amplitude-time characteristics of displacement on the surface of the studied structures

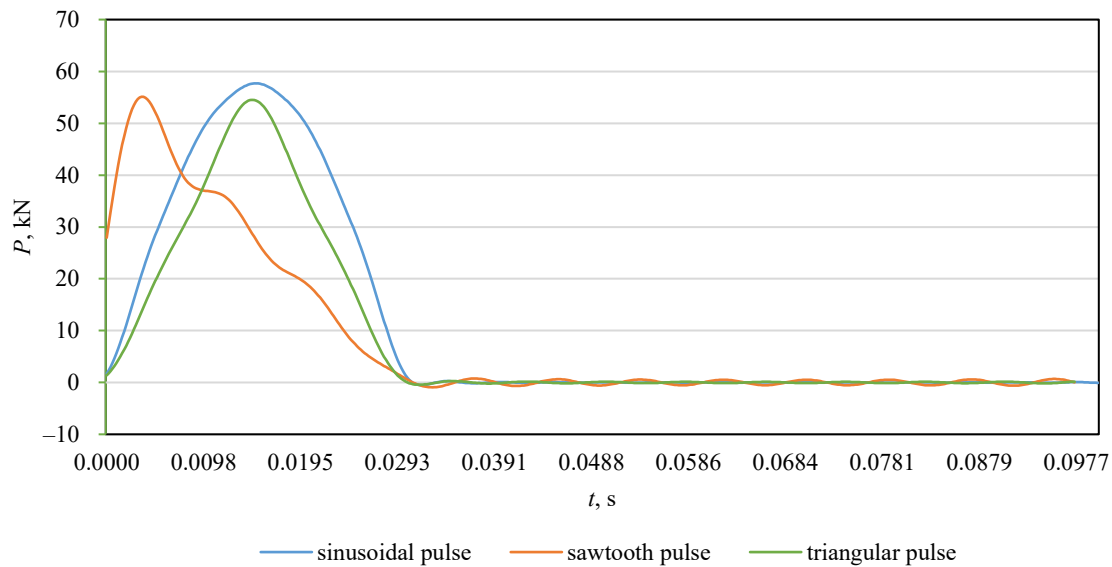


Fig. 7. Calculated load pulse shapes on the surface of the road pavement 4

The results of constructing dynamic hysteresis loops and the results of determining the dynamic deformation energy are presented in Figure 8 and in Table 2, respectively.

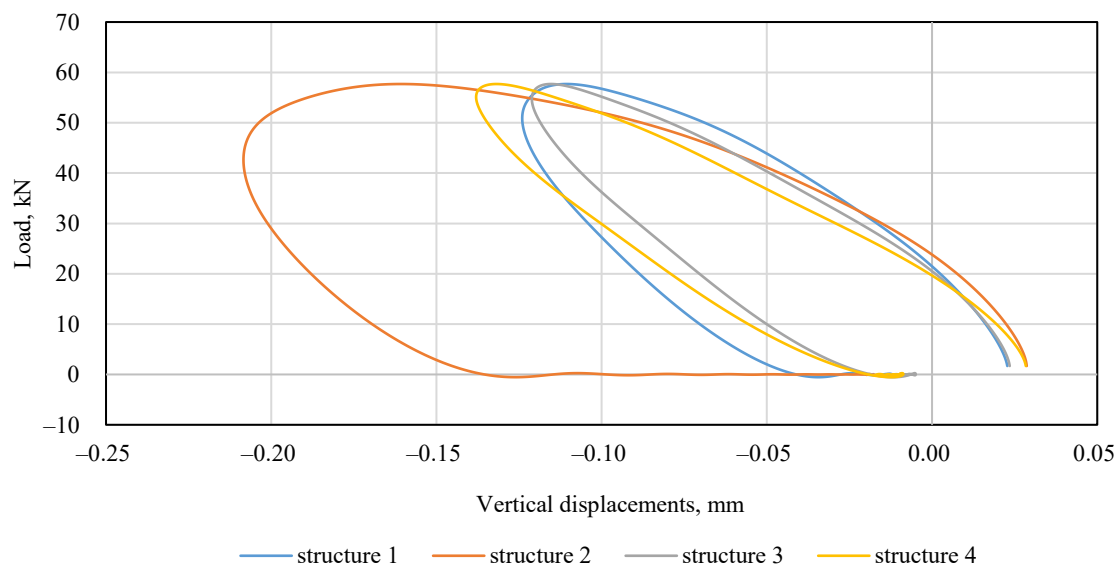


Fig. 8. Dynamic hysteresis loops calculated on the surface of road pavement structures

Table 2

Calculated Value of Deformation Energy Dissipated in Structures

Layers	Deformation energy, J/m ³
Structure 1	9.43
Structure 2	3.00
Structure 3	3.27
Structure 4	3.56

To experimentally confirm the results obtained, measurements are carried out using the FWD PRIMAX 1500 shock loading unit on the real operating road pavement, whose design is similar to structures 1, 3 and 4 shown in Table 1. The obtained experimental shapes of the dynamic hysteresis loops are shown in Figure 9, and the experimental values of the deformation energy dissipated in the structure are presented in Table 3.

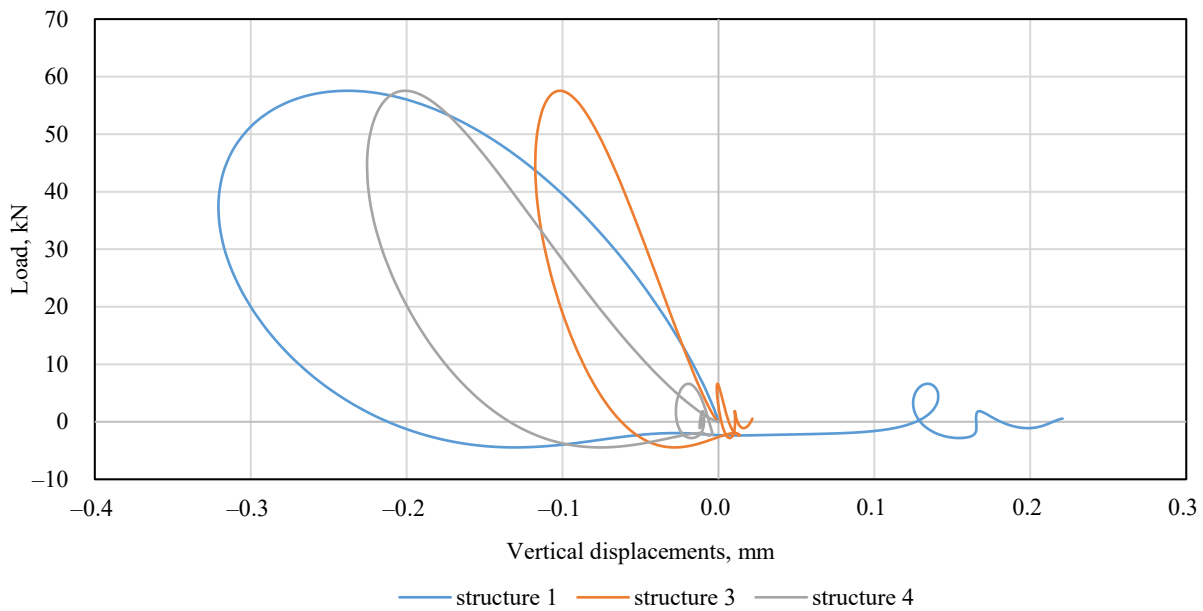


Fig. 9. Dynamic hysteresis loops recorded instrumentally on the surface of road pavement structures

Table 3

Experimental Value of Deformation Energy Dissipated in Structures

Layers	Deformation energy, J/m ³
Structure 1	9.44
Structure 3	3.74
Structure 4	4.56

Design options for road pavement similar to design 2 are currently undergoing feasibility studies for their applicability and have not been implemented under the field conditions of the Russian road network.

Discussion. Analyzing the data in Tables 2 and 3, we can conclude that the highest value of deformation energy dissipation is characteristic of the traditional design option 1, in which the rigidity of the structural layers increases from bottom to top. The lowest value of energy dissipation is undoubtedly characteristic of the most rigid design, 2, which assumes the construction of all layers using binder reinforcement. However, it should be noted that a nearly identical effect can be reached by the reinforcement of the working subgrade layer in the first turn. The numerical modeling has shown that strengthening only the subgrade layer, even without installing a reinforced base layer beneath the asphalt concrete, reduces the dissipated deformation energy from 9.43 to 3.56 J/m³. It can also be concluded that the elastic modulus of the underlying half-space, which simulates the roadbed, has the greatest impact on the amount of dissipated energy. Therefore, the greatest effect, both technical and economic, can be reached through strengthening the top of the roadbed while preserving the loose layers at the base of the road structure (similar to structures 3 and 4). This solution will bring the road pavement performance closer to the elastic stage while reducing the risk of cracks appearing on the road pavement surface due to an excessively rigid reinforced base layer. These modeling results were generally validated by the results of a full-scale experiment, which found that the experimental deformation energy on the surface of unreinforced structure 1, which was 9.44 J/m³, decreased to 4.56 J/m³ in the presence of a reinforced subgrade layer, and to 3.74 J/m³ in the presence of a reinforced base layer under the asphalt concrete and a reinforced subgrade layer. This fact validates the qualitative agreement between the results of in-situ and computational experiments. The research results can be applied to substantiating competing road surface design options and also be developed for use in the road maintenance industry in assessing their residual service life [34, 35]. An important conclusion is the establishment of the greatest impact on the magnitude of deformation energy dissipation from the strengthening of the subgrade layer. In recent years, the issue of using various soil strengthening additives has been actively addressed at various levels [36–38]. Once more data on the strengthening of the roadbed using appropriate additives and stabilization is received, the results obtained can be applied to prove the effect of their introduction. Undoubtedly, this will require conducting research using dynamic loading and stamp testing equipment [39, 40], which makes it possible to directly register dynamic hysteresis loops and load-unloading curves, and obtain the necessary information about the design characteristics of such layers. The approach presented in the study can also be efficiently developed at accelerated testing sites for road pavement [41], and used to calibrate models when their operational condition deteriorates [42].

Conclusion. Thus, as a result of the analysis performed within the framework of this research on the dissipation of deformation energy in the structure of road pavement with various options for the arrangement of reinforced layers and the assessment of the most efficient options for the arrangement of reinforced layers in the structure of the road pavement, it was established that the greatest impact on the magnitude of the dissipation of deformation energy is exerted by the strengthening of the roadbed, modeled as an elastic half-space, unlimited in thickness. This conclusion was validated by experimental studies, which revealed a similar qualitative pattern of changes in the dissipated deformation energy in a structure consisting of only unreinforced layers; a structure with a reinforced subgrade layer; and a structure with a reinforced base layer and a reinforced subgrade layer. It has been shown that the use of reinforced base layers reduces the amount of deformation energy dissipated in the road pavement structure by more than 2–3 times.

References

1. Raza MS, Sharma SK. A Review of Mechanical and Durability Properties and Microstructure of Semi-Flexible Pavement. *Innovative Infrastructure Solutions*. 2024;9(4):83. <https://doi.org/10.1007/s41062-024-01393-w>
2. Ghanizadeh AR, Salehi M, Mamou A, Koutras EI, Jalali F, Asteris PG. Investigation of Subgrade Stabilization Life-Extending Benefits in Flexible Pavements Using a Non-Linear Mechanistic-Empirical Analysis. *Infrastructures*. 2024;9(2):33. <https://doi.org/10.3390/infrastructures9020033>
3. Bei Zhang, Di Wang, Yanhui Zhong, Xiaolong Li, Hongjian Cai, Tao Wang. Mechanical Analysis of Semi-Rigid Base Asphalt Pavement under the Influence of Groundwater with the Spectral Element Method. *Applied Sciences*. 2024;14(6):2375. <https://doi.org/10.3390/app14062375>
4. Klyuev SV, Klyuev AV, Ayubov NA, Fediuk RS, Levkina EV. Finite Element Design and Analysis of Sustainable Mono-Reinforced and Hybrid-Reinforced Fibergeopolymers. *Advanced Engineering Research (Rostov-on-Don)*. 2025;25(3):171–185. <https://doi.org/10.23947/2687-1653-2025-25-3-171-185>
5. Tretyakov DA, Osovik DS. Estimation of Stresses in a Plate with a Concentrator through Ultrasonic Measurements of Acoustic Anisotropy. *Advanced Engineering Research (Rostov-on-Don)*. 2024;24(4):307–315. <https://doi.org/10.23947/2687-1653-2024-24-4-307-315>
6. Babushkina NE, Lyapin AA. Determination of Dynamic Stresses and Displacements under the Action of an Impact Load on a Two-Layer Structure during the Indentation Process. *Advanced Engineering Research (Rostov-on-Don)*. 2024;24(3):264–273. <https://doi.org/10.23947/2687-1653-2024-24-3-264-273>
7. Tiraturyan AN, Lyapin AA. Analysis of the Deformation Energy Dissipation in a Layered Medium Under Dynamic Loading (On the Example of Highways). *Soil Mechanics and Foundation Engineering*. 2024;61:445–451. <https://doi.org/10.1007/s11204-024-09995-3>
8. Xinnan Xu, Mohan Zhao, Yu Liu, Chaofan Wu, Yuhao Pei, Chengmiao Zhang. Falling Weight Impact Acceleration-Time Signals Analysis for Road Modulus Detection: Theoretical and Experimental Investigations. *Case Studies in Construction Materials*. 2024;21:e03915. <https://doi.org/10.1016/j.cscm.2024.e03915>
9. Zhenlong Gong, Yinghao Miao, Lantieri C. Review of Research on Tire–Pavement Contact Behavior. *Coatings*. 2024;14(2):157. <https://doi.org/10.3390/coatings14020157>
10. Yongxiang Li, Longwei Zhao, Junfeng Gao, Yanyan Ru, Haiwei Zhang. Evaluation of the Fatigue Performance of Full-Depth Reclamation with Portland Cement Material Based on the Weibull Distribution Model. *Coatings*. 2024;14(4):437. <https://doi.org/10.3390/coatings14040437>
11. Yongxiang Li, Chuangdan Luo, Kuiliang Ji, Haiwei Zhang, Bowei Sun. Laboratory Evaluation of Strength Performance of Full-Depth Reclamation with Portland Cement Material. *Coatings*. 2024;14(5):573. <https://doi.org/10.3390/coatings14050573>
12. Mendoza-Sanchez JF, Alonso-Guzman EM, Martinez-Molina W, Chavez-Garcia HL, Soto-Espitia R, Delgado-Alamilla H, et al. A Critical Review of Pavement Design Methods Based on a Climate Approach. *Sustainability*. 2024;16(16):7211. <https://doi.org/10.3390/su16167211>
13. Karki B, Prova S, Isied M, Souliman M. Neural Network Approach for Fatigue Crack Prediction in Asphalt Pavements Using Falling Weight Deflectometer Data. *Applied Sciences*. 2025;15(7):3799. <https://doi.org/10.3390/app15073799>
14. Chunru Cheng, Linbing Wang, Xingye Zhou, Xudong Wang. Predicting Rutting Development Using Machine Learning Methods Based on RIOCHTrack Data. *Applied Sciences*. 2024;14(8):3177. <https://doi.org/10.3390/app14083177>
15. Cheng Shen, Zhengguang Wu, Peng Xiao, Aihong Kang, Yangbo Wang. Experimental Research on the Anti-Reflection Crack Performance of Basalt Fiber Modified Rubber Asphalt Stress-Absorbing Layer. *Materials*. 2024;17(9):2013. <https://doi.org/10.3390/ma17092013>
16. Rui Ma, Yiming Li, Peifeng Cheng, Xiule Chen, Aoting Cheng. Low-Temperature Cracking and Improvement Methods for Asphalt Pavement in Cold Regions: A Review. *Buildings*. 2024;14(12):3802. <https://doi.org/10.3390/buildings14123802>
17. Rui Pan. Fatigue Performance Evaluation of Warm-Mixed Rubber Asphalt Mixture for Stress Absorption Layer in Cold Area. *Buildings*. 2024;14(12):3817. <https://doi.org/10.3390/buildings14123817>

18. Ashraf A, Sophian A, Bawono AA. Crack Detection, Classification, and Segmentation on Road Pavement Material Using Multi-Scale Feature Aggregation and Transformer-Based Attention Mechanisms. *Construction Materials*. 2024;4(4):655–675. <https://doi.org/10.3390/constrmater4040036>
19. Bhattacharya S, Taylor R, D'Melo D, Campbell C. Sustainable Design of Pavements: Predicting Pavement Service Life. *Infrastructures*. 2024;9(9):165. <https://doi.org/10.3390/infrastructures9090165>
20. Zhen Liu, Bingyan Cui, Qifeng Yang, Xingyu Gu. Sensor-Based Structural Health Monitoring of Asphalt Pavements with Semi-Rigid Bases Combining Accelerated Pavement Testing and a Falling Weight Deflectometer Test. *Sensors*. 2024;24(3):994. <https://doi.org/10.3390/s24030994>
21. Asres E, Ghebrab T, Ekwaro-Osire S. Framework for Design of Sustainable Flexible Pavement. *Infrastructures*. 2022;7(1):6. <https://doi.org/10.3390/infrastructures7010006>
22. Chun-Hua Hsing, Jun-Han Siao, Yu-Min Wang. A Study on the Design Depth of Permeable Road Pavement through Dynamic Load Experiment. *Materials*. 2022;15(13):4391. <https://doi.org/10.3390/ma15134391>
23. Kryukov KM. Assessing the Benefits and Challenges of Implementing 4D Modeling in Construction. *Modern Trends in Construction, Urban and Territorial Planning*. 2025;4(2):75–84. <https://doi.org/10.23947/2949-1835-2025-4-2-75-84>
24. Al-Zgul IKh, Sheina SG, Morozova NE. Problems and Prospects of Risk-Oriented Management in Construction: A Review of Current Research. *Modern Trends in Construction, Urban and Territorial Planning*. 2025;4(3):65–76. <https://doi.org/10.23947/2949-1835-2025-4-3-65-76>
25. Tiraturyan AN. Backcalculation of Elastic Moduli for Layered Media Based on Dynamic Deformation Analysis (Example of Highways). *Russian Journal of Nondestructive Testing*. 2024;60(8):947–954. <https://doi.org/10.1134/S1061830924602010>
26. Xuefeng Ye, Na Yang, Huina Chen, Manman Yang, Tingyao Wu. Damage Identification and Safety Threshold During the Construction and Operation Phases of Cast-in-Place Continuous Rigid Frame Bridges. *Buildings*. 2025;15(18):3282. <https://doi.org/10.3390/buildings15183282>
27. Babeshko VA, Evdokimova OV, Babeshko OM, Zaretskaia MV, Gorshkova EM, Mukhin AS, et al. On the Behavior of Materials with Defective Coating under Different Contact Conditions. *Materials Physics and Mechanics*. 2018;36(1):67–75. https://doi.org/10.18720/MPM.3612018_7
28. Lyapin A, Beskopylny A, Meskhi B. Structural Monitoring of Underground Structures in Multi-Layer Media by Dynamic Methods. *Sensors*. 2020;20(18):5241. <https://doi.org/10.3390/s20185241>
29. Tiraturyan AN, Uglova EV, Nikolenko DA, Nikolenko MA. Model for Determining the Elastic Moduli of Road Pavement Layers. *Magazine of Civil Engineering*. 2021;103(3):10308. <https://doi.org/10.34910/MCE.103.8>
30. Zhen Liu, Bingyan Cui, Qifeng Yang, Xingyu Gu. Sensor-Based Structural Health Monitoring of Asphalt Pavements with Semi-Rigid Bases Combining Accelerated Pavement Testing and a Falling Weight Deflectometer Test. *Sensors*. 2024;24(3):994. <https://doi.org/10.3390/s24030994>
31. Tutka P, Nagórski R, Zlotowska M. The Impact of Dynamic Effects on the Results of Non-Destructive Falling Weight Deflectometer Testing. *Materials*. 2024;17(17):4412. <https://doi.org/10.3390/ma17174412>
32. Xia Hua, Wael Zatar, Xiangle Cheng, Gang S Chen, Yini She, Xiaotian Xu, et al. Modeling and Characterization of Complex Dynamical Properties of Railway Ballast. *Applied Sciences*. 2024;14(23):11224. <https://doi.org/10.3390/app142311224>
33. Meng Wang, Qunding Yu, Yuanjie Xiao, Wengi Li. Resilient Modulus Behavior and Prediction Models of Unbound Permeable Aggregate Base Materials Derived from Tunneling Rock Wastes. *Materials*. 2022;15(17):6005. <https://doi.org/10.3390/ma15176005>
34. Fang Wang, Shiyi Zhang, Muiyang Huang, Kai Liu, Chaoliang Fu. Assessment of Fatigue Life in Grouted Polyurethane Composites for Pavement Maintenance. *Materials*. 2025;18(8):1806. <https://doi.org/10.3390/ma18081806>
35. Gensheng Hu, Gongzuo Shi, Runhua Zhang, Jianfeng Chen, Haichang Wang, Junzhe Wang. Assessment of Intelligent Unmanned Maintenance Construction for Asphalt Pavement Based on Fuzzy Comprehensive Evaluation and Analytical Hierarchy Process. *Buildings*. 2024;14(4):1112. <https://doi.org/10.3390/buildings14041112>
36. Piechowicz K, Szymanek S, Kowalski J, Lendo-Siwicka M. Stabilization of Loose Soils as Part of Sustainable Development of Road Infrastructure. *Sustainability*. 2024;16(9):3592. <https://doi.org/10.3390/su16093592>
37. Muhudin AA, Zami MS, Budaiwi IM, Abd El Fattah A. Experimental Study of Thermal Conductivity in Soil Stabilization for Sustainable Construction Applications. *Sustainability*. 2024;16(3):946. <https://doi.org/10.3390/su16030946>
38. Petrillo A, Fraternali F, Acampora A, Di Chiara G, Colangelo F, Farina I. Innovative Solidification and Stabilization Techniques Using Industrial By-Products for Soil Remediation. *Applied Sciences*. 2025;15(7):4002. <https://doi.org/10.3390/app15074002>
39. Jiacheng Cai, Yingchao Luo, Bing Zhang, Lei Chen, Lu Liu. Method for Extracting Impact Signals in Falling Weight Deflectometer Calibration Based on Frequency Filtering and Gradient Detection. *Sensors*. 2025;25(11):3317. <https://doi.org/10.3390/s25113317>

40. Kuttah D. Using Repeated Light-Weight Deflectometer Test Data to Predict Flexible Pavement Responses Based on the Mechanistic–Empirical Design Method. *Construction Materials*. 2024;4(1):216–237. <https://doi.org/10.3390/constrmater4010012>
41. Ni Guangcong, Tiraturyan AN, Uglova EV, Vorobev AV. Study on Dynamic Response Characteristics of Different Asphalt Pavement Structures Based on ALF Test. *Advanced Engineering Research (Rostov-on-Don)*. 2023;23(3):241–256. <https://doi.org/10.23947/2687-1653-2023-23-3-241-256>
42. Elshamy MM, Tiraturyan AN, Uglova EV. Evaluation of the Elastic Modulus of Pavement Layers Using Different Types of Neural Networks Models. *Advanced Engineering Research (Rostov-on-Don)*. 2021;21(4):364–375. <https://doi.org/10.23947/2687-1653-2021-21-4-364-375>

About the Author:

Artem N. Tiraturyan, Dr.Sci. (Eng.), Professor of the Motorways Department, Don State Technical University (1, Gagarin Sq., Rostov-on-Don, 344003, Russian Federation), [SPIN-code](#), [ORCID](#), [ScopusID](#), Ttiraturjan@list.ru

Conflict of Interest Statement: the author declares no conflict of interest.

The author has read and approved the final version of manuscript.

Об авторе:

Артем Николаевич Тиратуриян, доктор технических наук, профессор кафедры «Автомобильные дороги» Донского государственного технического университета (344003, Российская Федерация, г. Ростов-на-Дону, пл. Гагарина, 1), [SPIN-код](#), [ORCID](#), [ScopusID](#), Ttiraturjan@list.ru

Конфликт интересов: автор заявляет об отсутствии конфликта интересов.

Автор прочитал и одобрил окончательный вариант рукописи.

Received / Поступила в редакцию 13.09.2025

Reviewed / Поступила после рецензирования 19.10.2025

Accepted / Принята к публикации 06.11.2025

INFORMATION TECHNOLOGY, COMPUTER SCIENCE AND MANAGEMENT ИНФОРМАТИКА, ВЫЧИСЛИТЕЛЬНАЯ ТЕХНИКА И УПРАВЛЕНИЕ



UDC 681.515

Original Empirical Research

<https://doi.org/10.23947/2687-1653-2025-25-4-2209>

Observer-Based Finite-Time Adaptive Reinforced Super-Twisting Sliding Mode Control for Robotic Manipulators

Hoang Duc Long

Le Quy Don Technical University, Hanoi, Vietnam

✉ longhd@lqdtu.edu.vn

EDN: OZLBEC

Abstract

Introduction. Robotic manipulators operate in dynamic environments under uncertainties, external disturbances, and actuator faults, posing a critical challenge to their control design. While traditional control strategies, such as PID or computed torque control, offer simplicity, they often lack robustness to unmodeled dynamics. The development of robust and practically implementable control algorithms is becoming increasingly important with the growing use of manipulators in dangerous, precise and ultra-fast operations (industrial automation, medicine, space and service robots). Conventional PID controllers and torque calculation methods are simple but not robust enough to handle unmodeled effects. Sliding Mode Control (SMC), particularly the Super-Twisting variant (STA), provides strong robustness, but suffers from chattering and typically requires prior knowledge of system bounds. Recent advancements like Adaptive Global Integral Terminal Sliding Mode Control (AGITSMC) improve finite-time convergence but may result in overestimated control gains and residual switching effects. This research addresses a critical gap in current methods: the lack of a unified control approach that ensures finite-time convergence, suppresses chattering, and compensates for both unknown disturbances and actuator faults using observer feedback. The objective of this work is to design and analyze an Observer-Based Finite-Time Adaptive Reinforced Super-Twisting Sliding Mode Control (OFASTSMC) framework that adaptively adjusts its gains, estimates disturbances online, and guarantees smooth, robust performance even in the presence of severe nonlinearities and faults. The objective of this study is to develop and analyze an Observer-Based Finite-Time Adaptive Reinforced Super-Twisting Sliding Mode Control (OFASTSMC) framework that unifies finite-time observer feedback, adaptive gain tuning, and reinforced sliding surfaces to achieve robust trajectory tracking of robotic manipulators under disturbances and actuator faults, while effectively minimizing chattering and ensuring practical implementability.

Materials and Methods. This study considers the standard dynamic model of an n -DOF robotic manipulator derived using Lagrangian mechanics. The model accounts for nonlinear coupling effects, viscous friction, external disturbances, and additive actuator faults. To achieve robust finite-time control, a reinforced sliding surface is constructed using nonlinear error terms with adaptive power exponents, which accelerates error convergence. A finite-time extended state observer (ESO) is incorporated to estimate lumped disturbances and actuator fault torques in real time. Based on these estimates, the control law integrates a super-twisting sliding mode algorithm with adaptive gain tuning and boundary-layer smoothing to reduce chattering while ensuring strong robustness. The closed-loop system stability is formally analyzed within a Lyapunov framework, where rigorous proofs confirm finite-time convergence of the tracking error under the proposed controller. The proposed OFASTSMC algorithm is implemented in MATLAB/Simulink and validated on a 2-DOF planar robotic manipulator. The manipulator is subjected to time-varying disturbances and actuator degradation scenarios. For benchmarking, the method is directly compared with AGITSMC, using identical initial conditions, model parameters, and reference trajectories to ensure a fair and consistent performance evaluation.

Results. Simulation results demonstrate that the proposed OFASTSMC method significantly outperforms the benchmark AGITSMC in terms of tracking precision, robustness, and control smoothness. Specifically, the maximum joint position errors were reduced by over 40% compared to AGITSMC, and the settling time to reach the desired trajectory was

shortened by approximately 25%. Additionally, the proposed method effectively mitigated chattering in the control signal due to the use of saturation functions and gain limits, resulting in smoother actuator commands. The adaptive observer accurately estimated the lumped disturbance and fault inputs in real time, providing effective fault compensation without prior knowledge. These improvements were validated across multiple scenarios including abrupt actuator failures, nonlinear load torques, and varying trajectory speeds. The sliding surface convergence was achieved in finite time, confirming the theoretical guarantees of the method.

Discussion. The results validate that OFASTSMC achieves robust, high-precision tracking for robotic manipulators operating under real-world uncertainties. Its novelty lies in the integration of adaptive exponent tuning, finite-time observer feedback, and gain-limited super-twisting control into a unified and practical framework. Unlike previous methods that rely on fixed gain structures or ignore observer feedback, OFASTSMC adapts in real-time and maintains finite-time convergence guarantees with minimal chattering.

Conclusion. The results obtained confirm that OFASTSMC is an efficient and robust solution to the trajectory tracking problem in the presence of uncertainties. The method is computationally efficient and easy to implement in digital control systems, making it suitable for practical deployment in industrial robots, service manipulators, or surgical arms. Future research will focus on extending this method to task-space control and real hardware implementation under sensor noise and model mismatches.

Keywords: robotic manipulators, finite-time stability, super-twisting algorithm, sliding mode control, actuator fault, adaptive control, observer-based control

Acknowledgements. The author would like to thank the colleagues at the Department of Automation and Computing Techniques, Le Quy Don Technical University, for assistance in preparing the text of the article.

For Citation. Long HD. Observer-Based Finite-Time Adaptive Reinforced Super-Twisting Sliding Mode Control for Robotic Manipulators. *Advanced Engineering Research (Rostov-on-Don)*. 2025;25(4):337–349. <https://doi.org/10.23947/2687-1653-2025-25-4-2209>

Оригинальное эмпирическое исследование

Наблюдательно-адаптивное управление скользящим режимом с конечным временем сходимости на основе усиленного супер-скручивающего алгоритма для роботизированных манипуляторов

Хоанг Дык Лонг 

Технический университет имени Ле Куи Дона, Ханой, Вьетнам

✉ longhd@lqdtu.edu.vn

Аннотация

Введение. Роботизированные манипуляторы эксплуатируются в условиях изменчивой среды с неопределённостями, внешними возмущениями и возможными отказами приводов, что существенно осложняет проектирование надёжных систем управления. Важность разработки робастных и практически реализуемых алгоритмов управления возрастает с ростом применения манипуляторов в опасных, точных и сверхбыстрых операциях (промышленная автоматизация, медицина, космические и сервисные роботы). Традиционные ПИД-регуляторы и методы вычисления момента просты, но недостаточно устойчивы к немоделированным воздействиям. Управление скользящим режимом, в частности алгоритм супер-скручивания (STA), обеспечивает повышенную робастность и конечную сходимость, однако страдает эффектом дрожания и часто требует априорной информации о границах возмущений. Современные модификации (например, AGITSMC) достигают конечного времени сходимости и снижают дрожание, но могут вызывать завышение управляющих усилий и сохраняющиеся огрехи при оценке возмущений и отказов. В литературе замечен пробел: отсутствует интегрированный подход, который одновременно обеспечивает конечновременную сходимость, адаптивную компенсацию неизвестных возмущений и отказов, подавление дрожания и практическую реализуемость. Поэтому целью данной работы стало разработать и проанализировать новую структуру управления OFASTSMC (Observer-Based Finite-Time Adaptive Reinforced Super-Twisting Sliding Mode Control), объединяющую конечновременный наблюдатель, адаптивную настройку усилий и сглаженное супер-скручивающее управление. Решаемые задачи: построение конечновременного наблюдателя для оценки возмущений и отказов в режиме онлайн; разработка адаптивного механизма настройки усилий для предотвращения завышения управляющих сигналов; внедрение сглаженной STA для минимизации дрожания; проведение анализа устойчивости; выполнение численных и экспериментальных проверок на роботизированных манипуляторах.

Материалы и методы. Рассматривается стандартная динамическая модель роботизированного манипулятора с n степенями свободы, построенная на основе лагранжевой механики. Модель учитывает нелинейные связи, вязкое трение, внешние возмущения и аддитивные отказы приводов. Для обеспечения робастного управления с конечным временем сходимости была разработана усиленная скользящая поверхность, использующая нелинейные ошибки с адаптивными степенями — это ускоряет процесс сходимости. В схему управления включён конечно-временной расширенный наблюдатель состояния (ESO), позволяющий в реальном времени оценивать суммарные возмущения и моменты отказов приводов. На основе этих оценок закон управления реализован в виде супер-скручивающего алгоритма скользящего режима с адаптивной настройкой коэффициентов и использованием граничного слоя для снижения дрожания при сохранении высокой робастности. Устойчивость замкнутой системы строго проанализирована с использованием аппарата теории Ляпунова — это позволило доказать достижение конечного времени сходимости ошибок слежения под действием предложенного регулятора. Предложенный алгоритм OFASTSMC реализован в среде MATLAB/Simulink и проверен на примере плоского роботизированного манипулятора с двумя степенями свободы. Манипулятор подвергался действию переменных возмущений и сценариев деградации привода. Для объективного сравнения эффективности метод сопоставлялся с AGITSMC при идентичных начальных условиях, параметрах модели и опорных траекториях.

Результаты. Численные эксперименты демонстрируют, что предложенный метод OFASTSMC значительно превосходит AGITSMC по точности слежения, устойчивости и плавности управления. В частности, максимальные ошибки по положению звеньев снижены более чем на 40%, а время установления траектории уменьшено примерно на 25%. Метод эффективно устраняет дрожание в управляющем сигнале за счёт функций насыщения и ограничений усиления, обеспечивая более плавное управление приводами. Адаптивный наблюдатель точно оценивает суммарные возмущения и входы отказов в реальном времени, обеспечивая компенсацию без предварительной информации. Эффективность метода подтверждена в различных сценариях: резкие отказы приводов, нелинейные нагрузки, переменные скорости траектории. Сходимость на скользящей поверхности достигается за конечное время, что подтверждает теоретические гарантии.

Обсуждение. OFASTSMC обеспечивает высокоточную и робастную траекторию слежения в условиях неопределённостей. Основное преимущество метода — интеграция адаптивной настройки степеней, наблюдательной обратной связи и ограниченного супер-скручивающего управления в единую структуру. В отличие от подходов с фиксированными усилениями или без наблюдательной обратной связи, предложенная схема адаптируется в реальном времени, что позволяет поддерживать сходимость и существенно снижать дрожание управления. Метод сочетает адаптивность, наблюдательную коррекцию и ограниченное супер-скручивание, обеспечивая устойчивую сходимость и минимизацию дрожания.

Заключение. Полученные результаты подтверждают, что OFASTSMC является эффективным и робастным решением для задачи траекторного слежения в присутствии неопределённостей. Метод демонстрирует вычислительную эффективность и простоту реализации, что делает его пригодным для практического применения. Для дальнейшего развития исследования планируется переход к реализации управления в пространстве задач и проведение экспериментов на физическом оборудовании с учётом шумов и модельных несоответствий.

Ключевые слова: роботизированные манипуляторы, устойчивость за конечное время, алгоритм супер-скручивания, управление на основе скользящего режима, отказ привода, адаптивное управление, управление с наблюдателем

Благодарность. Автор выражает благодарность коллегам с кафедры автоматики и вычислительной техники Технического университета Ле Куи Дона за помощь в подготовке текста статьи.

Для цитирования. Хоанг Дык Лонг. Наблюдательно-адаптивное управление скользящим режимом с конечным временем сходимости на основе усиленного супер-скручивающего алгоритма для роботизированных манипуляторов. *Advanced Engineering Research (Rostov-on-Don)*. 2025;25(4):337–349. <https://doi.org/10.23947/2687-1653-2025-25-4-2209>

Introduction. Robotic manipulators play a pivotal role in modern industries such as manufacturing, logistics, minimally invasive surgery, space exploration, and service robotics [1–3]. Their widespread deployment in safety-critical tasks requires not only high-precision trajectory tracking but also resilience against uncertainties, actuator degradation, and time-varying disturbances [4–6]. With the growing complexity of Industry 4.0 systems and the rise of human–robot collaboration, the demand for robust and adaptive control solutions has become more pressing than ever [7–9].

Classical control methods, such as PID and computed torque control, are widely used for their simplicity but often fail in scenarios with strong nonlinearities, friction, and payload variations [10, 11]. Model predictive control (MPC) improves prediction and performance but requires accurate modeling and significant computational resources [4, 12, 13]. Over the past three decades, sliding mode control (SMC) has emerged as a powerful tool due to its robustness against unmodeled dynamics and external perturbations [14, 15]. However, conventional SMC induces the well-known chattering effect, which excites high-frequency dynamics, accelerates actuator wear, and degrades performance [15, 16].

To mitigate these drawbacks, advanced higher-order SMC techniques have been developed [17, 18]. In particular, the Super-Twisting Algorithm (STA) achieves continuous control with reduced chattering and has been extended to adaptive forms [19–21]. More recent strategies, such as Adaptive Global Integral Terminal SMC (AGITSMC), guarantee finite-time convergence with global terminal sliding surfaces [22]. Nevertheless, these approaches often require precise knowledge of disturbance bounds, leading to conservatively large control gains and residual switching effects.

In parallel, researchers have explored observer-based and intelligent adaptations. Disturbance observers, neural networks, and fuzzy approximators have been integrated into SMC frameworks to improve adaptability and fault tolerance [23–25]. Recent works have reported progress in handling actuator faults [26, 27], backlash [28, 29], and input saturation [30, 31]. Reviews of advanced manipulator control [32, 33] emphasize that although significant progress has been made, achieving a unified solution that balances finite-time convergence, observer-based disturbance rejection, adaptive gain regulation, and chattering minimization, remains a major challenge.

Motivated by these limitations, this study introduces an Observer-Based Finite-Time Adaptive Reinforced Super-Twisting Sliding Mode Control (OFASTSMC) framework. The proposed method integrates:

- a finite-time extended state observer for online estimation of lumped disturbances and actuator faults;
- a reinforced sliding surface with adaptive exponents to accelerate convergence;
- an adaptive super-twisting control law with boundary-layer smoothing to reduce chattering.

The main contributions of this work are:

1. Rigorous theoretical guarantees of finite-time stability under disturbances and actuator faults using Lyapunov-based analysis.
2. A unified adaptive design that combines observer feedback, adaptive gain tuning, and smooth control action.
3. Extensive validation on a 2-DOF robotic manipulator benchmark, demonstrating superior robustness, precision, and fault-tolerance compared to AGITSMC.

Materials and Methods

1. Mathematical Model of an n -DOF Robotic Manipulator

Robotic manipulators are governed by highly nonlinear and coupled dynamics due to their mechanical structure and interaction with the environment. For an n -degree-of-freedom (DOF) serial robotic manipulator operating in joint space, the dynamic equations of motion can be represented by the standard Lagrangian formulation as follows [22]:

$$H(q)\ddot{q} + C(q, \dot{q})\dot{q} + G(q) + F_v\dot{q} = \tau + \tau_d + \tau_f, \quad (1)$$

where $q \in \mathbb{R}^n$ — joint position vector; $\dot{q}, \ddot{q} \in \mathbb{R}^n$ — joint velocity and acceleration vectors; $H(q) \in \mathbb{R}^{n \times n}$ — positive definite and symmetric inertia matrix; $C(q, \dot{q}) \in \mathbb{R}^{n \times n}$ — Coriolis and centrifugal matrix; $G(q) \in \mathbb{R}^n$ — gravity torque vector, $F_v \in \mathbb{R}^{n \times n}$ — diagonal matrix of viscous friction coefficients; $\tau \in \mathbb{R}^n$ — control input torque; $\tau_d \in \mathbb{R}^n$ — unknown external disturbance torque; $\tau_f \in \mathbb{R}^n$ — actuator fault torque.

Actuator Fault and Disturbance Model. To model practical degradation and failures in actuators, we assume that actuator faults τ_f are additive, bounded, and possibly time-varying. The total unmodeled input is defined as:

$$\tau_u = \tau_d + \tau_f. \quad (2)$$

We assume that $\tau_u(t)$ is bounded as:

$$\|\tau_u(t)\| \leq a_0 + a_1 \|q(t)\| + a_2 \|\dot{q}(t)\|^2,$$

where $a_0, a_1, a_2 > 0$ are unknown positive constants.

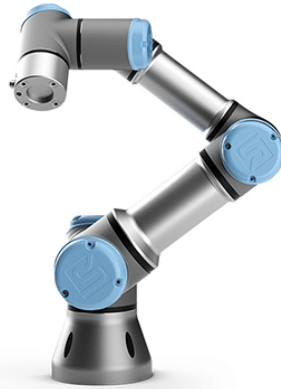


Fig. 1. n -DOF Robotic Manipulator

Properties of the Dynamics. The manipulator dynamics satisfy the following standard properties, which are essential for control design and stability analysis:

- **P1:** $H(q)$ is symmetric and uniformly positive definite.
- **P2:** $\dot{H}(q) - 2C(q, \dot{q})$ is skew-symmetric.
- **P3:** All terms $H(q)$, $C(q, \dot{q})$, $G(q)$ are locally Lipschitz and satisfy polynomial growth bounds in q , \dot{q} .

Objective. Given a desired trajectory $q_d(t) \in C^2$, the control objective is to design a robust, adaptive control law $\tau(t)$ such that:

$$\lim_{t \rightarrow T} \|q(t) - q_d(t)\| = 0 \quad \text{and} \quad \lim_{t \rightarrow T} \|\dot{q}(t) - \dot{q}_d(t)\| = 0, \quad (3)$$

in finite time $T < \infty$, despite the presence of unknown bounded disturbances τ_d , actuator faults τ_f , and parametric uncertainties.

2. Design of the OFASTSMC Algorithm

Define Tracking Errors:

$$e_1 = q - q_d(t), \quad e_2 = \dot{q} - \dot{q}_d(t). \quad (4)$$

Reinforced Sliding Surface

$$s = e_2 + \alpha_1 |e_1|^{p_1} \text{sign}(e_1) + \alpha_2 |e_1|^{p_2} \text{sign}(e_1), \quad (5)$$

with adaptive exponents $p_1(t), p_2(t) \in (0, 1)$ based on state magnitude:

$$p_1(t) = \frac{1}{1 + \kappa_1 e^{-|\dot{q}|}}, \quad p_2(t) = \frac{1}{1 + \kappa_2 e^{-|\ddot{q}_d|}}. \quad (6)$$

Finite-Time Observer (Modified ESO):

$$\hat{\tau}_d = \frac{\lambda_0 (s - s_{\text{prev}})}{dt}, \quad (7)$$

where $\lambda_0 > 0$, s_{prev} is the previous value of s .

Adaptive Gain Laws:

$$\dot{K}_1 = \gamma_1 |s|, \quad \dot{K}_2 = \gamma_2 |s|^p. \quad (8)$$

Control Law (OFASTSMC):

$$\tau = -\lambda s - K_1 s - K_2 |s|^p \text{sign}(s) - \hat{\tau}_d + C(q, \dot{q}) + G(q) + F_0 \dot{q} - H(q) \ddot{q}_d. \quad (9)$$

Advantages over existing approaches. Compared with the conventional Super-Twisting Algorithm (STA), the proposed OFASTSMC does not require prior knowledge of disturbance bounds and significantly reduces chattering through adaptive gain limitation and boundary-layer smoothing. Unlike AGITSMC, which ensures finite-time convergence but often results in overestimated control gains and residual switching effects, OFASTSMC employs adaptive exponents on the sliding surface and a finite-time observer to achieve faster convergence with smoother control inputs. Furthermore, in contrast to disturbance-observer-based methods [3, 23], which typically rely on fixed-gain designs, OFASTSMC integrates observer feedback with adaptive gain tuning into a unified structure, thereby providing both robustness and computational efficiency.

3. Stability Analysis

Assumption 1. Desired trajectory $q_d(t) \in C^2$, bounded with bounded derivatives.

Assumption 2. Disturbance and fault torque bounded:

$$\|\tau_d + \tau_f\| \leq a_0 + a_1 \|q(t)\| + a_2 \|\dot{q}(t)\|^2. \quad (10)$$

Lemma 1. Finite-Time Convergence of Sliding Variable

Consider the differential equation:

$$\dot{s}(t) = -k_1 s(t) - k_2 |s(t)|^p \text{sign}(s(t)), \quad k_1, k_2 > 0, \quad 0 < p < 1. \quad (11)$$

Then the sliding variable $s(t)$ converges to zero in finite time T_s , i.e., exists $T_s > 0$ such that $s(t) = 0$ for all $t \geq T_s$.

Proof.

We define a Lyapunov candidate function:

$$V(s) = \frac{1}{2}s^2. \quad (12)$$

The derivative of $V(s)$:

$$\begin{aligned} \dot{V}(s) &= s\dot{s} = s(-k_1s - k_2|s|^p \operatorname{sign}(s)) = s(-k_1s - k_2|s|^p \operatorname{sign}(s)) = \\ &= -k_1s^2 - k_2|s|^{1+p} = -2k_1V - k_2(2V)^{\frac{1+p}{2}}. \end{aligned} \quad (13)$$

Let $\alpha = \frac{1+p}{2} \in (0.5, 1)$, so:

$$\dot{V}(s) \leq -2k_1V - k_2(2V)^\alpha. \quad (14)$$

This is a differential inequality of the form:

$$\dot{V}(t) \leq -aV(t) - bV^\alpha(t), \quad a, b > 0, \quad 0 < \alpha < 1. \quad (15)$$

According to standard finite-time stability theory [23–25], this implies that: $V(t) \rightarrow 0$ in finite time.

Let us estimate the settling time. Ignoring the linear term $-2k_1V$, for a conservative bound:

$$\dot{V} \leq -k_2(2V)^\alpha = -CV^\alpha, \quad C = k_22^\alpha. \quad (16)$$

Separate variables:

$$\frac{dV}{V^\alpha} \leq -Cdt. \quad (17)$$

Therefore:

$$\int_{V(0)}^0 \frac{dV}{V^\alpha} \leq -C \int_0^{T_s} dt \Leftrightarrow \frac{1}{1-\alpha} [V^{1-\alpha}]_{V(0)}^0 = \frac{V^{1-\alpha}(0)}{1-\alpha} \geq CT_s \Rightarrow T_s \leq \frac{V^{1-\alpha}(0)}{C(1-\alpha)} = \frac{\left(\frac{s^2(0)}{2}\right)^{1-\alpha}}{k_22^\alpha(1-\alpha)}, \quad (18)$$

where $V(0)$ is the initial Lyapunov value and T_s is the maximum setting time. Thus, $s(t) \rightarrow 0$ in finite time.

Theorem 1. Finite-Time Stability of Tracking Error

For the nonlinear robotic manipulator system (1) under the observer-based finite-time adaptive super-twisting sliding mode control (OFASTSMC) (9) with the sliding surface (5) and adaptive gains (8), then the tracking error $e_1 = q - q_d$ converges to zero in finite time.

Proof.

From (4):

$$\dot{e}_2 = \ddot{q} - \ddot{q}_d = H^{-1}(\tau + \tau_d + \tau_f - C\dot{q} - G - F_v) - \ddot{q}_d. \quad (19)$$

Substitute control law (9) into (19), then:

$$\ddot{q} = H^{-1}(-\lambda s - K_1s - K_2|s|^p \operatorname{sign}(s) - \hat{\tau}_d + \tau_d + \tau_f). \quad (20)$$

From (5), the derivative of $s(t)$:

$$\dot{s} = \ddot{q} - \ddot{q}_d + (\alpha_1 p_1 |e_1|^{p_1-1} + \alpha_2 p_2 |e_1|^{p_2-1}) e_2. \quad (21)$$

So:

$$\dot{s} = -H^{-1}(\lambda s + K_1s + K_2|s|^p \operatorname{sign}(s) + \tilde{\tau}_d) + (\alpha_1 p_1 |e_1|^{p_1-1} + \alpha_2 p_2 |e_1|^{p_2-1}) e_2, \quad (22)$$

where $\tilde{\tau}_d = \hat{\tau}_d - (\tau_d + \tau_f)$.

We choose a Lyapunov candidate function:

$$V(s) = \frac{1}{2}s^T s. \quad (23)$$

The derivative of $V(s)$:

$$\begin{aligned}\dot{V}(s) &= s^T \dot{s} = s^T \left(-H^{-1} \left(\lambda s + K_1 s + K_2 |s|^p \operatorname{sign}(s) + \tilde{\tau}_d \right) + \left(\alpha_1 p_1 |e_1|^{p_1-1} + \alpha_2 p_2 |e_1|^{p_2-1} \right) e_2 \right) = \\ &= -s^T H^{-1} \left(\lambda s + K_1 s + K_2 |s|^p \operatorname{sign}(s) \right) - s^T H^{-1} \tilde{\tau}_d + s^T \Psi(q, \dot{q}, e_1),\end{aligned}\quad (24)$$

where $\Psi(q, \dot{q}, e_1) = \left(\alpha_1 p_1 |e_1|^{p_1-1} + \alpha_2 p_2 |e_1|^{p_2-1} \right) e_2$.

Now analyze each term.

Term 1. Negative Definite Dissipation

$$-s^T H^{-1} \left(\lambda s + K_1 s + K_2 |s|^p \operatorname{sign}(s) \right) \leq -\mu \lambda \|s\|^2 - \mu K_1 \|s\|^2 - \mu K_2 \|s\|^{1+p}. \quad (25)$$

Here, $\mu = \lambda_{\min}(H^{-1}) > 0$.

Term 2. Estimation Error Term

$$|s^T H^{-1} \tilde{\tau}_d| \leq \|s\| \|H^{-1}\| \|\tilde{\tau}_d\| \leq \mu_{\max} \|s\| \|\tilde{\tau}_d\|. \quad (26)$$

This is where estimation error comes in. If the observer is well designed, then:

$$\|\tilde{\tau}_d\| \rightarrow 0 \quad \text{as } t \rightarrow \infty. \quad (27)$$

So this is a bounded and vanishing term, eventually dominated by the strong negative dissipation in Term 1.

Term 3. Nonlinear “Bounded” Term $s^T \Psi$:

$$|s^T \Psi| = \left| s^T \left(\alpha_1 p_1 |e_1|^{p_1-1} + \alpha_2 p_2 |e_1|^{p_2-1} \right) e_2 \right| \leq \|s\| \|e_2\| \left(\alpha_1 p_1 |e_1|^{p_1-1} + \alpha_2 p_2 |e_1|^{p_2-1} \right). \quad (28)$$

Let $\eta(q, \dot{q}, t) = \left(\alpha_1 p_1 |e_1|^{p_1-1} + \alpha_2 p_2 |e_1|^{p_2-1} \right) \|e_2\|$. Then:

$$|s^T \Psi| \leq \|s\| \eta(q, \dot{q}, t) = \delta_1 \|s\|. \quad (29)$$

Combine (25), (26), (29) and (24):

$$\dot{V}(s) \leq -\mu(\lambda + K_1) \|s\|^2 - \mu K_2 \|s\|^{1+p} + \mu_{\max} \|s\| \|\tilde{\tau}_d\| + \delta_1 \|s\|. \quad (30)$$

Eventually, as:

$$- \|\tilde{\tau}_d\| \rightarrow 0;$$

– K_1, K_2 grow adaptively;

– the first two negative terms dominate the last two, and $\dot{V}(s) < 0$ with finite-time convergence.

From (30):

$$\dot{V}(t) \leq -2\mu(\lambda + K_1) \left(\frac{1}{2} \|s\|^2 \right) - 2^{\frac{1+p}{2}} \mu K_2 \left(\frac{1}{2} \|s\|^2 \right)^{\frac{1+p}{2}} = -c_1 V(t) - c_2 V^{\frac{1+p}{2}}(t), \quad (31)$$

with $c_1 = 2\mu(\lambda + K_1)$; $c_2 = 2^{(1+p)/2} \mu K_2 > 0$; $0 < \rho < 1$.

Then, by integrating the inequality using comparison theorems, we obtain a finite settling time T such that $V(t) = 0$ for all $t \geq T$, where:

$$T \leq \frac{1}{c_1} \ln \left(1 + \frac{c_1}{c_2 \left(1 - \frac{1+\rho}{2} \right)} V^{\frac{1-\rho}{2}}(0) \right). \quad (32)$$

Or more conservatively, if we ignore the linear term $-c_1 V(t)$, then:

$$\dot{V}(t) \leq -c_2 V^\alpha(t), \quad \alpha = \frac{1+\rho}{2} \in (0.5, 1). \quad (33)$$

As Lemma 1, integrating this gives the explicit finite-time convergence time:

$$T \leq \frac{V^{1-\alpha}(0)}{c_2(1-\alpha)}. \quad (34)$$

Results. To validate the effectiveness and robustness of the proposed Observer-Based Finite-Time Adaptive Reinforced Super-Twisting Sliding Mode Control (OFASTSMC), numerical simulations were conducted on a planar 2-DOF robotic manipulator [34–36]. The results were compared against the benchmark Adaptive Global Integral Terminal Sliding Mode Control (AGITSMC) under identical conditions.

Given link masses m_1, m_2 , lengths l_1, l_2 , and gravity g , the matrices are:

– Inertia matrix $M(q)$:

$$M(q) = \begin{bmatrix} m_1 l_1^2 + m_2 (l_1^2 + l_2^2 + 2l_1 l_2 \cos q_2) & m_2 (l_2^2 + l_1 l_2 \cos q_2) \\ m_2 (l_2^2 + l_1 l_2 \cos q_2) & m_2 l_2^2 \end{bmatrix}. \quad (35)$$

– Coriolis and centrifugal matrix $C(q, \dot{q})$:

$$C(q, \dot{q}) = \begin{bmatrix} -m_2 l_1 l_2 \sin q_2 \dot{q}_2 & m_2 (l_2^2 + l_1 l_2 \cos q_2) \dot{q}_2 \\ m_2 l_1 l_2 \sin q_2 \dot{q}_1 & 0 \end{bmatrix}. \quad (36)$$

– Gravity vector $G(q)$:

$$G(q) = \begin{bmatrix} (m_1 + m_2) g l_1 \sin q_1 + m_2 g l_2 \sin(q_1 + q_2) \\ m_2 g l_2 \sin(q_1 + q_2) \end{bmatrix}. \quad (37)$$

The external disturbance applied to each joint is defined as:

$$\tau_d(t) = \begin{bmatrix} \sin(t) \\ 0.5 \cos(2t) \end{bmatrix}. \quad (38)$$

The actuator fault model assumes a loss of effectiveness that activates at time $t = 3$ seconds. The fault torque is defined as:

$$\tau_f(t) = \begin{cases} \mathbf{0} & t \leq 3 \\ \begin{bmatrix} -0.4u_1(t) \\ -0.3u_2(t) \end{bmatrix} & t > 3 \end{cases}. \quad (39)$$

The desired joint trajectory was chosen to be smooth, bounded, and nonlinear to test the tracking performance under dynamic reference motion:

$$q_d(t) = \begin{bmatrix} 1.5 - e^{-t} \\ 1 + 0.5 \sin(0.5t) \end{bmatrix}. \quad (40)$$

The physical parameters of the 2-DOF planar manipulator used in the simulations are: $m_1 = 0.5(\text{kg})$, $m_2 = 1.5(\text{kg})$, $l_1 = 1.0(\text{m})$, $l_2 = 0.85(\text{m})$, $g = 9.81(\text{m/s}^2)$. OFASTSMC parameters: $\lambda = 10$, $\alpha_1 = 5$, $\alpha_2 = 3$, $\rho = 0.5$, $\gamma_1 = 10$, $\gamma_2 = 3$, $\kappa_1 = 2$, $\kappa_2 = 2$, $\phi = 0.05$, $K_1(0) = 5$, $K_2(0) = 5$. AGITSMC parameters: $\beta = 3$, $k_1 = 10$, $k_2 = 4$, $k_3 = 2$, $\gamma_3 = 5/3$; $\gamma_4 = 3/5$.

The angles of joints:

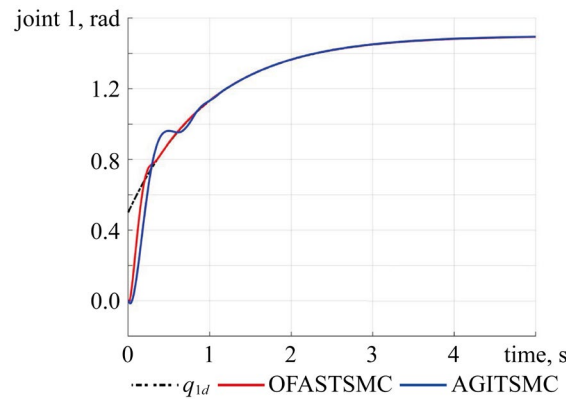


Fig. 2. Angle of Joint 1

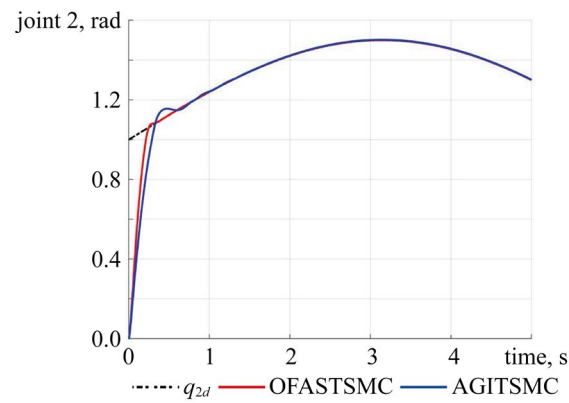


Fig. 3. Angle of Joint 2

The tracking errors of joints:

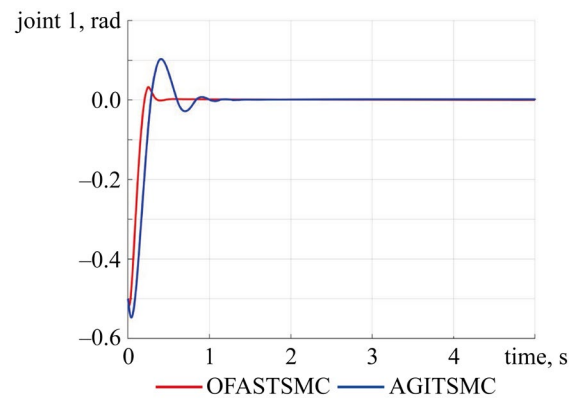


Fig. 4. Tracking error of Joint 1

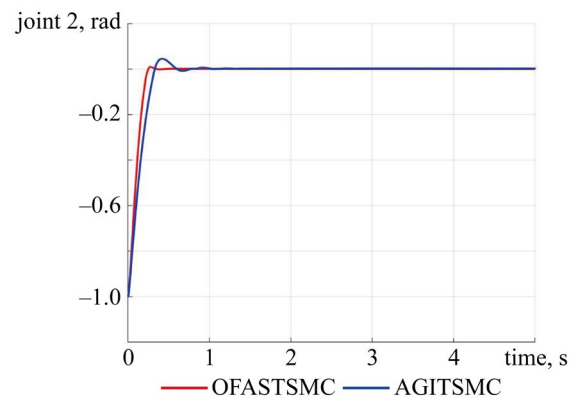


Fig. 5. Tracking error of Joint 2

The sliding surfaces of joints:

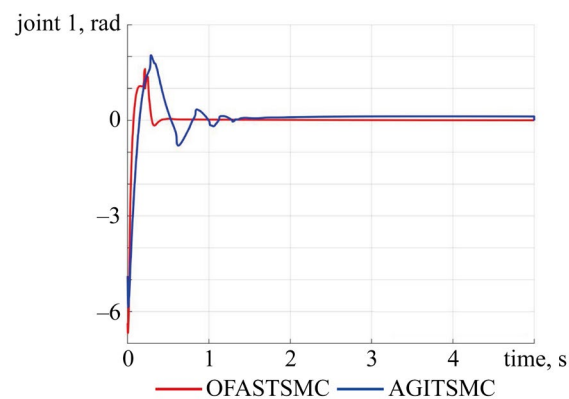


Fig. 6. Sliding surface of Joint 1

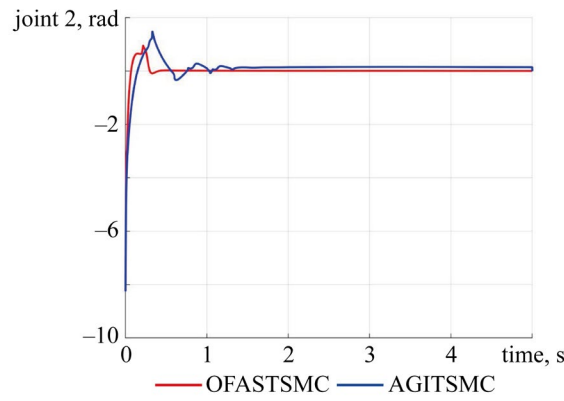


Fig. 7. Sliding surface of Joint 2

The control laws of joints:

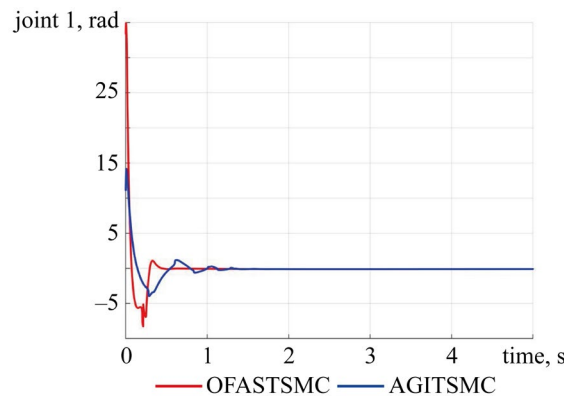


Fig. 8. Control law of Joint 1

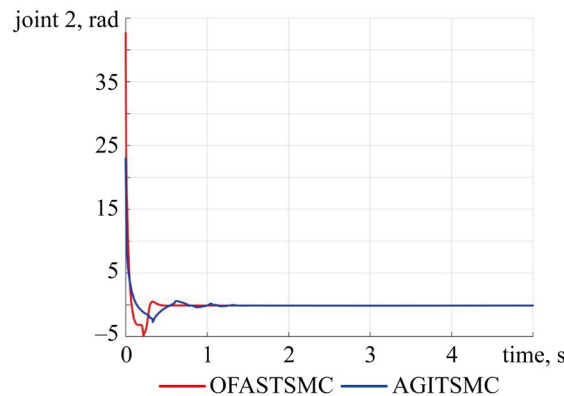


Fig. 9. Control law of Joint 2

Discussion. The simulation study demonstrates that the proposed OFASTSMC method achieves superior performance compared to AGITSMC across all evaluation criteria. Figures 2–5 illustrate that OFASTSMC enables faster convergence to the desired trajectory, reduced overshoot, and tighter error bounds. Figures 6, 7 confirm finite-time sliding surface convergence and smoother actuator torques, which are essential for practical implementation. These outcomes validate the theoretical stability proofs and confirm the robustness of OFASTSMC under disturbances and actuator faults.

In relation to existing works, the results highlight several advances. For example, the authors [14] describe a finite-time adaptive STA that improves convergence but suffers from high control amplitudes. Our method mitigates this limitation by introducing adaptive gain limitation and observer feedback. Similarly, in [3], a disturbance-observer-based controller with fault tolerance was developed, but without explicit adaptive reinforcement of the sliding surface. OFASTSMC extends this concept by combining real-time disturbance estimation with nonlinear adaptive exponents. Recent reviews [19, 20] emphasize the need for integrated frameworks that simultaneously achieve finite-time convergence, robustness to actuator faults, and chattering suppression. Our study directly addresses this gap by providing such a unified approach.

Conclusion. Based on the conducted research, the main conclusions are as follows:

1. Theoretical contribution. A novel observer-based finite-time adaptive reinforced super-twisting sliding mode control (OFASTSMC) algorithm has been developed. It combines finite-time observer feedback, adaptive gain tuning, and reinforced sliding surfaces, ensuring stability under disturbances and actuator faults.

2. Performance improvement. Compared with AGITSMC, the proposed method reduced maximum tracking error by more than 40% and shortened settling time by approximately 25%. Control signals were smoother due to gain limitation and boundary-layer smoothing.

3. Robustness and fault tolerance. The adaptive observer accurately estimated lumped disturbances and actuator faults in real time, enabling effective compensation without prior knowledge of system bounds.

4. Scientific novelty. Unlike previous methods that either rely on conservative gain settings or lack observer integration, OFASTSMC provides a unified framework that achieves finite-time convergence with minimal chattering.

Practical implications. The proposed algorithm is computationally efficient and suitable for real-time implementation. Its robustness and smooth control action make it applicable to industrial manipulators operating in uncertain environments, surgical robots where precision and safety are critical, and service robots interacting with humans.

Future research directions:

- Extension of OFASTSMC to task-space control for complex multi-DOF manipulators.
- Hardware validation on physical robotic platforms to confirm robustness under sensor noise and model uncertainties.
- Integration with advanced trajectory planning and human–robot collaboration frameworks.
- Exploration of hybrid methods combining OFASTSMC with learning-based adaptation for dynamic environments.

In summary, OFASTSMC offers a strong advancement in the field of fault-tolerant control for robotic manipulators, bridging theoretical innovation with practical applicability.

References

1. Tianli Li, Gang Zhang, Tan Zhang, Jing Pan. Adaptive Neural Network Tracking Control of Robotic Manipulators Based on Disturbance Observer. *Processes*. 2024;12(3):499. <https://doi.org/10.3390/pr12030499>
2. Aohua Liu, Bo Zhang, Weiliang Chen, Yiang Luo, Shuxian Fang, Ouyang Zhang. Reinforcement Learning Based Control for Uncertain Robotic Manipulator Trajectory Tracking. In: *Proc. China Automation Congress (CAC)*. New York City: IEEE; 2022. P. 2740–2745. <https://doi.org/10.1109/CAC57257.2022.10055583>
3. Zeeshan Anjum, Zhe Sun, Bo Chen. Disturbance-Observer-Based Fault-Tolerant Control of Robotic Manipulator: A Fixed-Time Adaptive Approach. *IET Control Theory and Applications*. 2024;18(11):1398–1413. <https://doi.org/10.1049/cth2.12672>
4. Pertuz SA, Podlubne A, Goehringer D. An Efficient Accelerator for Nonlinear Model Predictive Control. In: *Proc. IEEE 34th International Conference on Application-specific Systems, Architectures and Processors (ASAP)*. New York City: IEEE; 2023. P. 180–187. <https://doi.org/10.1109/ASAP57973.2023.00038>
5. Cruz-Ortiz D, Chairez I, Poznyak A. Adaptive Sliding-Mode Trajectory Tracking Control for State Constraint Master–Slave Manipulator Systems. *ISA Transactions*. 2022;127:273–282. <https://doi.org/10.1016/j.isatra.2021.08.023>
6. Yung-Hsiang Chen. Nonlinear Adaptive Fuzzy Hybrid Sliding Mode Control Design for Trajectory Tracking of Autonomous Mobile Robots. *Mathematics*. 2025;13(8):1329. <https://doi.org/10.3390/math13081329>
7. Marinelli M. From Industry 4.0 to Construction 5.0: Exploring the Path towards Human–Robot Collaboration in Construction. *Systems*. 2023;11(3):152. <https://doi.org/10.3390/systems11030152>
8. Jinhua Xiao, Kaile Huang. A Comprehensive Review on Human–Robot Collaboration Remanufacturing towards Uncertain and Dynamic Disassembly. *Manufacturing Review*. 2024;11:17. <https://doi.org/10.1051/mfreview/2024015>
9. Dhanda M, Rogers BA, Hall S, Dekoninck E, Dhokia V. Reviewing Human-Robot Collaboration in Manufacturing: Opportunities and Challenges in the Context of Industry 5.0. *Robotics and Computer-Integrated Manufacturing*. 2025;93:102937. <https://doi.org/10.1016/j.rcim.2024.102937>
10. Mohamed MJ, Oleiwi BK, Abood LH, Azar AT, Hameed IA. Neural Fractional Order PID Controllers Design for 2-Link Rigid Robot Manipulator. *Fractal and Fractional*. 2023;7(9):693. <https://doi.org/10.3390/fractalfract7090693>
11. Eltayeb A, Ahmed G, Imran IH, Alyazidi NM, Abubaker A. Comparative Analysis: Fractional PID vs. PID Controllers for Robotic Arm Using Genetic Algorithm Optimization. *Automation*. 2024;5(3):230–245. <https://doi.org/10.3390/automation5030014>
12. Gold T, Völz A, Graichen K. Model Predictive Interaction Control for Robotic Manipulation Tasks. *IEEE Transactions on Robotics*. 2023;39(1):76–89. <https://doi.org/10.1109/TRO.2022.3196607>
13. Jinxin Zhang, Hongze Wang. Online Model Predictive Control of Robot Manipulator with Structured Deep Koopman Model. *IEEE Robotics and Automation Letters*. 2023;8(5):3102–3109. <https://doi.org/10.1109/LRA.2023.3264816>

14. Zu-Ren Feng, Rui-Zhi Sha, Zhi-Gang Ren. A Chattering-Reduction Sliding Mode Control Algorithm for Affine Systems with Input Matrix Uncertainty. *IEEE Access*. 2022;10:58982–58996. <https://doi.org/10.1109/ACCESS.2022.3179580>
15. Zeinali M. Adaptive Chattering-Free Sliding Mode Control Design Using Fuzzy Model of the System and estimated uncertainties and its application to robot manipulators. In: *Proc. International Workshop on Recent Advances in Sliding Modes (RASMD)*. New York City: IEEE; 2015. P. 1–6. <https://doi.org/10.1109/RASMD.2015.7154652>
16. Boiko I. Chattering in Mechanical Systems under Sliding-Mode Control. In book: Oliveira TR, Fridman L, Hsu L (eds). *Sliding-Mode Control and Variable-Structure Systems. Studies in Systems, Decision and Control*. Cham: Springer; 2023. P. 337–356. https://doi.org/10.1007/978-3-031-37089-2_13
17. Minghao Liu, Qirong Tang, Yinghao Li, Changhui Liu, Min Yu. A Chattering-Suppression Sliding Mode Controller for an Underwater Manipulator Using Time Delay Estimation. *Journal of Marine Science and Engineering*. 2023;11(9):1742. <https://doi.org/10.3390/jmse11091742>
18. Rehman FU, Mufti MR, Din SU, Afzal H, Qureshi MI, Khan M. Adaptive Smooth Super-Twisting Sliding Mode Control of Nonlinear Systems with Unmatched Uncertainty. *IEEE Access*. 2020;8:177932–177940. <https://doi.org/10.1109/ACCESS.2020.3027194>
19. Mondal S, Mahanta Ch. Adaptive Integral Higher Order Sliding Mode Controller for Uncertain Systems. *Journal of Control Theory and Applications*. 2013;11:61–68. <https://doi.org/10.1007/s11768-013-1180-5>
20. Mirzaei MJ, Hamida MA, Plestan F, Taleb M. Super-Twisting Sliding Mode Controller with Self-Tuning Adaptive Gains. *European Journal of Control*. 2022;68:100690. <https://doi.org/10.1016/j.ejcon.2022.100690>
21. Shtessel YuB, Moreno JA, Plestan F, Fridman LM, Poznyak AS. Super-Twisting Adaptive Sliding Mode Control: A Lyapunov Design. In: *Proc. 49th IEEE Conference on Decision and Control (CDC)*. New York City: IEEE; 2010. P. 5109–5113. <https://doi.org/10.1109/CDC.2010.5717908>
22. Jiabin Hu, Xue Zhang, Dan Zhang, Yun Chen, Hongjie Ni, Huageng Liang. Finite-Time Adaptive Super-Twisting Sliding Mode Control for Autonomous Robotic Manipulators with Actuator Faults. *ISA Transactions*. 2024;144:342–351. <https://doi.org/10.1016/j.isatra.2023.10.028>
23. Xinyue Hu, Ban Wang, Yanyan Shen, Yifang Fu, Ni Li. Disturbance Observer-Enhanced Adaptive Fault-Tolerant Control of a Quadrotor UAV against Actuator Faults and Disturbances. *Drones*. 2023;7(8):541. <https://doi.org/10.3390/drones7080541>
24. Jiqing Chen, Qingsong Tang, Chaoyang Zhao, Haiyan Zhang. Adaptive Sliding Mode Control for Robotic Manipulators with Backlash. *Proceedings of the Institution of Mechanical Engineers, Part C: Journal of Mechanical Engineering Science*. 2023;237(24):5842–5852. <https://doi.org/10.1177/09544062231167555>
25. Jiqian Xu, Lijin Fang, Huaizhen Wang, Qiankun Zhao, Yingcai Wan, Yue Gao. Observer-Based Finite-Time Prescribed Performance Sliding Mode Control of Dual-Motor Joints-Driven Robotic Manipulators with Uncertainties and Disturbances. *Actuators*. 2024;13(9):325. <https://doi.org/10.3390/act13090325>
26. Shanchao Yi, Junyong Zhai. Adaptive Second-Order Fast Nonsingular Terminal Sliding Mode Control for Robotic Manipulators. *ISA Transactions*. 2019;90:41–51. <https://doi.org/10.1016/j.isatra.2018.12.046>
27. Tinoco V, Silva MF, Santos FN, Morais R, Magalhães SA, Moura P. A Review of Advanced Controller Methodologies for Robotic Manipulators. *International Journal of Dynamics and Control*. 2025;13:36. <https://doi.org/10.1007/s40435-024-01533-1>
28. Romero S, Valero J, Garcia AV, Rodriguez CF, Montes AM, Marin C, et al. Trajectory Planning for Robotic Manipulators in Automated Palletizing: A Comprehensive Review. *Robotics*. 2025;14(5):55. <https://doi.org/10.3390/robotics14050055>
29. Kharrat M, Alhazmi H. Fixed-Time Adaptive Control for Nonstrict-Feedback Nonlinear Systems with Input Delay and Unknown Backlash-Like Hysteresis. *Neural Processing Letters*. 2025;57:52. <https://doi.org/10.1007/s11063-025-11749-7>
30. Huanqing Wang, Zhu Meng. Fixed-Time Adaptive Neural Tracking Control for High-Order Nonlinear Switched Systems with Input Saturation and Dead-Zone. *Applied Mathematics and Computation*. 2024;480:128904. <https://doi.org/10.1016/j.amc.2024.128904>
31. Bhat SP, Bernstein DS. Finite-Time Stability of Continuous Autonomous Systems. *SIAM Journal of Control and Optimization*. 2000;38(3):751–766. <https://doi.org/10.1137/S0363012997321358>
32. Amato F, Ambrosino M, Ariola M, Consentino C, De Tommasi G. *Finite-Time Stability and Control*. New York, NY: Springer; 2013. 146 p. <https://doi.org/10.1007/978-1-4471-5664-2>
33. Honglei Xu. Finite-Time Stability Analysis: A Tutorial Survey. *Complexity*. 2020;9:1–12. <https://doi.org/10.1155/2020/1941636>
34. Khalid K, Zaidi AA, Ayaz Y. Optimal Placement and Kinematic Design of 2-DoF Robotic Arm. In: *Proc. International Bhurban Conference on Applied Sciences and Technologies (IBCAST)*. New York City: IEEE; 2021. P. 552–559. <https://doi.org/10.1109/IBCAST51254.2021.9393255>

35. Hameed WN, Khawwaf JO. Robust Sliding Mode Control for 2-Dof Robot Manipulator Position Control System. In: *Proc. 2nd International Conference on Emerging Trends and Applications in Artificial Intelligence*. 2024;2024(34):282–288. <https://doi.org/10.1049/icp.2025.0096>

36. Bouzid R, Gritli H, Narayan J. Optimized Inverse Kinematics of a 2-DoF Robotic Manipulator Using a Hybrid Approach Combining an ANN with a Metaheuristic Algorithm. In: *Proc. IEEE International Conference on Artificial Intelligence & Green Energy (ICAIGE)*. New York City: IEEE; 2024. P. 1–6. <https://doi.org/10.1109/ICAIGE62696.2024.10776675>

About the Author:

Hoang Duc Long, PhD, Lecturer of the Department of Automation and Computing Techniques, Le Quy Don Technical University (236, Hoang Quoc Viet, Hanoi, 10065, Vietnam), [ORCID](#), [ScopusID](#), [ResearcherID](#), longhd@lqdtu.edu.vn

Conflict of Interest Statement: the author declares no conflict of interest.

The author has read and approved the final manuscript.

Об авторе:

Хоанг Дык Лонг, PhD, преподаватель кафедры «Автоматизация и вычислительная техника» Технического университета имени Ле Куи Дона (10065, Вьетнам, Ханой, ул. Хоанг Куок Вьет, 236), [ORCID](#), [ScopusID](#), [ResearcherID](#), longhd@lqdtu.edu.vn

Конфликт интересов: автор заявляет об отсутствии конфликта интересов.

Автор прочитал и одобрил окончательный вариант рукописи.

Received / Поступила в редакцию 01.09.2025

Reviewed / Поступила после рецензирования 26.09.2025

Accepted / Принята к публикации 10.10.2025

INFORMATION TECHNOLOGY, COMPUTER SCIENCE AND MANAGEMENT ИНФОРМАТИКА, ВЫЧИСЛИТЕЛЬНАЯ ТЕХНИКА И УПРАВЛЕНИЕ



UDC 656.11

Original Empirical Research

<https://doi.org/10.23947/2687-1653-2025-25-4-2215>

Comparative Analysis of Neural Network and Machine Learning Models for Short-Term Traffic Flow Prediction on Shenzhen Expressway



EDN: DWKVUM

Ivan V. Topilin , Mengyi Han , Anastasia A. Feofilova , Nikita A. Beskopylny

Don State Technical University, Rostov-on-Don, Russian Federation

✉ ivan_top@mail.ru

Abstract

Introduction. With highway congestion increasing, the efficiency of intelligent transportation systems depends on high-quality short-term traffic prediction. Statistical methods do not adequately account for nonlinear and dynamic traffic changes. Long short-term memory (LSTM) and support vector machines (SVR) offer more promising solutions. However, they are not ranked in terms of accuracy, as there are no studies comprehensively comparing their adequacy for short-term traffic flow prediction. The proposed study fills this gap. The research objective is to compare the accuracy of LSTM and SVR, and select the optimal approach for traffic flow prediction on Shenzhen Meiguang Expressway.

Materials and Methods. Traffic detector data was collected on the Meiguan Expressway in June 2021. Data preprocessing methods were used, including weighted mean imputation and normalization. Autocorrelation analysis was used for feature extraction, along with the creation of an interaction variable between speed and detector occupancy. Models were trained and tested on data collected from detectors at 5-minute intervals.

Results. LSTM performed 17.86% better in terms of root mean square error, 19.82% better in terms of mean absolute error, and 25.78% better in terms of mean absolute percentage error. In periods with the lowest flow rate prediction error, RMSE, MAE, and MAPE for the LSTM model were 36.5%, 34.3%, and 42.3% lower, respectively. In periods with the highest error, RMSE, MAE, and MAPE for the LSTM model were 73.2%, 65.4%, and 64.4% lower, respectively. The Wilcoxon signed-rank test <0.05 confirmed the statistical significance of the differences.

Discussion. The superior predictive performance of LSTM stems from its architecture, namely, the combination of interaction variables and lag metrics. LSTM accounts better for flow time dependences, adapts to complex, long-term dynamic changes, and remains accurate even with significant fluctuations. The lower predictive performance of SVR stems from its weak, nonlinear approximation ability. Sudden flow changes increase significantly error rates.

Conclusion. When choosing between a neural network and a machine learning model for short-term traffic flow prediction on an expressway, the neural network model, such as LSTM, should be preferred. These research results can be useful in predictive strategies for reducing congestion. Short-term prediction based on LSTM can serve as a basis for optimizing traffic management, reducing congestion and pollutant emissions, and for optimizing intelligent transportation systems. A promising direction is the development of hybrid architectures that integrate contextual data (weather, infrastructure, accidents) to improve real-time predictions.

Keywords: short-term traffic flow prediction, traffic flow prediction error, long short-term memory (LSTM) model, support vector machine for regression (SVR)





Acknowledgements. The authors would like to thank the Editorial board and the reviewers for their attentive attitude to the article and the specified comments that helped the authors to improve its quality.

For Citation. Topilin IV, Han M, Feofilova AA, Beskopylny NA. Comparative Analysis of Neural Network and Machine Learning Models for Short-Term Traffic Flow Prediction on Shenzhen Expressway. *Advanced Engineering Research (Rostov-on-Don)*. 2025;25(4):350–362. <https://doi.org/10.23947/2687-1653-2025-25-4-2215>

Оригинальное эмпирическое исследование

Сравнительный анализ нейросетевой и машинной моделей для краткосрочного прогнозирования транспортного потока на скоростной автомагистрали

Мэйгуан Шэньчжэня

И.В. Топилин , М. Хань , А.А. Феофилова , Н.А. Бескопыльный 

Донской государственный технический университет, г. Ростов-на-Дону, Российская Федерация

✉ ivan_top@mail.ru

Аннотация

Введение. При растущей загруженности автомагистралей эффективность интеллектуальных транспортных систем зависит от качественного краткосрочного прогнозирования потоков. Статистические методы недостаточно точно учитывают нелинейные и динамические изменения трафика. Более перспективны модель долгой краткосрочной памяти (LSTM) и метод опорных векторов (SVR). Однако они не ранжированы в плане корректности, так как нет работ по комплексному сопоставлению их адекватности для краткосрочного прогнозирования потоков. Представленное исследование восполняет этот пробел. Цель работы — сравнительный анализ точности LSTM и SVR и выбор оптимального подхода для прогнозирования транспортного потока на автомагистрали Мэйгуан Шэньчжэня.

Материалы и методы. Данные детекторов транспорта собраны в июне 2021 года на автомагистрали Мэйгуан. Использовались методы предварительной обработки данных, включая заполнение взвешенным средним и нормализацию. Для извлечения признаков применили автокорреляционный анализ, а также создание переменной взаимодействия скорости и занятости детектора. Модели обучались и тестировались на данных, полученных с детекторов с 5-минутными интервалами.

Результаты исследования. Показатели LSTM лучше на 17,86 % по среднеквадратической, на 19,82 % — по средней абсолютной и на 25,78 % — по средней абсолютной процентной ошибке. В периодах с наименьшей ошибкой прогнозирования интенсивности потока RMSE, MAE и MAPE для модели LSTM оказались меньше на 36,5 %, 34,3 % и 42,3 % соответственно. В периодах с наибольшей ошибкой RMSE, MAE и MAPE для LSTM оказались меньше на 73,2 %, 65,4 % и 64,4 % соответственно. Критерий Уилкоксона $<0,05$ подтвердил статистическую значимость различий.

Обсуждение. Лучшие прогнозные возможности LSTM обусловлены ее архитектурой, а именно комбинированием переменных взаимодействия и лаговых показателей. LSTM лучше учитывает временные зависимости потока, адаптируется к его сложным, долгосрочным динамическим изменениям и остается точной даже при значительных колебаниях. Меньшая прогнозная эффективность SVR обусловлена слабой, нелинейной аппроксимирующей способностью. При резких изменениях потока существенно увеличиваются показатели ошибок.

Заключение. При краткосрочном прогнозировании транспортного потока на скоростной автомагистрали, выбирая между нейросетевой и машинной моделью, следует предпочесть нейросетевую — например, LSTM. Результаты исследования целесообразно использовать в предиктивных стратегиях снижения заторов. Краткосрочное прогнозирование на основе LSTM может быть базой для оптимизации управления дорожным движением, снижения заторов и загрязняющих выбросов, а также для оптимизации интеллектуальных транспортных систем. Перспективное направление — разработка гибридных архитектур, интегрирующих контекстные данные (погода, инфраструктура, аварии) для улучшения прогнозов в режиме реального времени.

Ключевые слова: краткосрочное прогнозирование транспортных потоков, ошибка прогнозирования интенсивности потока, модель долгой краткосрочной памяти (LSTM), метод опорных векторов для регрессии (SVR)

Благодарности. Авторы выражают благодарность редакции и рецензентам за внимательное отношение к статье и замечания, которые позволили повысить ее качество.

Для цитирования. Топилин И.В., Хань М., Феофилова А.А., Бескопыльный Н.А. Сравнительный анализ нейросетевой и машинной моделей для краткосрочного прогнозирования транспортного потока на скоростной автомагистрали Мэйгуан Шэньчжэня. *Advanced Engineering Research (Rostov-on-Don)*. 2025;25(4):350–362. <https://doi.org/10.23947/2687-1653-2025-25-4-2215>

Introduction. The solution to the pressing global problem of efficient traffic management relies on accurate traffic analysis and prediction. Urbanization and globalization are transforming and overburdening road transport systems, requiring fundamentally new and universal approaches to manage them. Obviously, neural network solutions and adequate machine models can provide such solutions. Their testing and training should be based on data obtained on high-speed highways in megacities. In this case, the results can be extrapolated to similar systems, i.e., major highways with heavy traffic.

This research utilized data collected in Shenzhen, a large city in southeastern China. With a population exceeding 17.5 million, motorization is growing at an annual rate of 8%. Consequently, the metropolis faces increasing congestion on its 386-kilometer-long highways¹. The rapid development of the road network, on the one hand, contributes to significant economic growth in Chinese newest megacity, but on the other, it overloads the transport network and leads to disruptions [1]. Thus, Shenzhen problem is not a local anomaly, but a typical example of the “success disease” facing megacities worldwide. The current situation directly contradicts the following key UN Sustainable Development Goals (SDG)².

SDG 3 “Good Health and Well-Being”. Congestion is not just a waste of time. It is a source of chronic stress, increased noise, and, most importantly, air pollution (PM2.5, NOx). According to the WHO, air pollution is one of the leading health risks.

It is important to note that the electrification of transport, which Shenzhen is actively promoting, is only part of the solution. Decarbonization by reducing the number of private cars is also needed.

SDG 9 “Industry, Innovation, and Infrastructure”. Chronic congestion reduces economic competitiveness of the city. Losses from congestion increase logistics costs, reduce labor productivity, and make areas less attractive for investment.

SDG 11 “Sustainable Cities and Communities”. Congestion makes cities unsustainable. It reduces the efficiency of urban systems, increases the time and cost of travel, impairs access to basic services (healthcare, education), and reduces quality of life.

SDG 13 “Climate Action”. The transport sector is a major source of greenhouse gases. Congestion significantly increases CO₂ emissions per passenger-kilometer or ton-kilometer for passenger and freight transport, respectively.

The global scale of the problem stimulates scientific research in this area. One of the fundamental challenges of effective traffic management is high-quality operational (short-term) prediction. Currently, this task has not been solved, which is proved by the analysis of literary sources presented below. In most cases, the data presented therein is either fragmentary or does not take into account the specifics of high-speed highways.

Short-term traffic flow prediction (STTFP), a key task of intelligent transportation systems (ITS), enables proactive congestion management through dynamic pricing, route optimization, and rapid response to traffic incidents [2]. However, the nonlinear, seasonal, and stochastic nature of road traffic limits the efficiency of traditional statistical forecasting methods [3]. Examples include the autoregressive integrated moving average (ARIMA) model [4] and k -nearest neighbors (k NN), which do not always adequately reflect complex spatiotemporal dependences [5].

Recent advances in deep machine learning have revolutionized short-term traffic prediction. Long short-term memory (LSTM) models with a memory cell architecture are excellent at reproducing sequential data and are ideal for traffic prediction [6]. Support vector regression (SVR) also has its advantages [7]. It is kernel-based, robust, and computationally efficient in high-dimensional spaces [8]. Machine learning advancements have also promoted the widespread use of SVR, which utilizes kernel techniques to handle nonlinear dependences [9]. Deep learning models, especially LSTMs, dominate recent STTFP research [10].

A comparative analysis of LSTM and SVR showed good applicability of these methods to various traffic density variations. Furthermore, high accuracy in predicting traffic flow speed was demonstrated [11].

Despite the widespread use of these methods, there are still few comparative studies for highways with heavy, high-speed traffic. There is some information on point-type objects such as urban intersections or local highway sections. At the same time, there is not enough research with a comprehensive analysis of the highway network.

This paper is aimed to fill this gap. The Meiguang Expressway in the Chinese metropolis of Shenzhen is used as a case study. The objective of the paper is to compare the accuracy of LSTM and SVR models and select the optimal approach for predicting traffic flow on the Meiguang Expressway in Shenzhen. To reach this objective, the authors developed an integrated approach to data preprocessing and feature extraction. The potential for practical application of the models in ITS systems was explored.

¹ China Statistical Yearbook 2023. URL: <https://www.stats.gov.cn/sj/ndsj/2023/indexeh.htm> (accessed: 06.10.2024).

² Sustainable Development Goals. United Nations. (In Russ. URL: <https://www.un.org/sustainabledevelopment/ru/sustainable-development-goals/> (accessed: 21.10.2025).

Materials and Methods. The Meiguan Expressway (Fig. 1), located in Shenzhen, Guangdong Province, China, is a 19.3-kilometer section of the G94 Expressway (Pearl River Delta Ring Road). The design speed is 100 km/h.

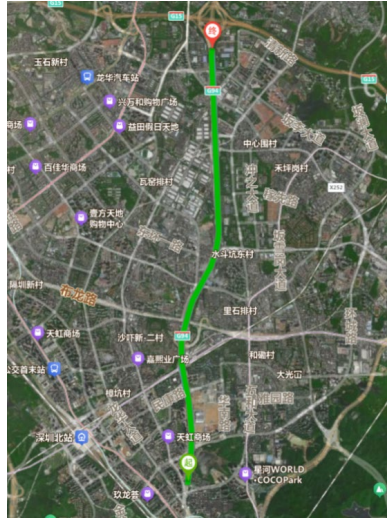


Fig. 1. Experimental section of the Meiguan Expressway (screenshot of a map from open sources)

The study focused on the south-north direction of the Meiguan Expressway. Data was collected using six inductive loop detectors (ILD) installed in the inner and outer pathways.

The following parameters were recorded at 5-minute intervals:

- traffic volume (units/5 min);
- detector occupancy (%);
- average speed (km/h);
- date and time interval (5 min);
- observation period: 7 days (from June 15 to June 21, 2021).

Total data volume: 1,144 records.

To improve the quality of analysis and modeling, preliminary data processing was performed [12]. The following were its stages.

1. Data screening. A selection from a set for identifying data that was valid and relevant to the model. Initially, the source dataset was divided by dates to select records with the most complete data, without obvious gaps. Invalid records with obvious gaps were removed. From the selected dates with complete data, consecutive dates were selected to study temporal variations in the flow.

2. Completing missing data. To provide accurate data collection, the equipment must operate without interruption. This can be hampered by random factors such as malfunctions, vehicle detector failures, weather conditions, power outages, etc. Therefore, the collected data was sometimes incomplete and contained gaps. However, they might contain important information about the process patterns. As a result, the prediction model did not receive sufficient data and became unstable, reducing the prediction reliability. Thus, before building a prediction model, it was required to fill in the missing data.

To compensate for periodically occurring time gaps in the traffic flow data, the presented work used the weighted mean method [13].

Step 1. Obtaining the mean value of traffic intensity for n points in time preceding the current moment:

$$f_1(t) = \frac{f^k(t-1) + f^k(t-2) + \dots + f^k(t-n)}{n}.$$

Step 2. Mean traffic intensity at the current moment, for the previous m days:

$$f_2(t) = \frac{f^{(k-m)}(t) + f^{(k-(m-1))}(t) + \dots + f^{(k-1)}(t)}{m}.$$

Step 3. Filling in missing data:

$$f^{(k)}(t) = af_1(t) + (1-a)f_2(t),$$

where $f^{(k)}(t)$ — reconstruction of traffic flow data at time t of day k , a — weight coefficient, $a = 0.6$.

The method is the basic one when working with missing data. It takes into account such properties of traffic volume data as:

- cyclical nature — $f_1(t)$;
- temporal nature — $f_2(t)$, i.e., the effect of traffic data from previous time points.

3. Normalization. Traffic flow data can vary significantly depending on the time of day, road segment, and other factors, resulting in a wide spread of values. The activation function of some neural nodes takes values in the range $[0, 1]$. Therefore, normalization is performed before training [14]. This eliminates the impact of outliers in the data (samples that deviate significantly from others), and also speeds up network training and improves convergence.

The basic normalization methods are linear, nonlinear, and 0-mean normalization. The activation function takes values from 0 to 1, therefore, this article uses the maximum-minimum linear normalization method to transform traffic flow values into the range $[0, 1]$:

$$f(t) = \frac{f - f_{\min}}{f_{\max} - f_{\min}},$$

where f — raw traffic flow data; f_{\min} — minimum value in traffic flow data; f_{\max} — maximum value in traffic flow data; $f(t)$ — normalized value of traffic flow.

The processed data were reduced using the inverse normalization formula after the prediction model was derived:

$$f = (f_{\max} - f_{\min})f(t) + f_{\min}.$$

The data sampling frequency was 5 minutes, and the final preprocessed data volume was 3,168 records. Some of these records, obtained on June 17, 2021, are presented in Table 1.

Table 1

Examples of Preprocessed Experimental Data

Traffic intensity, units/5 min	Detector occupancy, %	Traffic flow speed, km/h	Time interval, 5 min
258	13.93	83.62	1
255	14.48	79.88	2
223	12.08	82.25	3
340	18.39	82.04	4
254	13.86	83.3	5
263	13.98	84.87	6
231	12.49	85.89	7
151	7.87	84.94	8
223	11.96	83.81	9
226	11.95	86.92	10
166	8.59	86.17	11
140	7.45	83.29	12
143	7.85	83.99	13
231	12.67	84.71	14
147	7.55	89.53	15
96	4.90	90.74	16
128	7.02	83.94	17
106	5.75	81.99	18
128	7.24	79.4	19
136	6.99	84.57	20

Feature extraction is a key step in building an effective traffic flow prediction model. Traffic data analysis and processing provide key feature information, which improves model performance and accuracy.

1. Time-lag feature extraction.

Data from one time series depends on other time series, and the autocorrelation function (ACF) describes the correlation of a time series with different lags, i.e., the degree of linear correlation between the series itself and its own lagged values [15]. This determines the relationship between current and past values. When analyzing time series, the relationship between the current value Y_t and its value Y_t at some previous point in time is of interest. Period of Lag k is the time interval between the current time point t and k -th time point in the past $t-k$.

When predicting traffic flows, ACF was used to determine periodicity and trends in time series data. This made it possible to select an appropriate lag step as a feature and reflect the dynamics of changes in traffic flow parameters (Fig. 2).

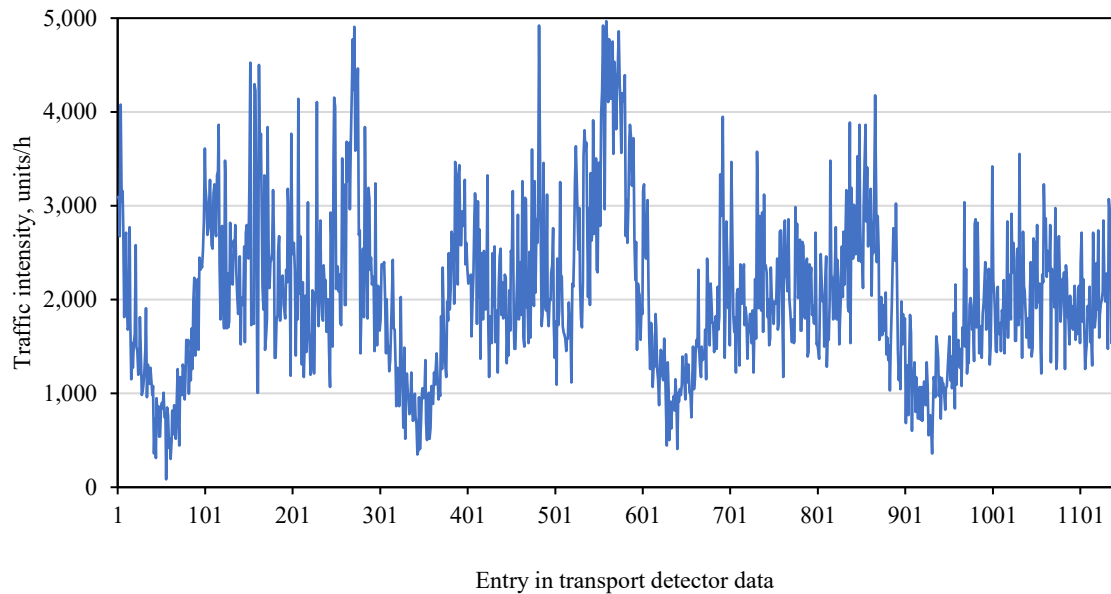


Fig. 2. Traffic dynamics on Meiguan Expressway

For the time series of traffic flow data, the ACF was calculated and the correlation between different time lags (e.g., $t-1$, $t-2$, ..., $t-n$) and the current moment t . The calculation results are presented in Figure 3.

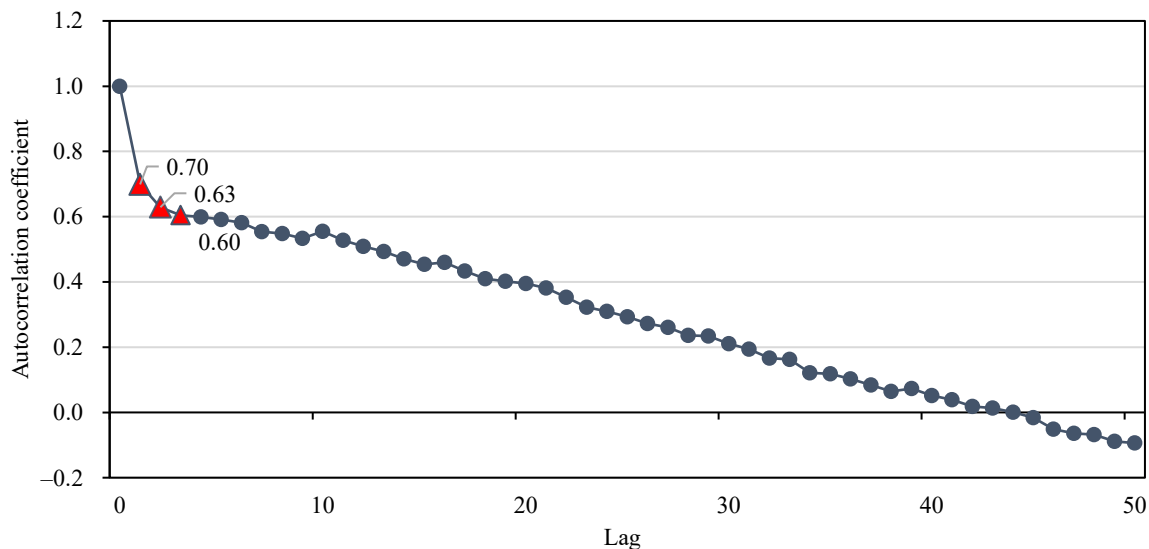


Fig. 3. Autocorrelation coefficients for different lag steps

Using the ACF threshold filtering method, three time lags with an autocorrelation coefficient >0.6 were selected: (Lag 1: 0.70, Lag 2: 0.63, Lag 3: 0.60). These lags were chosen as input features for the model. This approach enhances the model's ability to capture temporal patterns and provides a reliable data base for subsequent prediction models.

2. Interaction of speed and detector occupancy.

The product of speed and detector occupancy is used as a complex metric to represent the spatial-temporal variation of traffic flow [16]. Detector occupancy and speed are important traffic flow metrics. Their product can be used as a “feature interaction” term. This creates a new feature that better reflects the complexity and dynamics of traffic flow. Adding interaction terms can improve the expressiveness and approximation capabilities of machine learning models, specifically those such as LSTM and SVR. Interaction terms provide more information, helping the model better understand patterns and relationships in the data.

Model Architecture and Estimates

1. Support vector regression (SVR) is an extension of the support vector machine (SVM) algorithm [17]. The SVR model is suitable for solving complex nonlinear regression problems. It adapts well to nonlinear characteristics of traffic flow data, is highly robust to outliers, and can adapt to various data characteristics through adjusting the kernel function and regularization parameters. Therefore, in this paper, the SVR model is used as a comparative model for traffic flow prediction.

2. The long short-term memory (LSTM) neural network model is a variant of a recurrent neural network that is specifically designed to solve problems with long-term temporal dependences [18]. An LSTM directed recurrent neural network is capable of deeply revealing temporal dependences in predicting problems and effectively approximating nonlinear data. It can also retain information from time series for a long time [19]. This provides high efficiency of the model when working with data that has long time intervals and high latency. The advantages of LSTM in time series prediction and its high accuracy in long-term predictions are well known [20]. At the same time, the model has good robustness and flexibility, which allows it to be used for predicting traffic flows under vehicle-road coordination conditions. It is important to note that the LSTM structure combined interaction variables and lag indicators to improve prediction accuracy.

This paper evaluates the model prediction performance using the following representative performance metrics:

- mean absolute error;
- mean absolute percentage error;
- root mean square error [21].

This approach allows us:

- to quantitatively evaluate the accuracy of LSTM and SVR models;
- to visualize the discrepancy between actual traffic flow and the prediction results obtained using LSTM.

To test the statistically significant difference between the prediction errors of the LSTM and SVR models, this paper uses the Wilcoxon signed-rank test [22]. This is a nonparametric test for paired data in statistics. It is especially useful for small samples and when the data does not follow a normal distribution. The initial hypothesis (H_0) of the test is that there is no significant difference between the prediction errors of the LSTM and SVR models. P -value is a probability value used to detect a significant difference between two related samples. If P is less than a specified significance level (usually 0.05), the null hypothesis is rejected. In this case, it is assumed that the distribution of the difference between the two samples varies, meaning the sum of the ranks is significantly dissimilar. This paper demonstrates a significant difference in the prediction performance of LSTM and SVR. The calculation steps are described below.

Step 1. Calculating the difference in prediction errors between two models. The difference in prediction errors for each observation is calculated using the formula:

$$d_i = e_i^{(LSTM)} - e_i^{(SVR)}.$$

Step 2: Calculating the absolute values of the differences and ranking them.

Step 3: Calculating the sums of positive and negative ranks.

Step 4: Calculating the Wilcoxon P and comparing it to the critical value.

Results. In this study, Python was used to preprocess traffic data. The experimental dataset consisted of traffic data from June 17 to 20, 2021 (Table 2). The data was recorded at 5-minute intervals and contained 1,144 records. For traffic flow prediction and model evaluation, the data was divided into training and test sets.

Statistical Information about Datasets

Table 2

Indicator	Traffic intensity (units/h)
Minimum value	84
Maximum value	4968
Mean value	2052
Median	1944
Standard Deviation	864

The minimum traffic volume value is 84, and the maximum is 4968, indicating significant data dispersion. This suggests extremely low traffic volumes during certain periods of the day (e.g., early morning) and extremely high traffic volumes during rush hours. The mean value is 2052, and the median is 1944. The fact that the median is slightly smaller than the mean indicates the right-skewed data distribution. This means that traffic volume is high in most time intervals, while some periods of low volume (primarily early morning and late night) reduce the overall mean value. A standard deviation of 864 confirms significant flow fluctuations and sudden changes in traffic volume. Thus, the dataset is suitable for studying long-term dependences and nonlinear characteristics of time series and can serve as an experimental sample for traffic flow prediction.

As noted above, to improve prediction efficiency, this study uses the lag characteristic and the interaction variable between speed and detector occupancy as input features. This allows for a full accounting of the relationships between time series information and flow characteristics.

The SVR method uses the radial basis function (RBF kernel) as a kernel to capture nonlinear relationships.

Key parameters:

- 1) penalty coefficient $C = 2$ (tolerable error control);
- 2) maximum number of iterations — 120.

The LSTM parameters used in this study are described below.

- 1) Input layer: time step is the feature extraction delay step, which is equal to 1, 2, 3.
- 2) Hidden layer: single-layer LSTM structure containing 150 cells using the tanh activation function.
- 3) Regularization: a 10% dropout mechanism used to prevent overfitting.
- 4) Output Layer: a fully connected layer using a linear activation function to ensure continuous predicted values.
- 5) Training Strategy: Adam optimizer, learning rate = 0.08, batch size = 128, number of training rounds (epochs) = 120.

Figures 4 and 5 show the comparison of predicted and true values for the LSTM and SVR models.

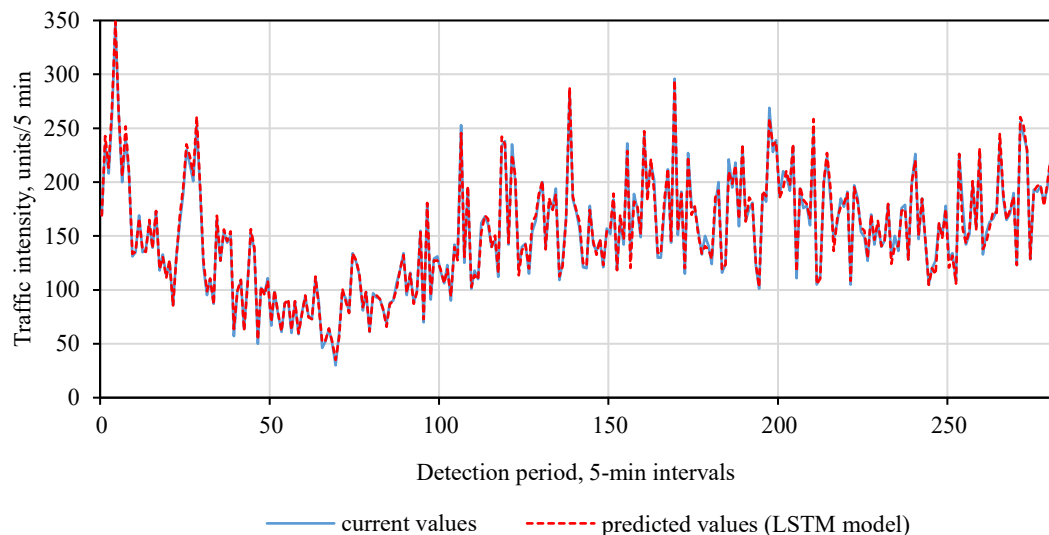


Fig. 4. Comparison of predicted and true values of LSTM

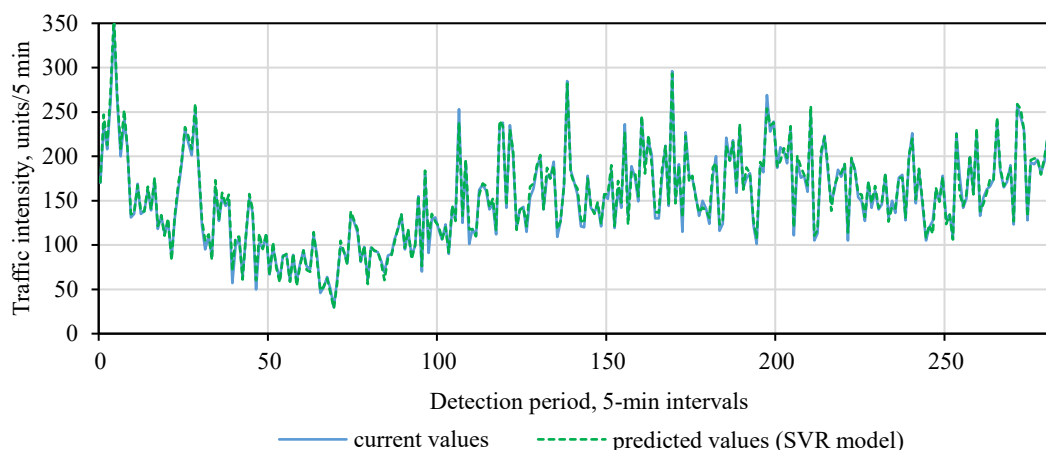


Fig. 5. Comparison of predicted and true values of SVR

The graphs show that the predicted values of the LSTM and SVR models reproduce real traffic flow dynamics well, with a small range of prediction errors. Therefore, these models were selected as control models for further evaluation of the efficiency of various methods in traffic flow prediction.

To increase the reliability of the experimental results and further validate the efficiency of the predictive models, this study conducted 10 training runs with different random initial values. In each experiment, the results for root mean square errors (RMSE), mean absolute errors (MAE), and mean absolute percentage errors (MAPE) were recorded.

To more clearly evaluate predictive performance, RMSE was chosen as the primary metric. From 10 experiments for each model, the five best results were selected, from which average values were calculated for comparative analysis.

Table 3 shows the prediction accuracy of the LSTM and SVR models. The RMSE, MAE, and MAPE errors for the LSTM model were 17.86%, 19.82%, and 25.78% lower, respectively, indicating higher prediction accuracy. MAPE reflects the percentage of prediction error relative to actual values. A lower MAPE score indicates more little relative errors for LSTM at different flow levels. LSTM demonstrates prediction stability during both peak and minimum periods, while SVR is more sensitive to extreme values.

Table 3

Prediction Errors of LSTM and SVR Models

Model	RMSE	MAE	MAPE
LSTM	4.6	3.48	2.39%
SVR	5.6	4.34	3.22%

Figure 6 shows the absolute percentage error of the predicted values relative to the actual values for each time interval along the flow time series. It is clearly seen that the absolute percentage error of the LSTM model is lower at most time points.

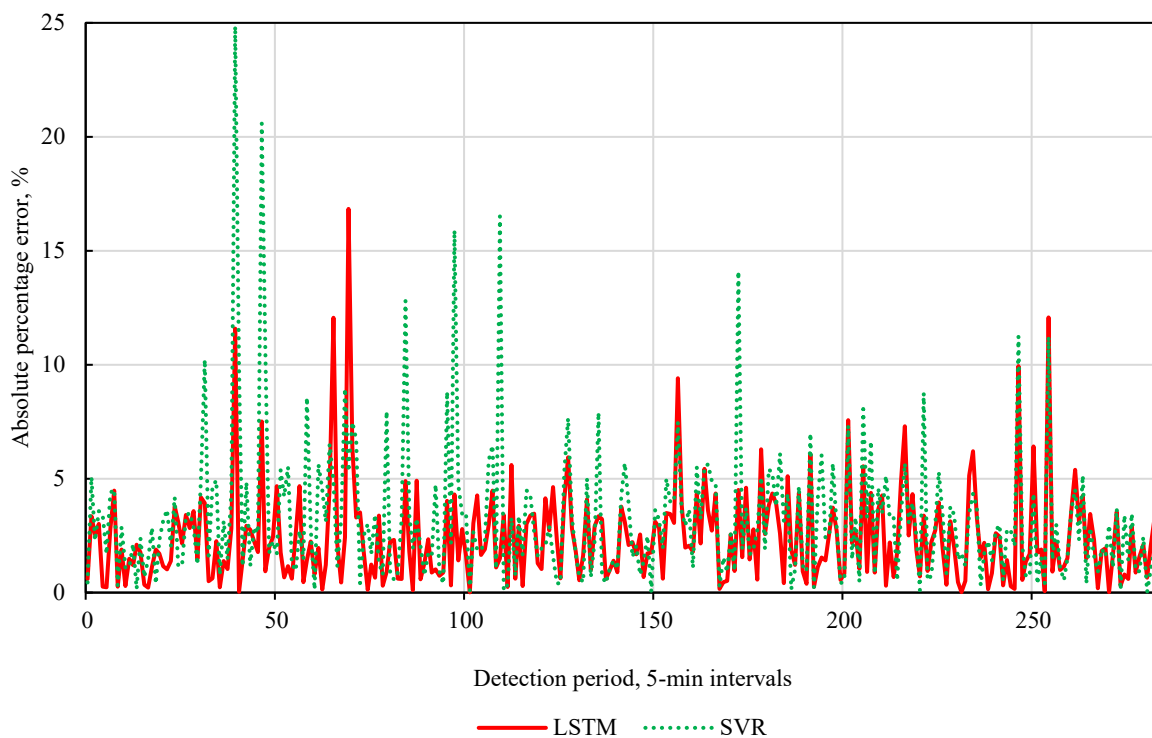


Fig. 6. Absolute percentage error for different time slices of LSTM and SVR

Comparing Figure 6 and Figure 4 (real values) shows that the peaks in the graph with large prediction errors correspond to time intervals with sharp changes in flow intensity. LSTM produces more stable prediction results and outperforms SVR in capturing flow peaks with nonlinear dynamic changes.

From Figure 6, we extracted the time intervals with the greatest error (timeslice: 36–72) and the least error (timeslice: 108–144). The numbers represent the 5-minute intervals. Data from these two periods was used in training models and predicting traffic flow to compare the ability of LSTM and SVR to capture dynamic characteristics of traffic flow. Figure 7 shows the prediction results of the LSTM and SVR models for the two specified time periods compared to the actual values.

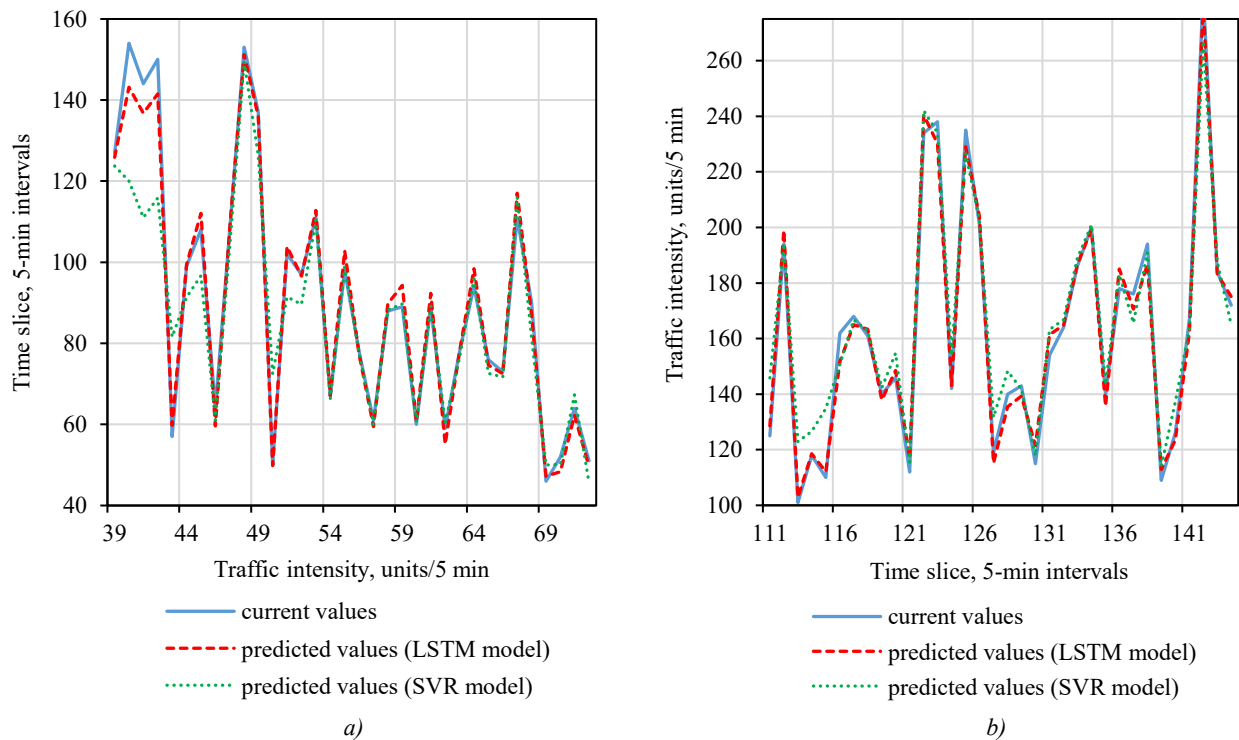


Fig. 7. Prediction curves by time periods: *a* — for time slices with the greatest error;
b — for time slices with the least error

Table 4 presents the prediction results of the two models for the periods with the greatest and least errors.

Table 4

Data on the Least and Greatest Prediction Errors of LSTM and SVR

Period	Model	RMSE	MAE	MAPE
With the least error	LSTM	6.14	4.84	2.99%
	SVR	9.67	7.37	5.19%
With the greatest error	LSTM	3.32	2.57	2.88%
	SVR	12,39	7.43	8.09%

The comparison shows that LSTM demonstrates better accuracy in periods with the least flow rate prediction error: the RMSE, MAE, and MAPE errors for the LSTM model are 36.5%, 34.3%, and 42.3% lower, respectively. In periods with the greatest flow rate prediction error, the advantage of LSTM is particularly noticeable: the RMSE, MAE, and MAPE errors for the LSTM model are 73.2%, 65.4%, and 64.4% lower, respectively. This shows the higher adaptability of this model.

To statistically test the significance of differences between the models, the Wilcoxon signed-rank test is used. The result ($P = 2.44e-15$) is tangibly less than 0.05. Therefore, the null hypothesis of no difference in prediction errors should be rejected. This proves a statistically significant difference in the performance of the models.

Along with RMSE, MAE, and MAPE evaluation, it is confirmed that the LSTM error is significantly lower and the error distribution is more concentrated, indicating higher prediction stability. The results convincingly demonstrate the advantages of LSTM when working with traffic flow time series data.

Discussion. Thus, prediction quality depends on the model architecture. Combining interaction variables and lag metrics in the LSTM structure resulted in improved prediction accuracy. Experiments revealed that LSTM outperformed SVR in terms of root-mean-square, mean absolute, and mean absolute percentage errors. This confirmed its superior predictive power under various traffic flow conditions. Flow stability affected prediction accuracy, but LSTM, thanks to its superior time series modeling capabilities, was able to more effectively account for flow temporal dependences and maintain high accuracy even under significant fluctuations. It is worth noting that LSTM not only effectively accounted for traffic flow temporal dependences but also adapted to complex, long-term dynamic changes. Hence — the more accurate results of short-term prediction.

The advantages of LSTM were significantly more pronounced in periods with the greatest flow rate prediction errors. The gain of this model in absolute percentage error in periods with the least error reached 42.3%, while in periods with the greatest error, it was 64.4%. For RMSE and MAE, the difference was twofold or almost twofold. The RMSE figures were 36.5% (periods with the least error) and 73.2% (periods with the greatest error). The corresponding figures for MAE were 34.3% and 65.4%.

The SVR method adapts well to nonlinear characteristics of traffic flow data, it is robust to outliers, and can adapt to various data characteristics through adjusting the kernel function and regularization parameters. Its computational efficiency is higher. However, this model is more sensitive to data noise due to the complexity of modeling long-term time dependence, which reduces prediction stability, especially in the presence of dynamic traffic flow fluctuations with great errors. The predictive performance of SVR is limited by its weaker, nonlinear approximation ability to sudden flow changes due to limitations of its own architecture, resulting in a significant increase in errors.

Conclusion. This study compared the performance of long short-term memory (LSTM) networks and support vector machine regression (SVR) for short-term traffic flow prediction on the Meiguan Expressway in Shenzhen. The LSTM model performed 17.86% better than the SVR in terms of mean squared error, 19.82% better in terms of mean absolute error, and 25.78% better in terms of mean absolute percentage error.

LSTM is also supported by its higher accuracy in periods with both the least error and the greatest one. In the first case, compared to SVR, the LSTM errors were 34.3–42.3% lower, in the second — by 64.4–73.2 %.

Thus, when choosing between a neural network and a machine learning model for short-term traffic flow prediction on a highway, the neural network model, in this case LSTM, should be preferred.

Let us outline three major results of this study for solving the problem of high-quality short-term prediction of traffic flows in large cities.

1. Using the Shenzhen Expressway as an example, it has been experimentally proven that LSTM as part of an intelligent transportation system can predict traffic flows quite reliably.

2. The differences in prediction accuracy between LSTM and SVR models were quantified, providing an objective basis for selecting algorithms for building traffic management systems. Statistical analysis confirmed the significance of the differences.

3. The following conclusions are important for the practice of traffic management on highways in large cities.

- LSTM effectively adapts to the temporal characteristics of traffic flows on highways.
- LSTM provides accurate predictions even under conditions of sharp fluctuations in traffic volume.
- The research findings enable the development of predictive strategies to reduce congestion.

Short-term traffic flow prediction based on LSTM allows for relatively accurate traffic volume prediction. This can serve as a basis for optimizing traffic management strategies, reducing congestion and pollutant emissions, and optimizing intelligent transportation systems.

A promising area for further research is the development of hybrid architectures that integrate contextual data (e.g., weather conditions, traffic incidents, or infrastructure features). This will improve the reliability and robustness of real-time prediction.

References

1. Garg T, Kaur G. A Systematic Review on Intelligent Transport Systems. *Journal of Computational and Cognitive Engineering*. 2022;2(3):175–188. <https://doi.org/10.47852/bonviewJCCE2202245>
2. Vlahogianni EI, Matthew GK, Golias JC. Short-Term Traffic Forecasting: Where We Are and Where We're Going. *Transportation Research. Part C: Emerging Technologies*. 2014;43(1):3–19. <https://doi.org/10.1016/j.trc.2014.01.005>
3. Williams BM, Hoel LA. Modeling and Forecasting Vehicular Traffic Flow as a Seasonal ARIMA Process: Theoretical Basis and Empirical Results. *Journal of Transportation Engineering*. 2003;129(6):664–672. [https://doi.org/10.1061/\(ASCE\)0733-947X\(2003\)129:6\(664\)](https://doi.org/10.1061/(ASCE)0733-947X(2003)129:6(664))
4. Lippi M, Bertini M, Frasconi P. Short-Term Traffic Flow Forecasting: An Experimental Comparison of Time-Series Analysis and Supervised Learning. *IEEE Transactions on Intelligent Transportation Systems*. 2013;14(2):871–882. <https://doi.org/10.1109/TITS.2013.2247040>
5. Zhenjin Huang, Hao Ouyang, Yiming Tian. Short-Term Traffic Flow Combined Forecasting Based on Nonparametric Regression. In: *Proc. International Conference of Information Technology, Computer Engineering and Management Sciences*. New York City: IEEE; 2011. P. 316–319. <https://doi.org/10.1109/ICM.2011.89>
6. Polson NG, Sokolov VO. Deep Learning for Short-Term Traffic Flow Prediction. *Transportation Research. Part C: Emerging Technologies*. 2017;79:1–17. <https://doi.org/10.1016/j.trc.2017.02.024>
7. Ceperic E, Ceperic V, Baric A. A Strategy for Short-Term Load Forecasting by Support Vector Regression Machines. *IEEE Transactions on Power Systems*. 2013;28(4):4356–4364. <https://doi.org/10.1109/TPWRS.2013.2269803>

8. Weiwei Zhu, Jinglin Wu, Ting Fu, Junhua Wang, Jie Zhang, Qiangqiang Shanguan. Dynamic Prediction of Traffic Incident Duration on Urban Expressways: A Deep Learning Approach Based on LSTM and MLP. *Journal of Intelligent and Connected Vehicles*. 2021;4(2):80–91. <https://doi.org/10.1108/JICV-03-2021-0004>
9. Peng Chen, Yong-zai Lu. Extremal Optimization for Optimizing Kernel Function and Its Parameters in Support Vector Regression. *Journal of Zhejiang University Science C*. 2011;12:297–306. <https://doi.org/10.1631/jzus.C1000110>
10. Feihu Ma, Shiqi Deng, Sang Mei. A Short-Term Highway Traffic Flow Forecasting Model Based on CNN-LSTM with an Attention Mechanism. *Journal of Physics: Conference Series*. 2023;2491:012008. <https://doi.org/10.1088/1742-6596/2491/1/012008>
11. Liu Mingyu, Wu Jianping, Wang Yubo, He Lei. Traffic Flow Prediction Based on Deep Learning. *Journal of System Simulation*. 2018;30(11):4100–4106. URL: <https://dc-china-simulation.researchcommons.org/journal/vol30/iss11/7> (accessed 09.09.2025).
12. García S, Ramírez-Gallego S, Luengo J, Benítez JM, Herrera F. Big Data Preprocessing: Methods and Prospects. *Big Data Analytics*. 2016;1:9. <https://doi.org/10.1186/s41044-016-0014-0>
13. Robin Kuok Cheong Chan, Joanne Mun-Yee Lim, Rajendran Parthiban. A Neural Network Approach for Traffic Prediction and Routing with Missing Data Imputation for Intelligent Transportation System. *Expert Systems with Applications*. 2021;171:114573. <https://doi.org/10.1016/j.eswa.2021.114573>
14. Chahinez Ounoughi, Sadok Ben Yahia. Sequence to Sequence Hybrid Bi-LSTM Model for Traffic Speed Prediction. *Expert Systems with Applications*. 2024;236:121325. <https://doi.org/10.1016/j.eswa.2023.121325>
15. Rong Chen, Lijian Yang, Christian Hafner. Nonparametric Multistep-Ahead Prediction in Time Series Analysis. *Journal of the Royal Statistical Society. Series B: Statistical Methodology*. 2004;66(3):669–686. <https://doi.org/10.1111/j.1467-9868.2004.04664.x>
16. Aqib M, Mehmood R, Alzahrani A, Katib I, Albeshri A, Altowaijri SM. Smarter Traffic Prediction Using Big Data, In-Memory Computing, Deep Learning and GPUs. *Sensors*. 2019;19(9):2206. <https://doi.org/10.3390/s19092206>
17. Xian Yao Ling, Xinxin Feng, Zhonghui Chen, Yiwen Xu, Haifeng Zheng. Short-Term Traffic Flow Prediction with Optimized Multi-kernel Support Vector Machine. In: *Proc. IEEE Congress on Evolutionary Computation (CEC)*. New York City: IEEE; 2017. P. 294–300. <https://doi.org/10.1109/CEC.2017.7969326>
18. Zhou Zhao, Ashok Srivastava, Lu Peng, Qing Chen. Long Short-Term Memory Network Design for Analog Computing. *ACM Journal on Emerging Technologies in Computing Systems (JETC)*. 2019;15(1):1–27. <https://doi.org/10.1145/3289393>
19. Srivastava N, Hinton G, Krizhevsky A, Sutskever I, Salakhutdinov R. Dropout: A Simple Way to Prevent Neural Networks from Overfitting. *Journal of Machine Learning Research*. 2014;15:1929–1958. URL: https://www.jmlr.org/papers/volume15/srivastava14a/srivastava14a.pdf?utm_content=buffer79b4 (accessed: 21.10.2025).
20. Yang Zhu, Yijun Gao, Zhenhao Wang, Guansen Cao, Renjie Wang, Song Lu, et al. A Tailings Dam Long-Term Deformation Prediction Method Based on Empirical Mode Decomposition and LSTM Model Combined with Attention Mechanism. *Water*. 2022;14(8):1229. <https://doi.org/10.3390/w14081229>
21. Pan B, Demiryurek U, Shahabi C. Utilizing Real-World Transportation Data for Accurate Traffic Prediction. In: *Proc. IEEE 12th International Conference on Data Mining*. New York City: IEEE; 2012. P. 595–604. <https://doi.org/10.1109/ICDM.2012.52>
22. Moors G, Vriens I, Gelissen JP, Vermunt JK. Two of a Kind. Similarities Between Ranking and Rating Data in Measuring Values. *Survey Research Methods*. 2016;10(1):15–33. <https://doi.org/10.18148/srm/2016.v10i1.6209>

About the Authors:

Ivan V. Topilin, Cand.Sci. (Eng.), Associate Professor of the Department of Organization of Transportation and Road Traffic Management, Don State Technical University (1, Gagarin Sq., Rostov-on-Don, 344003, Russian Federation), [SPIN-code](#), [ORCID](#), [ScopusID](#), ivan_top@mail.ru

Mengyi Han, Postgraduate student of the Department of Organization of Transportation and Road Traffic Management, Don State Technical University (1, Gagarin Sq., Rostov-on-Don, 344003, Russian Federation), [ORCID](#), hanmengyi@mail.ru

Anastasia A. Feofilova, Cand.Sci. (Eng.), Associate Professor of the Department of Organization of Transportation and Road Traffic Management, Don State Technical University (1, Gagarin Sq., Rostov-on-Don, 344003, Russian Federation), [SPIN-code](#), [ORCID](#), [ScopusID](#), afeofilova@donstu.ru

Nikita A. Beskopylny, Postgraduate student of the Department of Organization of Transportation and Road Traffic Management, Don State Technical University (1, Gagarin Sq., Rostov-on-Don, 344003, Russian Federation), [SPIN-code](#), [ORCID](#), [ResearchGate](#), [ScopusID](#), nbeskopylnyi@donstu.ru

Claimed Contributorship:

IV Topilin: conceptualization, supervision.

AA Feofilova: validation, writing – review & editing.

M Han: investigation, validation, writing – original draft preparation.

NA Beskopylny: investigation, validation, writing – original draft preparation.

Conflict of Interest Statement: the authors declare no conflict of interest.

All authors have read and approved the final manuscript.

Об авторах:

Иван Владимирович Топилин, кандидат технических наук, доцент кафедры «Организация перевозок и дорожного движения» Донского государственного технического университета (344003, Российская Федерация, г. Ростов-на-Дону, пл. Гагарина, 1), [SPIN-код](#), [ORCID](#), [ScopusID](#), ivan_top@mail.ru

Мэньи Хань, аспирант кафедры «Организация перевозок и дорожного движения» Донского государственного технического университета (344003, Российская Федерация, г. Ростов-на-Дону, пл. Гагарина, 1), [ORCID](#), hanmengyi@mail.ru

Анастасия Александровна Феофилова, кандидат технических наук, доцент кафедры «Организация перевозок и дорожного движения» Донского государственного технического университета (344003, Российская Федерация, г. Ростов-на-Дону, пл. Гагарина, 1), [SPIN-код](#), [ORCID](#), [ScopusID](#), afeofilova@donstu.ru

Никита Алексеевич Бескопыльный, аспирант кафедры «Организация перевозок и дорожного движения» Донского государственного технического университета (344003, Российская Федерация, г. Ростов-на-Дону, пл. Гагарина, 1), [SPIN-код](#), [ORCID](#), [ResearchGate](#), [ScopusID](#), nbeskopylnyi@donstu.ru

Заявленный вклад авторов:

И.В. Топилин: разработка концепции, научное руководство.

А.А. Феофилова: валидация результатов, написание рукописи – рецензирование и редактирование.

М. Хань: проведение исследования, анализ результатов, подготовка черновика научной статьи.

Н.А. Бескопыльный: проведение исследования, анализ результатов, подготовка черновика научной статьи.

Конфликт интересов: авторы заявляют об отсутствии конфликта интересов.

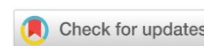
Все авторы прочитали и одобрили окончательный вариант рукописи.

Received / Поступила в редакцию 18.08.2025

Reviewed / Поступила после рецензирования 11.09.2025

Accepted / Принята к публикации 29.09.2025

INFORMATION TECHNOLOGY, COMPUTER SCIENCE AND MANAGEMENT ИНФОРМАТИКА, ВЫЧИСЛИТЕЛЬНАЯ ТЕХНИКА И УПРАВЛЕНИЕ



UDC 519.6:316.472.45

Original Empirical Research

<https://doi.org/10.23947/2687-1653-2025-25-4-2208>

Identification of the Activity Function of Social Network Users in a Linear Diffusion Model

Margarita A. Tolstykh , Victor K. Tolstykh 
Donetsk State University, Donetsk, Donetsk People's Republic
[✉ physicisto@yandex.ru](mailto:physicisto@yandex.ru)



EDN: CCULZU

Abstract

Introduction. Improving the accuracy of mathematical models for disseminating information in social networks is directly related to the ability to correctly identify their parameters. In numerous papers, the fundamental complexity of this problem is actually bypassed by substituting the direct identification of the desired functions for the selection of parameters for their heuristic approximations, which inevitably leads to a decrease in both the accuracy and universality of the model. In the linear diffusion model describing the spatiotemporal dynamics of information, one of the key parameters is the function characterizing user activity. The objective of this study includes the development and numerical implementation of an algorithm for direct parametric identification of user activity functions based on a direct extreme approach, which makes it possible to completely abandon heuristic approximations, and the evaluation of its computational efficiency in comparison to the classical gradient method.

Materials and Methods. A direct extreme approach was used to solve the parametric identification problem. Unlike the classical steepest descent technique, the proposed method with adjustable descent direction adapted the search trajectory to local features of the quality functional through introducing a control parameter. The numerical solution to the direct and adjoint problems was implemented using an implicit finite-difference scheme. The method was verified using synthetic data.

Results. For the identification algorithm, an analytical expression of the gradient of the target functional was obtained through the solution to the adjoint problem. The identifiability limits of the desired parameter conditioned by the inertia of the diffusion process and the network response time were determined. A comparative study of gradient algorithms was conducted. The classical steepest descent approach demonstrated slow and uneven convergence, requiring 13,217 iterations to reach the stopping criterion, whereas the method with adjustable descent direction provided convergence to the same level of accuracy in 376 iterations.

Discussion. The obtained results confirm the theoretical assumptions about the need to take into account the spatial heterogeneity of the functional gradient when solving infinite-dimensional optimization problems. The classical gradient technique exhibits low efficiency in reconstructing nonstationary parameters due to gradient nonuniformity, while the method with adjustable descent direction reaches uniform and rapid convergence. This demonstrates that adapting the algorithm to the specifics of an infinite-dimensional problem is a key success factor. The main contribution of the research is the development of a computing apparatus for the direct determination of functional parameters, which expands the methodological arsenal for analyzing systems described by partial differential equations.

Conclusion. The key findings of this research are the development and verification of an efficient algorithm for direct identifying user activity functions in a linear diffusion model of a social network. The practical significance consists in the creation of more accurate and interpretable tools for modeling information flows without resorting to a priori approximations. The developed algorithm has demonstrated significant advantages in speed and convergence. However, the interpretation of the physical meaning of the identified function within this model requires further development. A promising direction is the application of the method to more sophisticated models that take into account the spatial heterogeneity of user activity, as well as its extension to the identification of the function vector.

Keywords: social networks, diffusion model, parameter identification, direct extreme approach, infinite-dimensional optimization

Acknowledgements. The authors would like to thank the research team of the Department of Computer Technologies, Donetsk State University, for fruitful discussions of the research materials.

Funding Information. The work is done with the financial support from the Azov-Black Sea Mathematics Center for conducting fundamental scientific research (Agreement No. 075-02-2025-1608 dated February 27, 2025).

For Citation. Tolstykh MA, Tolstykh VK. Identification of the Activity Function of Social Network Users in a Linear Diffusion Model. *Advanced Engineering Research (Rostov-on-Don)*. 2025;25(4):363–370. <https://doi.org/10.23947/2687-1653-2025-25-4-2208>

Оригинальное эмпирическое исследование

Идентификация функции активности пользователей социальной сети в линейной диффузионной модели

М.А. Толстых , В.К. Толстых 

Донецкий государственный университет, г. Донецк, Донецкая Народная Республика

✉ physicisto@yandex.ru

Аннотация

Введение. Повышение точности математических моделей распространения информации в социальных сетях напрямую связано с возможностью корректной идентификации их параметров. Во многих работах фундаментальную сложность этой задачи фактически обходят, подменяя прямую идентификацию искомым функциями подбором параметров их эвристических аппроксимаций, что неизбежно приводит к снижению как точности, так и универсальности модели. В линейной диффузионной модели, описывающей пространственно-временную динамику распространения информации, одним из ключевых параметров выступает функция, характеризующая активность пользователей. Целью данного исследования является разработка и численная реализация алгоритма прямой параметрической идентификации функции активности пользователей на основе прямого экстремального подхода, позволяющего полностью отказаться от эвристических аппроксимаций, а также оценка его вычислительной эффективности в сопоставлении с классическим градиентным методом.

Материалы и методы. Для решения задачи параметрической идентификации был использован прямой экстремальный подход. В отличие от классического метода наискорейшего спуска, предложенный метод с регулируемым направлением спуска адаптирует траекторию поиска к локальным особенностям функционала качества за счет введения параметра регулирования. Численное решение прямой и сопряженной задач осуществлено по неявной конечно-разностной схеме. Верификация метода проводилась на синтетических данных.

Результаты исследования. Для алгоритма идентификации получено аналитическое выражение градиента целевого функционала через решение сопряженной задачи. Установлены границы идентифицируемости искомого параметра, обусловленные инерционностью диффузионного процесса и временем установления реакции сети. Проведено сравнительное исследование градиентных алгоритмов. Классический метод наискорейшего спуска продемонстрировал медленную и неравномерную сходимость, потребовав для достижения критерия остановки 13 217 итераций, тогда как метод с регулируемым направлением спуска обеспечил сходимость к тому же уровню точности за 376 итераций.

Обсуждение. Полученные результаты подтверждают теоретические предпосылки о необходимости учета пространственной неоднородности градиента функционала при решении бесконечномерных задач оптимизации. Классический градиентный метод демонстрирует низкую эффективность при восстановлении нестационарных параметров вследствие неоднородности градиента, в то время как метод с регулируемым направлением спуска позволяет достичь равномерной и быстрой сходимости. Это свидетельствует о том, что адаптация алгоритма к специфике бесконечномерной задачи является ключевым фактором успеха. Основной вклад исследования заключается в развитии вычислительного аппарата для прямого определения функциональных параметров, что расширяет методологический арсенал анализа систем, описываемых уравнениями в частных производных.

Заключение. Основными результатами работы являются разработка и верификация эффективного алгоритма прямой идентификации функции активности пользователей в линейной диффузионной модели социальной сети. Практическая значимость состоит в создании более точных и интерпретируемых инструментов для моделирования информационных потоков без привлечения априорных аппроксимаций. Разработанный алгоритм продемонстрировал значительное преимущество по скорости и характеру сходимости. Тем не менее, интерпретация физического смысла идентифицируемой функции в рамках данной модели требует дальнейшего развития. Перспективным направлением является применение метода к более совершенным моделям, учитывающим пространственную неоднородность активности пользователей, а также его расширение на идентификацию вектора функций.

Ключевые слова: социальные сети, диффузионная модель, идентификация параметров, прямой экстремальный подход, бесконечномерная оптимизация

Благодарности. Авторы выражают признательность научному коллективу кафедры «Компьютерные технологии» Донецкого государственного университета за плодотворное обсуждение материалов работы.

Финансирование. Работа выполнена при финансовой поддержке Азово-Черноморского математического центра на проведение фундаментальных научных исследований (Соглашение от 27.02.2025 № 075-02-2025-1608).

Для цитирования. Толстых М.А., Толстых В.К. Идентификация функции активности пользователей социальной сети в линейной диффузионной модели. *Advanced Engineering Research (Rostov-on-Don)*. 2025;25(4):363–370. <https://doi.org/10.23947/2687-1653-2025-25-4-2208>

Introduction. Social media have become an integral part of modern society, serving not only as entertainment but also as a tool for shaping public opinion and creating a community environment for various interests (everyday, political, extremist, etc.). Therefore, the tasks of studying, forecasting, and regulating the dissemination of information, as well as identifying and classifying communities on social media, are becoming hot issues. Solving these challenges requires the development of precise mathematical models of such processes.

There is a wide variety of social platforms, each with its own structure and information transfer mechanisms. The constant evolution and emergence of new algorithms for social networking operations leads to significant diversity in their mathematical models. Epidemic models SI, SIR, SEIR [1] and their modern, more sophisticated versions in the form of mean-field models [2] classify nodes (users) in a social network by state, and describe the quantitative change of nodes of a certain class. At the same time, graph models in the form of linear threshold and cascade [3] emphasize the cumulative effect of information dissemination and are often used to find opinion leaders in a social network. Each of the aforementioned models describes only specific aspects of information dissemination, without encompassing this process in its spatiotemporal fullness.

In recent years, machine learning-based models capable of accurately predicting information dissemination dynamics have gained widespread popularity [4]. However, such models typically operate on a “black box” principle and do not provide interpretable parameters (for example, virality, network throughput, or user activity). The lack of such parameters limits researchers' ability to evaluate social network clusters and manage information dissemination processes, which jeopardizes the application of models in problems requiring an understanding of the internal mechanisms of diffusion.

In [5, 6], the feasibility of constructing a fundamentally general model that is not linked with the constantly changing algorithms of social network functioning is noted. In [7], in order to reach this objective, the use of the mathematical apparatus of partial differential equations, namely, the linear diffusion model, is proposed:

$$\frac{\partial v}{\partial t} - p \frac{\partial^2 v}{\partial x^2} - rhv = 0, \quad x, t \in \Omega = (x_a, x_b) \times (t_0, t_1), \quad (1)$$

where t — time; x — distance in a network graph, measured by the minimum number of edges along which information can be transmitted $V(x, t) \in L_2(\Omega)$ (for example, in the form of the number of reposts of a certain news item); L_2 — Euclidean space of square-integrable functions.

The authors define the parameters of the model as follows: p — popularity of information (virality, speed of diffusion of information in the network); h — capacity of the social network (the maximum number of users who can take part in the dissemination of information); r — user activity (rate of growth of information in the network).

Model (1) takes into account the spatiotemporal patterns of information dissemination, and its parameters can be adjusted to reflect the characteristics of specific social networks [7]. In this case, the key problem is the task of parametric identification of the model. In general, all specified parameters should be functions: $p(x)$, $h(x)$, $r(t)$. The authors of model (1) propose approximating these functions with various heuristic dependences, which leads to the problem of parametric identification of the set of coefficients-numbers included in these dependences [8, 9]. This simplification does not allow us to reach maximum accuracy, which is possible only when identifying the functions directly specified, rather than their approximations, since the set of parameters included in the model may differ significantly for different social networks and even clusters of a single social network. The authors [10] reasonably point out that it is often impossible to analytically find optimal parameter functions, and classical numerical methods prove ineffective.

In [11], the problem of direct identification of function $h(x)$ is considered. To find its optimal value, a direct extreme approach [12] is used, based on the direct minimization of the quality criterion of identification $J(h)$ by extreme algorithms with gradient $\nabla J(h; x)$. Although an attempt was made in [11] to directly identify $h(x)$, the problem of identifying the time function $r(t)$ for similar models has not been systematically studied in the literature. The objective of this paper is to fill this gap through developing and numerically implementing an algorithm for direct parametric identification of the user activity function in the linear diffusion model (1) based on the direct extreme approach. The main task is to evaluate the efficiency of gradient algorithms for reaching this goal. The solution to this problem will create a methodological basis for the subsequent identification of other parameters (for example, $p(x)$ or the simultaneous identification of a vector of parameter functions) and the transition to more complex nonlinear models. Parameters $h(x)$ and $p(x)$ are considered known in this paper and are taken from [5] for isolation and detailed analysis of the target problem.

Materials and Methods. To model the processes of information dissemination according to equation (1) in the studied cluster of the network graph, boundary conditions of the first and second kind are specified:

$$v = 1 \text{ on } \Gamma_a = x_a \times (t_0, t_1), \quad \frac{\partial v}{\partial x} = 0 \text{ on } \Gamma_b = x_b \times (t_0, t_1).$$

Here, we assume that the information source is located at node x_a and at time $t = t_0$ generates information $v(x_a, t_0)$ in the form of a single news item. Value x_b determines the distance at which the information flow disappears.

The initial condition corresponds to the absence of the news item in question in the network:

$$v = 0 \text{ on } \Gamma_0 = (x_a, x_b] \times t_0.$$

The quality criterion of model identification is specified as the deviation of the model state v from the experimentally observed v_e in the real network over the entire spatiotemporal region Ω in the form of the following functional:

$$J(r) = \iint_{\Omega} (v - v_e)^2 dx dt. \quad (2)$$

The problem of parametric identification of the optimal value of the function $r_*(t)$ is formulated as an extremum problem:

$$r_* = \arg \min_{r \in L_2(S)} J(r).$$

To solve this problem, an infinite-dimensional gradient algorithm is used:

$$r^{k+1}(t) = r^k(t) - b^k \alpha(t) \nabla J(r^k; t), \quad t \in S_{\Delta} \subset S, \quad k = 0, 1, \dots, \quad (3)$$

where k — iteration number; b^k — step multiplier (selected using the golden section method); $\alpha(t)$ — parameter for regulating the direction of descent. If $\alpha(t) = 1$, then algorithm (3) is reduced to the classical steepest descent method (SDM). Otherwise, this algorithm is a method with adjustable direction of descent (ADDM) [12]. Parameter $\alpha(t)$ regulates the direction of descent to the optimum to provide uniform convergence of the functions $r^{k+1}(t)$ to $r_*(t)$ on $S_{\Delta} \subset S$, where uniform convergence is, in principle, possible. For ADDM, according to [12], the parameter for regulating the direction of descent can be set:

$$\alpha(t) = \frac{r^0(t)}{|\nabla J(r^0; t)|}.$$

To implement algorithm (3), it is required to find an analytical expression for the gradient of the objective functional (2), which depends implicitly on the control. This is the main difficulty in infinite-dimensional identification. The gradient is found through solving the adjoint problem, the technique for obtaining which is widely described in the literature [13, 14].

To evaluate the efficiency of the solution to the problem of parametric identification of the user activity function in model (1) through the direct extreme approach (3), the following test problem was set.

The original and adjoint linear parabolic equations were solved numerically using the implicit Crank-Nicolson finite-difference scheme by the sweep method. The spatiotemporal grid was defined by the values $n = 50$, $m = 500$. This corresponded to the distance of five edges of the network graph over which the news spread from the source, and time $t_1 - t_0 = 72$ hours. It was assumed that $t_{\Delta} = 5$ hours.

To construct the synthetic data v_e , parameters p and h were assumed to be known and were taken from [5]:

$$p(x) = e^{-x}, \quad h(x) = -0.03x^2 + 0.2x.$$

A test optimal value was set, which was also proposed in [5]:

$$r_*(t) = \frac{0.0059}{1.5526} - e^{-1.5526t} \left(\frac{0.0059}{1.5526} - 1 \right).$$

The direct problem for model (1) was solved. The resulting state $v(x, t)$ was taken as the “experimental” $v_e(x, t)$. Next, the initial approximation $r^0(t) = 0.3$ was specified, and the iterative process of solving the inverse identification problem using the extremal algorithm (3) began to recover function $r_*(t)$.

The condition for stopping iterations was the following criterion for the practical termination of convergence:

$$\frac{u^k - u^{k-1}}{u^{k-1}} \leq 10^{-5}.$$

Research Results. For algorithm (3), the gradient is found:

$$\nabla J(r; t) = - \int_{x_a}^{x_b} h v f dx \in L_2(S_\Delta). \quad (4)$$

It is determined through solving the following adjoint problem f :

$$-\frac{\partial f}{\partial t} - p \frac{\partial^2 f}{\partial x^2} - f r h + 2(v - v_e) = 0, \quad x, t \in \Omega, \quad (5)$$

with the corresponding boundary and initial (terminal) conditions:

$$p f = 0 \text{ on } \Gamma_a, \quad p \frac{\partial f}{\partial x} = 0 \text{ on } \Gamma_b, \quad f = 0 \text{ on } \Gamma_1 = [x_a, x_b] \times t_1.$$

The adjoint problem is solved in the reverse time direction from the initial zero state f on Γ_1 . For a nonoptimal value $r(t)$, after some time t_Δ due to free term $2(v - v_e)$ in equation (5), a nonzero state f is formed. If we conduct a controllability analysis, we obtain a controllability set on which function $r(t)$ can be identified:

$$S_\Delta = (t_0 + t_\Delta, t_1 - t_\Delta), \quad (6)$$

where t_Δ , on the one hand, is the waiting time for network users to begin reacting to the published news. Identifying user activity before their reaction is impossible. On the other hand, this is the onset time of the impact of term $2(v - v_e)$ in the adjoint problem on the entire spatial domain of the network cluster under consideration.

Figure 1 shows the initial value of the gradient. The identification results are presented in Figure 2 *a*. The convergence of the method ends at iteration $k = 13,217$ with nonuniform convergence on S_Δ . The dash-dotted curve is an example of the value of function $r^{20}(t)$ at the 20th iteration.

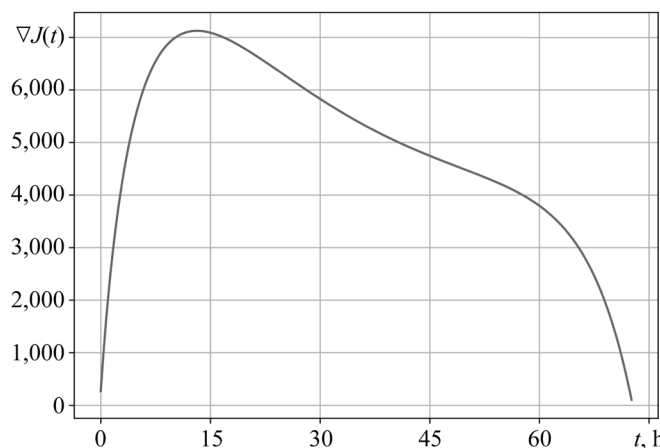


Fig. 1. Initial value of gradient $\nabla J(r^0; t)$

The results of the ADDM identification are shown by the dotted curve in Figure 2 *b*. Convergence was completed after $k = 376$ iterations. The resulting function $r^{376}(t)$ visually matches the exact test value $r_*(t)$. The dash-dotted line is an example of $r(t)$ at iteration $k = 20$. The final value of the objective functional in both methods was approximately the same.

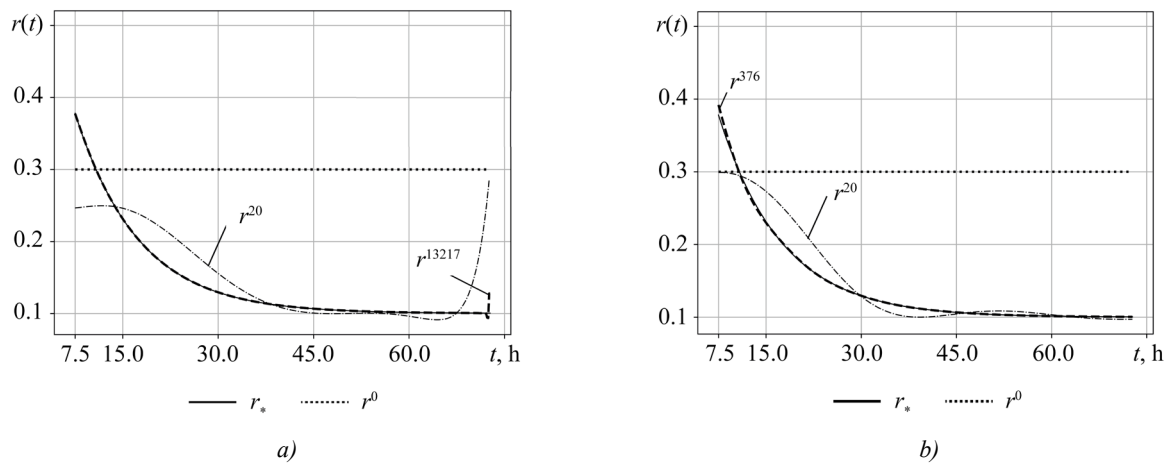


Fig. 2. Identification of $r(t)$:
a — by SDM; b — by ADDM

Discussion. The obtained results allow us to draw a number of important conclusions about the nature of the identification problem and the efficiency of the proposed method. The significant nonuniformity of the initial gradient $\nabla J(r^0; t)$ (Fig. 1) with a uniform initial approximation $r^0(t)$ is a direct consequence of the spatiotemporal dynamics of model (1) and limited controllability (6) of the system at the edges of the interval S . This explains why the classical SDM, which does not take this heterogeneity into account, exhibits slow and uneven convergence (Fig. 2 a). The algorithm spends significant computational resources on compensating for the gradient features, which leads to the need for 13,217 iterations.

In turn, the ADDM effectively compensates for this heterogeneity due to parameter $\alpha(t)$, adapting the search direction to the local features of the functional. This is confirmed by the uniform $r^k(t) \rightarrow r_*(t)$ on the entire set S_Δ (Fig. 2 b) and a reduction in the number of iterations by two orders of magnitude (376 versus 13,217). This result is in good agreement with the theoretical assumptions presented in [12] and confirms that for infinite-dimensional problems, the key factor is not simply minimization, but taking into account the heterogeneity of the gradient functional.

As for consistency with previous research, success in direct identification $r(t)$ develops the ideas embedded in [11] for identifying $h(x)$, and demonstrates the universality of the direct extreme approach for functional parameters in distributed systems. At the same time, our approach offers a solution to the problem identified in [10], where the inefficiency of classical numerical methods was noted.

For comparison, similar problems for systems of ordinary differential equations in the identification of a vector of numbers were considered in [15]. It was shown that the problem was not in the problem itself, but in the need to use specialized adaptive algorithms. Establishing the domain of identifiability S_Δ is also an important methodological contribution.

This result highlights a fundamental limitation associated with the inertia of the diffusion process and the time it takes for the network to react, which must be considered when correctly formulating such inverse problems.

Conclusion. This paper addresses the pressing problem of direct parametric identification of the user activity function $r(t)$ in a linear diffusion model (1) describing the dissemination of information in a social network. The developed and verified algorithm, based on a direct extreme approach with an adjustable descent direction, has demonstrated a more than twofold improvement in convergence rate compared to the classical gradient method, proving its high efficiency for this class of problems.

The practical significance of this research lies in the creation of a computational tool that eliminates a priori heuristic approximations of parameters and moves to direct function reconstruction, critically increasing the accuracy and validity of information dissemination models. This opens up opportunities for developing more reliable systems for predicting and managing information flows in social networks.

The basic limitation of the current work is the use of synthetic data for method validation. Also, the interpretation of the physical meaning and dimensionality of $r(t)$ function itself requires further in-depth study. Future research will focus on the development of model representations and adaptation of the proven method to more complex nonlinear models. A key challenge for the future is to expand the method for simultaneous identification of several functional parameters, which is a more complex but also more practically valuable task.

References

1. Mei Li, Xiang Wang, Kai Gao, Shanshan Zhang. A Survey on Information Diffusion in Online Social Networks: Models and Methods. *Information*. 2017;8(4):118. <https://doi.org/10.3390/info8040118>
2. Glukhov AI, Shishlenin MA, Trusov NV. Modeling the Dynamics of Social Protests: Mean Field Games and Inverse Problems. *Differential Equations*. 2025;61(6):802–822. <https://doi.org/10.7868/S3034503025060067>
3. Alshahrani M, Zhu Fuxi, Sameh A, Mekouar S, Sheng Huang. Efficient Algorithms Based on Centrality Measures for Identification of Top-K Influential Users in Social Networks. *Information Sciences*. 2020;527:88–107. <https://doi.org/10.1016/j.ins.2020.03.060>
4. Dritsas E, Trigka M. Machine Learning in Information and Communications Technology: A Survey. *Information*. 2025;16(1):8. <https://doi.org/10.3390/info16010008>
5. Haiyan Wang, Feng Wang, Kuai Xu. *Modeling Information Diffusion in Online Social Networks with Partial Differential Equations*. Cham: Springer; 2020. 144 p. <https://doi.org/10.48550/arXiv.1310.0505>
6. Ying Hu, Rachel Jeungeun Song, Min Chen. Modeling for Information Diffusion in Online Social Networks via Hydrodynamics. *IEEE Access*. 2017;5:128–135. <https://doi.org/10.1109/ACCESS.2016.2605009>
7. Feng Wang, Haiyan Wang, Kuai Xu, Jianhong Wu, Xiaohua Jia. Characterizing Information Diffusion in Online Social Networks with Linear Diffusive Model. In: *Proc. IEEE 33rd International Conference on Distributed Computing Systems*. New York City: IEEE; 2013. P. 307–316. <https://doi.org/10.1109/ICDCS.2013.14>
8. Zvonareva TA, Kabanikhin SI, Krivorotko OI. Numerical Algorithm for Source Determination in a Diffusion–Logistic Model from Integral Data Based on Tensor Optimization. *Computational Mathematics and Mathematical Physics*. 2023;63(9):1513–1523. <https://doi.org/10.31857/S0044466923090193>
9. Krivorotko O, Kabanikhin S, Shuhua Zhang, Kashtanova V. Global and Local Optimization in Identification of Parabolic Systems. *Journal of Inverse and Ill-Posed Problems*. 2020;28(6):899–913. <https://doi.org/10.1515/jiip-2020-0083>
10. Zoppoli R, Sanguineti M, Gnecco G, Parisini Th. The Basic Infinite-Dimensional or Functional Optimization Problem. In book: *Neural Approximations for Optimal Control and Decision*. Cham: Springer; 2020. P. 1–38. https://doi.org/10.1007/978-3-030-29693-3_1
11. Tolstykh VK. *Direct Extreme Approach for Optimizing Distributed Parameter Systems*. Donetsk: Yugo-Vostok; 1997. 177 p. (In Russ.)
12. Tolstykh MA. Identifying the Capacity of a Social Network. *Moscow University Computational Mathematics and Cybernetics*. 2024;48:59–64. <https://doi.org/10.3103/S0278641924010084>
13. Miele A. *Theory of Optimum Aerodynamic Shapes*. New York: Academic Press; 1965. 455 p.
14. Marchuk GI, Shutyaev VP. Adjoint Equations and Iterative Algorithms in Problems of Variational Data Assimilation. *Proceedings of the Steklov Institute of Mathematics (Supplement Issues)*. 2012;276(2):138–152. <https://doi.org/10.1134/S0081543812020113>
15. Kabanikhin SI, Krivorotko OI. Optimization Methods for Solving Inverse Problems of Immunology and Epidemiology. *Journal of Computational Mathematics and Mathematical Physics*. 2020;60(4):590–600. <https://doi.org/10.31857/S0044466920040109>

About the Authors:

Margarita A. Tolstykh, Junior Research Associate, Mathematics Center, Donetsk State University (24, Universitetskaya Str., Donetsk, 283001, Donetsk People's Republic), [SPIN-code](#), [ORCID](#), [ResearchGate](#), physicisto@yandex.ru

Victor K. Tolstykh, Dr.Sci. (Phys.-Math.), Dr.Sci. (Eng.), Professor of the Computer Technology Department, Donetsk State University (24, Universitetskaya Str., Donetsk, 283001, Donetsk People's Republic), [SPIN-code](#), [ORCID](#), [ScopusID](#), [ResearcherID](#), mail@tolstykh.com

Claimed Contributorship:

MA Tolstykh: data curation, investigation, visualization, writing – original draft preparation.

VK Tolstykh: methodology, writing – review & editing.

Conflict of Interest Statement: the authors declare no conflict of interest.

All authors have read and approved the final manuscript.

Об авторах:

Маргарита Анатольевна Толстых, младший научный сотрудник, научно-образовательный математический центр «Математический центр Донецкого государственного университета» (283001, Донецкая Народная Республика, г. Донецк, ул. Университетская, д. 24), [SPIN-код](#), [ORCID](#), [ResearchGate](#), physicisto@yandex.ru

Виктор Константинович Толстых, доктор физико-математических наук, доктор технических наук, профессор кафедры «Компьютерные технологии» Донецкого государственного университета (283001, Донецкая Народная Республика, г. Донецк, ул. Университетская, д. 24), [SPIN-код](#), [ORCID](#), [ScopusID](#), [ResearcherID](#), mail@tolstykh.com

Заявленный вклад авторов:

М.А. Толстых: курирование данных, проведение исследования, визуализация, написание черновика рукописи.

В.К. Толстых: разработка методологии, написание рукописи — внесение замечаний и исправлений.

Конфликт интересов: авторы заявляют об отсутствии конфликта интересов.

Все авторы прочитали и одобрили окончательный вариант рукописи.

Received / Поступила в редакцию 04.09.2025

Reviewed / Поступила после рецензирования 23.09.2025

Accepted / Принята к публикации 01.10.2025

INFORMATION TECHNOLOGY, COMPUTER SCIENCE AND MANAGEMENT ИНФОРМАТИКА, ВЫЧИСЛИТЕЛЬНАЯ ТЕХНИКА И УПРАВЛЕНИЕ



UDC 004.75

Original Empirical Research

<https://doi.org/10.23947/2687-1653-2025-25-4-2238>

Concept of a Multilevel Network Infrastructure for Monitoring Agricultural Facilities Based on Wireless Sensor Networks

Vladimir V. Samoylenko

Stavropol State Agrarian University, Stavropol, Russian Federation

✉ samoilenko.vv@stgau.ru

EDN: CLJRZJ

Abstract

Introduction. In the context of digitalization of the agricultural sector, precision farming becomes a key driver of sustainability: wireless sensor networks (WSN) provide continuous monitoring of edaphoclimatic parameters and plant health, supporting yield forecasting and resource optimization while reducing operational risks. Despite significant progress in research on energy efficiency, routing, and topologies of WSN, the issue of their systemic reliability in real agricultural scenarios has been addressed only fragmentarily. Existing theoretical approaches rely on graph theory, Markov and quasi-deterministic models to assess connectivity and fault tolerance but do not sufficiently account for battery degradation, radio channel variability, and external factors (microclimate, interference), as well as their combined effects. The objective of this article is to develop a methodological approach to enhance the reliability of WSN for monitoring agricultural objects through a multilevel model that integrates network parameters, hardware properties, and external actions.

Materials and Methods. To develop the model, methods of system analysis were used, including analysis and synthesis of previously known models and algorithms for controlling the WSN for various levels of network interaction. At the first stage, analytical models of each level were examined: operating conditions of radio devices; physical channels with interference and hardware distortions; energy losses of nodes in channels with variable environmental characteristics; linear WSN with heterogeneous radio communication segments and clustering of WSN. At the second stage, an analysis of WSN control algorithms was conducted: selection of transmission modes with minimal signal distortion; optimization of signal structure with minimal Bit Error Rate (BER); control of data packet length and transmitter power; balancing of energy losses in relay nodes, as well as routing with minimal time and energy losses. At the third stage, the synthesis of the obtained results was performed, presenting a hierarchical monitoring infrastructure for the agricultural object that considered all levels of WSN interaction, parameters of sensor nodes, and the external actions.

Results. A methodological multilevel approach to increasing the reliability of WSN for monitoring agricultural facilities has been proposed and substantiated. This approach integrates network parameters, equipment properties, and external actions. It is validated by modeling the improvement of energy efficiency, reduction of delays, and increase in fault tolerance. Within this framework, a five-tier hierarchical concept of multilevel network infrastructure for monitoring agro-industrial objects based on WSN has been developed. It incorporates models and algorithms at the levels of: devices, physical channels, data transmission channels, linear routes, and networks. Single-level and inter-level dependences linking performance indicators, destabilizing factors, and controllable parameters have been established.

Discussion. The presented approach addresses the gap between energy models and the consideration of dynamic/information constraints of nodes, while also taking into account the actual operating condition of modems, and the thermal dependence of power sources. The multilevel integration of criteria (from signal shape correlation indicators to network probabilistic metrics of WSN integrity) allows for the alignment of local optimization and system goals,

reducing the risk of conflicts between levels. The principle of level matching and external augmentation provides iterative adjustments of requirements and parameters, which increases the robustness of decision-making to environmental uncertainty and channel heterogeneity. Constraints of the current work include the need to calibrate models for specific hardware profiles, the dependence of efficiency on available PHY/MAC modes and ARQ protocols, and sensitivity to the accuracy of interference environment and temperature assessments.

Conclusion. The developed models and algorithms across five levels provide the specified metrics of interference resilience, delivery time and energy consumption with the minimum required involvement of resources, which increases the survivability and service life of the WSN. The proposed approach creates the basis for the transition to systemically designed, reproducible solutions in precision agriculture. It reduces resource costs and environmental impact, and also increases the sustainability and profitability of agricultural production. Scaling requires field testing and publication of reference configurations and codes for reproducibility.

Keywords: wireless sensor network, agricultural facility, reliability, network infrastructure, physical data transmission channel, signal distortion, routing algorithms

Acknowledgements. The author would like to thank the Editors and reviewers for their attentive attitude to the article and the comments they made, which allowed us to improve its quality.

For Citation. Samoylenko VV. Concept of a Multilevel Network Infrastructure for Monitoring Agricultural Facilities Based on Wireless Sensor Networks. *Advanced Engineering Research (Rostov-on-Don)*. 2025;25(4):371–382. <https://doi.org/10.23947/2687-1653-2025-25-4-2238>

Оригинальное теоретическое исследование

Концепция многоуровневой сетевой инфраструктуры мониторинга агропромышленных объектов на основе беспроводных сенсорных сетей

В.В. Самойленко 

Ставропольский государственный аграрный университет, г. Ставрополь, Российская Федерация

✉ samoilenko.vv@stgau.ru

Аннотация

Введение. В условиях цифровизации агросектора точное земледелие становится ключевым драйвером устойчивости: беспроводные сенсорные сети (БСС) обеспечивают непрерывный мониторинг почвенно-климатических параметров и состояния растений, поддерживая прогнозирование урожайности и ресурсную оптимизацию при снижении операционных рисков. Несмотря на значительный прогресс в исследованиях энергоэффективности, маршрутизации и топологий БСС, проблема их системной надежности в реальных агросценариях освещена фрагментарно. Существующие теоретические подходы опираются на теорию графов, марковские и квазидетерминированные модели для оценки связности и отказоустойчивости, но недостаточно учитывают деградацию батарей, вариативность радиоканала и внешние факторы (микроклимат, помехи), а также их совместное влияние. Цель данной статьи — разработать методический подход к повышению надежности БСС для мониторинга агрообъектов посредством многоуровневой модели, интегрирующей сетевые параметры, свойства аппаратуры и внешние воздействия.

Материалы и методы. Для разработки модели были применены методы системного анализа, в т.ч. анализа и синтеза ранее известных моделей и алгоритмов управления БСС для различных уровней сетевого взаимодействия. На первом этапе рассмотрены аналитические модели каждого уровня: технического состояния радиоустройств; физического канала с помехами и аппаратурными искажениями; энергопотерь узлов в канале с переменными характеристиками среды; линейной БСС с гетерогенными участками радиосвязи и кластеризации БСС. На втором этапе произведен анализ алгоритмов управления БСС: выбора режима передачи с минимальными искажениями сигналов; оптимизации структуры сигнала с минимальным BER; управления длиной пакета данных и мощностью передатчика; маршрутной балансировки энергопотерь в узлах ретрансляции, а также маршрутизации с минимальными потерями времени и энергии. На третьем этапе произведен синтез полученных результатов, представлена иерархическая инфраструктура мониторинга агропромышленного объекта, учитывающая все уровни взаимодействия БСС, параметры сенсорных узлов и влияние внешних факторов.

Результаты исследования. Предложен и обоснован методический многоуровневый подход к повышению надежности БСС для мониторинга агрообъектов, интегрирующий сетевые параметры, свойства аппаратуры и внешние воздействия, подтвержденный моделированием повышения энергоэффективности, снижения задержек и роста отказоустойчивости. В рамках этого разработана пятииерархическая концепция многоуровневой сетевой инфраструктуры для мониторинга агропромышленных объектов на базе БСС, интегрирующая модели и алгоритмы на уровнях: устройства, физического канала, канала передачи данных, линейного маршрута и сети. Получены одноуровневые и межуровневые зависимости, связывающие показатели эффективности, дестабилизирующие факторы и управляемые параметры.

Обсуждение. Представленный подход устраняет выявленный в литературе разрыв между энергетическими моделями и учетом динамических/информационных ограничений узлов, а также учитывает реальное техническое состояние модемов и термозависимость источников питания. Многоуровневая интеграция критериев (от корреляционных показателей формы сигнала до сетевых вероятностных метрик целостности БСС) позволяет согласовывать локальные оптимизации и системные цели, уменьшая риск конфликтов между уровнями. Принцип согласования уровней и внешнего дополнения обеспечивает итеративную корректировку требований и параметров, что повышает устойчивость принятия решений к неопределенности среды и гетерогенности каналов.

Ограничениями текущей работы являются: необходимость калибровки моделей под конкретные аппаратные профили, зависимость эффективности от доступных режимов PHY/MAC и протоколов ARQ, а также чувствительность к точности оценок помеховой обстановки и температурных режимов.

Заключение. Разработанные модели и алгоритмы на пяти уровнях обеспечивают достижение заданных показателей помехоустойчивости, времени доставки и энергопотребления при минимально необходимом задействовании ресурсов, что повышает живучесть и срок службы БСС. Предложенный подход создает основу для перехода к системно спроектированным, воспроизводимым решениям в точном земледелии, снизит ресурсные затраты и экологическую нагрузку, а также повысит устойчивость и рентабельность агропроизводства. Для масштабирования необходимы полевые испытания и публикация эталонных конфигураций и кодов для воспроизводимости.

Ключевые слова: беспроводная сенсорная сеть, агропромышленный объект, надежность, сетевая инфраструктура, физический канал передачи данных, искажение сигнала, алгоритмы маршрутизации

Благодарности. Автор выражает благодарность редакции и рецензентам за внимательное отношение к статье и указанные замечания, которые позволили повысить ее качество.

Для цитирования. Самойленко В.В. Концепция многоуровневой сетевой инфраструктуры мониторинга агропромышленных объектов на основе беспроводных сенсорных сетей. *Advanced Engineering Research (Rostov-on-Don)*. 2025;25(4):371–382. <https://doi.org/10.23947/2687-1653-2025-25-4-2238>

Introduction. The development of the agricultural industry is inextricably linked to the implementation of modern digital control systems through the concept of the Internet of Things (IoT) [1]. One of the key technological concepts of precision agriculture is wireless sensor networks (WSN) [2]. The use of this technology allows for the transition from reactive to predictive and precise control. WSN is actively used for monitoring agricultural facilities, including:

- soil condition monitoring [3] (measuring moisture, temperature, pH, NPK (nitrogen, phosphorus, potassium) content, and salinity level) [4, 5];
- microclimate control in greenhouses and vegetable storage facilities (measuring air temperature, relative humidity, illumination level, CO₂ concentration [6];
- monitoring plant health, identifying diseases and pests, and predicting productivity (measuring leaf area index (LAI), chlorophyll levels, and temperature stress) [7];
- management of livestock enterprises (determining the location of animals (GPS, RFID), measuring physical activity, body temperature, and heart rate) [8].

The key benefits of digitalization in agricultural production include optimized energy consumption, which reduces costs for water, electricity, fertilizers, and pesticides by 20–30%, and increases yield and product quality by 10–15%. From an environmental perspective, precision management reduces greenhouse gas emissions through optimizing logistics and agrochemical application. A systematic approach to digitalizing agribusiness enables remote monitoring and management, as well as data-driven decision-making.

Despite the achievements, the problem of providing the reliability of WSN has not yet found a complete solution to most applied problems, although the first studies in this area date back to the early 2000s [9]. A common shortcoming of existing research on the reliability of WSN is the emphasis on the dynamic and information constraints of nodal modules, rather than on their energy potential. This leads to an incomplete consideration of factors affecting reliability. For example, in [10], despite the consideration of the energy consumption model and the power supply capacity, the volume of data and energy costs for communication remain without due attention because of their impact on the interlayer performance indicators of the WSN.

On the other hand, overestimating the impact of destabilizing environmental factors causes irrational and excessive consumption of energy resources. Some of these shortcomings are taken into account in [11], where the reliability assessment is based on the hierarchical trust rule base method. Nevertheless, a significant number of factors affecting the reliability of WSN remain, including:

1. limited computing power and capacity of sensor nodes.
2. non-renewable power sources in most practical applications.
3. simple architecture and software of nodes, which do not allow for complex computing tasks.
4. vulnerability of WSN to attacks due to the use of open communication methods.
5. deployment of sensor nodes under difficult operating conditions leading to their premature failure.

However, numerous studies fail to take into account the actual technical condition of sensor nodes. Mass production technology for inexpensive electronic devices does not provide high accuracy and reproducibility of their characteristics. The major challenge in deploying WSN remains the limited energy supply of sensor nodes, with no ability to recharge or quickly replace batteries. Therefore, minimizing energy consumption becomes paramount even at the network design stage. Improving the energy efficiency of sensor network nodes is a priority [12].

Scientific research on the analysis of operating time of the WSN node shows that the most energy-dependent operating modes are the active traffic transmission modes [13]. This is due to the operation of the network interface during the reception, transmission and waiting for data.

Power supply reliability plays a key role, as in numerous cases there is no redundancy. A power supply failure, particularly a reduction in its capacity, can disable a local sensor node and, consequently, affect the operation of the entire network. The problem is compounded by the limited maximum capacity of the batteries used and the significant cost difference between higher-capacity power supplies.

A number of methods are proposed to reduce the energy consumption of sensor nodes, in particular: approaches aimed at saving energy through optimizing the operating cycles of the transmitter; methods for adapting the transmitter and receiver to changing external conditions; methods for optimizing routing and correcting the network topology taking into account the energy consumption of each node [14]. Various energy balancing methods are used to equalize the power consumption of all network nodes. Furthermore, one solution to this problem is to optimize WSN coverage, including cluster and non-cluster approaches [15].

However, known studies lack sufficient scientific groundwork in the area of multi-level research into WSN designed for monitoring agroindustrial facilities. A method for analyzing local and global states of hierarchical multicomponent systems under uncertainty is presented in [16]. However, without adaptive tracking of the boundaries of the uncertain impact of environmental factors, it is difficult to formulate decisions on the economical use of network resources. The multilevel synthesis methodology developed in [17] offers a set of iterative procedures for end-to-end system design, from the formation of the initial design to working detailing, but its applicability is limited to the initial phases of the life cycle, including development and design.

A number of principles and models for making coordinated decisions for various levels and stages of the functioning of the WSN are presented in [18]. Most of these studies rely on the principle of vertical “top-down” decomposition, according to which the characteristics of the synthesized system are determined using a multi-level procedure: from a general system model with corresponding indicators, parameters of conditions, constraints and control — to lower-level models with their indicators and parameters. The disadvantage of this approach is the rigidity and low efficiency of management, since the decision-making process does not include a preliminary detailed analysis of the resource potential of lower-level elements.

Current research [19] proposes the implementation of multilevel synthesis of WSN based on the principles of level coordination and external supplementation. According to the first principle, requirements formed at any level of the system act as constraints when selecting models and determining the functional capabilities of the underlying levels. If these requirements cannot be met, iterative adjustments to the conditions and results of modeling at higher levels are made. The principle of external supplementation involves obtaining results at the lower level, verifying them through data and methods from higher levels, and, if necessary, refining these results when moving on to the synthesis of the higher-level system.

Despite the significant benefits of using modern digital technologies to intensify agricultural production, including a 20–30% reduction in production costs and a 10–15% increase in yields, the active implementation of such solutions is hampered by the lack of a systematic approach to the technical implementation of digital infrastructure. Each of the solutions discussed in the literature contributes to improving the energy efficiency of the food processing system. However, in the context of the objectives posed in this study, their direct application is difficult or impossible.

The literature review revealed a significant gap in scientific knowledge: lack of comprehensive, multilevel models of precision farming systems based on the WSN platform. Such models should be designed to comprehensively address issues related to energy resource depletion and limitations of sensor node radio transmission elements.

The objective of this research is to develop a new methodological approach to providing the reliability of wireless communication systems. The approach is based on the creation of a comprehensive, multilevel model of the network infrastructure for monitoring agricultural facilities, taking into account not only WSN parameters and external factors, but also the synergistic effect of their interaction, including structural-energy, frequency-dynamic, and topological-dynamic aspects.

Materials and Methods. To develop a comprehensive multilevel model of network infrastructure for monitoring agro-industrial facilities (Fig. 1), a systems approach was used. Decomposing the hierarchical model into five levels formed the basis of the study. Specific models and algorithms were previously developed for each level to provide a synergistic effect. The research methodological framework included original results obtained and published by the authors. The key models and algorithms summarized in the developed model are presented below.

A model of the technical condition of the facilities was used at the device level. The coefficient of mutual correlation of the reference and distorted signals was used as a criterion for assessing the state of the radio equipment [20]. This indicator demonstrated a high sensitivity to types of degradation, such as intersymbol distortions and additive noises. To optimize power consumption at this level, algorithms for selecting a transmission mode with minimal distortion were used. These algorithms analyze the communication channel quality in real time and dynamically switch the modulation and transmitter power, providing a balance between communication reliability and efficient resource use. This approach improves both the reliability and battery life of the device.

At the physical channel level, a channel model with interference and hardware signal distortions was used [21]. Analytical models of WSN communication channels represented the dependence of the bit error probability during incoherent reception of messages on the energy and stochastic parameters of the distorted signal and additive interference at the receiver input. These models provide highly accurate predictions of communication quality under unstable fading and impulse noise conditions. This level utilizes an algorithm for optimizing the signal structure with a minimum bit error rate (BER). Its operation is based on the adaptive symbol duration selection and the use of hidden error-correcting coding, which guarantees reliable data transmission while maintaining total channel throughput.

At the data link channel level, a model of node energy losses in a channel with variable environmental characteristics was used [22]. This model established an analytical relationship between the bit error probability (BEP), node heating temperature, signal fading depth in the channel (Rician K factor), and signal-to-noise ratio (SNR). Taking into account the thermal state of the node allowed us to predict its energy consumption and reliability during operation. A specialized algorithm was used to manage data packet length and transmitter power. It dynamically balanced the need to retransmit short packets and the energy costs of transmitting long ones, minimizing the total energy loss in a changing interference environment. This significantly increased network battery life without compromising the reliability of transmitted information.

At the route level, a linear WSN model with heterogeneous radio sections and algorithms for route balancing of energy losses in relay nodes were used [23]. Analytical models of time and energy losses took into account internode distances, transmitter power, and the characteristics of multipath signal propagation. Based on the dependence of time losses on the number of relays, heterogeneous WSN deployment algorithms with a criterion for minimizing network delay were used, which did not limit resources. This provided scheduling flexibility for both resource-rich and resource-constrained tasks. Balancing algorithms redistributed the load between nodes, preventing premature failure due to energy depletion and extending the overall network lifespan. Thus, this combination of models and algorithms optimized the key network metrics — energy efficiency, latency, and survivability.

At the network level, a WSN clustering model was used that took into account mutual interference in channels and the residual charge of node batteries, as well as routing algorithms with minimal time and energy losses [24]. The conducted research made it possible to form a sufficient number of connections between nodes that met communication reliability criteria, standardized in accordance with the requirements for noise immunity and timeliness of data packet transmission. Routing algorithms dynamically adapted to changing interference levels and node residual energy, selecting a path that balanced delivery speed and energy consumption. The simulation results enabled the implementation of network topology and clustering management algorithms. These algorithms provided self-healing of the network in the event of key node failures and allowed for load redistribution to prevent overload of individual clusters. This approach increased fault tolerance and overall network lifespan in dynamic interference environments.

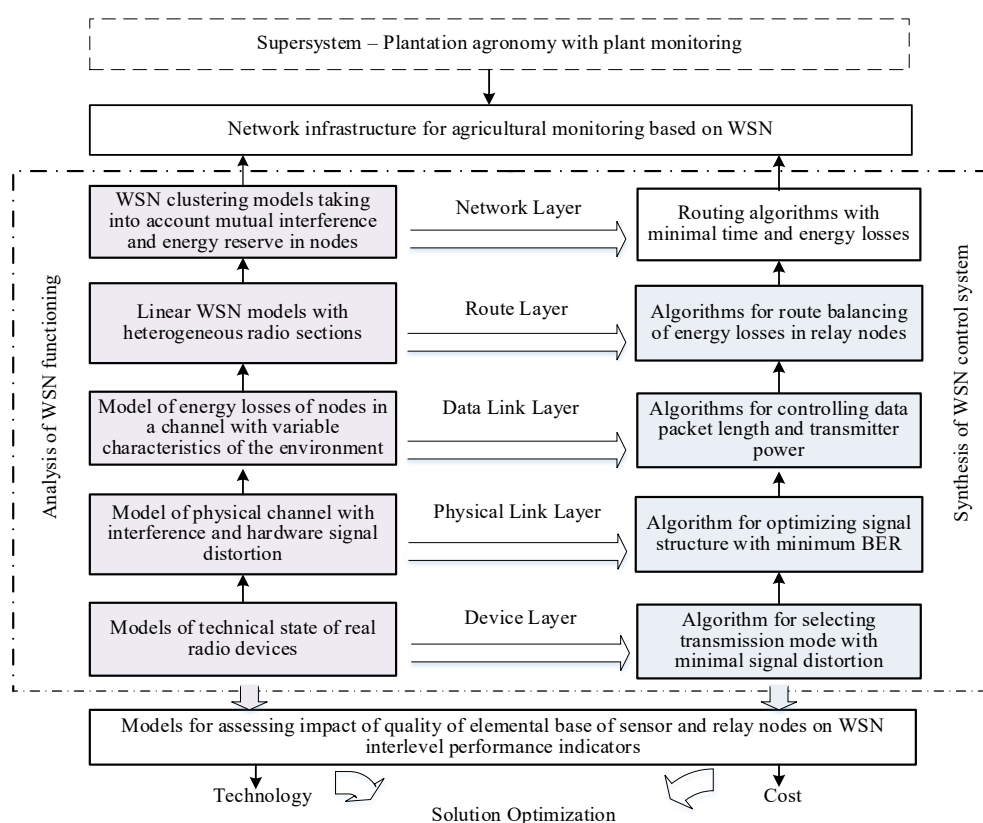


Fig. 1. Scheme of a multilevel network infrastructure for monitoring agricultural facilities based on wireless sensor networks

Results. The research resulted in a multilevel network infrastructure for monitoring agricultural facilities. The components of this system are presented in Table 1.

Table 1

Components of a Multilevel Reliability Management System for WSN
with Account of Various Destabilizing Factors

Level v of	Destabilizing factors $\xi^{(v)}$	Performance indicators $\varphi^{(v)}$	Managing optimized parameters $\omega^{(v)}$	Resource limitations Ω_v	Additional (proposed for consideration) conditions $\zeta^{(v)}$
1 – device	Hardware defects that distort signal	Relative signal distortion index	Redistribution of energy in signal frequency band	Regime	Radio frequency fingerprints of modems with various defects
2 – physical channel	Off-net interference with variable frequency	Bit error rate (BER)	Selection of phase- code structure of signal	Structural- code	Unevenness of signal spectra and interference
3 – data link channel	Variability of ambient temperature, multipath signals	Packet loss probability (PER), retransmission rate. Node energy loss per communication round	Data packet fragmentation. Optimization of transmission power level	Energy; presence of ARQ protocol	Temperature- dependent discharge characteristics of batteries
4 – linear route	Heterogeneity of different route sections	End-to-end packet delay. Node energy balance	Adaptive alternation of node activity	Hardware; dynamic	Features of radio wave propagation
5 – network	Mutual interference from neighboring nodes	Number of alternative data transmission routes	Network topology and clustering management	Topological	Topographic conditions of node placement

Based on the results obtained, the method of multilevel synthesis of WSN is defined as an iterative process consisting of the sequential determination of signal parameters, functional and mobile modes of network nodes, taking into account the limited resources of each level.

As shown in Figure 1, this study presents the following levels of analysis and synthesis of WSN: Θ_1 — device; Θ_2 — physical channel; Θ_3 — data link; Θ_4 — linear route; Θ_5 — network.

Each group of characteristics $\Theta_v = \{\varphi^{(v)}, \xi^{(v)}, \varpi^{(v)}\}$, where $v = 1, 2, 3, 4, 5$, includes the following indicators:

1) **performance indicators** $\varphi^{(v)} \in \Phi_v$, determining the level of achievement of target noise immunity factors as a result of the application of synthesized algorithms. In the context of the subject area under consideration, such indicators include: $\varphi^{(1)}$ — coefficients of mutual correlation of the distorted and reference signals (characterizing the degree of their overlap in the frequency-time domain); $\varphi^{(2)}$ — bit error probability; $\varphi^{(3)}$ — packet retransmission frequency upon detection of a corrupted bit; $\varphi^{(4)}$ — end-to-end delay of the transmitted packet, energy balance of nodes along the route; $\varphi^{(5)}$ — probability that the time of the integral state of the WSN is not less than the period required by the supersystem (for example, the growing season of an agricultural crop);

2) **key destabilizing factors** $\xi^{(v)} \in \Xi_v$, that directly affect the values of parameters $\varphi^{(v)}$: $\xi^{(1)}$ — hardware defects in the node modem that distort the generated signal; $\xi^{(2)}$ — interference with a spectrum within the receiver passband; $\xi^{(3)}$ — changing ambient temperature and radio wave propagation conditions; $\xi^{(4)}$ — heterogeneity of different sections of the linear route; $\xi^{(5)}$ — mutual interference from neighboring nodes;

3) **control parameters** $\varpi^{(v)} \in \Omega_v$, that is, parameters of resource distribution algorithms of a certain level, that enable to compensate for the destabilizing effect of the environment, reflected by the selection conditions: $\varpi^{(1)}$ — vector of energy redistribution between orthogonal components of the signal at the level of changing the modem operating mode; $\varpi^{(2)}$ — selection of the phase-code structure of the signal with rejection of the spectrum section affected by interference; $\varpi^{(3)}$ — fragmentation of the packet length or selection of the optimal gradation of the transmitter power in order to reduce energy losses of the node; $\varpi^{(4)}$ — schedule of the sequence of changes in the activity states of the “wake-sleep” node; $\varpi^{(5)}$ — matrix of selection of coordinates of the next location of the WSN nodes and schedule of change of the heads of clusters;

4) **resource constraints** Ω_v of control parameters: Ω_1 — types of changeable modem modes; Ω_2 — nomenclature of signal-code structures; Ω_3 — data packet formats, transmitter power gradations; Ω_4 — optional capabilities for controlling radio path activity; Ω_5 — resource of mobile vehicles and possible locations for WSN nodes.

The upper-level parameters given by the expression $\{\varpi^{(v+1)}\}$, are constraints for the lower level:

$$\Omega_v \subset \{\varpi^{(v+1)}\} \in \Omega_{v+1}. \quad (1)$$

Parameters Φ_v, Ξ_v, Ω_v are the ranges of acceptable values for the corresponding indicators. The radio communication system model is a system of deterministic and statistical relationships that combine performance indicators, operating conditions, and control parameters at all hierarchical levels.

The following types of dependences are distinguished.

Single-level dependences that establish a relationship between performance indicators $\varphi^{(v)}$, conditions $\xi^{(v)}$ and selection parameters $\varpi^{(v)}$ at each v -th level:

$$\varphi^{(v)} = f_v[\varpi^{(v)}, \xi^{(v)}]. \quad (2)$$

Despite the widespread use of these dependences for solving local problems of providing noise immunity within a separate level, their use creates significant difficulties in developing solutions for the optimal distribution of limited system resources between levels.

Interlevel dependences that determine the relationship between performance indicators of the v -th and $(v-1)$ -th levels, conditions of the v -th and $(v+1)$ -th levels, and the selection parameters of the v -th level:

$$\varphi^{(v)} = f_{v, v-1, v+1}[\varphi^{(v-1)} \geq \varphi_{mp}^{(v-1)}, \varpi^{(v)} \in \Omega_v \subset \{\varpi^{(v+1)}\}, \xi^{(v)}]. \quad (3)$$

Efficiency index $\varphi^{(v-1)}$ of the underlying level can be taken into account during the synthesis using the “bottom-to-top” pattern, which is typical for the operational stage (including the reliability control of WSN), in contrast to the design stage, which uses “top-to-bottom” synthesis [25].

At each hierarchical level, the object synthesis is realized through optimization of the controlled variables $\varpi^{(v)}$ within the established constraints Ω_v . These constraints are formed by the values of the parameters of the adjacent upper level $\{\varpi^{(v+1)}\}$. The need to move to a higher level arises when it is impossible to provide the required energy reliability with local resources, which involves the system resources. This decision is made with a comprehensive consideration of environmental factors at the synthesized level, including temperature conditions and interference environment.

Following the procedure for the mathematical description of complex objects adopted in the systems approach [26], the key stage of modeling is the formation of a system of performance indicators and optimization criteria. These parameters serve as the basis for the synthesis of optimal resource allocation algorithms that provide the required reliability of the WSN and allow for the evaluation of the efficiency of management decisions under conditions of multilevel external actions. At the same time, the selected indicators and criteria should provide a quantitative assessment of the degree of implementation of basic functions by network nodes at all hierarchical levels, guaranteeing the achievement of the established target values in accordance with the system intended purpose.

The criterion for the operation of an object in a v -th level system defines the range of acceptable values of the performance indicator Φ_v^* , where $\varphi^{(v)} \in \Phi_v^*$. In the context of providing the reliability of WSN, it is advisable to distinguish two criteria: suitability and optimality.

With limited resources and scalar indicator $\varphi^{(v)}$, the suitability criterion $\varphi^{(v)} \geq \varphi_{\text{доп}}^{(v)}$ defines the target area $\Phi_v^* = [\varphi_{\text{доп}}^{(v)}, 1]$, where $\varphi_{\text{доп}}^{(v)}$ — permissible value of the indicator. This allows us to formulate the problem of synthesizing energy efficiency algorithms as an inverse optimization problem — to find the minimum values of resources $\varpi^{(v)} \in \Omega_v$ that provide the achievement of permissible values of the efficiency indicators.

For optimality criterion $\varphi^{\wedge}\{v\} \rightarrow \max_{\varpi^{(v)} \in \Omega_v}$, region Φ_v^* degenerates into a point corresponding to the maximum value $\varphi^{(v)}$ for admissible values of the selection parameters $\varpi^{(v)} \in \Omega_v$ and given selection conditions. In this context, the development of control algorithms is reduced to solving the direct problem of optimal resource allocation.

Local use of the analyzed criteria does not allow for a comprehensive consideration of the specifics of WSN reliability assurance processes under varying network node operating modes. Therefore, it is advisable to implement a multilevel reliability management process based on the principle of sufficiency, which provides improved system performance with minimal additional resource expenditure.

The practical implementation of the sufficiency principle is based on an iterative parameter selection process, where migration between hierarchical levels occurs with increasing resource expenditures required to obtain specified reliability indicators. At each step, the sufficiency of the solutions generated to meet established performance standards is verified. The tools for implementing this approach include a set of suitability criteria and a hierarchical set of models that provide information support for making design decisions at all stages of the synthesis of the complex system.

Additional conditions for selecting solutions $\zeta^{(v)}$, taken into account in this work, include: $\zeta^{(1)}$ — radio frequency fingerprints of modems with various defects; $\zeta^{(2)}$ — unevenness of signal spectra and interference; $\zeta^{(3)}$ — temperature-dependent discharge characteristics of batteries; $\zeta^{(4)}$ — features of radio wave propagation; $\zeta^{(5)}$ — topographic conditions of node placement.

Taking into account the hierarchical organization of resources described by a chain of nested sets:

$$\dots, \varpi^{(v-1)} \in \Omega_{v-1} \subset \{\varpi^{(v)}\}, \varpi^{(v)} \in \Omega_v \subset \{\varpi^{(v+1)}\}, \varpi^{(v+1)} \in \Omega_{v+1} \subset \{\varpi^{(v+2)}\}, \dots,$$

where the volume and cost of resources grow with increasing system level, the selection of solutions to provide a given level of noise immunity requires prioritizing the use of lower-level resources. In this case, the general problem statement is as follows:

— *based on the known* and developed single-level and multilevel models of types (2) and (3) of the radio communication system, taking into account both basic conditions $\xi^{(v)}$ — destabilization factors, and additional conditions $\zeta^{(v)}$ for selecting a solution, *to determine* the minimum level v^* of the system under study, at which, due to the optimal distribution of the resource $\varpi^{(v)} \in \Omega_v$, the performance quality indicator of WSN $\varphi^{(v)*}$ is ensured to be not lower than the permissible (required) value $\varphi_{\text{доп}}^{(v)}$. In this case, value $\varphi_{\text{доп}}^{(v)}$ is calculated taking into account the required reliability of the WSN, determined by the supersystem.

In the mathematical formulation, this problem has the form:
needs to be determined

$$v^* = \min \left\{ v = f^{-1} \left[\max_{\varpi^{(v)}} \left\{ \varphi^{(v)} \right\} \geq \varphi_{\text{доп}}^{(v)}, \varpi^{(v)*}, \xi^{(v)}, \zeta^{(v)} \right] \right\}, \quad (4)$$

at which

$$\begin{aligned} & \dots\dots\dots \\ \varphi^{(v-1)*} &= \max_{\varpi^{(v-1)} \in \Omega_{v-1}} \left\{ \varphi^{(v-1)} \left[\varphi^{(v-2)}, \varpi^{(v-1)}, \xi^{(v-1)}, \zeta^{(v-1)} \right] \right\} < \varphi_{\text{доп}}^{(v-1)}; \\ \varphi^{(v)*} &= \max_{\varpi^{(v)} \in \Omega_v} \left\{ \varphi^{(v)} \left[\varphi^{(v-1)}, \varpi^{(v)}, \xi^{(v)}, \zeta^{(v)} \right] \right\} \geq \varphi_{\text{доп}}^{(v)}; \\ \varphi^{(v+1)*} &= \max_{\varpi^{(v+1)} \in \Omega_{v+1}} \left\{ \varphi^{(v+1)} \left[\varphi^{(v)}, \varpi^{(v+1)}, \xi^{(v+1)}, \zeta^{(v+1)} \right] \right\} \geq \varphi_{\text{доп}}^{(v+1)}. \\ & \dots\dots\dots \end{aligned} \quad (5)$$

The general scientific problem is solved step-by-step (in accordance with the considered levels of reliability assurance of the WSN) through sequentially checking the fulfillment of inequalities (5). The left-hand side of each of the inequalities (5) represents the solution to a specific research problem, in the formulation of which the optimality criterion is used. Taking into account certain characteristics of the multilevel representation of the WSN, the specific research problems are:

- 1) minimization of hardware distortions of the signal shape relative to the reference signal:

$$\varphi^{(1)}\left[\varpi^{(1)}, \xi^{(1)}, \zeta^{(1)}\right] \rightarrow \max_{\varpi^{(1)}}, \varpi^{(1)} \in \Omega_1; \quad (6)$$

- 2) optimal distribution of signal energy between orthogonal components taking into account the probability distribution of the interference frequency in the signal spectrum:

$$\varphi^{(2)}\left[\varphi^{(1)}, \varpi^{(2)}, \xi^{(2)}, \zeta^{(2)}\right] \rightarrow \max_{\varpi^{(2)}}, \varphi^{(1)} \geq \varphi_{\text{don}}^{(1)}; \varpi^{(2)} \in \Omega_2; \quad (7)$$

- 3) optimization of transmitter power and packet length in order to reduce the node energy consumption per communication round:

$$\varphi^{(3)}\left[\varphi^{(2)}, \varpi^{(3)}, \xi^{(3)}, \zeta^{(3)}\right] \rightarrow \max_{\varpi^{(3)}}, \varphi^{(2)} \geq \varphi_{\text{don}}^{(2)}; \varpi^{(3)} \in \Omega_3; \quad (8)$$

- 4) optimization of the schedule of alternating node activity in “wake-sleep” modes for the purpose of route balancing of energy losses:

$$\varphi^{(4)}\left[\varphi^{(3)}, \varpi^{(4)}, \xi^{(4)}, \zeta^{(4)}\right] \rightarrow \max_{\varpi^{(4)}}, \varphi^{(3)} \geq \varphi_{\text{don}}^{(3)}; \varpi^{(4)} \in \Omega_4; \quad (9)$$

- 5) optimal network clustering that provides the required number of alternative routes with an acceptable reduction in nodal energy resources:

$$\varphi^{(5)}\left[\varphi^{(4)}, \varpi^{(5)}, \xi^{(5)}, \zeta^{(5)}\right] \rightarrow \max_{\varpi^{(5)}}, \varphi^{(4)} \geq \varphi_{\text{don}}^{(4)}; \varpi^{(5)} \in \Omega_5; \quad (10)$$

As follows from expressions (6)–(10), the ranges of change of the variable parameters $\varpi^{(v)}$ are limited by the resource capabilities of the system Ω_v at the corresponding control level v , in particular:

- 1) at the device level — by the presence of modes for correcting (pre-distorting) the spectrum of generated signals for optimal redistribution of energy in the modem bandwidth;
- 2) at the physical level — by the ability to select phase-code designs with direct spectrum expansion to minimize the impact of interference and hardware distortions on the reliability of message reception;
- 3) at the data link channel level — by the presence of an ARQ protocol in the event of detection of distorted bits upon reception, followed by optimization of the transmission mode;
- 4) at the route level — by limited hardware and dynamic resources that allow for adaptive control of node activity (in sleep/wake modes));
- 5) at the network level — by the ability to reconfigure the network structure when forming clusters and backup data transmission routes (Table 1).

The integration of additional conditions $\zeta^{(v)}$, not previously taken into account in single-level models, into the procedure for optimizing algorithms for providing the reliability of the WSN contributes to the development of the methodological apparatus, confirms the scientific novelty of the formulation and solution to applied research problems.

Discussion. The analytical analysis has shown that the traditional methodologies for studying the energy reliability of wireless sensor systems often suffer from fragmentation, which reduces their efficiency. The major problem with these approaches is their ignorance of the impact of the technical states of low-level nodes on the output indicators of high-level systems. This reduces the accuracy of the assessment and leads to suboptimal resource allocation.

In the presented study, this problem is solved by an iterative multilevel approach based on the principle of sufficiency. Its key advantage is the search for the minimum hierarchical level v at which the resource distribution $\varpi^{(v)}$ provides the required value of the quality indicator $\varphi^{(v)} \geq \varphi_{\text{don}}^{(v)}$. Compared to known methods [16], the application of this approach allows achieving target reliability indicators with minimal resource costs.

The scientific novelty of the work is expressed in the integration of new conditions $\zeta^{(v)}$ into the model, which were not previously taken into account in papers [20–24]. This provides more accurate and practice-oriented control algorithms, which is of key importance in improving the reliability of WSN. The developed multilevel model of network infrastructure demonstrates how a systems approach to design can improve reliability management.

It allows for the integration of parameters of the technical condition of sensor nodes, which ultimately improves the accuracy of predicting the operating characteristics of the system and allows its operation to be adapted to real-time conditions.

A multilevel model of network infrastructure, built on the principles of hierarchical synthesis, demonstrates the possibility of consistently accounting for the parameters of individual sensor nodes [13] in the context of global network performance indicators. Compared to the models in which node states are described in an aggregated manner, the proposed approach provides a more detailed and, at the same time, systemic representation, which improves the accuracy of performance prediction and the stability of control decisions.

The developed reliability management methodology based on the sufficiency principle balances the operational quality and resource constraints. Unlike the studies that prioritize either maximizing reliability or minimizing energy consumption, this approach proposes a mechanism for aligning these criteria at each hierarchical level. This is reflected, specifically, in routing algorithms that take into account the residual energy of nodes and the interference environment in the communication channel. Their use not only improves energy efficiency and extends the network service life, but also ensures the required reliability under changing external actions.

Thus, the presented approach provides a more comprehensive and practice-oriented basis for managing WSN energy reliability compared to the existing solutions. It combines detailed consideration of low-level states with a high-level system description, expanding the network ability to adapt to real-world operating conditions and optimize the use of limited resources.

Conclusion. Despite the results obtained, a critical understanding of the limitations and capabilities of the models used remains urgent. The directions outlined in this paper require further research, including a deeper understanding of the mechanics of the interactions between destabilizing factors and systemic responses. To validate the results obtained and assess their stationarity, field tests and similar research under various agroclimatic conditions are required.

This study not only confirms the need for a multilevel approach to WSN reliability management but also provides a basis for further research in this area. A detailed analysis and integration of factors affecting reliability and energy efficiency potentially opens new horizons for the application of WSN in the agricultural industry and other areas that require an efficient and reliable monitoring.

Practical implementation could include the deployment of heterogeneous WSN, in which router nodes collect data from sensors, balancing energy consumption based on the developed integrated multilayer model of the network infrastructure for monitoring agricultural facilities. For example, the proposed algorithms could be used to generate digital field maps, automate irrigation and application of crop protection products, and minimize costs and environmental impacts.

References

1. Mazitov AA. Web Application for Mathematical Modeling of Unsteady Oil Flow in Porous Medium. *Advanced Engineering Research (Rostov-on-Don)*. 2023;23(4):422–432. <https://doi.org/10.23947/2687-1653-2023-23-4-422-432>
2. Samoylenko I, Fedorenko V, Samoylenko V. Adaptive Data Relay Transmission in Wireless Sensor Networks for Reliable Crop Growth Monitoring. *Computers and Electronics in Agriculture*. 2025;234:110367. <https://doi.org/10.1016/j.compag.2025.110367>
3. Hamouda F, Puig-Sirera À, Bonzi L, Remorini D, Massai R, Rallo G. Design and Validation of a Soil Moisture-Based Wireless Sensors Network for the Smart Irrigation of a Pear Orchard. *Agricultural Water Management*. 2024;305:109138. <https://doi.org/10.1016/j.agwat.2024.109138>
4. Xinqing Xiao. Sustainable Agriculture with Self-Powered Wireless Sensing. *Agriculture*. 2025;15:234. <https://doi.org/10.3390/agriculture15030234>
5. Al-Attafi MKR, Yesaulko AN, Kotova AS. Optimization of Macro- and Microelement Content in Soil for Sunflower Cultivation under Unstable Moisture Conditions of the Central Ciscaucasus Region. *Agrarian Bulletin of the North Caucasus*. 2025;15(2):74–84. <https://doi.org/10.31279/2949-4796-2025-15-2-74-84>
6. Jingxin Yu, Jiang Liu, Congcong Sun, Jiaqi Wang, Jianchao Ci, Jing Jin, et al. Sensing Technology for Greenhouse Tomato Production: A Systematic Review. *Smart Agricultural Technology*. 2025;11:101020. <https://doi.org/10.1016/j.atech.2025.101020>
7. Dinn C, Adhikari R, Hassan E, Shakshuki E, Eaman A. Developing a New IoT Network Topology for Effective Greenhouse Monitoring and Control. *Procedia Computer Science*. 2025;265:285–292. <https://doi.org/10.1016/j.procs.2025.07.183>
8. Sharma B, Koundal D. Cattle Health Monitoring System Using Wireless Sensor Network: A Survey from Innovation Perspective. *IET Wireless Sensor Systems*. 2018;8(4):143–151. <https://doi.org/10.1049/iet-wss.2017.0060>
9. Sisinni E, Saifullah A, Song Han, Jennehag U, Gidlund M. Industrial Internet of Things: Challenges, Opportunities, and Directions. *IEEE Transactions on Industrial Informatics*. 2018;14(11):4724–4734. <https://doi.org/10.1109/TII.2018.2852491>
10. Tsarev OYu, Tsarev YuA. Validation of Reliability Indices during Experimental Development of a Complex Technical Series System. *Advanced Engineering Research (Rostov-on-Don)*. 2023;23(1):26–33. <https://doi.org/10.23947/2687-1653-2023-23-1-26-33>

11. Wei He, Guan-Yu Hu, Zhi-Jie Zhou, Pei-Li Qiao, Xiao-Xia Han, Yuan-Yuan Qu, et al. A New Hierarchical Belief-Rule-Based Method for Reliability Evaluation of Wireless Sensor Network. *Microelectronics Reliability*. 2018;87:33–51. <https://doi.org/10.1016/j.microrel.2018.05.019>
12. Lajara R, Pelegri-Sebastiá J, Solano JJP. Power Consumption Analysis of Operating Systems for Wireless Sensor Networks. *Sensors*. 2010;10(6):5809–5826. <https://doi.org/10.3390/s100605809>
13. Lajara R, Perez-Solano JJ, Pelegri-Sebastia J. Predicting the Batteries' State of Health in Wireless Sensor Networks Applications. *IEEE Transactions on Industrial Electronics*. 2018;65(11):8936–8945. <https://doi.org/10.1109/TIE.2018.2808925>
14. Maltseva NS, Azhmuratova RR, Bondarenko DS. Extending the Service Life of a Wireless Sensor Network Environmental Monitoring. *Engineering and Construction Bulletin of the Caspian Region*. 2023;46(4):99–103. <https://doi.org/10.52684/2312-3702-2023-46-4-99-103>
15. Nam-Tuan Le, Yeong Min Jang. Energy-Efficient Coverage Guarantees Scheduling and Routing Strategy for Wireless Sensor Networks. *International Journal of Distributed Sensor Networks*. 2015;11:612383. <https://doi.org/10.1155/2015/612383>
16. Reformat MZ, Yager RR. Multi-Level State Evaluation in Complex Systems: Information Granules and Evidence Theory Approach. *Granular Computing*. 2024;9:57. <https://doi.org/10.1007/s41066-024-00477-3>
17. Volchenkov D. Mathematics of Multi-Level Complex Systems. *Discontinuity, Nonlinearity, and Complexity*. 2014;3(3):223–225. <https://doi.org/10.5890/DNC.2014.09.001>
18. Khan MA, Shalu, Naveed QN, Lasisi A, Kaushik S, Kumar S. A Multi-Layered Assessment System for Trustworthiness Enhancement and Reliability for Industrial Wireless Sensor Networks. *Wireless Personal Communications*. 2024;137:1997–2036. <https://doi.org/10.1007/s11277-024-11391-x>
19. Ojeda F, Mendez D, Fajardo A, Ellinger F. On Wireless Sensor Network Models: A Cross-Layer Systematic Review. *Journal of Sensor and Actuator Networks*. 2023;12(4):50. <https://doi.org/10.3390/jsan12040050>
20. Fedorenko V, Samoylenko V, Vinogradenko A, Samoylenko I, Sharipov I, Anikuev S. Mathematical Aspects of Stable State Estimation of the Radio Equipment in Terms of Communication Channel Functioning. In book: Vishnevskiy VM, Samouylov KE, Kozyrev DV (eds). *Distributed Computer and Communication Networks*. Cham: Springer; 2019. P. 547–59. https://doi.org/10.1007/978-3-030-36625-4_44
21. Listova NV, Fedorenko VV, Samoylenko IV, Emelyanenko IV, Samoylenko VV. The Communications Channels Models in Wireless Sensor Networks, Based on the Structural-Energetic Interaction between Signals and Interferences. In: *Proc. Moscow Workshop on Electronic and Networking Technologies (MWENT)*. New York City: IEEE; 2018. P. 1–4. <https://doi.org/10.1109/MWENT.2018.8337298>
22. Fedorenko V, Samoylenko I, Samoylenko V. Fragmentation of Data Packets in Wireless Sensor Network with Variable Temperature and Channel Conditions. *Computer Communications*. 2024;214:201–214. <https://doi.org/10.1016/j.comcom.2023.12.001>
23. Fedorenko V, Oleinikov D, Samoylenko I, Samoylenko V. Criteria for the Deployment of a Heterogeneous Linear WSN: Operability vs Energy Efficiency. *Ad Hoc Networks*. 2023;147:103202. <https://doi.org/10.1016/j.adhoc.2023.103202>
24. Fedorenko VV, Samoylenko VV, Alduschenko DV, Emelyanenko IV. Methods of Modeling Wireless Sensor Networks Topology Considering Internodal Interference. *Vestnik of Astrakhan State Technical University. Series: Management, Computer Science and Informatics*. 2020;(3):34–44. <https://doi.org/10.24143/2072-9502-2020-3-34-44>
25. Lei Zou, Zidong Wang, Jun Hu, Yurong Liu, Xiaohui Liu. Communication-Protocol-Based Analysis and Synthesis of Networked Systems: Progress, Prospects and Challenges. *International Journal of Systems Science*. 2021;52(14):3013–3034. <https://doi.org/10.1080/00207721.2021.1917721>
26. Buldakova T. Approaches to the Development of Complex Systems Models. In: *Proc. XXI International Conference. Complex Systems: Control and Modeling Problems (CSCMP)*. New York City: IEEE; 2019. P. 374–378. <https://doi.org/10.1109/CSCMP45713.2019.8976542>

About the Author:

Vladimir V. Samoylenko, Cand.Sci. (Eng.), Associate Professor of the Department of Engineering and IT-Solutions, Stavropol State Agrarian University (12, Zootechnicheskyy Lane, Stavropol, 355035, Russian Federation), [SPIN-code](#), [ORCID](#), [ResearchGate](#), [ScopusID](#), samoylenko.vv@stgau.ru

Conflict of Interest Statement: the author declares no conflict of interest.

The author has read and approved the final version of manuscript.

Об авторе:

Владимир Валерьевич Самойленко, кандидат технических наук, доцент кафедры «Инжиниринг и IT-решения» Ставропольского государственного аграрного университета (355000, Российская Федерация, г. Ставрополь, пер. Зоотехнический, 12), [SPIN-код](#), [ORCID](#), [ResearchGate](#), [ScopusID](#), samoilenko.vv@stgau.ru

Конфликт интересов: автор заявляет об отсутствии конфликта интересов.

Автор прочитал и одобрил окончательный вариант рукописи.

Received / Поступила в редакцию 15.09.2025

Reviewed / Поступила после рецензирования 01.10.2025

Accepted / Принята к публикации 20.10.2025